

Developmental Signals in Murine Postnatal Cardiac Growth

Amy Margaret Nicks, BSc. (Hons)

Submitted in accordance with the requirements degree of
Doctor of Philosophy

The University of Leeds
Faculty of Biological Sciences

November 2016

The candidate confirms that the work submitted is her own, except where work which has formed part of jointly authored publications has been included. The contribution of the candidate and the other authors to this work has been explicitly indicated below. The candidate confirms that appropriate credit has been given within the thesis where reference has been made to the work of others.

Li, M., Iismaa, S. E., Naqvi, N., Nicks, A., Husain, A. & Graham, R. M. 2014. Thyroid hormone action in postnatal heart development. *Stem Cell Res*, 13, 582-91.

This review was a collaborative effort, which has been referenced in the General Introduction.

This copy has been supplied on the understanding that it is copyright material and that no quotation from the thesis may be published without proper acknowledgement.

© 2016 The University of Leeds and Amy Margaret Nicks

The right of Amy Margaret Nicks to be identified as Author of this work has been asserted by her in accordance with the Copyright, Designs and Patents Act 1988.

Acknowledgements

Firstly, I would like to thank my supervisor Professor Bob Graham for the opportunity to work at the Victor Chang Cardiac Research Institute (Sydney) with his team. I am not sure how Bob manages the institute and the lab; it is a wonderful place to work with so many multi-disciplinary teams. Bob is an outstanding man, sometimes he may be difficult to keep up with (both intellectually and practically) but he always has time to discuss science. There is so much to thank you for. Thanks for bringing me here, for entrusting me with this project, and for teaching me to think critically, not only about my work but also the work of others. My study in Australia would not have been possible without the complete support of my UK supervisor, Professor Derek Steele, from the University of Leeds- thank you. I would like to also thank my co-supervisor in Sydney, Dr Siiri Iismaa, for her undivided attention, bouncing ideas around, answering all of my endless questions and her incredible eye for detail, especially in the last few months of writing. I would like to also thank my second co-supervisor in Sydney, Dr Nicola Smith, for welcoming me with open arms to Australia and the lab, who has given me her full moral support throughout and indispensable experimental guidance. Thanks must go to all past and present members of the Graham lab for their unwavering support, particularly Mrs Sara Holman and Ms Andrea Chan.

The Institute is really a wonderful place to work, including all of my colleagues on level 5 (and security), who have been so kind and generous, not only with their reagents, but also with their advice, time, and friendship. I would especially like to thank Dr Alastair Stewart, Dr Ali McCorkindale, Daniella Beniamen, and Claire Smith, who have directly helped me and made my time here extra enjoyable. Every day on my way to work in Darlinghurst, I have two motivations, a coffee from the great people in Latteria and the sign-posted quote:

“Logic will get you from A to B. Imagination will take you everywhere.” - Albert Einstein

And last but not least, thanks must go to my incredible husband, family and friends. Tom is one-of-a-kind following me to Sydney and we have made so many special memories along the way especially on our engagement and wedding day. Thank you for everything. A huge thank you to my beloved parents and sister who I have missed seeing so much while I have been here, they are my inspiration and my rock. I would also like to thank my friends from near and afar for their love and amazing support.

I confirm that the work submitted is my own except those mentioned below. I confirm that the appropriate credit has been given to experimental contributors and in the referenced work of others.

I would like to thank those that contributed to this research for their help and expertise in the lab: Mrs Sara Holman, Ms Andrea Chan, Dr Jianxin Wu, Dr Ming Li, Dr Siiri Iismaa, and Galina Shevchenko, from the Graham Lab, and outside of the lab, the BioCORE animal facility, Dr Scott Kesteven, Mr Rob Saloman, Dr David Humphreys and Dr Joshua Ho.

Their contributions have been as follows: Dr Ming Li, Dr Scott Kesteven, and Dr Jianxin Wu, performed suprarenal aortic banding (SAC) surgery, echocardiography, and micromanometry, respectively. To efficiently isolate, enrich, and purify CMs from multiple hearts within a day, Sara, Andrea and myself, worked as a team, and without their help and expertise this would not have been possible. Histology was performed and images were generated by Andrea in Chapter 3 (Figure 3.7, I collected and sectioned tissues for this experiment), and Chapter 6 (Figure 6.4, we collected tissues for this experiment). Three independent RT-qPCR experiments were performed in Chapter 5 by Dr Siiri Iismaa (Figure 5.4C), Galina (Figure 5.4B), and myself (Figure 5.4A). The experiment for staining and imaging cells in Chapter 6 (Figure 6.7, Figure 6.8, Figure 6.9, and Figure 6.10) was performed by both Andrea (who also set up the confocal microscope to take tiled images) and myself. Mr Rob Saloman, who is head of the Garvan Flow Cytometry Facility, provided assistance with flow cytometry experiments, data collection and analyses (Figure 6.6). Dr David Humphreys constructed and sequenced poly(A) and miRNA cDNA libraries from the Genomic Core Facility at the Victor Chang Cardiac Research Institute. Drs David Humphreys and Joshua Ho advised on the analyses of RNA-Seq data, and direct contributions were made by David in Chapter 7 and 8 (Figure 7.1 and Figure 8.1). And a big thank you to all the staff at the BioCORE animal facility, who have taught me everything I know about mice and looked after the animals.

Abstract

Cardiovascular disease is the leading cause of death worldwide, and is increasing in an ageing and growing population. Heart failure in adults results from a loss of functional cardiomyocytes (CMs), which are not replaced because the terminally differentiated state of adult CMs severely limits the capacity of the heart to regenerate. Thus, there is a need to develop strategies that enhance endogenous CM proliferation and enable cardiac repair.

This thesis describes the characterisation of a surgical model of pressure overload, suprarenal aortic constriction (SAC), which results in hypertension and left ventricular hypertrophy. This model can be used to investigate candidates for cardiac regeneration. Previous work in our laboratory suggested that under hypertensive stress, mice with inhibited signalling of the tyrosine kinase receptor, c-Kit, had improved cardiac function and survival due to CM proliferation. Thus, the expression of c-Kit was evaluated in wild-type mice and was found at very low levels in developing and adult CMs, and was not re-expressed in adults following SAC. Therefore, c-Kit is unlikely to contribute to the maintenance of CM terminal differentiation and is not a suitable therapeutic target for CM proliferation.

Another approach to identifying candidates for regeneration is to understand the changes in gene expression and regulatory networks that lead to CM proliferation and terminal differentiation. Characterisation of postnatal cardiac growth identified pivotal postnatal days (P) of CM maturation with high CM proliferation (P2), a transition between CM division and enlargement (P10 and P13), and CM terminal differentiation (P70). A standardised protocol for mice of any age was developed to rapidly purify CMs (~95% purity). Poly(A) RNA was extracted from purified CMs at the aforementioned time points for high-throughput sequencing, which identified ~3,800 differentially expressed mRNAs that underpin CM maturation. Thus, this data has enormous potential to identify molecular targets for cardiac regeneration.

Table of Contents

Acknowledgements	iii
Abstract	v
Table of Contents	vi
List of Tables	xi
List of Figures	xii
List of Abbreviations	xv
Chapter 1 General Introduction	1
1.1 Cardiovascular disease	1
1.1.1 Hypertensive heart disease (HHD) and heart failure (HF)	1
1.1.2 Pathological versus physiological hypertrophy	2
1.1.3 Signals in cardiac hypertrophy	6
1.1.4 Renin-angiotensin aldosterone system (RAAS).....	7
1.1.5 Surgical models of HF in mice.....	8
1.1.6 Treatments of LVH	11
1.1.7 Endogenous cardiomyocyte (CM) turnover in the adult heart	12
1.2 Stem cell factor receptor (c-Kit)	13
1.2.1 c-Kit structure and signalling	13
1.2.2 c-Kit expression in the heart.....	17
1.2.3 c-Kit expression after cardiac injury	18
1.2.4 Cardiac injury in mice with mutations in the c-Kit/SCF pathway	19
1.3 Postnatal cardiac growth	22
1.3.1 Comparative physiology of heart growth.....	22
1.3.2 Factors that affect postnatal cardiac growth.....	23
1.3.3 Cell cycle, ploidy and nucleation status in CMs	24
1.3.4 Phases of CM growth	28
1.3.5 Metabolic switch in postnatal CM maturation	31
1.3.6 Pathophysiology in postnatal cardiac growth.....	33
1.3.7 Clues for regeneration in postnatal cardiac growth.....	35
1.4 Cardiomyocyte transcriptome	37

1.4.1	Microarray versus high-throughput sequencing (HTS).....	37
1.4.2	Sampling the CM transcriptome.....	40
1.4.3	Discordant adult and neonatal CM isolation procedures.....	40
1.5	Aims of this study	43
Chapter 2	General Methods	44
2.1	Animals	44
2.2	Tissue collection	44
2.3	Cardiac puncture	44
2.4	CM isolation and enrichment	45
2.5	CM area quantification.....	46
2.6	RNA extraction	46
2.7	Real-time quantitative polymerase chain reaction (RT-qPCR).....	47
2.8	Preparing cells for immunocytochemistry	48
2.9	Histology.....	48
2.10	Statistical analyses	49
Chapter 3	Characterisation of a surgical mouse model of LVH.....	50
3.1	Introduction.....	50
3.2	Materials and Methods.....	52
3.2.1	Suprarenal aortic constriction (SAC)	52
3.2.2	Echocardiography.....	55
3.2.3	Micromanometry	55
3.2.4	Tissue and CM collection.....	56
3.2.5	Immunocytochemistry.....	56
3.2.6	Plasma renin concentration and activity.....	57
3.2.7	RT-qPCR.....	58
3.2.8	Staining for cardiac fibrosis	59
3.3	Results.....	60
3.3.1	Effects of SAC on blood pressure	60
3.3.2	Effects of SAC on cardiac function.....	62
3.3.3	Gross morphology of LVH following SAC	64
3.3.4	Evaluation of pathological hypertrophy markers and fibrosis.....	68
3.3.5	RAAS activation following SAC	71

3.4	Discussion	72
Chapter 4	The role of c-Kit in cardiomyocytes after LVH.....	75
4.1	Introduction.....	75
4.2	Materials and Methods.....	77
4.2.1	Animal models	77
4.2.2	Tissue and CM collection.....	78
4.2.3	Cell culture of HEK293T and MEL cells.....	78
4.2.4	Stem cell factor (SCF) stimulation of MEL cells.....	79
4.2.5	Protein extraction, immunoprecipitation and Western blotting.....	80
4.2.5.1	Protein extraction	80
4.2.5.2	Immunoprecipitation	80
4.2.5.3	SDS-PAGE and transfer.....	81
4.2.5.4	Western blot	82
4.2.5.5	Densitometry of Western blots.....	83
4.2.6	RT-qPCR.....	84
4.2.7	Immunocytochemistry.....	84
4.3	Results.....	85
4.3.1	Identification of specific anti-c-Kit antibodies for Western blot analyses	85
4.3.2	Characterisation of c-Kit expression in MEL cells and in three cardiac-specific c-Kit transgenic mouse lines	87
4.3.3	Characterisation of c-Kit expression in the WT heart and in CMs	91
4.3.4	c-Kit expression following SAC	95
4.3.5	SCF stimulation of mature c-Kit in MEL cells	98
4.4	Discussion.....	100
Chapter 5	Postnatal murine cardiac growth.....	105
5.1	Introduction.....	105
5.2	Materials and Methods.....	108
5.2.1	Inbred C57BL/6J colony	108
5.2.2	Heart collection, CM isolation and fixation	110
5.2.3	Total T ₃ assay	110
5.2.4	RT-qPCR.....	111

5.2.5	Immunocytochemistry.....	111
5.3	Results.....	113
5.3.1	Postnatal heart and body weights	113
5.3.2	Levels of triiodothyronine (T ₃) hormone in postnatal development	116
5.3.3	Cell cycle gene expression during postnatal cardiac growth.....	117
5.3.4	Morphology of developing postnatal CMs.....	119
5.4	Discussion	121
Chapter 6	Purification of cardiomyocytes from neonatal, preadolescent, and adult mouse hearts.....	128
6.1	Introduction.....	128
6.2	Materials and Methods.....	130
6.2.1	CM isolation, enrichment and purification from neonatal, preadolescent, and adult hearts.....	130
6.2.1.1	Materials for cannulation and perfusion of the heart.....	130
6.2.1.2	Buffers.....	133
6.2.1.3	Extraction and cannulation of the heart.....	136
6.2.1.4	Perfusion of postnatal hearts	139
6.2.1.5	Isolation of CMs.....	140
6.2.1.6	Enrichment of preadolescent and adult CMs.....	141
6.2.1.7	Purification of preadolescent and adult CMs	141
6.2.1.8	Purification of neonatal CMs	143
6.2.2	Histology	144
6.2.3	Flow cytometry	144
6.2.3.1	Fixing cells for flow cytometry	144
6.2.3.2	Staining for flow cytometry	144
6.2.3.3	Flow cytometry.....	145
6.2.4	Immunocytochemistry.....	145
6.2.4.1	Counting cell populations.....	146
6.3	Results.....	147
6.3.1	Modification of the method for isolation and enrichment of adult CMs	147
6.3.2	Adapting the purification of CMs from adult hearts to neonatal and preadolescent hearts	149

6.3.3	Characterisation of isolated and enriched CMs.....	151
6.3.4	Characterisation of purified CMs.....	153
6.4	Discussion.....	161
Chapter 7	Transcriptional profiles of CM maturation.....	166
7.1	Introduction.....	166
7.2	Materials and Methods.....	168
7.2.1	Purification of CMs.....	168
7.2.2	RNA extraction.....	168
7.2.3	RNA concentration and quality.....	169
7.2.4	cDNA library construction from poly(A) and small RNA.....	170
7.2.4.1	Enrichment of poly(A) and small RNA.....	170
7.2.4.2	cDNA library construction.....	171
7.2.5	Alignment of reads and gene counts.....	173
7.2.6	Analyses of RNA-Seq data.....	174
7.2.7	Functional biological category analyses of differentially expressed (DE)-mRNAs.....	174
7.3	Results.....	176
7.3.1	Characterisation of CM inputs for RNA-Seq.....	176
7.3.2	Alignment of unique reads.....	177
7.3.3	Distinct transcriptional profiles of postnatal CMs.....	178
7.3.4	Identifying DE-mRNAs in CM maturation.....	180
7.3.5	Expression levels of cardiac cell-type specific markers in purified preparations of CMs.....	182
7.3.6	Expression of developmental and growth signals across postnatal CM maturation.....	183
7.3.7	Functional biological category analyses of DE-mRNAs.....	185
7.4	Discussion.....	188
Chapter 8	General Discussion.....	193
	List of References.....	205
	Appendix.....	225

List of Tables

Table 1.1: Relative contributions of metabolic pathways to the production of ATP during rabbit cardiac development.....	32
Table 3.1: Timeline for sham and SAC surgeries	53
Table 3.2: Taqman probe sequences for RT-qPCR.....	58
Table 3.3: Primer sequences for SYBR Green RT-qPCR.....	58
Table 3.4: Gross morphology, micromanometry and echocardiography measurements one week post- sham or SAC surgery	65
Table 3.5: Acute and short-term effects of SAC on renin levels.....	71
Table 4.1: c-Kit, phospho-c-Kit and GAPDH antibodies.....	83
Table 5.1: Primers sequences for SYBR Green RT-qPCR.....	111
Table 5.2: Heart-to-body weight measurements in postnatal murine development....	115
Table 6.1: Buffers for CM isolation and purification.....	134
Table 6.2: Preparing digestion buffer (DB) for neonatal hearts	136
Table 6.3: Detailed procedure for the purification of CMs from murine neonatal and adult hearts	138
Table 7.1: CM input samples for RNA-Seq.....	176

List of Figures

Figure 1.1: Illustration of the changes in cardiac geometry of a normal heart that undergoes either concentric or eccentric hypertrophy.....	5
Figure 1.2: Illustration of different surgical models of pressure overload (PO) by aortic banding	9
Figure 1.3: c-Kit domains and tyrosine phosphorylation sites	14
Figure 1.4: Structural surface representation of c-Kit homodimerisation and c-Kit mutations.....	16
Figure 1.5: Schematic of the cell cycle	26
Figure 3.1: Images of SAC surgery	54
Figure 3.2: Micromanometry measurements one week post- sham or SAC surgery	61
Figure 3.3: Echocardiography measurements six days post- sham or SAC surgery	63
Figure 3.4: Gross morphology of the heart, LV and CMs one week post- sham or SAC surgery	67
Figure 3.5: Correlation between SBP and LV/TL, before and after applying the exclusion criteria.....	68
Figure 3.6: Expression of pathological hypertrophy markers in the LV and in CMs one week post- sham or SAC surgery	69
Figure 3.7: Histological transverse LV sections stained for fibrosis one week post- sham or SAC surgery	70
Figure 4.1: The construct used to generate transgenic c-Kit mouse models: Tg(α MHC-Kit ^{Wv}), Tg(α MHC-Kit.1) and Tg(α MHC-Kit.2).....	77
Figure 4.2: Western blot analyses to determine the specificity of c-Kit antibodies	86
Figure 4.3: Characterisation of c-Kit expression in HEK293T and MEL cells, and in WT and Tg(α MHC-Kit ^{Wv}) hearts.....	88
Figure 4.4: Characterisation of c-Kit expression in WT and Tg(α MHC-Kit ^{Wv}) CMs	89
Figure 4.5: Characterisation of c-Kit expression in WT, Tg(α MHC-Kit ^{Wv}), Tg(α MHC-Kit.1) and Tg(α MHC-Kit.2) transgenic mouse models	91
Figure 4.6: Western blotting and immunoprecipitation conditions were optimised to improve the detection of c-Kit protein.....	93
Figure 4.7: Characterisation of c-Kit in WT hearts and in CMs	95
Figure 4.8: Characterisation of c-Kit in WT CMs and in LVs one week post - sham or -SAC surgery	97

Figure 4.9: Detection of c-Kit activity after SCF stimulation of MEL cells	99
Figure 5.1: Phenotype of inbred C57BL/6J mouse pups from birth to two weeks	109
Figure 5.2: Heart-to-body weight ratios of C57BL/6J mice from litters of an average size.....	114
Figure 5.3: Endogenous serum total T ₃ levels during postnatal development	116
Figure 5.4: Expression of cell cycle genes throughout postnatal cardiac development.....	118
Figure 5.5: Gross morphology of developing postnatal CMs	120
Figure 5.6: A comparison of reported murine heart-to-body weight ratios.....	123
Figure 5.7: Correlation between heart weight and CM size in postnatal cardiac development.....	127
Figure 6.1: Surgical instruments and Langendorff apparatus used to cannulated and perfuse murine hearts	132
Figure 6.2: Immuno-magnetic separation of ECs from CMs	143
Figure 6.3: Enriched CM fraction contaminated with ECs.....	148
Figure 6.4: Histological sections of aortae and hearts from neonatal, preadolescent and adult mice.....	150
Figure 6.5: The percentage of rod-shaped CMs that were fixed prior to the dissociation of cardiac tissue or after	152
Figure 6.6: Flow cytometric analyses of purified neonatal, preadolescent, or adult CMs	154
Figure 6.7: Isolation and purification of P2 CMs	156
Figure 6.8: Isolation, enrichment and purification of P10 CMs.....	157
Figure 6.9: Isolation, enrichment and purification of P13 CMs.....	158
Figure 6.10: Isolation, enrichment and purification of adult CMs	159
Figure 6.11: The proportion of CMs, ECs or other cell types quantified at various stages of the CM purification procedure.....	160
Figure 7.1: The distribution of unique poly(A) reads to the reference genome from CMs across postnatal cardiac development	177
Figure 7.2: Principle component analyses (PCA) of mRNA, lncRNA and miRNA, from CMs across postnatal cardiac development	179
Figure 7.3: The number of DE-mRNAs from CMs across postnatal cardiac growth were determined using cpm, fold-change, and statistical significance criteria.....	181
Figure 7.4: Expression of cardiac cell markers in purified CMs	182

Figure 7.5: Expression of developmental and growth signalling genes in CMs purified over the course of postnatal cardiac development	184
Figure 7.6: Heatmap of clustered DE-mRNAs reveal functional biological categories that associate with key developmental time points in postnatal CM maturation	186
Figure 8.1: Expression patterns of mRNA-lncRNAs-miRNAs from the Igf2/H19 locus over the time course of postnatal CM maturation	200

List of Abbreviations

AAC	abdominal aortic constriction
Ab	antibody
Ang II	angiotensin II
ANP	atrial natriuretic peptide
BNP	brain natriuretic peptide
bp	base pair
bpm	beats per minute
BW	body weight
CHD	congenital heart disease
CM	cardiomyocyte
CO	cardiac output
CPC	cardiac progenitor cell
cpm	counts per million
CSC	cardiac stem cell
CVD	cardiovascular disease
DB	digestion buffer
DBP	diastolic blood pressure
DE	differentially expressed

EC	endothelial cell
ECL	enhanced chemiluminescence
FS	fractional shortening
G	gauge
GFP	green fluorescent protein
h	LV wall thickness
HF	heart failure
HHD	hypertensive heart disease
HR	heart rate
HW	heart weight
IB	isolation buffer
IGF1	insulin-like growth factor 1
IGF1R	insulin-like growth factor 1 receptor
IHD	ischaemic heart disease
IP	immunoprecipitation
lncRNA	long noncoding RNA
LV	left ventricle
LVEDP	left ventricular end-diastolic pressure
LVEF	left ventricular ejection fraction
LVH	left ventricular hypertrophy

LVSP	left ventricular systolic pressure
MAP	mean arterial pressure
MI	myocardial infarction
miRNA	micro RNA
mRNA	messenger RNA
P	postnatal day
PB	perfusion buffer
PFA	paraformaldehyde
PO	pressure overload
R	internal LV chamber radius
RAAS	renin-angiotensin aldosterone system
RIN	RNA integrity number
RNA-Seq	RNA sequencing
RT	room temperature
SAC	suprarenal aortic constriction
SBP	systolic blood pressure
SCF	stem cell factor
SEM	standard error of the mean
TB	transfer buffer
TF	transcription factor

Tg	transgenic
TH	thyroid hormone
TL	tibia length
UTR	untranslated region
VSMC	vascular smooth muscle cell
WT	wild-type
α -MHC	alpha-myosin heavy chain
α -SKA	alpha-skeletal actin
β -MHC	beta-myosin heavy chain

Chapter 1 General Introduction

1.1 Cardiovascular disease

Cardiovascular disease (CVD) is the leading cause of death worldwide. From 1990 to 2013, the number of deaths from CVD increased by 41% due to an ageing and growing population (Naghavi *et al.*, 2015; Roth *et al.*, 2015). In 2011, the World Health Organization (WHO) set a goal, “25 by 25”, to reduce premature deaths from CVD by 25% before 2025 in persons aged between 30 and 70 years-old. CVD risk factors and comorbidities, such as: obesity, smoking, diabetes, and hypertension, may lead to sudden cardiac death, or mortality. Current strategies to alleviate CVD involve lifestyle changes (diet and exercise), medication, and surgery. Heart failure (HF) is a common end-result of a variety of CVDs, including ischemic and hypertensive heart disease (IHD and HHD), whereby heart transplantation is the only cure for patients with end-stage HF, but is limited by the number of donors, and requires lifelong administration of immunosuppressive drugs. To obviate these problems, the potential to stimulate cardiac regeneration to repair the heart is a novel approach to treating CVDs, although a major hurdle to realising this approach is the terminally differentiated state of adult cardiomyocytes (CMs), which severely limits regenerative repair after cardiac injury. This is in contrast to other organs, such as the liver and skin, which retain their regenerative potential throughout life, allowing scarless repair after injury with complete restoration of organ function.

1.1.1 Hypertensive heart disease (HHD) and heart failure (HF)

In the Framingham Heart Study (Levy *et al.*, 1988), left ventricular (LV) mass and blood pressures were determined in ~5000 participants of 17- 90 years of age. This showed that hypertension preceded HF in 75% of patients and was the primary cause of pathological left ventricular hypertrophy (LVH) (Ho *et al.*, 1993). Indeed, LVH is an independent predictor of cardiovascular morbidity and mortality (Lloyd-Jones *et al.*, 2002; Levy *et al.*, 1988). The clinical diagnosis for hypertension is an elevated blood pressure of >140/90 mmHg, and if blood pressure increases above 160/100 mmHg, the risk of HF doubles (Lloyd-Jones *et al.*, 2002). In response to hypertensive stress, the adult heart is restricted to hypertrophic growth

to normalise wall stress and preserve cardiac output (CO). The prevalence of LVH is 16% in women and 19% in men, which was determined by echocardiography measurements (Levy *et al.*, 1988). Hypertensive heart disease (HHD) involves a sequence of events that lead to pathological hypertrophy associated with systolic and/or diastolic dysfunction, which may progress into overt HF (Drazner, 2011). HF patients are classified into four classes depending on the severity of their symptoms according to the New York Heart Association framework, which is based on exercise tolerance and fatigue, from class I: no limit of physical activity, to class IV: cannot undertake physical activity without discomfort (Jessup *et al.*, 2009). A sensitive biomarker of HF is the circulating level of brain natriuretic peptide (BNP), which is determined to guide therapy (Jessup *et al.*, 2009; Horwich *et al.*, 2003).

1.1.2 Pathological versus physiological hypertrophy

Cardiac “hypertrophy” is from the Greek for “increased growth” (Maillet *et al.*, 2013) and others refer to it as “above normal growth” of the heart (Dorn, 2007). An increase in workload on the heart leads to both physiological and pathological hypertrophy resulting from the cellular enlargement of CMs rather than from cell division because CMs become terminally differentiated after birth. This does not occur with other cell types in the heart, such as endothelial cells (ECs), fibroblasts, or vascular smooth muscle cells (VSMCs), which all retain proliferative capacity (Maillet *et al.*, 2013). Hypertension-induced pathological hypertrophy is initially adaptive to maintain CO but becomes maladaptive with cardiac remodelling, which as a result progresses to cardiac dysfunction. This progression is due to altered cardiac geometry, activation of the “fetal gene program”, fibrosis, and inadequate angiogenesis leading to decreased myocardial perfusion and coronary blood flow in the heart (Dorn, 2007; Maillet *et al.*, 2013). In comparison, physiological hypertrophy also results in altered cardiac geometry but with enhanced coronary blood flow and no re-expression of the fetal gene program or fibrosis.

In the compensatory or adaptive phase of cardiac growth, high blood pressure increases the afterload on the heart, which is counteracted by thickening of the LV wall to normalise wall stress and maintain CO. At the cellular level, cardiac growth is achieved by an increase in CM width as sarcomeres replicate in parallel with a subsequent increase in LV wall thickness (h) compared with the internal chamber radius (R), increasing the LV wall

thickness- to -internal chamber ratio (h/R) (Figure 1.1) (Grossman *et al.*, 1975; Lorell and Carabello, 2000). This type of cardiac growth caused by pressure overload (PO) is characterised as concentric hypertrophy, as the circumference of the resultant hypertrophic LV is concentric with that of the original heart. Other cardiac diseases that result from PO include valvular stenosis, which obstructs the outflow of blood and, hence, increases afterload (Maillet *et al.*, 2013). Over time, persistent haemodynamic overload leads to a decrease in the LV wall thickness to internal chamber radius ratio (h/R), which is due to an increase in CM length, and not width, caused by the serial replication of sarcomeres (Figure 1.1). The resulting dilatation of the LV and ensuing volume overload is characteristic of eccentric hypertrophy (circumference of the dilated LV chamber has moved laterally and is no longer concentric with that of the original heart) (Lorell and Carabello, 2000). Other volume overload cardiac diseases include mitral valve regurgitation, arterio-venous shunts or a large myocardial infarction (MI). The altered geometry of the LV and chamber dilation leads to cardiac dysfunction (Dorn, 2007).

The hallmark of pathological hypertrophy is the re-expression of the fetal genes: atrial and brain natriuretic peptides (ANP and BNP), α -skeletal actin (α -SKA) and β -myosin heavy chain (β -MHC) (Schoenfeld *et al.*, 1998; Gulick *et al.*, 1991). In addition the expression of fetal genes, LVH is associated with fibrosis due to the increased deposition and accumulation of collagen resulting from the proliferation of fibroblasts, which heterogeneously alters tissue structure and causes myocardial stiffness (Cuspidi *et al.*, 2006; Weber and Brilla, 1991). Together with fibrosis and insufficient arteriogenesis to maintain adequate myocardial perfusion, decompensatory hypertrophy ensues with systolic and/or diastolic dysfunction due to chamber stiffness and impaired relaxation, a substrate for ventricular arrhythmias and sudden cardiac death, and also indicates the onset of HF (Kahan and Bergfeldt, 2005; Houser *et al.*, 2012). Chronic LVH and diastolic dysfunction results in severe congestive HF that requires repeated hospitalization (Lorell and Carabello, 2000). Thus, there are many factors that contribute to pathological cardiac remodelling and its progression to overt HF.

Physiological hypertrophy is distinguishable from pathological hypertrophy as it is associated with normal LV systolic and diastolic function, and does not progress to HF (Maillet *et al.*, 2013; Dorn, 2007). Physiological hypertrophy, which occurs with normal

cardiac development, pregnancy and exercise, is reversible, unlike pathological hypertrophy, which is usually irreversible if increased workload is not ameliorated (Dorn, 2007) (Maillet *et al.*, 2013). Normal cardiac development involves the development of both pressure and volume overload, and therefore, consists of both concentric and eccentric hypertrophy (Maillet *et al.*, 2013; Naqvi *et al.*, 2014). Exercise-induced physiological hypertrophy also develops into either concentric or eccentric hypertrophy depending on the type of training, i.e., if it is isometric (such as weight-lifting) or isotonic (such as cycling), respectively (Dorn, 2007; Maillet *et al.*, 2013). However, athletes that undertake prolonged endurance training regimes and increase their aerobic rather than anaerobic capacity, are more likely to develop pathological hypertrophy and CVD (Dorn, 2007; Maillet *et al.*, 2013). In contrast, only volume overload occurs with pregnancy resulting in eccentric hypertrophy (Dorn, 2007) , which is reversible postpartum.

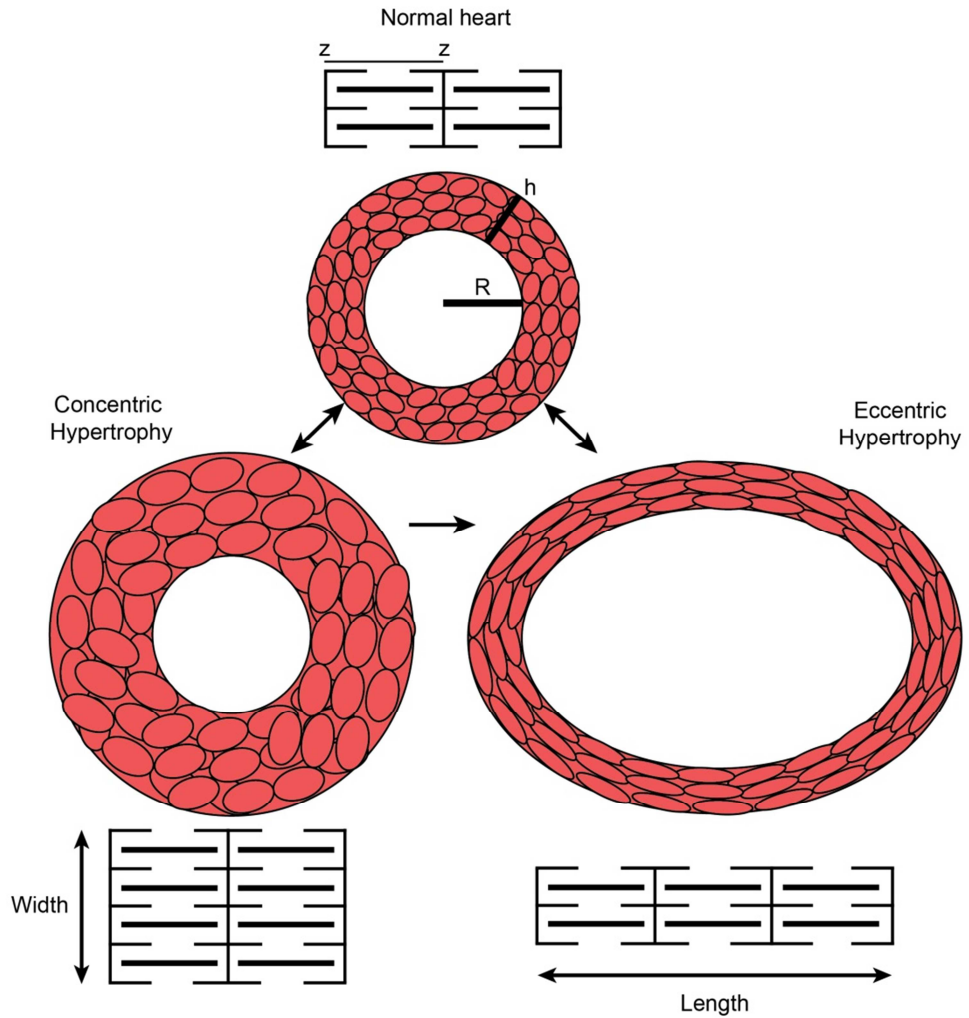


Figure 1.1: Illustration of the changes in cardiac geometry of a normal heart that undergoes either concentric or eccentric hypertrophy

Cardiac hypertrophy involves concentric or eccentric growth of the heart due to an increased workload on the heart. Concentric hypertrophy leads to an increase in the LV wall thickness (h) relative to the internal chamber radius (R) resulting from an increase in CM cell width due to the parallel addition of sarcomere. Eccentric hypertrophy leads to chamber dilation and a reduction in the wall thickness ration (h/R) with an increase in CM cell length, rather than width, due to the serial addition of sarcomere. Sarcomere units are shown under each LV chamber with thin actin filaments aligned along the z-discs and thick myosin filaments aligned in-between.

The underlying molecular phenotypes of pathological and physiological hypertrophy are different, and include changes in energy metabolism, contractility, fetal gene expression, fibrosis, and neurohumoral pathways. CMs contain many mitochondria that continually supply ATP primarily via the oxidation of fatty acids and also by the oxidation of glucose. In pathological hypertrophy, there is a shift from fatty acid to glucose metabolism, whereas both pathways are augmented in physiological hypertrophy leading to enhanced aerobic capacity (Dorn, 2007; Hou and Kang, 2012). Furthermore, the fetal gene program is activated in pathological hypertrophy but not in physiological hypertrophy (Maillet *et al.*, 2013). This leads to an increase in the ratio of slow twitch contractile protein, β -MHC, to the fast twitch contractile protein, α -MHC, which has higher ATPase activity. The increase in the β -MHC/ α -MHC ratio is energetically favourable but also disadvantageous since contractility is reduced (Krenz and Robbins, 2004). In human hearts, β -MHC is the predominant isoform and the expression of α -MHC decreases by 15-fold with end-stage HF (Miyata *et al.*, 2000). In contrast, the contractile protein that represents the thin filament, α -SKA, increases with CM stretch and wall stress, and is associated with increased contractility (Hewett *et al.*, 1994). Overall, contractility is reduced, which is also due to impaired Ca^{2+} homeostasis, and in particular, the reduced expression of the sarcoplasmic reticulum Ca^{2+} -ATPase 2A (SERCA2A) (Hou and Kang, 2012). Another change that occurs with pathological but not physiological hypertrophy, is increased fibrosis caused by the greater deposition of collagen types I and III (Dorn, 2007; Hou and Kang, 2012). Pathological hypertrophy leads to increases in ANP and BNP levels, which counteract high blood pressure and fibrosis, respectively (Gardner, 2003). ANP does this by targeting the renin-angiotensin-aldosterone system (RAAS) system to inhibit renin and aldosterone secretion, it is also an antagonist of vasoconstriction, acting as a relaxant to reduce total peripheral resistance, and therefore, reduces blood pressure and volume (Atlas *et al.*, 1986). Whereas BNP is produced by fibroblasts and inhibits collagen deposition, and moreover, *Nppb*^{-/-} mice with reduced BNP expression, have higher levels of fibrosis after PO (Gardner, 2003; Tamura *et al.*, 2000).

1.1.3 Signals in cardiac hypertrophy

There are many signalling pathways that are activated with pathological or physiological hypertrophy, and the neurohumoral pathway is one of these. Indeed, the main signalling

pathway that promotes pathological hypertrophy is through G protein-coupled receptors (GPCRs) that are activated by angiotensin II (Ang II), endothelin, and catecholamines (Heineke and Molkentin, 2006) (Dorn, 2007). Upon ligand binding, heterotrimeric $G\alpha_{q/11}$ proteins couple to GPCRs, and the G proteins recruit phospholipase C β , resulting in the hydrolysis of phosphatidylinositol 4, 5 bisphosphate (PIP₂) into diacylglycerol (DAG) and inositol 1, 4, 5 triphosphate (IP₃) (Salazar *et al.*, 2007). DAG activates protein kinase C, which initiates the expression of pro-hypertrophic genes. IP₃ leads to sustained Ca²⁺ release from sarco-endoplasmic reticulum stores, which in turn causes the activation of calcineurin and the downstream transcription factor (TF), nuclear factor of activated T-cells (NFAT), which translocates to the nucleus (Salazar *et al.*, 2007; Heineke and Molkentin, 2006). Both NFAT and calmodulin kinase II stimulate the expression of prohypertrophic genes and cardiac growth (Salazar *et al.*, 2007).

Physiological hypertrophy is promoted by insulin-like growth factor 1 (IGF1) that activates the phosphoinositide 3-kinase (PI3K) and serine/threonine-protein kinase (Akt) pathway (Dorn, 2007) (Maillet *et al.*, 2013). IGF1 is synthesised and secreted from the liver in response to growth hormone stimulation, and is also produced by target tissues (Maillet *et al.*, 2013). IGF1 binds to heterodimers of the tyrosine kinase receptors: insulin receptor and IGF1 receptor (IGF1R) or to homodimers of IGF1R, which recruit adaptor proteins that interact with PI3K (Jung and Suh, 2014). PI3K is a heterodimer that consists of a p85 regulatory subunit and a p110 (α , β or δ) catalytic subunit, which phosphorylates phosphatidylinositol 4, 5-bisphosphate to generate phosphatidylinositol 3, 4, 5-triphosphate (Heineke and Molkentin, 2006; Dorn, 2007). This leads to Akt recruitment and phosphorylation at the cell membrane, and its activation promotes protein synthesis through activating the mammalian target of rapamycin (mTOR) and inhibiting glycogen synthase kinase (GSK). Furthermore, the p110 α isoform of PI3K, regulates heart and CM size in normal cardiac development and exercise (Shioi *et al.*, 2000; McMullen *et al.*, 2003).

1.1.4 Renin-angiotensin aldosterone system (RAAS)

Pathological hypertrophy is also associated with abnormal activation of RAAS, although the exact mechanisms for the dysregulation of RAAS components are not completely understood (Atlas, 2007). Renin is synthesised and secreted by the juxtaglomerular (JG)

cells in the kidney, which detect a reduction in blood pressure, or renin is released when there is a decrease in the delivery of sodium and chloride ions to the macular densa of the distal tubules. Once released, renin cleaves circulating angiotensinogen (secreted by the liver), forming angiotensin I (Ang I) (Atlas, 2007), although the decapeptide has no biological activity, it is hydrolysed to the active octapeptide, Ang II, by membrane-bound angiotensin converting enzyme (ACE), and to a lesser extent by the mast cell protease, chymase (chymotryptic-like protease). Ang II acts at the Ang II type 1 (AT₁) receptor located in vessel walls resulting in vascular smooth muscle constriction, which increases vascular resistance leading to an increase in blood pressure. Ang II also stimulates the release of aldosterone from the adrenal glands and the antidiuretic hormone (ADH) from the posterior pituitary gland. This causes an increase in blood volume and pressure due to salt and water retention (Atlas, 2007). In addition, Ang II and aldosterone negatively regulate renin release while the synthesis of Ang II is also inhibited by ANP and nitric oxide (Atlas, 2007).

1.1.5 Surgical models of HF in mice

Surgical models have contributed greatly to our understanding of the pathogenesis and treatment of LVH. In addition to myocardial infarction, surgical models of HF by aortic constriction result in systemic hypertension and the rapid development of cardiac hypertrophy. These can be performed in mice, which are the preferred species for genetic studies and aid “proof of principle” research. Mice are also economically beneficial, with relatively low housing costs and a short gestational period (~21 days) (Tarnavski *et al.*, 2004; Patten and Hall-Porter, 2009). However, there are very few laboratories that have the expertise to perform microsurgery, especially techniques involving aortic banding in mice (Tarnavski *et al.*, 2004).

Abdominal and suprarenal aortic constrictions (AAC and SAC) are performed by partially ligating the abdominal aorta either between the right and left renal artery or above the origin of both renal arteries, respectively (Figure 1.2). Both AAC and SAC are more commonly performed in rats. SAC surgeries carried out in mice are often incorrectly referred to as AAC, however, in rats, AAC specifically describes banding between the right and left renal. Nevertheless, both AAC and SAC reduce renal blood flow and increase systemic blood

pressure, resulting in PO-induced LVH. Thoracic aortic constriction (TAC), established by Rockman *et al.* (1991), is more commonly performed in mice compared with SAC. TAC mimics aortic stenosis, whereby the banding is located around the aortic arch between the innominate and left carotid arteries (Figure 1.2), which directly increases cardiac afterload and, thus, the workload placed on the heart (Rockman *et al.*, 1991). Thus, all aortic banding models restrict blood flow through the aorta, leading to increased vascular resistance and high blood pressure proximal to the constriction. PO-induced LVH is evident by an increase in LV mass and wall thickness due to cellular hypertrophy, which in turn results in cardiac remodelling and decompensatory hypertrophy. This leads to impaired diastolic (relaxation of the heart) and systolic (contractility of the heart) function, depressed LV ejection fraction (LVEF), and, depending on the severity and duration of the constriction, the development of end-stage HF, which can manifest within weeks (Breckenridge, 2010; van Nierop *et al.*, 2013).

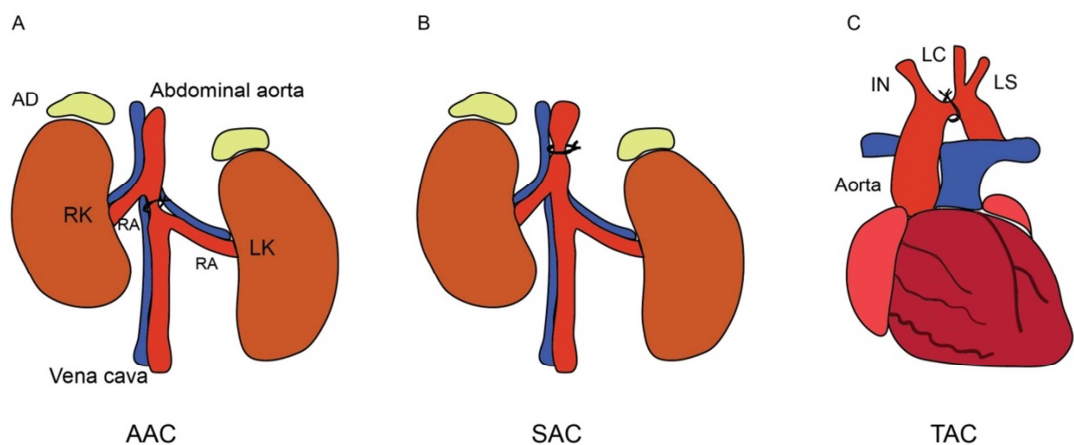


Figure 1.2: Illustration of different surgical models of pressure overload (PO) by aortic banding

A, Abdominal aortic constriction (AAC) between the right and left renal artery; B, suprarenal aortic constriction (SAC) proximal to the origin of the renal arteries; C, thoracic aortic constriction (TAC) between the innominate and left common carotid arteries. AD, adrenal glands; RK, right kidney; LK, left kidney; RA, renal artery; IN, innominate artery; LC, left carotid; LS, left subclavian.

In general, it is difficult to make comparisons of surgical models given the difference in methods used between studies, such as the species, surgical technique, severity of constriction, study duration, and the location of banding. Rockman *et al.* (1991) reported a ~33% increase in the heart-to-body weight ratio (HW/BW) after one week of TAC surgery (27 G) in C57BL/6J x SJL mice, resulting in an immediate pressure gradient of 70 mmHg in the left carotid and 115 mmHg in the right carotid, which were both 75 mmHg prior to constriction. Comparisons of PO phenotypes have been made post-TAC with varying degrees of constriction in C57BL/6J mice, in which ambulatory blood pressures were monitored over a 24-hour period at four weeks after surgery (Duan *et al.*, 2007). The aorta was partially ligated in the presence of differently sized needles: 25 G, 26 G, and 27 G, which was then removed; this resulted in elevated SBPs that were ~130 mmHg, ~145 mmHg, and ~190 mmHg, and increases in the ventricle-to-body weight of ~11%, ~27%, and ~56%, respectively (Duan *et al.*, 2007). Moreover, the degree of constriction was correlated to the severity of LVH, whereby the higher the blood pressure the greater the fibrosis and expression of hypertrophy markers.

Resulting SAC phenotypes are also dependent on the degree of aortic constriction and length of study. In one study, two weeks of SAC with a 29 G needle using C57BL/6 mice, SBP increased by 59 mmHg and LV/BW increased by ~48%, which was accompanied with a re-expression in fetal genes (Wettschureck *et al.*, 2001). Our laboratory has previously used the SAC model with a 29 G needle in C57BL/6J mice and the LV/BW increased by ~45% and MAP was elevated by ~ 33% after one week of surgery (Li *et al.*, 2008). In another study, SAC was performed with a 25 G needle in FVB/N mice, and HW/BW increased by ~20 % after two weeks of the surgery but blood pressures were not measured (De Windt *et al.*, 2001). There have been fewer reports of SAC compared with TAC in the literature, although there are some long-term SAC studies. At eight weeks post-SAC with a 28 G needle using C57BL/6J mice, HW/BW increased by ~ 19% and the right carotid blood pressure was elevated by 15 mmHg compared with shams (Wu *et al.*, 2002). In this study, the aortae of sham controls were also ligated with a 20 G needle, which is not usually performed with sham operations. Patients with hypertension often have abnormal RAAS activation (Atlas, 2007), and yet the activity of RAAS in mice with aortic banding has not been established. Our laboratory has previously treated mice with an ACE inhibitor from the time of SAC surgery, and this reduced blood pressure to levels that were comparable to shams at three days post-SAC (Li *et al.*, 2004). In addition, AT₁ receptor blockers abrogated

hypertrophy after two weeks of TAC surgery (Takeda *et al.*, 2010; Li *et al.*, 2010). These studies clearly demonstrate the effects of aortic banding on LV mass and blood pressure, which involves the RAAS but its role is not clear. In addition, they illustrate the variability amongst different reports of SAC surgeries and highlight the importance of characterising PO models of aortic banding, especially since data are lacking for short-term studies of SAC-induced LVH in mice.

One of the main differences between SAC and TAC mouse surgeries is the higher mortality rate in SAC (30-40%) compared with TAC (10-20%) (Rockman *et al.*, 1991; deAlmeida *et al.*, 2010; Wu *et al.*, 2002; Duan *et al.*, 2007; Li *et al.*, 2008), in which most deaths occur within a 24-hour period of the surgery. Moreover, these surgeries lead to chamber dilation and congestive HF after 3, 6, and 15 weeks of surgery depending on the experimental conditions (Breckenridge, 2010; deAlmeida *et al.*, 2010; Hara *et al.*, 2002). One criticism of all of these models is the rapid development of LVH caused by the instantaneous increase in blood pressure, which is unlike the slower progression of stenosis/hypertension in the clinical setting, and therefore, of LVH (Patten and Hall-Porter, 2009). Nonetheless, the rapid development of LVH is a valuable tool for developing and identifying novel targets in the treatment of HF.

1.1.6 Treatments of LVH

Current treatments for LVH usually involve a combination of antihypertensive drugs such as ACE inhibitors, nitrates, and Ca²⁺ channel blockers (dilate blood vessels), diuretics (reduce blood volume), AT₁ receptor antagonists (block Ang II-mediated effects), and β -adrenergic blockers (reduce heart rate). Although therapeutic interventions may prevent or delay the progression of LVH to end-stage HF, the only definitive treatment of severe HF is a heart transplant, which involves a major surgical procedure, requires life-long immunosuppressive therapy and monitoring, is expensive, and is often not feasible due to the limited availability of donors.

1.1.7 Endogenous cardiomyocyte (CM) turnover in the adult heart

The adult heart has long been termed a post-mitotic organ, although data has recently surfaced suggesting there is a low level of CM renewal in humans. Indeed, Bergmann *et al.* (2009) used carbon dating to evaluate the age of CMs by measuring the incorporation of ^{14}C into DNA after nuclear bomb testing during the Cold War. This indicated that CM turnover was ~1% per year at the age of 25, and declined with age to 0.45% at 75 years. Conversely, Kajstura *et al.* (2010) estimated an average 20% renewal of CMs per year from a pool of resident cardiac stem cells (CSCs) that expanded with age. Mollova *et al.* (2013) reported a ~1.9% turnover of CMs in a young adult heart (19 years-old), similarly to Bergmann *et al.* (2009). Senyo *et al.* (2013) detected a comparable annual CM turnover of 0.76% in mice by using the non-radioactive isotope, ^{15}N thymidine (a marker of DNA synthesis), in combination with genetic fate mapping to label the majority of CMs with green fluorescent protein (GFP). Senyo *et al.* (2013) showed that pre-existing CMs undergo DNA synthesis to form new mononucleated GFP⁺ CMs. These sorts of methods are very limited in humans, and thus, it is more difficult to elucidate whether newly formed adult CMs arose from stem cells or differentiated CMs (Mollova *et al.*, 2013). Nonetheless, the low level of CM renewal in the heart is not enough to enable self-repair after cardiac injury.

In the past 20 years, the field of cardiac repair or regeneration has been evolving (Laflamme and Murry, 2011). The ultimate goal is to therapeutically manipulate innate pathways to stimulate the endogenous regeneration of CMs. If we can manipulate the pathway of self-renewal in CMs to alleviate the workload placed on individual CMs, this may translate into a novel therapy for cardiac regeneration after injury. Importantly, our laboratory has for the first time shown CM proliferation in adulthood in response to PO, using mice with genetic mutations of stem cell factor receptor, c-Kit, had better preserved cardiac function and survival, which was markedly improved compared with wild-type (WT) mice where the response is limited to hypertrophy (Li *et al.*, 2008).

1.2 Stem cell factor receptor (c-Kit)

Stem cell factor receptor (c-Kit) signalling mediates cell survival, migration, differentiation, and proliferation, and is important for haematopoiesis, pigmentation and fertility. Overactive c-Kit mutations are implicated in diseases such as: leukaemia, gastrointestinal tumours, testicular carcinoma and mastocytosis, in which more than 500 mutations of c-Kit have been reported (Lennartsson and Ronnstrand, 2012). The role of c-Kit in the heart is less clear, although c-Kit is expressed in CSCs it diminishes upon cell differentiation into different cardiac cell types (Tallini *et al.*, 2009; Fransioli *et al.*, 2008; Li *et al.*, 2008).

1.2.1 c-Kit structure and signalling

c-Kit was identified from homology with the oncogene v-kit from the Hardy-Zuckerman 4 feline sarcoma virus (Besmer *et al.*, 1986), and is localised on human chromosome 4 and mouse chromosome 5. c-Kit is over 1,000 amino acids long and has a core molecular weight of 110 kDa but post-translational heterogeneous *N*-linked glycosylation generates mature and precursor forms of c-Kit of 145-160 kDa and 125 kDa in size, respectively (Yarden *et al.*, 1987; Lennartsson and Ronnstrand, 2012). c-Kit is a member of the membrane bound sub-family of receptor tyrosine kinases (RTK), which structurally consist of an N-terminal domain, an extracellular domain (ECD) that comprises five immunoglobulin-like domains, a single hydrophobic transmembrane domain (TMD), a juxtamembrane domain (JMD), a kinase domain split into two parts (a N-lobe and C-lobe) by a kinase insert, and lastly a C-terminal domain (Figure 1.3 and Figure 1.4).

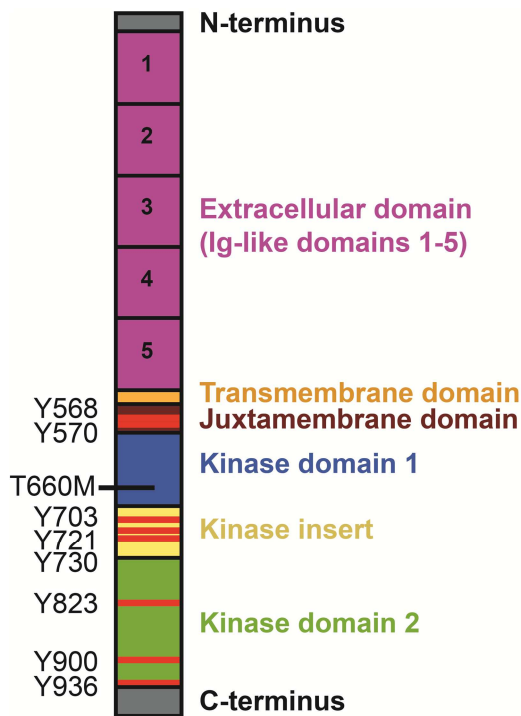


Figure 1.3: c-Kit domains and tyrosine phosphorylation sites

c-Kit domains proportional to their lengths, and a number of intracellular tyrosine phosphorylation sites are shown. Adapted from Roskoski (2005).

c-Kit is an archetypal RTK that undergoes ligand-induced dimerization, activation and degradation. The ligand of c-Kit, stem cell factor (SCF; also known as Kit-ligand or steel factor) is a cytokine that exists as both a membrane bound and soluble protein. Soluble SCF forms a dimer that binds to two c-Kit monomers, resulting in c-Kit dimerisation and autophosphorylation. A schematic of c-Kit activation is shown in Figure 1.4 and is based on the crystal structure of c-Kit bound to SCF. Dimeric soluble SCF associates strongly with the extracellular domain of c-Kit at Ig-like domains 1-3. Ig-like domains 4 and 5 are not involved in SCF binding but their interaction with each other is essential for tyrosine phosphorylation. Upon SCF-induced dimerisation, the two transmembrane domains of c-Kit move within 15Å of each other, which initiates transphosphorylation of intracellular tyrosine residues (Lennartsson and Ronnstrand, 2012). These occur systematically in the following order: juxtamembrane domain (Y568 and Y570), the kinase insert (Y703, Y721 and Y730), kinase domain 2 (Y823 and Y900) and C-terminus (Y936). Phosphorylation of these tyrosine residues results in the recruitment of multiple effectors involved in many

signalling pathways, including: PI3K, Src kinases, mitogen-activated protein kinases (MAPKs), phospholipase C and D, and adaptor proteins (Lennartsson and Ronnstrand, 2012). Only the mature form of c-Kit is phosphorylated while the precursor form of c-Kit is not phosphorylated and is not expressed at the cell surface (Lennartsson and Ronnstrand, 2012; Blume-Jensen *et al.*, 1991). c-Kit internalisation is mediated by Cbl phosphorylation, which directly or indirectly binds at the phosphorylation sites, blocking activation (Lennartsson and Ronnstrand, 2012). Cbl proteins function as E3 ligases resulting in the ubiquitylation and proteasomal degradation of c-Kit (Zeng *et al.*, 2005).

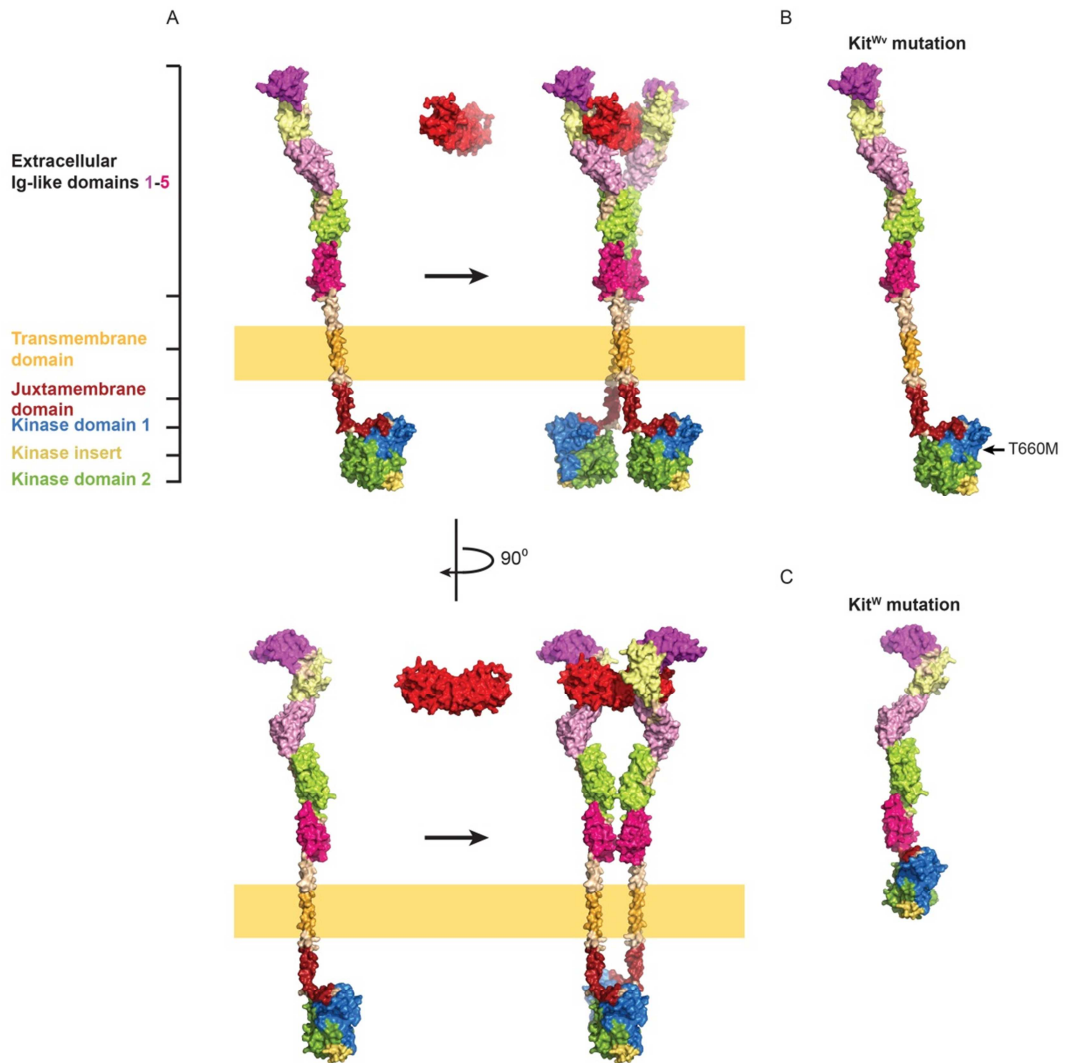


Figure 1.4: Structural surface representation of c-Kit homodimerisation and c-Kit mutations

A, the dimeric soluble SCF ligand induces homodimerisation of c-Kit in the plasma membrane resulting in the phosphorylation of intracellular tyrosines that are brought into close contact. B, Kit^{Wv} is a missense mutation at T660M in kinase domain 1. C, Kit^W is a 78 amino acid deletion of the transmembrane domain. The domains are similarly coloured to those presented in Figure 1.3. These models were made using PDBIDs: 2e9w and 2ec8, and images were generated using PyMol that were kindly provided by Dr Alastair Stewart.

1.2.2 c-Kit expression in the heart

There is a subpopulation of resident cardiac c-Kit⁺ stem cells (CSCs) in the heart, however, their abundance is very low (Barile *et al.*, 2007). Endogenous CSCs that express c-Kit are self-renewing, clonogenic, and differentiate *in vitro* and *in vivo* into all three cardiac lineages; CMs, ECs, and VSMCs (Beltrami *et al.*, 2003; Tallini *et al.*, 2009; Ellison *et al.*, 2013). c-Kit⁺ cardiac progenitor cells (CPCs) express proteins that identify with one of the cardiac lineages, e.g., GATA4 or sarcomeric tropomyosin for CMs, α -smooth muscle actin for VSMCs, or Pecam1 for ECs, and thus are partially committed (Fransioli *et al.*, 2008; Kovacic *et al.*, 2005). Furthermore, CPCs were found to form CMs, ECs, and fibroblasts *in vivo*, regulating cardiac homeostasis and repair in the adult heart (Hosoda *et al.*, 2009). Once cultured CPCs fully differentiate into one of the cardiac lineages, c-Kit expression is lost (Fransioli *et al.*, 2008; Tallini *et al.*, 2009). In contrast, Zaruba *et al.* (2010) found that the cardiomyogenic potential of adult and neonatal c-Kit⁺ cells was very limited *in vitro* and *in vivo*.

Expression of c-Kit⁺ cells during postnatal cardiac development is not well documented. Fransioli *et al.* (2008) generated transgenic mice that express GFP under the control of the c-Kit promoter to evaluate the number of CSCs that co-express GFP, and therefore c-Kit, in the heart. Such cells were found infrequently in cardiac tissues at: 7.2, 7.1, 0.3, and 0 per mm², at postnatal day 2 (P2), P7, P14, and P70, respectively (Fransioli *et al.*, 2008). In agreement with this study, our laboratory found that c-Kit expression in cardiac tissues was much greater at P1-P2 than P10 by immunohistochemistry and by RT-qPCR (Li *et al.*, 2008). However, c-Kit co-localised with β -MHC suggesting CMs were the source of c-Kit rather than CSCs. In another study, Tallini *et al.* (2009) reported that c-Kit was expressed in CPCs found in the embryonic, neonatal (P2-3), and adult hearts, reaching a maximum number at P2 but decreasing progressively to extremely low levels in the adult (<1%). This was investigated using a Kit^{BAC}-eGFP mouse that was generated using a bacterial artificial chromosome, which expressed enhanced GFP (eGFP) under the control of the *c-Kit* locus. This was similar to Zaruba *et al.* (2010), who determined the total proportion of c-Kit⁺ cells in the neonatal heart was 0.65% and in the adult heart was 0.5% by fluorescence-activated cell sorting (FACS). Overall, these studies indicate that c-Kit is most abundant at P2, although it is unclear as to which cell types are responsible for c-Kit expression. This is important to know since the role of c-Kit in heart development has not been established.

1.2.3 c-Kit expression after cardiac injury

In addition to studying the basal expression of c-Kit, its role in cardiac cells has also been studied in adult mammalian hearts after cardiac injury. The initial work by Beltrami *et al.* (2003) showed improved cardiac function following two injections of EGFP⁺ CSCs in the heart after MI. This resulted in the regeneration of CMs, ECs, and VSMCs. In another study, the number of c-Kit expressing cells was higher after MI and these cells, which were recruited to the site of injury, increased the number of CSCs and CPCs that differentiated into all three cardiac lineages (CMs, ECs, VSMCs) (Fransioli *et al.*, 2008). In a neonatal MI model, CPCs differentiated into ECs and CMs, partially regenerating the myocardium, but after the same MI injury performed in the adult heart, CPCs only differentiated into cells with a vascular lineage (Jesty *et al.*, 2012). Tallini *et al.* (2009) reported that after cryo-injury there was an increased population of c-Kit⁺ cells that mostly formed ECs or fibroblasts, and only the occasional differentiated CMs expressed c-Kit, which did not lead to cardiomyogenesis. On the contrary, newly formed CMs after MI and PO injury were reportedly due to the differentiation of CSCs (Hsieh *et al.*, 2007). It has also been suggested that the expansion of endogenous CSCs and their differentiation into CMs is sufficient to repair the heart after acute myocardial death (8-10% of the LV) using a single dose of isoproterenol (Ellison *et al.*, 2013); a finding that has recently been challenged (Wallner *et al.*, 2016). In the latter study, it was shown that a single injection of isoproterenol caused membrane injury in 10% of CMs, which was reversible, and, hence, CMs recovered in the absence of a contribution from the CSC population (Wallner *et al.*, 2016).

In contrast to the aforementioned work, Senyo *et al.* (2013) reported that the adult heart only has a very limited capacity to repair after MI, and that newly formed CMs are derived from the replication of pre-existing CMs and not by the maturation of stem cells. Replication of endogenous CMs after injury has also been shown in neonatal mice after apical resection (Porrello *et al.*, 2011b) and in zebrafish after apical resection (Kikuchi *et al.*, 2010; Jopling *et al.*, 2010). Thus, the origin, frequency, and propensity of CSCs to differentiate into CMs *in vivo* is controversial and highly debated.

In summary, the field of cardiac regeneration is in disagreement with respect to the basal expression and contribution of c-Kit expressing cells following injury, which may be context dependent (i.e., the type of injury model used). This is concerning since CSCs are

being clinically trialled (Bolli *et al.*, 2011). For these reasons, the careful evaluation of c-Kit in different cardiac cell types of the heart after injury is important, especially as it may help to establish its role in the heart.

1.2.4 Cardiac injury in mice with mutations in the c-Kit/SCF pathway

c-Kit co-localises to the same allele as the dominant white-spotting (W) locus. Mutations at this locus were first observed more than a century ago in black-eyed white mice that had loss of skin and iris pigmentation (Durham, 1908; Little, 1917). The W mutation is the result of a 78 amino acid deletion of the transmembrane domain, and results in a protein of 125 kDa, which is not expressed at the cell surface of Kit^{W/W} mast cells (Nocka *et al.*, 1990). W^v is a missense mutation, where threonine has been replaced with methionine at position 660, resulting in a dominant-negative effect on c-Kit signalling, shown in Figure 1.3 and Figure 1.4. Kit^{W/W} homozygotes die *in utero* or shortly after birth (Nocka *et al.*, 1989), whereas Kit^{W^v/W^v} homozygotes have a less severe phenotype but are sterile and anaemic that are black-eyed white mice due to a loss of pigmentation. Compound heterozygote Kit^{W/W^v} are also black-eyed white mice, are anaemic due to defective haematopoiesis, are deficient in tissue mast cells, and have sterility issues (Nocka *et al.*, 1990; Theoharides *et al.*, 1993; Galli *et al.*, 1987; Nocka *et al.*, 1989).

Original investigations in our laboratory focussed on PO in the Kit^{W/W^v} mice, which are deficient in tissue mast cells, and therefore have impaired secretion of the mast cell protease, chymase, which forms Ang II in the heart (Li *et al.*, 2004; Nishimura *et al.*, 1996). Unexpectedly, Kit^{W/W^v} hearts showed profound CM proliferation after one week of SAC-induced PO. Of interest, the cardiac morphology and function of adult Kit^{W/W^v} and WT mice were indistinguishable at baseline in terms of their mean arterial pressure (MAP), LV/BW, and CM area (cross-sectional area). Furthermore, microarray profiling of untreated Kit^{W/W^v} and WT hearts showed that only 8 of some >40,000 transcripts were differentially expressed. After one week of PO, the MAP and LV/BW increased similarly between WT and Kit^{W/W^v} mice, however, the degree of CM hypertrophy, which was determined by CM cross-sectional area, was markedly greater in WT hearts (WT: ~36% vs Kit^{W/W^v}: 10%). Although there were equivalent increases in LV mass between the WT and Kit^{W/W^v} mice post-SAC, in the latter this was due to a remarkable ~40% addition of CMs. Moreover, there

were a significant number (>150) of differentially expressed mRNAs relative to WT mice post-SAC, with many of the up-regulated transcripts being involved in cycle re-entry and cell proliferation. Further evidence of CM proliferation in Kit^{W/W^v} hearts post-SAC was the expression of cell cycle markers: Ki67 (all phases of cell cycle), phosphorylated histone H3 (onset of mitosis), and aurora kinase B (cytokinesis) in mature Kit^{W/W^v} CMs but not in WT CMs. In addition, pulse chase experiments using bromodeoxyuridine (BrdU), an analogue of thymidine, was incorporated into Kit^{W/W^v} CM nuclei with DNA replication but absent in WT CM nuclei post-SAC. This meant the number of CMs that re-entered the cell cycle increased by >1000-fold in Kit^{W/W^v} hearts compared with WT (WT, 0.004%; vs Kit^{W/W^v}, 4%). Importantly, the hyperplastic response observed in the Kit^{W/W^v} mice post-SAC resulted in better cardiac function and survival compared with their congenic WT littermates.

In these studies, the basal number of LV c-Kit⁺ interstitial cells was low in the adult WT and Kit^{W/W^v} myocardium (10 cells/ mm²) and were mostly resident CSCs. Interestingly, inhibition of c-Kit signalling in the Kit^{W/W^v} mice prevented the differentiation of CSCs into CPCs (GATA4⁺), which were reduced by 14-fold and 64-fold post-SAC, respectively, compared with WT hearts. Although the total number of c-Kit⁺ interstitial cells in the WT LV did not increase post-SAC, the CPC population expanded by 50%, whereas there was only a 10% increase in the number of CSCs in Kit^{W/W^v} hearts. Hence, there was a disproportionate expansion of CSCs and not CPCs in Kit^{W/W^v} hearts.

Given that c-Kit signalling is inactivated ubiquitously in all Kit^{W/W^v} tissues, a transgenic mouse overexpressing the Kit^{W^v} mutation under the control of the CM-specific α -MHC promoter (characterised and provided by Jeffrey Robbins (Gulick *et al.*, 1991; Subramaniam *et al.*, 1991)) was used to generate Tg(α -MHC-Kit^{W^v}) mice at the University of Alabama's Transgenic and Embryonic Stem Cell facility by Li *et al.* (2008) to study the effects of heart-specific inactivation of c-Kit signalling. After one week of PO, proliferative markers were present in Tg(α -MHC-Kit^{W^v}) CMs, consistent with cell cycle re-entry. These data suggest that not only does the ubiquitous inactivation of c-Kit signalling in Kit^{W/W^v} mice, but also CM-specific inhibition c-Kit signalling from birth, prevents CM cell cycle exit, allowing CM cell division and proliferation after PO.

There have been very few studies that investigate the effects and/or phenotype of mice with impaired c-Kit signalling after cardiac injury, however in one such study, SAC-induced PO resulted in compensatory hypertrophy after 4 weeks and congestive HF after 15 weeks in WT mice, but HF was not observed in Kit^{W/W^v} mice (Hara *et al.*, 2002). In agreement with Li *et al.* (2008), cardiac function was better preserved in Kit^{W/W^v} mice than in WT mice post-SAC. Furthermore, Kit^{W/W^v} had reduced perivascular fibrosis and pathological cardiac remodelling (Hara *et al.*, 2002). This was attributed to the deficiency of mast cells because when WT mice were administered tranilast, a stabiliser of mast cells, the progression of PO to HF was abrogated. The work of Hara *et al.* (2002) also highlights a beneficial phenotype of better cardiac function in Kit^{W/W^v} mice post-SAC, which was due to absence of tissue mast cells, however, the proliferation of CMs was not evaluated (Hara *et al.*, 2002).

In contrast to the PO model, Fazel *et al.* (2006) reported reduced cardiac function and increased mortality in Kit^{W/W^v} mice after three weeks of MI. This was due to the impaired mobilisation of bone marrow-derived endothelial progenitor cells, and thus, reduced EC proliferation, which prevented angiogenesis. Moreover, they found the Kit^{W/W^v} hearts were larger and the extent of CM hypertrophy was greater. In a complementary study, the c-Kit ligand, SCF, was overexpressed in CMs resulting in an increased number of endothelial progenitor cells and enhanced angiogenesis that led to a decrease in CM apoptosis, thus improving cardiac function and survival after 30 days of MI (Xiang *et al.*, 2009).

Overall, these studies demonstrate that there are a variety of mechanisms and cell types that are involved in the cardiac injury process in mice with impaired c-Kit signalling. c-Kit activates a plethora of signalling pathways and c-Kit⁺ precursor cells can give rise to all three cardiac lineages. The question we posed is whether active c-Kit signalling in CMs is a signal for differentiation and thus may restrict the heart to hypertrophic growth in response to PO, rather than the hyperplastic growth by CM proliferation, which was observed in both mice with global and CM-restricted inactivation of c-Kit signalling.

1.3 Postnatal cardiac growth

Another approach to identifying pathways of regenerative potential is to characterise cardiac growth, and more specifically, the phases of cardiac growth that govern: CM proliferation, terminal differentiation, and enlargement, in the context of the postnatal environment.

1.3.1 Comparative physiology of heart growth

The heart is the first organ to form in the embryo and continues to grow as the body grows throughout infancy, childhood, preadolescence and into adulthood. Heart weight is directly related to body surface area (Gutgesell and Rembold, 1990) and body weight (Scholz *et al.*, 1988). Haemodynamic load is the main determinant for heart and body growth during development, and when the body stops growing so does the heart. Physiological and pathological cardiac growth are tightly coupled to preload and/or afterload. The increased circulatory demand during body growth drives an expansion in blood volume, increasing arterial blood pressure, LV wall thickness, heart rate, and CO, in the early postnatal period. These changes result in chamber dilation and eccentric hypertrophy that has similarities to those observed with volume overload, which occur simultaneously with the development of the coronary vasculature bed (Naqvi *et al.*, 2014; Mrowka *et al.*, 1996; Fleming *et al.*, 2011). Once fully developed, the heart pumps blood to meet the circulatory demand and metabolic energy requirements of the body, which vary markedly across species. For example, at rest the blue whale heart contracts at 6 bpm, which is one of the slowest heart rates known (Dobson, 2003), whereas the ruby-throated hummingbird heart contracts at one of the fastest rates at 615 bpm (Odum, 1945); differences in heart rate are commensurate with the massive difference in body mass. This highlights the direct relationship between blood volume, heart and body mass, which are inversely proportionate to heart rate (Holt *et al.*, 1968).

The average adult male human heart has been variously reported to weigh ~ 370 g (n= 44, 20-40 years) (Friedman, 1951), ~300 g (n=85, 20-69 years) (Womack, 1983), ~371 g (n=218, 20-39 years) (Hanzlick and Rydzewski, 1990), and ~310 g (n=232, 18-35 years) (Molina and DiMaio, 2012). In a much smaller sample size, the average female heart weight was reported to be 285 g (n=17, 20-40 years) (Friedman, 1951) and ~230 g (n= 24, 20-69

years)(Womack, 1983). In contrast, the non-diseased heart of a newborn weighs ~20 g (Coppoletta and Wolbach, 1933). Thus, the heart grows by approximately 13- to 17- fold from birth in females and males, respectively; an estimated heart growth that is similar to the 20-fold increase reported by Zak (1973). Male hearts are 15-30% larger than females after puberty (de Simone *et al.*, 1995). Heart weight also changes depending on disease status and age. Interestingly, hearts of animals that run shortly after birth (sheep, goats, and cattle) are one-third of the adult size compared with those that do not, which are one-sixth of the adult heart size (rabbits, dogs and cats). Thus, the rate of heart growth is also species dependent (Hudlicka and Brown, 1996). Moreover, human cardiac growth is accelerated within the first year of birth relative to body weight, in that the HW/BW ratio is twice of that observed in adults (Smith, 1928; Holt *et al.*, 1968). The acceleration of heart growth (HW/BW) has also been reported in rats but only occurs within the first 4-5 days after birth (Anversa *et al.*, 1980; Li *et al.*, 1996). In mice, the HW/BW has been presumed to be constant throughout postnatal growth with no fluctuations from birth to adulthood (Soonpaa *et al.*, 1996). However, our laboratory recently found that the HW/BW increases markedly in preadolescent mice between P10 and P20, in mice (Naqvi *et al.*, 2014). It has been suggested that differences in heart size between species is determined by the total number of cells rather than by cell size (Zak, 1973; Campbell *et al.*, 1987). If true, this implies that cell growth or enlargement is conserved across species, which may help to elucidate common growth-dependent signalling pathways that also underlie postnatal human heart growth.

1.3.2 Factors that affect postnatal cardiac growth

In addition to the haemodynamic changes that occur with the switch from the fetal to the postnatal circulation, cardiac development is also affected by nutrition and oxygen levels.

Intrauterine growth restriction (IUGR) has been associated with the development of CVD. An epidemiological study of ~5,600 men in Hertfordshire (England) reported that those born with low birth weights had higher death rates from ischaemic heart disease (Barker *et al.*, 1989). Thus, it was recommended that the period of postnatal development is an important time to treat or promote growth in babies with low birth weights. Offspring born to rats fed a low protein diet during pregnancy had lower body and heart weights, and significantly fewer CMs at birth (Corstius *et al.*, 2005). Nutrition-related effects have also

been observed postpartum. When litters of newborn rats were adjusted to 16 (slow-growing), 8 (normal) or 4 (fast growing) pups per litter, the average LV mass at P21 was approximately -40% in the slow-growing and +30% in the fast-growing group compared with the normal litter (Rakusan *et al.*, 1978; Bai *et al.*, 1990). This correlated to the number and size of CMs, both of which were significantly reduced in the slow-growing group. Thus, it has been proposed that CM proliferation contributes to rapid cardiac growth that is observed in the early postnatal period (Rakusan *et al.*, 1978).

Suboptimal exposure to oxygen also affects cardiac growth. Prenatal exposure to hypoxia increased the CM cross-sectional area despite comparable LV weights between normoxic and hypoxic groups, and, therefore, it was suggested this was due to a reduced number of CMs (Bae *et al.*, 2003). In addition, prenatal hypoxia has been associated with the increased expression of hypoxia-inducible factor 1 α (HIF-1 α) in fetal hearts (Bae *et al.*, 2003). Newborn rats that were subjected to hypoxia at levels of 12-15% O₂ for 21 days were found to have significantly larger LVs and enhanced CM proliferation (Hollenberg *et al.*, 1976). A more recent report suggested that postnatal oxygenation in mice induces oxidative stress, increasing the production of reactive oxygen species, which causes cell cycle arrest and CM hypertrophy within one week of birth (Puate *et al.*, 2014). Thus, fetal and postnatal oxygen levels influence the total population of CMs during postnatal cardiac growth, which is also highly context-dependent.

1.3.3 Cell cycle, ploidy and nucleation status in CMs

Active molecular components of the cell cycle have been widely used to measure DNA synthesis and cell proliferation in CMs. The cell cycle distributed over a 24-hour period and consists of four transitional phases starting with gap 1 (G1), DNA synthesis (S), gap 2 (G2), and mitosis (M), (Figure 1.5). Cellular growth occurs during G1 and G2 phases in preparation for DNA synthesis or mitosis, respectively. From G1, cells enter the S phase where sister chromatids replicate, and the number of chromosomes and DNA content doubles. The cell then enters G2 and progresses to mitosis, which is categorised into four parts; prophase, metaphase, anaphase, and telophase. Mitosis encompasses nuclear division that results in two daughter nuclei (karyokinesis), and shortly afterwards, cytoplasmic division into two daughter cells (cytokinesis). In the first stage of mitosis, prophase,

chromosomes condense and the nuclear membrane disintegrates, after which, chromosomes align along a metaphase plate and sister chromatids separate from the centrosome (early anaphase). In late anaphase, sister chromatids segregate to polar ends of the cell and are partitioned by a contractile actomyosin ring. This brings the plasma membrane inwards, forming a cleavage furrow, thus, initiating cytokinesis. During cytokinesis, nuclear membranes reform producing two daughter nuclei. Towards the end of mitosis, the progressive contraction of the actomyosin ring leads to the formation of an intercellular bridge or midbody in the cleavage furrow of the dividing plasma membrane. This undergoes abscission and the daughter cells split apart, i.e., the process of cytokinesis (Steigemann and Gerlich, 2009; Lacroix and Maddox, 2012).

Cell progression through each phase of the cell cycle is positively regulated by the cyclical or transient expression of cyclins that form holoenzymes with cyclin-dependent kinases (CDKs) upon phosphorylation (Hochegger *et al.*, 2008). These cyclin-CDK couplings correspond to different phases of the cell cycle (Figure 1.5). Upon holoenzyme activation, retinoblastoma susceptibility (Rb) protein is phosphorylated releasing bound E2F (E2 promoter binding factor). E2Fs are a family of transcription factors (TFs) that initiate the expression of target genes such as cyclin E and A, and CDK1 (also known as Cdc2), which regulate G1, S and M phase (E2F integrates cell cycle progression with DNA repair, replication, and G₂/M checkpoints) (Ahuja *et al.*, 2007; Doree and Hunt, 2002). Indeed, E2Fs bind to ~130 promoters of genes that regulate the cell cycle (Ren *et al.*, 2002). Conversely, the Rb family (including p107 and p130, also called pocket proteins) binds and represses the E2F-mediated transcription of cell cycle genes, thereby eliciting cell cycle exit and terminal differentiation. The cell cycle is also regulated by CDK inhibitors (CKIs), specifically the INK4 family (p15, p16, p18, and p19), which compete with cyclins for CDKs (particularly CDK4/6) and, therefore, prevent their phosphorylation and activation. CDK1/2/4/6 are also inhibited by the Cip/Kip family (p21, p27, and p57) of CKIs (Ahuja *et al.*, 2007). Hence, the kinase activity of cyclin-CDKs are tightly regulated, and signalling can be terminated by inhibiting the holoenzyme through protein binding of CKIs, or inhibition at CDK phosphorylation sites, or proteosomal degradation via the ubiquitin-proteolytic pathway (Lim and Kaldis, 2013; Hochegger *et al.*, 2008).

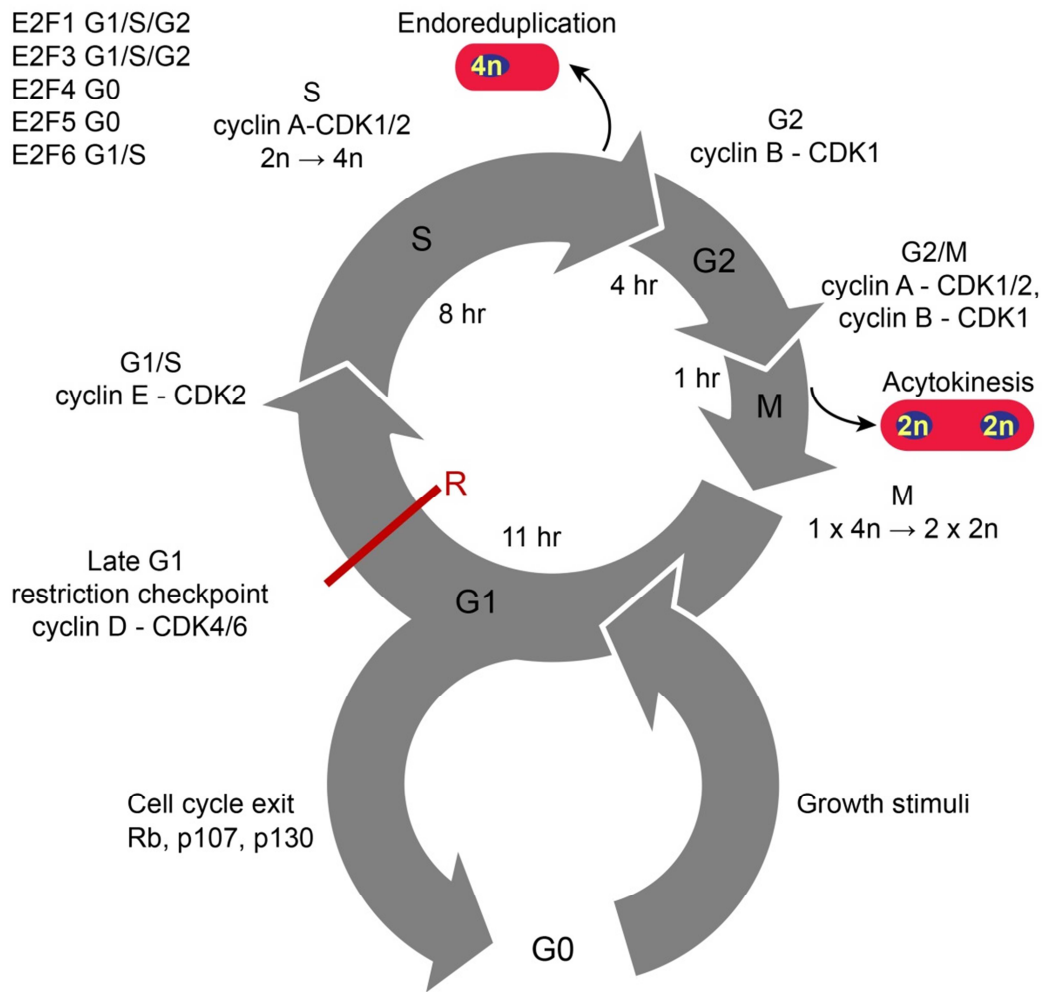


Figure 1.5: Schematic of the cell cycle

The cell cycle consists of four phases: G1, S, G2, and M, which are regulated by the E2F family of TFs and specific cyclin and cyclin dependent kinase (CDK) holoenzymes (Ahuja *et al.*, 2007). During G1, the cell continually grows and if it passes the regulatory restriction point (R) in late G1, is committed to progress into the DNA synthesis (S) phase (Cooper, 2000). In the S phase, the DNA content of a cell doubles, i.e., from 2n to 4n, which may become octoploid (8n) or hexadecaploid (16n) depending on its original DNA content. After the S phase, a cell progresses into G2 during which the cell grows and prepares for mitosis (M). The M phase usually results in the division of one cell into two daughter cells, i.e., 1 x 4n to 2 x 2n. After mitosis, cells enter G1 phase and either undergo another round of cell division, or remain in G1 and grow to a size similar to that of the mother cell, and then permanently exit the cell cycle (G0). In the example of skin fibroblasts, platelet-derived growth factor is a growth stimulus for cells to re-enter the cell cycle from G0 (Cooper, 2000). Human CMs exit the cell cycle after DNA synthesis (endoreduplication), whereas rodent CMs exit the cell cycle after karyokinesis without the completion of cytokinesis (acytokinesis). Cell cycle exit may also be regulated by Rb-proteins (including p107 and p130) (Ahuja *et al.*, 2007). The timing of each phase differs as indicated above (Cooper, 2000).

Genes encoding proteins such as: aurora kinase A/B, Ki67, polo-like kinase 1 (Plk1), cyclin B, survivin, anillin and phosphorylated histone H3 (Mollova *et al.*, 2013; Naqvi *et al.*, 2014), are often transiently expressed during mitosis, and are considered to be markers of cell proliferation, although Ki67 is expressed in all phases of the cell cycle except for G0 and is more likely to be a marker of cells that are cycling. Some of these gene products interact with each other during mitosis and function as follows: aurora kinase B phosphorylates histone H3 and regulates chromosomal segregation; it also associates with survivin, Plk1 and other proteins that form the *chromosomal passenger complex*, which is necessary for central spindle formation of the midbody in late cytokinesis (Steigemann and Gerlich, 2009; Crane *et al.*, 2004). Survivin also regulates microtubule formation during interphase (Rosa *et al.*, 2006). The Plk family regulate all phases of the cell cycle, however, Plk1 is specifically expressed in mitosis (in microtubules and centrosomes during interphase) and cytokinesis (in kinetochores, centrosomes, microtubules, the central spindle, and the midbody) (Zitouni *et al.*, 2014). When Plk1 is expressed, it is phosphorylated by aurora kinase A and other co-factors that lead to cyclin B - CDK1 activity and entry into mitosis (Zitouni *et al.*, 2014). Furthermore, the regulatory control of Plk1 expression is multifaceted. Plk1 is repressed in G1 by the Rb proteins: p53 (cellular tumour antigen) and p21, and negatively regulated by the CDE-CHR (cell-cycle-dependent element and cell cycle homology region) element in its promoter. The transcription of Plk1 is then activated in the presence of the dREAM (Rb, E2F, and MYB) complex during the G2 phase of the cell cycle (Archambault and Glover, 2009). Another gene that is involved in mitosis is anillin, which is a Rho effector that aids the assembly of the actomyosin ring (composed of actin filaments, F-actin, and myosin) and is required for furrow ingression by recruiting GTPases (Eggert *et al.*, 2006; Lacroix and Maddox, 2012). In addition to these genes, there are many more genes (~1,200) that are active during the cell cycle and could be considered as developmental markers in cell proliferation and differentiation (cell cycle exit) (Ren *et al.*, 2002).

DNA content and cell cycle exit varies between rodents and humans. Polyploidy describes the DNA content within a cell that is greater than one set of chromosomes, with n being the haploid content and $2n$ the diploid content (Laflamme and Murry, 2011). Most rodent CMs (~80-95%) become binucleated within two weeks after birth due to karyokinesis without undergoing cytokinesis and nuclei are diploid ($2 \times 2n$) (acytokinesis, Figure 1.5) (Ahuja *et al.*, 2007; Li *et al.*, 1996; Soonpaa *et al.*, 1996; Brodsky *et al.*, 1991; Raulf *et al.*, 2015). In

contrast to rodent CMs, most human CMs do not become binucleated and the majority are mononucleated (~60-75%) and tetraploid (4n) (Mollova *et al.*, 2013; Laflamme and Murry, 2011; Olivetti *et al.*, 1996; Sandritter and Scomazzoni, 1964). The DNA content of ~40-58% of human CMs increases to be >2n from 0-1 to 10-20 years of age (Mollova *et al.*, 2013) or from infancy to adulthood (Eisenstein, 1970). An increase in ploidy without karyokinesis or cytokinesis indicates that the cell cycle has exited after DNA synthesis (i.e., endoreduplication, Figure 1.5) (Mollova *et al.*, 2013; Olivetti *et al.*, 1996).

1.3.4 Phases of CM growth

CMs comprise one-third of the total cell population in the rat heart but constitute 65-80% of the myocardial mass (Nag, 1980; McMullen and Jennings, 2007). More recent estimates of the proportion of CMs in the mouse heart are variable from ~15% (Pinto *et al.*, 2016; Raulf *et al.*, 2015) to 56% (Banerjee *et al.*, 2007) of cardiac cells. Postnatal cardiac growth is mainly achieved by the proliferation and enlargement of CMs. Indeed, Clubb and Bishop (1984) reported three phases of CM growth during postnatal rat development: CM proliferation in the neonatal period (P0-4), a transitional phase from CM proliferation to cellular enlargement in the neonatal to preadolescence period (P4-15), and exclusively cellular enlargement in preadolescence to adulthood (P16-P56+). The timing of these events is important since abnormal heart growth may result from a reduced number of CMs that in turn affects the cell size of a CM (i.e., CM hypertrophy) leading to CVDs. Determining developmental signals that regulate normal CM proliferation and enlargement could reveal changes in abnormal cardiac growth, in addition to identifying novel targets to develop cardiac regenerative therapies for HF.

The timing of the three phases of CM growth reported by Clubb and Bishop (1984) is contentious (Li *et al.*, 1996; Soonpaa *et al.*, 1996; Naqvi *et al.*, 2014). Earlier studies reported CM cell division occurs until weaning age at ~ 3 weeks postpartum in rats (Zak, 1973; Claycomb, 1975; Romyantsev, 1977). In two studies performed within the same year in rat (Li *et al.*, 1996) and mouse (Soonpaa *et al.*, 1996), different conclusions were reported for the timing of the transition from cell proliferation to terminal differentiation. In the first study using Sprague-Dawley rats (adjusted to litters of 10-12 pups), the number of CMs increased by 1.68-fold from P1 to P3, thereafter the cell volume increased by 2.5-fold from

day 3 to 12, and binucleation was completed by P12 (Li *et al.*, 1996). Thus, instead of a gradual decrease in cell proliferation, there was a rapid transition from cell proliferation to enlargement after birth at P3-4. Leu *et al.* (2001) have also reported in C57BL/6 mice that CM volume is constant from birth to P4 and then rapidly increases in the following 10 days. In contrast, Soonpaa *et al.* (1996) reported that CM proliferation ceases by the late fetal period in mice. Moreover, C3Heb/FeJ mice (adjusted to litters of 6 pups) were injected with [³H]-thymidine to detect DNA replication and sacrificed after a two-hour labelling period at P5 or P10. Ten percent of CM DNA had incorporated the isotope at P5, however, at P10 none of the CMs were positive for the isotope (detected by autoradiographic analysis). Therefore, P10 coincided with the completion of CM binucleation, whereby ~90% of the isotope was localised in binucleated CMs after a 48-hour labelling period with a single injection of the isotope at P6. In addition, cell cycle proteins involved in DNA synthesis (G1 and S phase: cyclin D1/D3, CDK4, and PCNA) showed similar levels of abundance in hearts at embryonic day 12 (E12) when CMs are actively proliferating and at P10 when CM nuclei are dividing, becoming binucleated. Altogether, Soonpaa *et al.* (1996) conclude that DNA synthesis in the fetal heart contributes to proliferation, while DNA synthesis in the heart contributes to binucleation. However, neither cell division, cell number nor mitosis-related markers were assessed in this study, which focussed mainly on the S phase of the cell cycle. In another study using C57BL/6J mice, the incorporation of BrdU and presence of Ki67 was evaluated at E14.5, P1, P4, P7, P14, and P21 (Walsh *et al.*, 2010). Both markers were higher at E14.5, P1, P4 and P7, compared with P14 and P21, and there were no data points collected between P7 and P14. The number of binucleated CMs increased to >98% between P5 and P8. Overall, more datasets are required for a consensus as to the timings of CM growth by establishing cell number and size, the presence of mitotic figures, especially cytokinesis to indicate cell division, as well as the changes in DNA synthesis and karyokinesis in rodents and humans.

More recently in human studies, cell division has been shown to continue beyond the neonatal period up to 20 years of age, resulting in a 3.4-fold increase in the CM population number, which was simultaneous with cellular enlargement (Mollova *et al.*, 2013). Extensive studies from our laboratory using C57BL/6J mice born in litters of 6-7 pups to normalise heart and body growth have shown that the proliferative capacity of CMs extends into preadolescence (Naqvi *et al.*, 2014). CM proliferation between P14-P18 substantially increased the total CM population by 1.4-fold (~500,000 CMs) (Naqvi *et al.*, 2014). This

was accompanied by the re-expression of mitosis-related genes at P15 relative to P13, P14, and P16, which were comparably lower. Furthermore, BrdU was administered by a single injection at P14 and by P18 ~11% of CM nuclei were BrdU⁺, indicating cells had entered S phase. However, ploidy remained the same at 2n, and therefore, cells had effectively undergone karyokinesis. Furthermore, aurora kinase B (a marker for mitosis) was evaluated by immunohistochemistry and immunocytochemistry, and was present in ~15% and ~30% of P15 CM nuclei, respectively, indicating these CMs were in the mitotic phase of the cell cycle. The latter percentage is likely to be more accurate since it is well known that CM nuclei are underrepresented by immunohistochemical analyses (Mollova *et al.*, 2013; Raulf *et al.*, 2015). There were also transient decreases of ~50% in the cell volume of mono- and bi-nucleated CMs at P15, suggesting the division of one CM into two smaller daughter cells. Altogether, these data indicate that the cell cycle re-entry of CMs extends beyond the early neonatal period into preadolescence and adolescence.

Naqvi *et al.* (2014) also demonstrated that heart growth (HW/BW) accelerated by 30% from P10 to P17 and that the α -MHC to β -MHC ratio was significantly increased between P10 and P14. This coincided with a surge in the levels of serum thyroid hormone, T₃, from P10, and peaked at P12. This was interesting given that α -MHC expression is regulated by T₃ (Chizzonite and Zak, 1984; Li *et al.*, 2014b). Inhibition of T₃ biosynthesis by administering propylthiouracil (PTU) from P7-P14 abolished the increase in HW/BW between P10 and P18, as well as CM proliferation. In addition, PTU treatment prevented an increase in the α -MHC/ β -MHC ratio at P15 relative to P10 (Naqvi *et al.*, 2014). The effects of T₃ were linked to the IGF1/PI3K/Akt pathway, whereby the expression of components in this pathway increased at P15 relative to P10. Interestingly, regulatory thyroid hormone (TH) responsive elements are present in the promoter of the IGF1 gene and mice with deletion of thyroid hormones receptors (TRs) have been shown to have altered expression of IGF1 (Xing *et al.*, 2012). Moreover, the number of CMs is also greatly enhanced (by ~35%) in transgenic mice with cardiac-restricted overexpression of IGF1 (Reiss *et al.*, 1996).

Cardiac regenerative capacity has been assessed at 1, 2, and 21 days post apical resection of P1 and P7 neonatal murine hearts (Porrello *et al.*, 2011b). The heart of a P1 pup fully regenerated due to CM proliferation, with minimal hypertrophy and fibrosis observed, however, P7 hearts failed to recover fully and had significant fibrosis (Porrello *et al.*,

2011b). Similar results were obtained in a MI model of cardiac injury that was performed in P1, P7, or P14 hearts, where, in contrast to P1 hearts, neither P7 nor P14 hearts were able to regenerate (Porrello *et al.*, 2013). The conclusion of these studies was that the cardiac regenerative window lies within the first week of life. Our laboratory subjected mice of different ages (P2, P15 or P21) to MI and at the three week follow-up, found P2 hearts fully regenerated, but significant injury was sustained in P21 hearts that did not regenerate, and an intermediate cardiac repair response resulting in a partial reduction of infarct size in P15 hearts (Naqvi *et al.*, 2014). The degree of regeneration correlated with CM cell cycle re-entry, which was robust at P2, lower at P15, and absent at P21 (Naqvi *et al.*, 2014).

1.3.5 Metabolic switch in postnatal CM maturation

In order for the cell to be completely functional and adapt to greater productivity during postnatal cardiac growth, the subcellular components of a CM must develop. During postnatal cardiac growth there are a number of cellular processes that take place in maturing CMs, including a shift in energy metabolism, mitochondrial biogenesis, improved excitation-contraction coupling, autonomic innervation of the heart, and the enhanced expression of contractile proteins, calcium handling proteins and ion channels (Maillet *et al.*, 2013; Li *et al.*, 2014b), many of which are regulated by growth hormones, such as IGF1 and TH (Maillet *et al.*, 2013; Li *et al.*, 2014b). The main cellular process that is important in CM maturation is the metabolic switch from anaerobic to aerobic respiration.

The metabolic pathways for generating energy in the form of adenosine triphosphate (ATP) (glycolysis, and lactate, glucose and fatty acid oxidation) are dependent on the availability of substrates and oxygen, which change during postnatal cardiac development (Lopaschuk and Jaswal, 2010). The supply of circulating lactate is higher than fatty acids at the neonatal stage of development compared with adults and mitochondrial oxidative capacity is reduced. The relative contributions of ATP from these metabolic pathways have been evaluated in the developing rabbit heart (shown in Table 1.1.). In the fetal and newborn period, the energy for CM proliferation is predominantly generated by anaerobic respiration in a low oxygen environment of 3-5% through glycolysis and lactate production (Lopaschuk and Jaswal, 2010), and the contribution of glucose and fatty acid oxidation to ATP is less. Fatty acids are metabolised by β -oxidation, the Krebs cycle and the electron transport chain, and

these yield more acetyl CoA, reduced coenzymes, as well as six times more ATP, compared with a molecule of glucose (Lodish *et al.*, 2000). This shift in metabolism during normal cardiac development has been well documented.

Table 1.1: Relative contributions of metabolic pathways to the production of ATP during rabbit cardiac development

	Fetal/ Newborn heart (P0)	Neonatal heart (P7)	Preadolescent heart (P21)
Glycolysis (%)	44	5	7
Lactate oxidation (%)	25	49	1
Glucose oxidation (%)	18	5	12
Fatty acid β -oxidation (%)	13	41	80

Adapted from Lopaschuk and Jaswal (2010).

1.3.6 Pathophysiology in postnatal cardiac growth

The transition from the fetal to postnatal environment causes an instantaneous increase in oxygenation, cardiac afterload and systemic arterial pressure (Jonker and Louey, 2016), which may be more problematic in babies born with CHD or born prematurely, as growth defects at birth affect subsequent postnatal cardiac development.

The prevalence of CHD has risen by >50% between 2000 and 2010, and occurs in 13 out of 1000 children (Marelli *et al.*, 2014). There are many types of CHD that are caused by abnormalities in cardiac structure and function due to genetic mutations, and altered haemodynamics and blood flow that regulate embryonic heart development, which affect the early postnatal period of cardiac growth (Bruneau, 2008; Rudolph, 1970). Hypoplastic left heart syndrome is a severe form of CHD that is fatal without surgical intervention within the first few days after birth, as the heart is unable to support circulation due to underdeveloped structures and CM hypoplasia. The hope for the future is to develop cardiac regenerative medicines to treat CHD in the postnatal period and aid cardiac development into adult life.

Preterm births (<37 weeks gestation) resulting from preeclampsia or IUGR occur in 1 out of 10 births worldwide (Goldenberg *et al.*, 2008; Beck *et al.*, 2010). The proportion of infant deaths arising from preterm births is high, accounting for 28% mortality within 7 days of birth (Lawn *et al.*, 2006), although the survival rate in developed countries is closer to 100% for preterm births > 32 weeks gestation (Slattery and Morrison, 2002). Preterm newborns with low birth weight (due to preeclampsia) had cardiac hypertrophy and greater LV outputs at birth compared with those born with a normal weight (n= ~30 per group). This was attributed to altered haemodynamics with disruptions in blood flow and volume (Leipala *et al.*, 2003a). LV mass was reported to increase by 56% in preterm infants compared with 35% in full term infants within the first month postpartum (n= ~20 per group) (Kozak-Barany *et al.*, 2001; Lewandowski *et al.*, 2013). However, it was unknown whether cardiac problems in preterm born infants extend into adult life. Indeed, a recent study involving participants aged between 20 and 39 years (n= ~100 per group), showed that adults born preterm had a greater LV mass of 19 g, compared with adults born at full term

(Lewandowski *et al.*, 2013). The increased LV mass in adults born preterm was associated with altered LV structures, higher blood pressures, and reduced systolic and diastolic function. Moreover, prematurity was an independent predictor of LV mass, which had a dose-dependent relationship with gestational age (i.e., the earlier the preterm birth the larger the LV mass in adults born preterm) (Lewandowski *et al.*, 2013; Norman, 2013). This study suggests that an increase in LV mass of 19 g would increase the risk of cardiovascular events in adults by >50% (Lewandowski *et al.*, 2013).

Another major developmental molecule that is important in postnatal cardiac maturation is T₃, which has profound effects on the cardiovascular system (Li *et al.*, 2014b; Mai *et al.*, 2004; Kolar *et al.*, 1992; Segar *et al.*, 2013). Indeed, hyperthyroidism is associated with increased blood volume, CO, contractility, heart rate and α -MHC expression, which are conversely decreased in hypothyroidism (Li *et al.*, 2014b). Thyroid hormone regulates the transcription of many genes upon binding to heterodimers of the nuclear thyroid hormone receptors (TR α and TR β) and retinoic acid receptor, which binds with high affinity to T₃ response elements located near the transcriptional start sites of T₃-responsive genes (Li *et al.*, 2014b). This regulates the postnatal shift from β -MHC to α -MHC, and results in an increase in the expression of the sarco-endoplasmic reticulum Ca²⁺ ATPase (SERCA2A), β 1-adrenergic receptor, sodium and potassium channels, sodium and calcium exchanger (NCX), cardiac troponin I, ANP, TR α 1, and adenylyl cyclase (AC) types V and VI (Maillet *et al.*, 2013).

TH is synthesised in the thyroid gland and is released in response to the secretion of thyroid stimulating hormone from the anterior pituitary that is regulated by thyrotropin releasing hormone from the hypothalamic paraventricular nucleus (Li *et al.*, 2014b). TH also exerts a negative feedback effect on the release of both thyrotropin releasing hormone and thyroid stimulating hormone (Li *et al.*, 2014b). Congenital hypothyroidism leads to growth delays, deafness, impaired neurogenesis and cardiac malformations (Li *et al.*, 2014b). The hypothalamic-pituitary-axis matures in humans at midgestation and levels of T₃ markedly increase within a few hours after birth (Fisher and Klein, 1981). In contrast to humans, the hypothalamic-pituitary-axis matures in rodents at a later stage between P12 and P15 and coincidentally levels of T₃ rise rapidly at P12-15 after an initial peak at P5-6 (Hadj-Sahraoui *et al.*, 2000). It is of interest, therefore, that newborns with CHD are susceptible to iodine-

induced hypothyroidism following surgical procedures involving the administration of iodinated contrast agents with cardiac catheterisation and/or topical use of iodine antiseptics (Thaker *et al.*, 2014; Linder *et al.*, 1996). In addition, treating CHD children with T₃ for 12 days following surgery significantly improves myocardial function (Bettendorf *et al.*, 2000). Hypothyroidism is more common in preterm newborns in which T₃ levels were depressed and reported to be less than half of that of full term newborns immediately after birth, however values normalise by P16 (Fisher and Klein, 1981). Thus, T₃ has important effects on cardiac function and growth during development (Brown, 2000).

1.3.7 Clues for regeneration in postnatal cardiac growth

Identifying molecules that are essential for CM terminal differentiation requires an understanding of the temporal molecular changes that occur in CMs as they start to withdraw from the cell cycle. The phases of CM maturation that regulate CM number and cardiac size consist of CM proliferation, enlargement and terminal differentiation, and these are likely to be interrelated events (Jonker and Louey, 2016). However, the molecular signals for the terminal differentiation of CMs are elusive (Katz *et al.*, 2016), thus, highlighting that many of the mechanisms involved are largely unknown.

Terminal differentiation describes cells that have permanently withdrawn from the cell cycle, and thus, are not able to proliferate. In general, adult CMs are terminally differentiated, although a very small subset of cells divide, contributing to the low turnover in adult hearts (Senyo *et al.*, 2013). The loss of a proliferative capacity leading to the terminally differentiated state of an adult CM is likely due to a sequence of events driven by master regulators. This may involve the inhibition of cell cycle genes, the loss of mitogenic stimuli, the effect of growth factors (IGF1, TH, Neuregulin 1 (NRG1) and fibroblast growth factor 1 (FGF1), the binucleation of CMs, cellular enlargement, or changes in CM architecture that prevent cell cycle re-entry, or the transcription of a series of master genes that regulate the transition from CM proliferation to enlargement (Porrello *et al.*, 2011b; Naqvi *et al.*, 2014; Soonpaa *et al.*, 1996; Li *et al.*, 1996; Ahuja *et al.*, 2007; Xin *et al.*, 2013). It is nearly impossible to discuss all the potential signalling pathways that regulate cell proliferation, enlargement, and terminal differentiation. Developmental signals will most certainly include regulators of gene expression such as TFs and miRNAs. One of the

pathways that governs transcriptional activity is the Hippo pathway, which negatively regulates Wnt signalling to control cardiac growth and CM proliferation (Xin *et al.*, 2013). Other cardiac TFs (NK2 homeobox 5 (Nkx2-5), zinc-finger-containing TF (GATA4), myocytes-enhancer factor-2 (MEF2), WNT, NFAT, serum response factor (SRF) have established roles in the embryonic cardiac development that orchestrate cell lineage commitment, cardiac morphogenesis and cell proliferation, and have been reported to target numerous genes involved in postnatal cardiac growth (Oka *et al.*, 2007; Xin *et al.*, 2013). Another TF, Meis1, was found to regulate the CM cell cycle by transcriptional activation of the CDKIs (p15, p16, and p21) (Mahmoud *et al.*, 2013). Furthermore, miRNAs have recently emerged as having a role in regulating cell cycle arrest and regeneration (Porrello *et al.*, 2011a; Katz *et al.*, 2016).

1.4 Cardiomyocyte transcriptome

Gene regulatory networks are highly conserved in embryonic cardiac development across species, and these are coordinated by TFs, including Nkx2-5, MEF2, GATA, and HAND, and their downstream target genes (Olson, 2006). Less is known about the cellular regulation and expression of mRNAs and noncoding RNAs during postnatal cardiac development, particularly in the narrow window from CM division to terminal differentiation. The transcriptome is the intermediate of two fundamentally important cellular processes of transcription (of DNA to mRNA or noncoding RNA) and translation (of mRNA to synthesise proteins). However, the abundance of mRNA is not always indicative of protein levels, since proteins are subject to post-translational modifications, including degradation (Vogel and Marcotte, 2012). Nevertheless, RNA-seq can be used to identify the molecular changes that underpin cardiac growth and may provide novel targets for regenerative medicine.

1.4.1 Microarray versus high-throughput sequencing (HTS)

The RNA content of a mammalian cell is ~10 pg depending on the cell type, however only one-hundredth of that RNA is mRNA (Tang *et al.*, 2011). Rodent CMs are mostly binucleated by P14 (80-95%), although it is not known if both nuclei are active and whether CMs contain more RNA as a result. To capture the expression of mRNAs and noncoding RNAs, technologies are evolving from microarray to high-throughput sequencing (HTS), which has the advantage of nucleotide resolution and a greater dynamic range. A comprehensive comparison of microarray hybridization and sequencing techniques has been reviewed by Wang *et al.* (2009), which are briefly discussed below. In addition, two of the most widely used sequencers, Ion Torrent Proton System and HiSeq, are compared.

Microarray assays are based on the hybridization of fluorescently-labelled cDNA samples, which bind to specific sequences of DNA that are printed onto a microarray chip using photolithography (Wang *et al.*, 2009; Latif and Garry, 2010). The chip is scanned with a laser to excite the dye and the intensity of the emitted light is captured as digital information that corresponds to the relative expression of a gene. Microarray is limited to pre-determined genomic sequences and has a smaller dynamic range of detection in the order of

100 to 300-fold (Wang *et al.*, 2009), whereby abundant transcripts emit high-levels of fluorescence that saturate, and lowly abundant transcripts emit low-levels of fluorescence below the detection threshold. In contrast, RNA-Seq has nucleotide-resolution and can be used to assemble and identify novel transcripts, isoforms and variants. It also has a broader dynamic range in the order of 9,000-fold and enables accurate quantification of the relative amount of molecules between samples. Moreover, RNA-Seq requires a smaller amount of RNA as starting material and generates data that is more reproducible than microarray (Wang *et al.*, 2009). Taken together, RNA-Seq is a revolutionary tool for capturing the whole transcriptome, including noncoding RNAs, to provide insights into cell biology and disease (Licatalosi and Darnell, 2010).

Today the most popular sequencing platform used for RNA-Seq is the HiSeq, which is manufactured by Illumina. Other technologies include the Ion Torrent Proton System by Life Technologies (Quail *et al.*, 2012; Loman *et al.*, 2012; Chu and Corey, 2012; Li *et al.*, 2014c). Both use sequencing-by-synthesis methods with a DNA polymerase. The basic workflow of a HTS experiment consists of enriching a RNA population of interest (i.e., polyadenylated RNA or small RNA), constructing cDNA libraries, sequencing cDNA reads, and then aligning reads to a reference genome, followed by bioinformatic data analysis (Chu and Corey, 2012). The most common method for polyadenylated, poly(A), RNA enrichment is the use of magnetic beads with oligo (dT) sequences bound to the bead surface that uses base pairing to capture the poly(A) tail of the mRNA. Small RNA enrichment may involve size selection with nucleic acid binding beads. HTS platforms require short lengths of cDNA molecules to sequence, and thus, larger RNA molecules are fragmented enzymatically (using RNase III), chemically or mechanically to sizes typically smaller than 300 nucleotides. RNA fragments or small RNAs are then ligated at the 5' and 3' end to adapters with specific DNA sequences that are designed differently for each sequencing platform (Chu and Corey, 2012). The adapters are incorporated into cDNA synthesis by reverse transcription polymerase chain reaction (RT-PCR) to amplify and identify samples. Small cDNA may be enriched by gel size selection after electrophoresis and eluted, and then amplified in another round of PCR. The resulting cDNA libraries are then sequenced in parallel.

For the sequencing of cDNA libraries, HiSeq technology uses adapters to hybridize and tether cDNA onto the surface of a glass flow cell coated with clusters of primer sequences that facilitate clonal bridge amplification of the forward and reverse fragment, producing paired-end reads (Shendure and Ji, 2008). In contrast, the Ion Torrent Proton System technology uses adapters to hybridize and tether cDNA onto the surface of beads that are mixed with PCR reagents and oil in emulsion-PCR. The bead and fragment are contained within a microdroplet and the fragment is clonally amplified, producing single-end reads (Shendure and Ji, 2008). HiSeq uses fluorescently-labelled nucleotides that after base-pairing to the cDNA with DNA polymerase emit light upon excitation that enables base calling (Quail *et al.*, 2012). Unlike most sequencing platforms, the Ion Torrent Proton System is the first “post-light” sequencer (Loman *et al.*, 2012) and has been likened to “the world’s smallest pH meter”. It utilises a semi conductance chip that is sequentially washed with one of four nucleotides, which then releases a hydrogen ion upon base-pairing with DNA. This alters the pH, which is detected as a change in voltage that aids base calling. Both of these platforms yield comparable RNA-Seq results (Li *et al.*, 2014c).

There are advantages and disadvantages to both platforms, for example, HiSeq sequencing takes longer (~27 hours) than the Ion Torrent Proton System (~6 hours). However, the amplification of cDNA libraries requires a more hands on approach using the Ion Torrent Proton System pipeline compared to HiSeq, which has this integrated into the sequencing process. Regardless, these technologies are rapidly evolving and newer versions continue to be released, reducing processing times and costs, while improving accuracy and accessibility. A major challenge of RNA-Seq is the downstream processing of large datasets that usually requires high performance computing resources and bioinformatic expertise.

1.4.2 Sampling the CM transcriptome

Gene expression data has been collected from microarray analyses of CPCs at specific stages of embryonic heart development, and this has been compared to embryonic stem cells and adult CMs (Masino *et al.*, 2004). These datasets have been valuable in identifying genes involved in morphogenesis, and moreover, distinct transcript signatures or molecular programs associated with specific stages of development (Latif and Garry, 2010). In general, transcriptome analysis can be used to identify downstream target genes of TFs and networks that direct cell differentiation and maturation, and to reveal important regulatory pathways (Latif and Garry, 2010). This demonstrates that sampling an isolated cell population at specific time points in development is useful to elucidate changes in gene expression that contribute to cardiogenesis (Masino *et al.*, 2004).

At the time that this work was undertaken, there were no sequencing datasets for purified CMs that have been isolated at different time points during postnatal cardiac growth. Gene expression studies have often used: fetal and adult cardiac tissues, CPCs, embryonic stem cell- or human induced pluripotent stem cell- derived CMs, immortalised CM cell lines (HL-1 and H9c2), enriched adult CMs, or cultured neonatal CMs. These samples were likely used with specific aims and end-points that mostly involve comparing embryonic to adult time points, or sham- operated to post-cardiac injury (such as apical resection, MI, hypertrophy or HF) (Latif and Garry, 2010). Nonetheless, gene expression datasets for purified populations of primary CMs from postnatal cardiac growth are lacking.

1.4.3 Discordant adult and neonatal CM isolation procedures

Purifying CMs at multiple time points during cardiac growth is complex. Indeed, the heart comprises many different cell types, including CMs, ECs and fibroblasts that lie within the intricate setting of extracellular matrix proteins, blood vessels and other supporting cell types. CMs comprise only 15-30% (Raulf *et al.*, 2015; Pinto *et al.*, 2016) or ~56% (Banerjee *et al.*, 2007) of the total population, however, they account for 65-80% of the adult heart mass (Nag, 1980; McMullen and Jennings, 2007). In addition, the populations of CMs and non-myocytes change during development (Soonpaa *et al.*, 1996; Olivetti *et al.*, 1980; Banerjee *et al.*, 2007).

The isolation of highly enriched populations of CMs is not trivial and requires the use of different protocols depending on the stage of development. Such protocols were originally established in neonatal and adult rats, and were subsequently adapted to the mouse; a species widely used for cardiovascular and genetic studies. Scaling the procedure for CM isolations from rats to mice, which are 10-fold smaller than rats, is technically challenging for both the adult and neonatal mouse hearts (Liao and Jain, 2007). In general, the different methods for the isolation of adult and neonatal CMs also have variable processing times (Louch *et al.*, 2011; Ehler *et al.*, 2013). For adult hearts, CMs are isolated after the heart is digested by Langendorff retrograde perfusion with proteolytic enzymes (usually collagenase II), which breaks down the extracellular matrix. The heart is then teased apart into tissue fragments that are dissociated into a single cell suspension by gentle trituration, and CMs are enriched after low-speed centrifugations combined with the gradual re-introduction of Ca^{2+} . CMs are either used after dissociation, enrichment, or cell culture depending upon the experiment. CM isolation from adult mouse hearts is more difficult compared with rat hearts because the aortae of the former are much smaller, and therefore, the cannulation of the heart for perfusion is more challenging.

The technicality of cannulating the neonatal mouse heart is further compounded in neonatal and younger mice, which are much smaller than adult mice. This has led to methodologies to disaggregate the heart, not by cannulation and Langendorff perfusion, but by using scissors or other mechanical means to mince cardiac tissues into pieces (typically multiple hearts are processed in a single batch of 5-15). The minced hearts are then incubated with digestion buffer at 4°C overnight and/or subjected to sequential incubation steps with proteolytic enzymes (trypsin and collagenase II) to breakdown the extracellular matrix for 10-20 minutes at 37°C (Ehler *et al.*, 2013; Louch *et al.*, 2011). Tissue fragments are dissociated into a cell suspension by trituration and the CM fraction is enriched by pre-plating cells using uncoated culture dishes for ~2 hours. This plating step differentially removes the majority of non-myocytes as these cells adhere to the uncoated plastic. The non-adherent CMs are then plated onto a collagen-coated culture dish for 12-18 hours (Ehler *et al.*, 2013; Chlopcikova *et al.*, 2001). The main disadvantages of this method are the harsher disaggregation techniques that require mechanical force and enzymatic digestion to isolate cells, and the duration of the procedure that is typically 1-2 days (Ehler *et al.*, 2013). Commercial kits have been developed for CM isolation following the digestion of multiple neonatal hearts over a period of 1-2 hours. These include the Pierce Cardiomyocyte

Isolation Kit (Thermo Fisher) that requires cell culture overnight to purify CMs, the Neonatal Heart Dissociation Kit (Miltenyi Biotec) followed by the Neonatal Cardiomyocyte Isolation Kit (Miltenyi Biotec) to purify CMs, and, the Neonatal Cardiomyocyte Isolation System (Worthington) that requires 1-2 days of cell culture to purify CMs. In addition, neonatal mouse hearts are more susceptible to over-digestion, whereby CM yield and viability is much lower than those from neonatal rat hearts (Ehler *et al.*, 2013).

Less attention has been given to the isolation of CMs from pups aged between P5 and P28, which are either categorized into the neonatal CM isolation protocol using sequential digestions (up to P10), or into the adult CM isolation protocol by Langendorff perfusion (>P17) (Lam *et al.*, 2002). This is due to the aforementioned reasons that the neonatal mouse heart is much smaller than the adult, thus cannulating the neonatal aorta for Langendorff retrograde perfusion is technically challenging. In addition, the isolation of >P10 CMs using the neonatal method of sequential digestions also results in low CM viability and yield.

CMs are usually cultured to improve their purity or a discontinuous Percoll gradient is used to separate CMs from non-myocytes after centrifugation (Louch *et al.*, 2011). The latter technique has been developed mainly for CMs that are larger from the neonatal and adult rat heart (Iwaki *et al.*, 1990; Nakagawa *et al.*, 1995; Maisch, 1981; Chlopcikova *et al.*, 2001), and is not so commonly used for neonatal or adult mice (Evans and Goodwin, 2007; Harada *et al.*, 2005). This method is also complicated and time-consuming (Louch *et al.*, 2011; Chlopcikova *et al.*, 2001). Indeed, some laboratories use two different protocols, one to purify neonatal rat CMs using Percoll gradients and another to purify neonatal mouse CMs by pre-plating (Nickson *et al.*, 2007).

Cell type-specific information on regulatory events at key time points during postnatal cardiac growth requires freshly purified populations of CMs that closely emulate the *in vivo* environment. It is also important to isolate CMs from neonatal, preadolescent, and adult hearts in a similar manner for direct comparisons in gene expression that are not influenced by using different techniques or cell culture. Revolutionary advances in high-throughput sequencing technologies would allow us to capture the changes in transcriptional activity during postnatal cardiac development.

1.5 Aims of this study

Although cardiac growth has been well studied in mice, the molecular determinants that contribute to the terminal differentiation of CMs remain unknown. The developmental signals associated with postnatal cardiac growth may be manipulated to stimulate endogenous CM proliferation as a means of cardiac regeneration for the treatment of many cardiovascular diseases (including CHD). One candidate gene that was identified to promote the terminal differentiation of CMs was stem cell factor receptor (c-Kit). In response to PO, genetic mouse models with global or CM-restricted inactivation of c-Kit exhibited CM proliferation rather than CM hypertrophy, which markedly improved survival outcomes.

Thus, there were two overarching aims in this study. The first aim was to investigate whether c-Kit is re-expressed in adult WT CMs after PO, and if so pharmacological inhibition of the receptor may be a novel therapeutic target for stimulating the proliferation of adult CMs. To address this aim, a cardiac injury model of LVH, SAC-induced PO, was characterised in adult WT mice (Chapter 3) and the expression of c-Kit in adult WT CMs post-SAC was evaluated (Chapter 4).

The second aim was to embark on the discovery of new candidates for cardiac regeneration by establishing the transcriptomic signatures of CMs during important stages of postnatal cardiac growth. To address this aim, (i) pivotal time points in postnatal cardiac growth were identified (Chapter 5), (ii) a standardised method to purify CM populations from any postnatal age was developed (Chapter 6), and (iii) transcriptomic profiles of CMs at those pivotal time points along the CM developmental trajectory were determined (Chapter 7).

Chapter 2 General Methods

2.1 Animals

Experimental procedures using C57BL/6J mice at the Victor Chang Cardiac Research Institute (Sydney) were approved by the local Garvan Institute /St Vincent's Hospital Animal Ethics Committee (AEC #: 13/07) in accordance with The Australian Code of Practice for the Care and Use of Animals for Scientific Purposes (2004). Mice were given food (pellets of rodent food that had been sterilised by irradiation; Gordon's Speciality Feeds) and water *ad libitum*.

2.2 Tissue collection

Mice were weighed prior to euthanasia. Neonatal mice were euthanised by decapitation (<P10) and older mice were euthanised by CO₂ asphyxiation and cervical dislocation. Hearts were excised by opening the thoracic cavity with surgical scissors and the ribcage was retracted to carefully and quickly excise the heart, which was rinsed in saline to remove blood. Heart tissues were gently blotted dry, weighed, and snap-frozen in liquid nitrogen, which were subsequently stored at -80°C or fixed in 2% paraformaldehyde (PFA) for 3 hours and then stored in 70% ethanol.

2.3 Cardiac puncture

Mice were anaesthetised with 2-4% isoflurane in an empty cage and then secured with surgical tape into a supine position on a heating pad at 37°C to maintain body temperature. Isoflurane (2-4%) was continually administered via a nose cone and the level of anaesthesia was assessed by the toe pinch reflex, which does not occur with a deep level of anaesthesia. Blood was drawn using a 25-gauge (G) needle attached to 1 ml syringe that was inserted at 45° through the diaphragm and into the cardiac ventricle. Mice were euthanised by exsanguination under anaesthesia followed by cervical dislocation.

2.4 CM isolation and enrichment

CMs were isolated from the heart after Langendorff retrograde perfusion with collagenase II (Worthington) and enriched for by differential centrifugation using the O'Connell et al. (2007) method.

Adult mice were injected with heparin (100 μ l; 1000 UI/ml; cat. #: 02112115; Pfizer) and euthanised by cervical dislocation. The aorta was cannulated *in situ* with a 6.0 silk suture at the level of the diaphragm with a cannula (24 G gavage needle) attached to a 2 ml syringe. The heart was then mounted onto Langendorff apparatus and perfused at 37°C for 3 minutes with Ca²⁺-free perfusion buffer (9 ml of perfusion buffer: 120mM NaCl, 15mM KCl, 0.5mM KH₂PO₄, 5mM NaHCO₃, 10mM HEPES 5mM glucose, pH 7) at a flow rate of 3 ml/min. The extracellular matrix was digested by perfusing the heart for 8 minutes with digestion buffer containing collagenase II and Ca²⁺ (24 ml of perfusion buffer with 3 mg/ml collagenase II and 43 μ M Ca²⁺). After digestion, the atria were removed by cutting the artioventricular junction, the ventricles of the heart were placed in a petri dish containing transfer buffer (perfusion buffer and 5% FCS). The heart tissue was teased apart with fine scissors and forceps and tissue was dissociated into cells by trituration with a wide bore transfer pipette (3 ml). Once tissues were dissociated, transfer buffer was added up to 10 ml and CMs were counted using a haemocytometer to obtain total CM yield and viability. The mixture of rod-shaped (healthy) and round (dead) CMs were readily visualised under the microscope. CMs were enriched in a series of three low-speed centrifugations simultaneously with Ca²⁺ re-introduction to produce Ca²⁺-tolerant CMs. After each centrifugation step, cells were resuspended in transfer buffer containing increasing concentrations of Ca²⁺ (0.1, 0.4, 0.9 mM). Smaller non-myocytes were discarded in the supernatant after each wash. After CM enrichment, cells were resuspended in transfer buffer (10 ml) and CMs were counted using a haemocytometer to obtain the total CM yield and viability. CMs were either snap-frozen in liquid nitrogen and stored at -80°C or fixed in 2% PFA for 3 hours and then stored in 70% ethanol for downstream experiments.

2.5 CM area quantification

A binary image (black/white) was used to measure CM area (μm^2), in which a cell outline was automatically detected using ImageJ software. The cell area was then calculated based on the number of pixels within the cell outline, and normalised to the scale bar.

2.6 RNA extraction

RNA was extracted by phenol-chloroform phase separation. Whole hearts, ventricles, or CMs were homogenised in 1 ml of TRIzol (Invitrogen) on a beaker of wet ice using a Polytron homogeniser. Phase separation was performed by adding chloroform (200 μl) to homogenates, which was mixed thoroughly by shaking for 15 s and incubated for 3 minutes at RT. Samples were centrifuged at 12,000 g for 15 minutes at 4°C. The upper aqueous phase was transferred to a new tube containing glycogen (5 μl ; 5mg/ml) and mixed thoroughly by shaking for a few seconds. Isopropanol (600 μl) was added and mixed thoroughly by shaking for a few seconds, which was then incubated for 10 minutes at RT. Samples were centrifuged at 12,000 g for 10 minutes at 4°C. After centrifugation, the supernatant was discarded, and residual supernatant was removed after a quick spin using a microcentrifuge. The pellet was washed with 75% ethanol (1 ml) and mixed thoroughly by vortexing, which was centrifuged at 7,500 g for 5 minutes at RT. After centrifugation, the supernatant was discarded, and residual supernatant was removed after a quick spin using a microcentrifuge. The RNA pellet was air-dried under a lamp for ~30-45 minutes and RNA was reconstituted in DEPC-treated water (90 μl). RNA was further purified overnight by ethanol precipitation. Sodium acetate (10 μl ; 3M) was added to RNA (100 μl) and thoroughly mixed by shaking for a few seconds. Ethanol (250 μl ; 100%) was added, mixed thoroughly by vortexing, and samples were incubated overnight at -20°C. On the following day, samples were centrifuged at 12,000 g for 15 minutes at 4°C. After centrifugation, the supernatant was discarded, and the residual supernatant was removed after a quick spin using a microcentrifuge. RNA pellets were resuspended in ethanol (1 ml; 75%), mixed thoroughly by vortexing, and centrifuged at 7,500 g for 5 minutes at 4°C. After centrifugation, the supernatant was discarded, and residual supernatant was removed after a quick spin using a microcentrifuge. RNA pellets were air-dried as before, reconstituted in DEPC-treated water (100 μl), and stored at -80°C.

2.7 Real-time quantitative polymerase chain reaction (RT-qPCR)

For RT-qPCR using Taqman probes, reverse transcription was performed with ~670 ng DNase-treated RNA (Turbo DNA-free, Ambion) using the SuperScript III First-Strand Synthesis System (Invitrogen) for cDNA synthesis. RT-qPCR reactions were set up in a 384-well plate using cDNA samples that were diluted at 1:20. Each well contained (10 μ l/well): cDNA (2 μ l), 2 x Taqman Gene Expression Master Mix (5 μ l; Applied Biosystems), RNase-free water (2 μ l), and Taqman probe (1 μ l). Triplicate samples were prepared as well as no template controls. The plate was assayed on a Roche LightCycler 480 using the following cycling conditions: denaturation at 95°C for 10 minutes with a 4.8°C/second ramp rate; 40x cycles of amplification at 95°C for 10 seconds with a 4.8°C/second ramp rate, 58°C for 30 seconds with 2.5°C/second ramp rate, 72°C for 30 seconds with a 4.8°C/second ramp rate; followed by cooling at 50°C for 10 seconds with a 2.5°C/second ramp rate. Relative quantification was performed using the $2^{-\Delta\Delta CT}$ method (Winer *et al.*, 1999).

For RT-qPCR using SYBR Green, reverse transcription was performed with ~400 ng RNA, which was DNase-treated and cDNA was synthesised using the QuantiTect Reverse Transcription Kit (Qiagen). RT-qPCR reactions were set up in a 384-well plate using cDNA samples that were diluted at 1:4. Each well (10 μ l/well) contained: cDNA (2 μ l), 2 x SYBR Green I Master (5 μ l; Roche), RNase-free water (1 μ l), forward and reverse primer (1 μ l; 5 μ M). Triplicate samples were prepared as well as no template controls. The plate was assayed on a Roche LightCycler 480 using the following cycling conditions: denaturation at 95°C for 10 minutes with a 4.4°C/second ramp rate; 40x cycles of amplification at 95°C for 10 seconds with a 4.4°C/second ramp rate, 62°C for 10 seconds with 2.2°C/second ramp rate, 72°C for 10 seconds with a 4.4°C/second ramp rate; melt at 60°C for 1 second; and cooling at 37°C for 1 second. Each primer pair was validated for SYBR Green assays by constructing a standard curve using cDNA dilutions of: 1 in 10, 1 in 100, 1 in 1000, 1 in 1000, and primers with an efficiency of ~2 were used. Relative quantification was performed using the $2^{-\Delta\Delta CT}$ method (Winer *et al.*, 1999).

2.8 Preparing cells for immunocytochemistry

Cells were fixed with 2% PFA in a 15 ml polypropylene tube for 5 minutes at RT. Cells were washed with PBS (10 ml) and the supernatant was removed after centrifugation at 100 g or 300 g for 3 minutes at RT. Cells were resuspended in PBS (1 ml) and stored at 4°C. Cells were mounted onto Superfrost slides (Lomb) using slide holders with sample chambers, and placed into a Cyto-Tek (Sakura) centrifuge. Cell suspensions were added to the sample chamber and slides were centrifuged at 500 g for 5 minutes at RT. Slides were then stored in PBS at 4°C.

2.9 Histology

Freshly dissected tissues were fixed in 4% PFA for 3 hours and stored in 70% ethanol. To prepare tissues for embedding, specimens were placed between two biopsy foam pads, which were then placed in a labelled embedding cassette before processing. Samples were processed by dehydrating, clearing, and embedding specimens in paraffin. The tissue cassettes were dehydrated in a series of incubations with 70%, 90%, and 95% ethanol for 30 minutes each on a rocker, followed by incubation with 100% ethanol for 1 hour on a rocker at RT (x2). Tissues were cleared of ethanol with xylene for 1 hour at RT (x2). Specimens were infiltrated with paraffin and xylene (50:50) for 1 hour at 60°C, followed by paraffin only for 1 hour at 60°C (x2). Tissues were then embedded into paraffin blocks by submerging samples into molten wax in a stainless steel mold, and a cassette was secured on top of the mold by topping up with molten wax over the cassette. The tissue-embedded blocks were then cooled on a cold plate for ~30 minutes until the wax had solidified and the samples were ready to be removed from the mold. The cassette blocks were stored at RT. Prior to sectioning, embedded specimens were placed on ice and individually sectioned at 5 µm using a Leica RM2255 microtome. Paraffin ribbons were floated onto the water surface in a water bath set at 46°C, and specimens were mounted onto slides. The slides were dried vertically overnight at RT. To better preserve the tissue, dried slides were placed in an oven at 60°C for 15-20 minutes to melt the paraffin and cover the tissue. Samples were stored in a slide storage box at RT.

2.10 Statistical analyses

Data were analysed and are presented as mean \pm standard error of the mean (SEM) using GraphPad Prism 6.0 software. Statistical significances were determined using a two-tailed unpaired Student's t-test, or, by one-way analysis of variance (ANOVA) followed by Tukey's *post hoc* test, or, two-way ANOVA followed by Bonferroni's *post hoc* test. Statistical significance was considered $p < 0.05$.

Chapter 3 Characterisation of a surgical mouse model of LVH

3.1 Introduction

Hypertension is a major cause of pathological left ventricular hypertrophy (LVH), which is an independent risk factor for HF, sudden cardiac death, and mortality (Lloyd-Jones *et al.*, 2002; Levy *et al.*, 1990). Hypertensive heart disease (HHD) is clinically diagnosed by an increase in blood pressure >140/90 mmHg, and the effect of LVH on cardiac function and morphology are evaluated by electrocardiography (ECG), echocardiography or magnetic resonance imaging (MRI) (Drazner *et al.*, 2005; Heckbert *et al.*, 2006; Lloyd-Jones *et al.*, 2002; Levy *et al.*, 1988; Breckenridge, 2010). The main characteristics of pathological LVH are not merely an increase in LV mass, which can also be observed with physiological hypertrophy, but a hypertrophy that also involves cardiac remodelling, changes in cardiac geometry, the re-expression of fetal gene and fibrosis. Although initially adaptive to maintain CO, pathological LVH is likely to be maladaptive even from the time of its initial onset, as it progresses to also involve reduced coronary blood flow that results in impaired cardiac function and the onset of HF (Lorell and Carabello, 2000; Schoenfeld *et al.*, 1998; Maillet *et al.*, 2013).

Surgical models of cardiac hypertrophy have contributed greatly to our understanding of the underlying pathophysiology and to the treatment of HF. The neurohumoral involvement is well known in cardiac hypertrophy and HF (Francis, 2001; Liao *et al.*, 2003). Suprarenal aortic constriction (SAC) models of pressure overload (PO) were developed in larger species, such as dogs (Zimmerman and Kraft, 1979), rabbits (Morris *et al.*, 1977), and rats (Freeman *et al.*, 1977), and it has since been adapted to mice, which are the preferred species for cardiovascular and genetic studies. Measurements of blood pressure and cardiac function in mouse models were previously limited by the small size of a mouse, which is one-tenth of that of a rat (Tarnavski *et al.*, 2004). Thus, microsurgery is technically challenging in the mouse and evaluation of cardiac haemodynamics and contractile function requires considerable expertise and technologies, such as ultra-high resolution echocardiography and micromanometry (Patten and Hall-Porter, 2009).

The severity of LVH in mice is determined by the degree of constriction of the aorta, in which a needle of a specified diameter reproducibly constrict the aorta, by placing the needle onto the aorta and then tightening a ligature around the aorta and needle; the latter is then removed to leave a fixed aortic constriction. The restriction of blood flow in the constricted aorta leads to elevations in blood pressure and increased cardiac afterload, resulting in concentric hypertrophy and pathological remodelling that advances to HF (Hara *et al.*, 2002). Our laboratory has performed SAC in mice to model PO-induced LVH and found a novel target with regenerative potential after cardiac injury, which will be explored in Chapter 4.

Given that the development of LVH can vary significantly depending on experimental conditions, the purpose of this study was to characterise the pathophysiology of SAC-induced hypertension and LVH in mice. This work also provides a background to determine c-Kit expression in CMs after PO in the following chapter (Chapter 4).

3.2 Materials and Methods

General Methods are described in Chapter 2.

3.2.1 Suprarenal aortic constriction (SAC)

Adult C57BL/6J male mice (8 week-old) were randomly assigned to sham or SAC surgeries. Mice were anaesthetised with 2-4% isoflurane and fur was shaved from the left side of the lower body. The mouse was then secured with surgical tape in a right lateral position on a heating pad at 37°C to maintain body temperature. Isoflurane was administered continuously at 2-4% via a nose cone. The surgical area was cleaned with an ethanol wipe. Surgery began with a lateral abdominal incision on the left side of the mouse using surgical scissors (Figure 3.1). The muscular wall of the abdomen was retracted for access and visualisation of the abdominal aorta, which was gently isolated from the surrounding tissue with forceps. A suture needle with 7.0 silk was used to ligate the aorta proximal to the origin of the renal arteries around a blunt and bent 29 G needle. Once the banding was tightly secured, the needle was removed. This resulted in a narrowing of the aortic area to approximately one-third of its original size without completely obstructing blood flow. Sham operations were similarly performed whereby the aorta was isolated without constriction. The muscular walls of the abdomen were sutured with 7.0 silk and the skin was closed with surgical wound clips. The area was then cleaned with iodine solution (Betadine). Mice were placed in recovery cages on a heating pad for 24-hours after surgery and food was softened with water to assist consumption. In the three days following surgery, mice were given buprenorphine by subcutaneous injection twice daily at 0.075mg/kg. Mice were weighed and monitored each day over the duration of the study.

To analyse cardiac function and structure, echocardiography was performed 6 days after surgery (cohort 1) and micromanometry was performed 7 days after surgery (cohort 1 and 2), at which time hearts or CMs were collected for subsequent analyses (Table 3.1). To measure plasma renin concentration and activity, blood was collected from sham and SAC-operated mice 24-hours after surgery (cohort 3).

Table 3.1: Timeline for sham and SAC surgeries

Cohort			Day: 0	1	2	3	4	5	6	7	
	1	n=11	sham	surgery						echo-cardiography	micromanometry and heart tissue collection
n=18		SAC									
2	n=10	sham								micromanometry and CM isolation	
	n=16	SAC									
3	n=10	sham			tissue collection at 24 hrs						
	n=15	SAC									

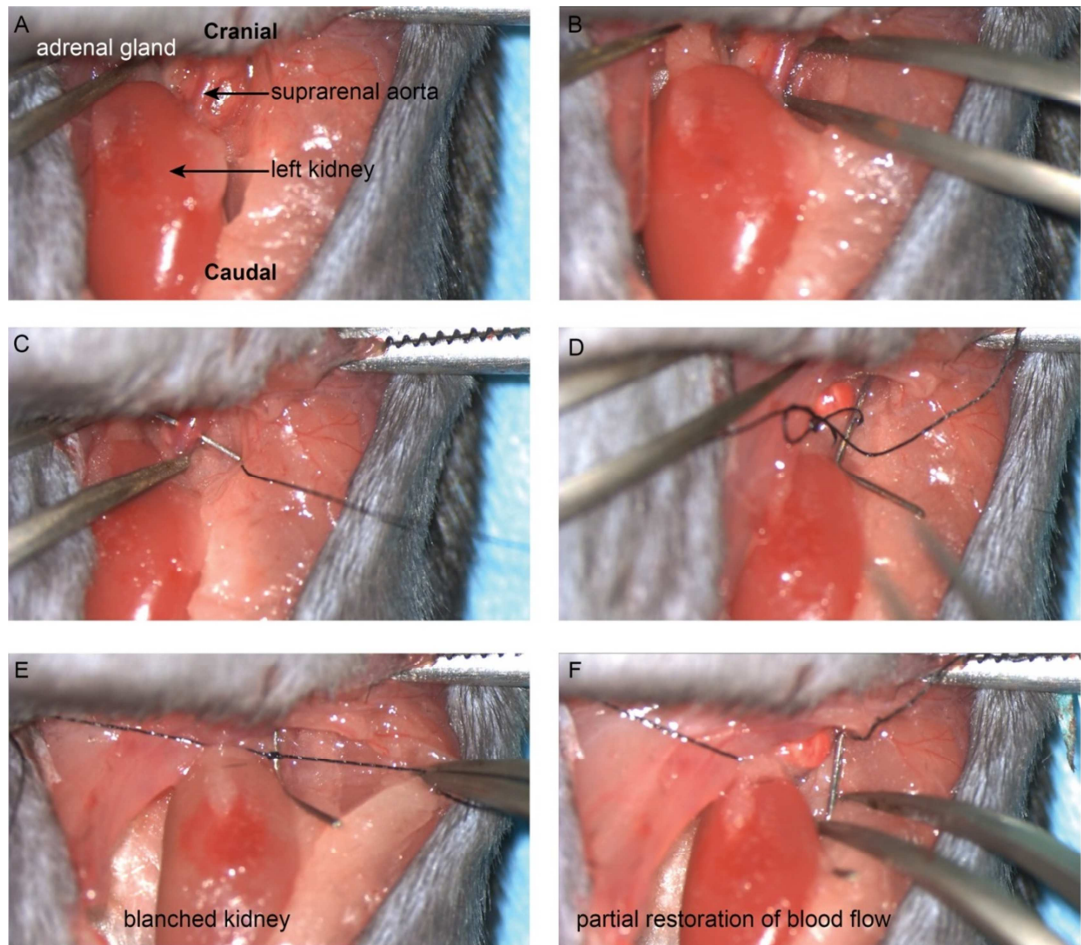


Figure 3.1: Images of SAC surgery

SAC surgeries were recorded and still frames were captured. These images depict the following: A, the left kidney and the aorta are exposed at the suprarenal level after a lateral incision; B, the aorta is isolated from surrounding tissue using forceps; C, a suture needle is used to guide the 7.0 silk around the aorta; D, silk is looped twice around the aorta and a blunted 29 G needle; E, blood flow is occluded blanching the kidney after a double knot is tightened; F, partial blood flow is restored after the needle is removed.

3.2.2 Echocardiography

In cohort 1, echocardiography was performed in a blinded fashion 6 days after sham or SAC surgeries (Table 3.1). Mice were anaesthetised with 3-5% isoflurane and the anterior chest area was shaved. Mice were placed in a supine position on an integrated heating pad with ECG electrodes to maintain 37°C. Isoflurane was continually administered at 1-2% through a nose cone. To monitor heart rate, pre-warmed ultrasound conductive gel was applied to all four limbs positioned near the electrodes. Gel was also applied to the thoracic region that was brought into contact with a MS400 transducer probe (18-38 MHz) connected to a VEVO 2100 echocardiography machine (VisualSonics, Canada). The probe was held in a clamp that was mounted onto a rack allowing sub-millimetre 3D control of its position. Recordings were made of the long and short LV axis that were analysed with Vevo Lab (VisualSonics, Canada) software.

3.2.3 Micromanometry

In cohorts 1 and 2, haemodynamic measurements were performed in a blinded fashion 7 days after sham or SAC surgery (Table 3.1). Mice were anaesthetised with 3-5% isoflurane and the ventral neck and thoracic anterior area was shaved. The mouse was secured onto a heating pad in a supine position and secured with surgical tape around all four limbs and the tail. Anaesthetic was continually administered through a nose cone using 1-2% isoflurane. A midline incision was made along the ventral neck where the right carotid artery was isolated with fine-tip haemostats and dilation forceps. The artery was retracted and elevated using three 6.0 silk loops, the first was looped around the artery proximal to the heart, a second loop lay around the artery between the first and third, and the third was positioned distal to the heart along the same vessel. The distal loop was tightened and ligated while tension was applied to the proximal loop to occlude blood flow. A 25 G needle was used to puncture the artery near the distal ligature, forming an opening where a 1.2 F pressure sensor catheter (Scisense, Canada) was inserted and progressed beyond the second loop, which was ligated to minimise blood loss. The tension from the proximal loop was released and the catheter tip advanced into the aortic root for blood pressure recordings and then further into the LV to record LV pressure. Pressure traces were acquired and analysed using AcqKnowledge (Biopac Systems, USA) software.

3.2.4 Tissue and CM collection

After micromanometry measurements were recorded, mice were euthanized by cervical dislocation. In cohort 1, the lungs, heart, liver and partial right kidney were quickly excised and rinsed in saline to remove blood. In cohort 1 and 3, the atria, right and left ventricles were sequentially isolated from the whole heart. Tissues were then gently blotted dry before weighing and were snap-frozen in liquid nitrogen and stored at -80°C. In cohort 1, LVs were dissected transversely into three sections, whereby the base and apex were snap-frozen in liquid nitrogen and stored at -80°C for downstream extraction of protein for Western blotting and RNA for RT-qPCR. The LV mid-section was fixed in 2% PFA for 3 hours and then stored in 70% ethanol for immunohistochemistry or histology. In cohort 1, the right tibia was removed from an incision made at the ankle and along the bone to the tibia-femur joint, and the tibia was cleaned of tissue and then stored in 100% ethanol at RT. The tibia length was measured in millimeters using the same pair of fine calibre callipers. Heart and LV weights were subsequently normalised to either body weight or tibia length.

In cohort 2, CMs (3 ml) were isolated and enriched (see Chapter 2, Section 2.4) from sham- and SAC- operated hearts and separated into three aliquots for Western blotting (2 ml), RT-qPCR (0.8 ml), and immunocytochemistry (0.2 ml). CMs were snap-frozen in liquid nitrogen and stored at -80°C for downstream extraction of protein and RNA or fixed in 2% PFA for 5 minutes and subsequently stored in PBS for staining.

3.2.5 Immunocytochemistry

Immunostaining of fixed cells was performed as follows. Slides were incubated with 80 µl per slide of blocking buffer (1% BSA and 0.2% Triton X-100 in PBS) for 1 hour at RT, which was removed by flicking slides individually. Cells were incubated overnight at 4°C with a primary antibody (Ab), rabbit anti-laminin (cat. #: ab11575, Abcam), diluted at 1:200 in blocking buffer. Slides were washed in PBS for 5 minutes at RT on an orbital shaker (x5). The following steps were performed in the dark. Cells were incubated for 1 hour at RT with a secondary Ab, goat anti-rabbit IgG Alex Fluor 555, diluted at 1:1000 in blocking buffer. Cells were washed in PBS for 5 minutes on an orbital shaker (x5). Cell nuclei were stained with DAPI (cat. #: D9542, Sigma) diluted at 1:5000 for 10 minutes at RT. Cells were

washed in PBS for 5 minutes on an orbital shaker (x5). Coverslips were secured onto each slide with PVA-DABCO mounting medium. Slides were then stored at 4°C. Stained cells were imaged with a confocal microscope using the same settings (Axio Imager microscope equipped with a LSM 700 confocal scan head, Zeiss).

3.2.6 Plasma renin concentration and activity

In cohort 3, blood was drawn by cardiac puncture at 24-hours after surgery and mixed by inversion with Na₂EDTA (1-2 mg/ml) in 1.5 ml microfuge tubes to inhibit converting enzymes and peptidases, thereby preventing protein degradation. After centrifugation at 12,000 g at 4°C, the supernatant containing plasma was collected and aliquots were stored at -80°C. Plasma renin concentration (PRC) and activity (PRA) were analysed in duplicate by radioimmunoassay (ProSearch International, Australia). PRC was measured by the generation of Ang I in the presence of the exogenous sheep renin substrate, Angiotensinogen. PRA was measured using endogenous levels of renin substrate and any Ang I that was already present in the plasma was subtracted (Sealey, 1991).

3.2.7 RT-qPCR

To measure the expression of hypertrophy markers, cDNA was synthesised using the Superscript III First Strand Synthesis System and RT-qPCR was performed using a Taqman assay. Taqman probes are detailed in Table 3.2.

Table 3.2: Taqman probe sequences for RT-qPCR

Gene	Gene ID	Taqman ID	Sequence
ANP	<i>Nppa</i>	Mm01255747_g1	GATGGATTTCAAGAACCTGCTAGAC
BNP	<i>Nppb</i>	Mm01255770_g1	GTTTGGGCTGTAACGCACTGAAGTT
β -MHC	<i>Myh7</i>	Mm00600555_m1	CGGGACATTGGTGCCAAGGGCCTGA
α -SKA	<i>Acta1</i>	Mm00808218_g1	CTTCCGGCCGTACCACCGGCATCGT
HPRT	<i>Hprt</i>	Mm01545399_m1	GGACTGATTATGGACAGGACTGAAA

To measure the expression of renin mRNA, cDNA was synthesised using the QuantiTect Reverse Transcription Kit and RT-qPCR was performed using a SYBR Green assay. The primers (Integrated DNA Technologies) used for renin and *Gapdh* mRNA expression are shown in Table 3.3.

Table 3.3: Primer sequences for SYBR Green RT-qPCR

Gene	Sequence	Reference
<i>Renin</i> Forward Primer	5'-GAG GCC TTC CTT GAC CCA TC-3'	Wu <i>et al.</i> , (2002)
<i>Renin</i> Reverse Primer	5'-TGT GAA TCC CAC AAG CAA GG-3'	Wu <i>et al.</i> , (2002)
<i>Gapdh</i> Forward Primer	5'-CTT GGG CTA CAC TGA GGA C-3'	
<i>Gapdh</i> Reverse Primer	5'-CTG TTG CTG TAG CCG TAT TC-3'	

3.2.8 Staining for cardiac fibrosis

Samples were fixed, processed, embedded, and sectioned, as described in the General Methods (Chapter 2).

Slides with LV tissue sections were rehydrated in a series of short incubations of 3 minutes to remove wax by incubating with xylene (x2) and rehydrating in ethanol at 100% (x2), 95% (x1), 70% (x1), followed by incubating in distilled water for 2 minutes. Nuclei were identified with Weigert's iron haematoxylin solution by staining for 8 minutes at RT, and protected from light. Specimens were then washed in distilled water for 10 minutes. LV sections were stained with 0.1% Sirius red (cat #: 365548, Sigma) and 0.1% Fast Green FCF (cat #: F7258, Sigma) in picric acid to identify collagen fibres (type I and III) and cytoplasm, respectively. Excess stain was removed with two quick rinses in 0.5% acidified water (glacial acetic acid), followed by one more rinse in distilled water. Specimens were then dehydrated in a short series of incubation steps for 1 minute each with increasing concentrations of ethanol: 70% (x1), 95% (x1), and 100% (x2), followed by xylene (x2). Coverslips were then mounted onto slides with Depex mounting media. Images of LV sections were taken with a DM6000B light microscope.

3.3 Results

3.3.1 Effects of SAC on blood pressure

Haemodynamic measurements were recorded by micromanometry, and the level of anaesthesia was adjusted to stabilise heart rates at 500 bpm. This was to limit the effects of variable heart rates on blood pressure measurements in sham and SAC groups (Figure 3.2). Previous surgical experience with the SAC model in our laboratory suggested that not every SAC surgery that is performed results in the induction of hypertension. Criteria were established *a priori* to define a successful SAC surgery as systolic blood pressure (SBP) that was two standard deviations (SD) above the mean of the sham-operated group, which was 127 mmHg. Thus, the threshold for a successful SAC surgery was $SBP > 127$ mmHg, where the mean SBP of sham-operated mice was 109 mmHg ± 9 mmHg (SD). This translated to a SAC surgery success rate of 68%, where one week after SAC surgery the SBP, diastolic blood pressure (DBP), and mean arterial pressure (MAP), were significantly elevated by 45 mmHg, 10 mmHg, and 18 mmHg, respectively, relative to shams. LV systolic pressure (LVSP) was similar to SBP, increasing by 38 mmHg, and LV end-diastolic pressure (LVEDP) was also significantly elevated in SAC relative to sham groups. However, cardiac contractility (dP/dt_{max} and dP/dt_{min}) was not altered post-SAC compared to shams.

Three mice were excluded from this study due to micromanometry technicalities. The mortality rate in SAC-operated mice was 32%. Half of these deaths occurred within 24-hours of SAC surgery and the remaining mice were culled for ethical reasons because of a significant loss in body weight ($\geq 10\%$) due to ill health. One of the mice culled due to ill health had severe systemic oedema, indicating congestive HF.

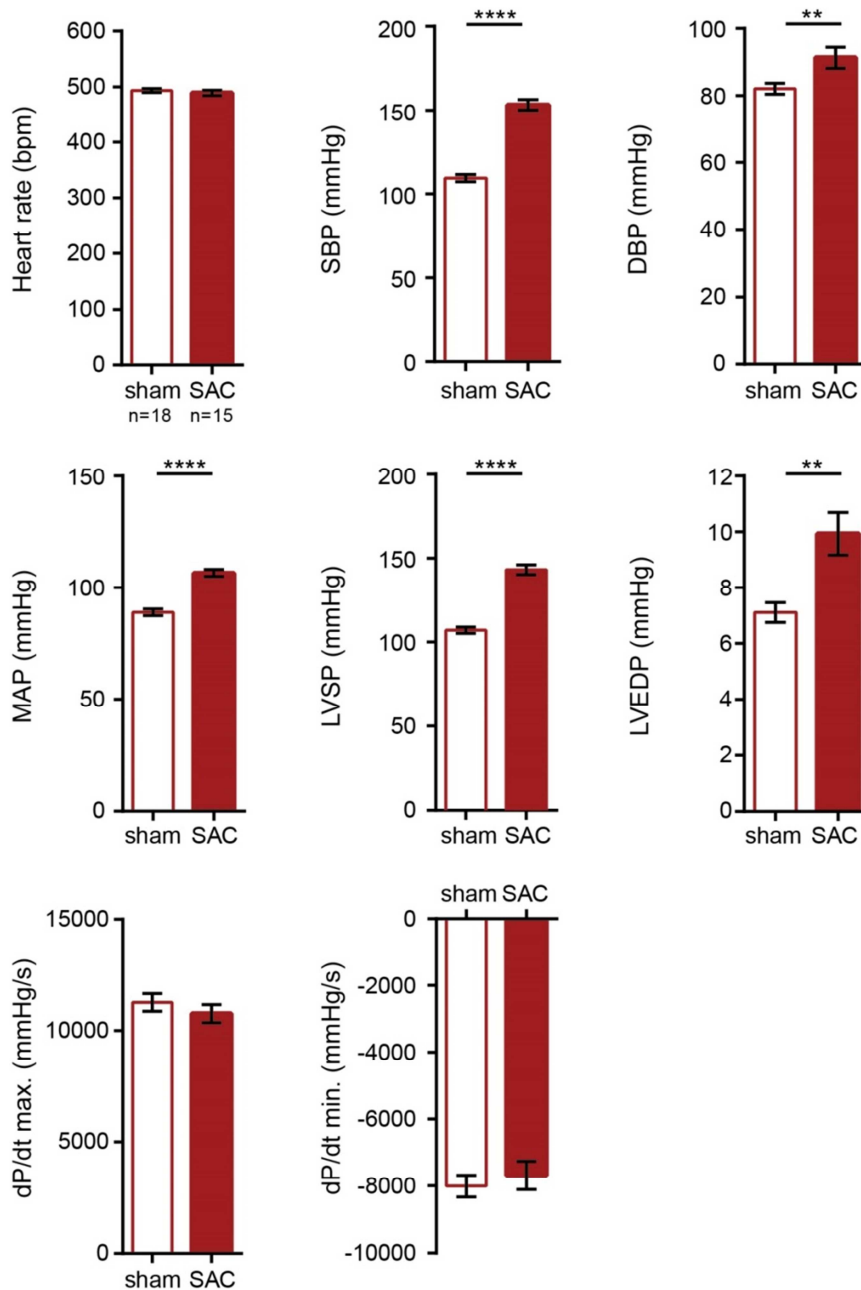


Figure 3.2: Micromanometry measurements one week post- sham or SAC surgery

Micromanometry was performed on adult male C57BL/6J mice (9-week old) one week post-surgery (sham, n=18; SAC, n=15) and analysed using AcqKnowledge software. Data are presented as means \pm SEM; independent comparisons were made by two-tailed Student's unpaired *t*-tests; **p*<0.05, ***p*<0.005, and *****p*<0.0001. DBP, diastolic blood pressure; SBP, systolic blood pressure; MAP, mean arterial pressure; dP/dt, contractility max and min; LVSP, left ventricular systolic pressure; LVEDP, left ventricular end-diastolic pressure.

3.3.2 Effects of SAC on cardiac function

Echocardiography was performed 6 days post-surgery and revealed a 20% increase in the relative LV wall thickness (h/R) of SAC-operated mice relative to sham-operated mice, indicating the development of concentric hypertrophy (Figure 3.3 and Table 3.4). There were also significant reductions in CO, LV ejection fraction (LVEF) and fractional shortening (FS) post-SAC relative to shams. Indeed, CO fell by 14%, which was consistent with an 8% reduction in LVEF due to an increase in the LV end-systolic volume (LVESV) that nearly doubles, and an 11% reduction in FS. Hence, less blood was ejected from the LV during systole post-SAC compared with shams. There were no significant changes in the LV end-diastolic volume (LVEDV) or stroke volume (SV) post-SAC relative to shams.

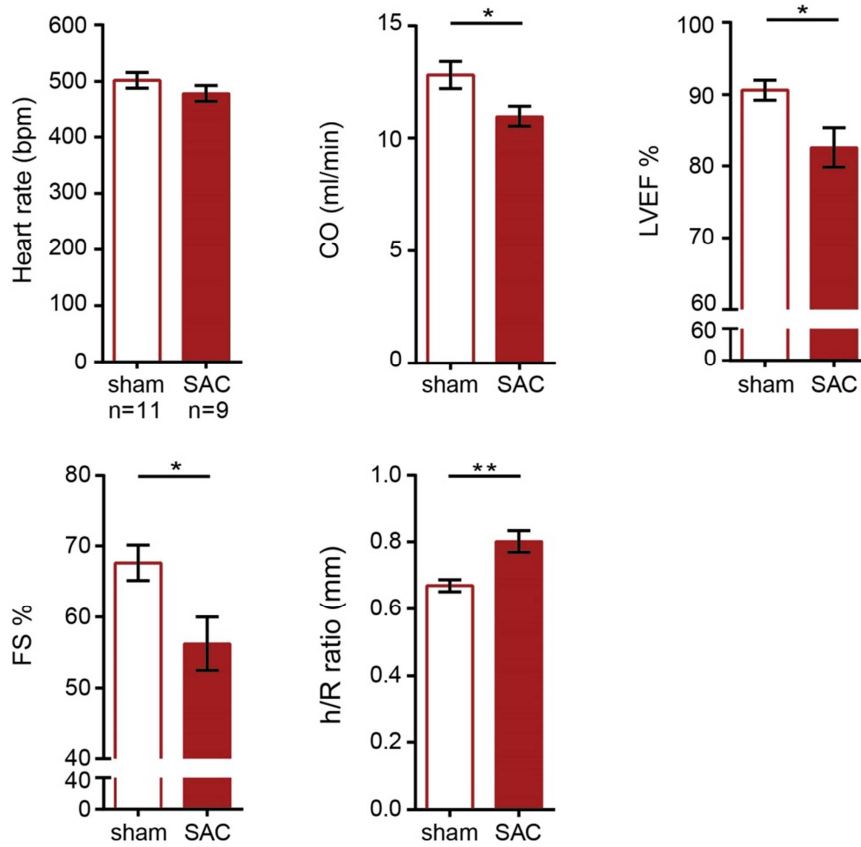


Figure 3.3: Echocardiography measurements six days post- sham or SAC surgery

Echocardiography was performed on adult male C57BL/6J mice (9-week old) six days post-surgery (sham, n=11; SAC, n=9). Data are presented as means \pm SEM; independent comparisons were made by two-tailed Student's unpaired *t*-tests; **p*<0.05, and ***p*<0.005. CO, cardiac output; LVEF, ejection fraction; FS, fractional shortening; h, LV wall thickness; R, internal LV chamber radius.

3.3.3 Gross morphology of LVH following SAC

There were no statistically significant differences in body weight or tibia length (TL) between sham- and SAC- operated mice (Table 3.4), thus data are presented for TL (Figure 3.4A). Consistent with the development of LVH, heart (HW/TL) and LV (LV/TL) mass increased significantly post-SAC by 39% and 48%, respectively, relative to shams (Figure 3.4). The weight of the lungs (lungs/TL) was comparable between sham and SAC mice, suggesting that the developing LVH phenotype had not advanced to HF. CMs were isolated from the cardiac ventricles, and were stained to measure cell size by CM area (Figure 3.4B), which shows CMs had enlarged by 17% post-SAC relative to shams.

In Figure 3.5, the relationship between LV/TL and SBP, determined using Pearson's correlation, before ($R^2=0.48$, Figure 3.5A) and after ($R^2=0.92$, Figure 3.5B), excluding animals that did not meet the criterion of $SBP > 127$ SBP (mmHg) is shown. The exclusion criterion clearly strengthened the correlation between SBP and LV/TL (Figure 3.5B), mainly due to the exclusion of one SAC-operated mouse that remained normotensive (SBP of 102mmHg) but showed a significant increase in LV mass of 90% (LV/TL= 9.1) relative to shams (LV/TL= 4.8). This data point is easily observed in Figure 3.5A.

Table 3.4: Gross morphology, micromanometry and echocardiography measurements one week post- sham or SAC surgery

	sham	SAC	p-value
<i>Gross morphology</i>	n=8	n=6	
BW (g)	22.55 ± 0.37	22.01 ± 0.36	ns
HW (mg)	119 ± 4	161 ± 4	****
LVW (mg)	78 ± 3	111 ± 3	****
TL (mm)	16.1	15.6	ns
Lungs (mg)	135.2 ± 4	126.5 ± 3	ns
HW/BW (mg/g)	5.3 ± 0.2	7.4 ± 0.3	****
LV/BW (mg/g)	3.5 ± 0.1	5.1 ± 0.2	****
HW/TL (mg/mm)	7.4 ± 0.3	10.3 ± 0.2	****
LV/TL (mg/mm)	4.8 ± 0.1	7.1 ± 0.1	****
Lungs/TL (mg/mm)	8.4 ± 0.2	8.6 ± 0.6	ns
Lungs/BW	6.0 ± 0.1	6.1 ± 0.4	ns
<i>Micromanometry</i>	n=18	n=15	
HR (bpm)	494 ± 4	490 ± 5	ns
DBP (mmHg)	82 ± 2	91 ± 3	*
SBP (mmHg)	109 ± 2	153 ± 3	****
MAP (mmHg)	89 ± 2	107 ± 2	****
dP/dt max (mmHg/S)	11266 ± 401	10763 ± 425	ns
dP/dt min (mmHg/S)	-8004 ± 313	-7682 ± 379	ns
LVSP (mmHg)	106.9 ± 2	144.9 ± 3	****
LVEDP (mmHg)	7.1 ± 0.4	9.9 ± 0.8	**
<i>Echocardiography</i>	n=11	n=9	
HR (bpm)	502 ± 4	479 ± 14	ns
LVEDV (mm ³)	28 ± 1	28 ± 2	ns
LVESV (mm ³)	2.7 ± 0.5	5.2 ± 1	*
SV (mm ³)	26 ± 1	23 ± 1	ns
CO (ml/min)	12.8 ± 0.6	11 ± 0.5	*

h (mm)	1.04 ± 0.02	1.22 ± 0.03	****
R (mm)	1.56 ± 0.03	1.53 ± 0.04	ns
h/R	0.669 ± 0.02	0.801 ± 0.03	**
LVEF (%)	90.6 ± 1.4	82.6 ± 2.9	*
FS (%)	67.6 ± 2.5	56.2 ± 3.8	*

Gross morphology, micromanometry, and echocardiography measurements from adult male C57BL/6J mice (9-week old) one week post-sham or –SAC surgery. Data are presented as mean ± SEM; independent comparisons were made by two-tailed Student's unpaired *t*-tests; **p*<0.05, ***p*<0.005, ****p*<0.0005, *****p*<0.0001 and ns, non-significant. BW, body weight; HW, heart weight; LVW, left ventricular weight; TL, tibia length; HR, heart rate; DBP, diastolic blood pressure; SBP, systolic blood pressure; MAP, mean arterial pressure; LVSP, left ventricular systolic pressure; LVEDP, left ventricular end-diastolic blood pressure; LVEDV, left ventricular end-diastolic volume; LVESV, left ventricular end-systolic volume; SV, stroke volume; CO, cardiac output, h, LV wall thickness; R, LV internal chamber radius; LVEF, left ventricular ejection fraction, LVEF= ((LVEDV – LVESV) / LVEDV) x100); FS, fractional shortening, FS= ((LVIDd – LVIDs) / LVIDd) x100); ID, internal diameter; s, systole; d, diastole.

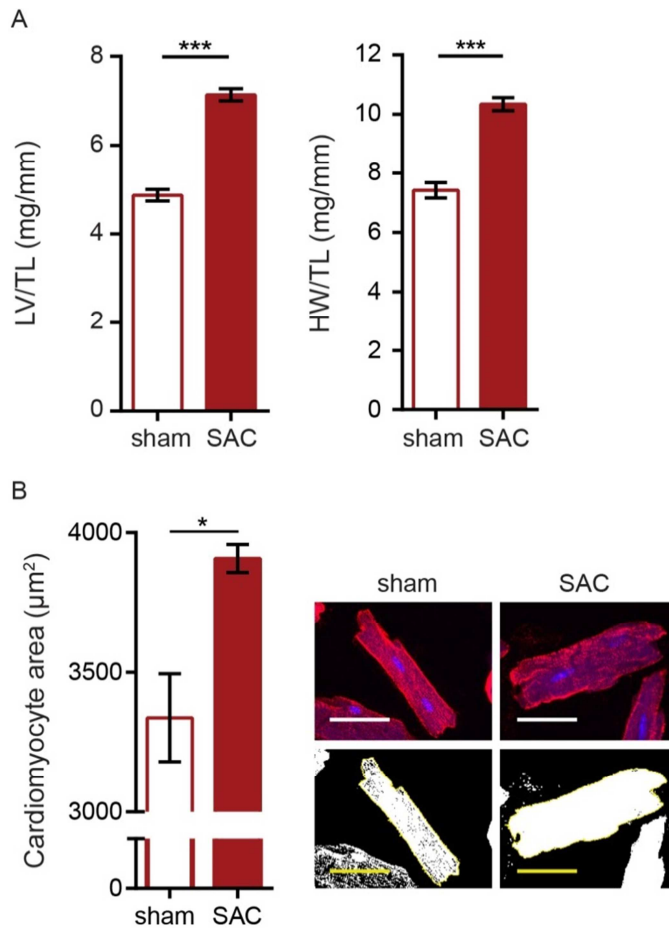


Figure 3.4: Gross morphology of the heart, LV and CMs one week post- sham or SAC surgery

Gross morphology measurements were made at one week after sham or SAC surgery in adult male C57BL/6J mice (9-week old). A, heart and LV weights were normalised to TL (n=6-8). B, CM areas were measured using ImageJ (n=3, 30-40 binucleated CM areas per slide) with representative images. Top, CM membranes were stained with laminin (red) and DNA with DAPI (blue); bottom, replica binary images show the cell area (white) within the outline of each CM, and CM areas were measured in ImageJ. Scale bar is 50 μm . Data are presented as means \pm SEM; independent comparisons were performed using two-tailed Student's unpaired *t*-tests; * $p < 0.05$, and *** $p < 0.0005$. LV, left ventricle; HW, heart weight; TL, tibia length.

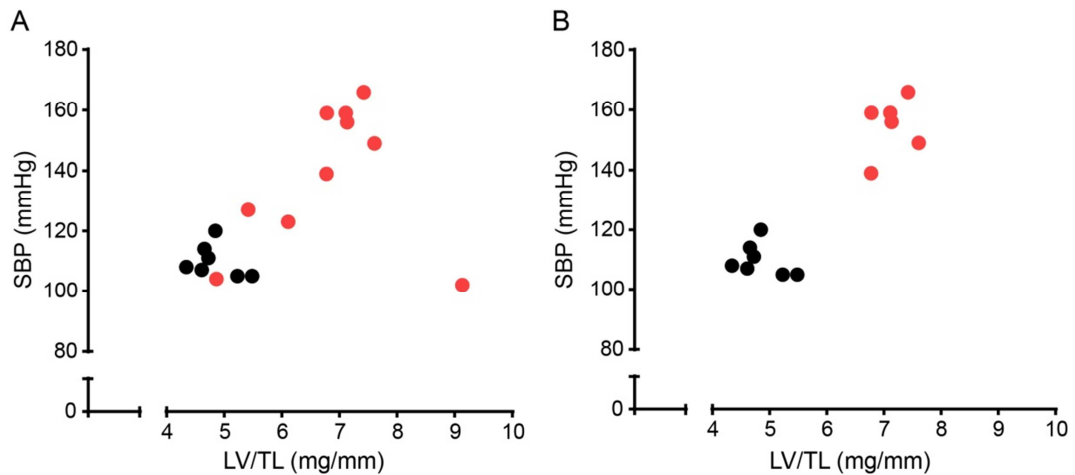


Figure 3.5: Correlation between SBP and LV/TL, before and after applying the exclusion criteria

Correlation between SBP and LV/TL ratio in sham- (black dots) or SAC- (red dots) operated mice one week after surgery; A, all sham- and SAC-operated mice were included (n=17); and B, only mice that had successful SAC surgery (SBP <127 mmHg) were included in the study (n=13). SBP, systolic blood pressure; LV, left ventricle; TL, tibia length.

3.3.4 Evaluation of pathological hypertrophy markers and fibrosis

A distinctive characteristic of pathological hypertrophy is the re-expression of fetal genes, specifically, ANP, BNP, β -MHC and α -SKA. The mRNAs for these hypertrophy markers were more abundant post-SAC compared with shams in both the LV (Figure 3.6A) and in enriched CM fractions (Figure 3.6B). ANP, BNP, β -MHC and α -SKA mRNAs were more abundant post-SAC in the LV by 6-, 1400-, 3-, and 7- fold, respectively, relative to shams. The fold-change of ANP, β -MHC and α -SKA mRNAs was greater in the CM-enriched fraction (12-, 25-, and 13- fold, respectively) compared with the LV post-SAC, whereas BNP increased by only 4-fold in the CM-enriched fraction compared with 1400-fold in the LV post-SAC, and hence, changes in BNP levels were higher in the LV than in CMs.

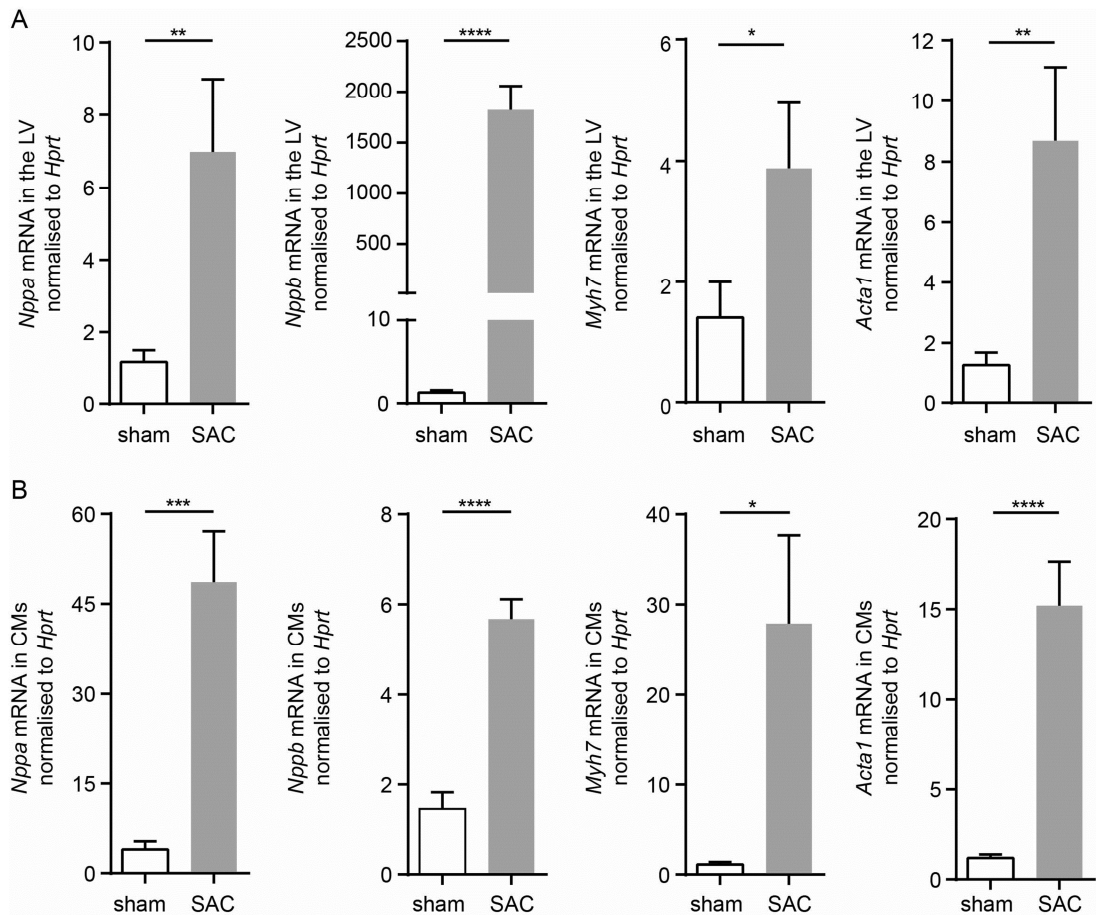


Figure 3.6: Expression of pathological hypertrophy markers in the LV and in CMs one week post- sham or SAC surgery

The expression of hypertrophy marker mRNAs, normalised to *Hprt* mRNA, were evaluated one week post -sham or -SAC surgery of adult male C57BL/6J mice (9- week old) from the (A) LV (sham, n=8; SAC, n=5) and (B) in enriched CM fractions (sham, n=7; SAC, n=8). Data are presented as means \pm SEM, independent comparisons were made by two-tailed Student's unpaired *t*-tests; * p <0.05, ** p <0.005, *** p <0.0005 and **** p <0.0001. *Nppa* encodes ANP, atrial natriuretic peptide; *Nppb* encodes BNP, brain natriuretic peptide; *Myh7* encodes β -MHC, beta- myosin heavy chain; *Acta1* encodes α -SKA, alpha- skeletal actin.

Furthermore, one week post-surgery there was evidence of perivascular fibrosis in SAC-operated mice compared with shams that was identified by Picrosirius Red staining, which detects collagen fibres (Figure 3.7). These transverse sections of the LV also demonstrated an increase in the thickness of the LV wall (h) relative to the radius of the internal LV chamber radius (R) post-SAC, and supports the h/R measurements from echocardiography data (Figure 3.3).

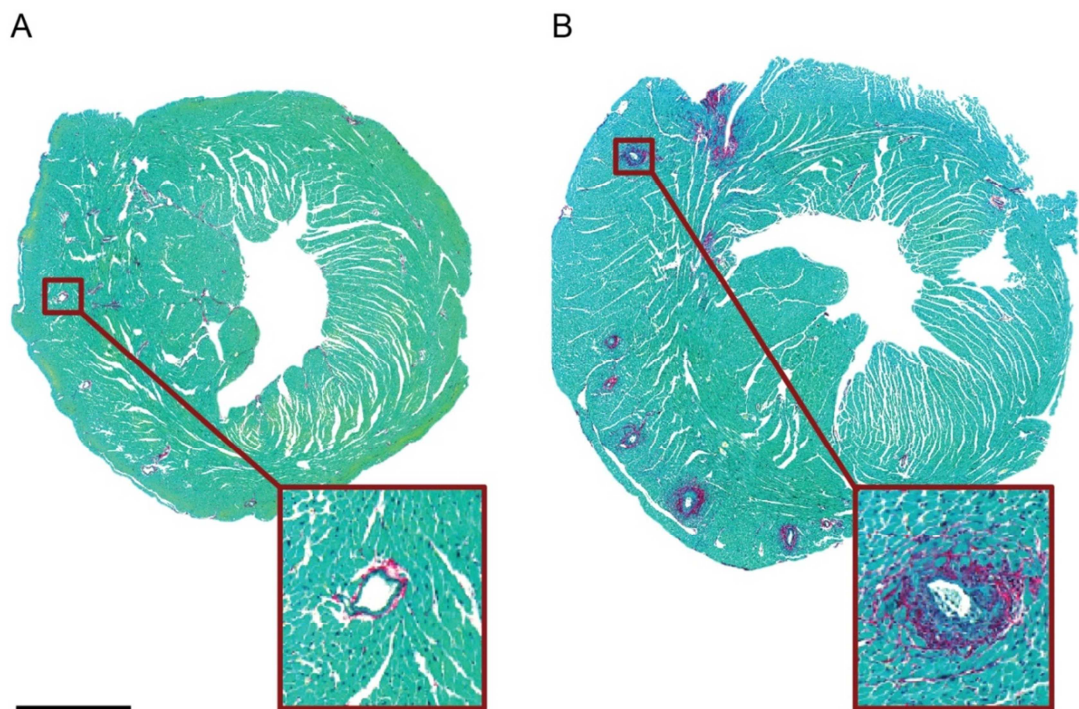


Figure 3.7: Histological transverse LV sections stained for fibrosis one week post-sham or SAC surgery

Representative LV sections show evidence of perivascular fibrosis (collagen deposition) around the coronary arteries post-SAC compared with shams. Transverse LV sections were stained with Fast Green and Picrosirius Red to identify the cytoplasm and collagen, respectively, one week after (A) sham- or (B) SAC- surgery in C57BL/6J adult mice (9-week old). Scale bar is 1 mm.

3.3.5 RAAS activation following SAC

To further determine whether the RAAS system was activated, plasma renin concentration and activity (PRC and PRA) were measured at 24-hours after surgery, as well as the expression of renin mRNA taken from the kidney one week after surgery. PRC and PRA remained unchanged post-SAC (Table 3.5). However, there was a slight upward trend in renin mRNA levels post-SAC relative to shams, but this did not reach statistical significance (Table 3.5). There were no differences in HW/BW ratios between sham or SAC groups 24-hours after surgery, as expected.

Table 3.5: Acute and short-term effects of SAC on renin levels

	sham	SAC	p-value
24-hours post-surgery	n=10	n=14	
HW/BW (mg/g)	4.84	4.98	ns
PRC (Ang I ng/mL/hr)	992.4 ± 104.7	1051 ± 94.93	ns
PRA (Ang I ng/mL/hr)	71.54 ± 7.26	71.68 ± 6.9	ns
One week post-surgery	n=7	n=5	
<i>Ren/Gapdh</i> mRNA	1.065 ± 0.2	1.75 ± 0.4	ns

At 24-hours post –sham or –SAC surgery of adult male C57BL/6J mice (8-week old), heart and body weights were recorded, and blood plasma was sent to ProSearch for radioimmunoassays to measure plasma renin concentration and activity (PRC and PRA). At one week post –sham or –SAC surgery, *Ren* mRNA levels were measured from the kidney of adult male C57BL/6J mice (9-week old) and normalised to *Gapdh*. *Ren* encodes renin protein and *Gapdh* encodes GAPDH protein. Data are presented as means ± SEM. Statistics were performed using a two-tailed Student’s unpaired *t*-tests; ns, non-significant. HW, heart weight; BW, body weight; PRC, plasma renin concentration, PRA, plasma renin activity.

3.4 Discussion

In this study hypertension-induced LVH after one week of SAC was characterised in mice. Post-SAC, blood pressures (SBPs) were elevated by 45 mmHg resulting in a 48% increase in LV mass (LV/TL), which is similar to that of previous reports in mice (Wettschureck *et al.*, 2001; Li *et al.*, 2008). The increased LV mass was due to CM hypertrophy, which was evident by the 17 % enlargement in CM area. This resulted in a thickening of the LV wall (i.e., an increase in h) and little changes to the internal LV chamber radius (R) and, hence, an increase in h/R; consistent with the development of concentric hypertrophy. The development of LVH resulted in impaired cardiac function, as evident by reductions in CO (-14%), LVEF (-8%) and FS (-11%). Moreover, and consistent with pathological hypertrophy, the re-expression of fetal genes increased post-SAC and there was also evidence of LV remodelling as shown by perivascular fibrosis compared with shams. Although there was no indication of abnormal RAAS activity, as determined by PRC and PRA at 24-hours post-SAC and renin mRNA one week post-SAC. Taken together, these results demonstrate that SAC leads to a reproducible model of hypertensive heart disease.

Blood pressures were significantly elevated in SAC-operated mice compared with shams (SAC, 154/91 mmHg, n=15; vs sham, 109/82 mmHg, n=18, $p < 0.0001$) at one week post-SAC (Table 3.4), which is analogous to that of hypertensive patients. For SAC surgery to have been successful, the criterion of >127 mmHg was used. This resulted in 68% of SAC surgeries that were successful and resulted in hypertension. The success (68%) and mortality rates (32%) were comparable to those reported for rats post-SAC (Kim *et al.*, 2015). Blood pressures that did not meet the criteria resulted in the exclusion of four of the SAC-operated mice from cohort 1 (heart tissue collection) and two from cohort 2 (CM isolation). Three of the four SAC-operated mice that were excluded from the tissue cohort, had comparable SBPs and LV weights compared with sham controls. However, one of the four mice that was excluded from this study was normotensive but had a marked increase in LV mass (LV/TL, +90%), and LV wall thickness compared with shams, with diminished cardiac contractility (dP_{\max}/dT_{\min}), indicating that LVH had progressed to HF.

The main defining characteristic of LVH is an increase in LV mass. One week post-SAC, LVs were significantly enlarged by 48% and CMs underwent hypertrophy, which is likely due to an increase in cell width (Figure 3.4B), and contributed to a thickening of the LV

wall (h/R), relative to shams. Representative images of histological transverse LV sections confirmed these findings (Figure 3.7). Overall, SAC resulted in the classical development of concentric hypertrophy, corresponding to clinical presentations of LVH (Grossman *et al.*, 1975; Drazner, 2011).

Pathological LVH has a distinctive transcriptome, with the re-activation of the fetal gene program, a hallmark that has been extensively described. Indeed, SAC-induced hypertrophy was accompanied by increases in ANP, BNP, β -MHC, and α -SKA mRNA expression compared with shams (Figure 3.6). Post-SAC, the fold-increase of ANP, β -MHC, and α -SKA, was greater in enriched fractions of CMs than in LV tissue, whereas the fold-increase in BNP was greater in LV tissues than in enriched CMs, relative to sham. After hypertensive stress, BNP is highly elevated in blood plasma and is also synthesised by proliferating cardiac fibroblasts. Both the blood plasma and fibroblasts would have been removed from the CM-enriched fraction, and hence, the expression of BNP mRNA was greater in the LV than in CMs (Gardner, 2003; Tsuruda *et al.*, 2002). Furthermore, perivascular fibrosis was observed post-SAC with an increase in collagen deposition, (Figure 3.7) indicating the proliferation of fibroblasts that have also been observed in patients with HHD (Diez, 2007). In addition, the RAAS system is a critical contributor to the development of myocardial fibrosis, specifically Ang II and aldosterone, by inducing the proliferation of cardiac fibroblasts (Diez, 2007; Cuspidi *et al.*, 2006; Weber and Brilla, 1991).

Although the presence of ANP and fibrosis post-SAC, indicate RAAS activation, plasma renin concentration and activity (PRC and PRA, 24-hours post-SAC) and kidney renin mRNA (one week post-SAC) were not elevated (Table 3.5). SAC involves banding the abdominal aorta above the origin of both renal arteries, which directly reduces renal blood flow. One explanation for the absence in renin changes is that the increase in blood pressure may have restored renal perfusion despite aortic constriction, thus reducing renin release. In two different surgical rat models, two kidney, 1 clip (2K1C, the left renal artery is clipped) and abdominal aortic constriction (AAC) model, renin mRNA levels increased in the left ischemic kidney but decreased in the contralateral right kidney after 28 days of 2K1C and 3 days of AAC (Moffett *et al.*, 1986), and coincided with elevations in PRA. Renin mRNA levels were also increased in the left ischemic kidney two weeks after 2K1C and one week after AAC in mice (Wiesel *et al.*, 1997; Zhang and Morgan, 1999). Studies in rats have

shown PRA increases within 15-30 minutes of SAC banding (Villarreal *et al.*, 1984) and one day after SAC but returned to control values after three days (Baker *et al.*, 1990), while others have not observed increased PRA levels in rats after 1, 3, 7 or 28 days of SAC surgery (Heller *et al.*, 1998; Kuwahara *et al.*, 2002). It has also been shown that cardiac renin mRNA levels do not increase at one week post-SAC in rats, nor did kidney renin mRNA or PRA levels increase at eight weeks post-SAC in mice (Heller *et al.*, 1998; Wu *et al.*, 2002). However, elevations in PRA were reported to be indicative of HF in rabbits (Morris *et al.*, 1977). Thus, measurements of renin and PRA vary depending on the species, the surgical model, the severity of aortic constriction, and on the length of the study.

Another possible explanation for the absence of elevated renin levels is that it is subject to negative feedback via Ang II, aldosterone, and ANP, which directly inhibit renin synthesis and release (Melo *et al.*, 2000; Kurtz *et al.*, 1986; Atlas *et al.*, 1986; Atlas, 2007). This may explain the transient and temporal patterns of renin expression that have been previously reported (Heller *et al.*, 1998; Moffett *et al.*, 1986; Baker *et al.*, 1990). This may also be reflected patients with LVH who also have variable PRA measurements. Altogether, the increased expression of ANP and fibrosis, which are co-regulated by aldosterone and Ang II, indicate RAAS activation (Ogawa *et al.*, 1999). Thus, cardiac remodelling is a complex sequence of events, coordinating the expression of pathological markers and fibrosis, both of which are influenced by RAAS activation. A further evaluation of RAAS components are required to assess its contribution to the SAC model in mice.

Overall, this study characterises SAC-induced LVH in mice, which has characteristics similar to those of patients with HHD, including LV enlargement, concentric hypertrophy, elevations in blood pressure and impaired cardiac function. Moreover, both the post-SAC mouse model and HHD patients, exhibit changes that are associated with pathological cardiac remodelling, including the re-expression of fetal genes and fibrosis. These findings suggest that this surgical model is a valuable research tool for understanding the molecular and biochemical changes underpinning LVH, which may be used for developing new treatments for HF. In addition, this work lays the foundation for, and extends upon our previously published data using a SAC model of LVH (Li *et al.*, 2008), in which we identified c-Kit as a target for CM regeneration, which will be explored in Chapter 4.

Chapter 4 The role of c-Kit in cardiomyocytes after LVH

4.1 Introduction

In the adult mammalian heart, CMs are terminally differentiated and have lost their proliferative capacity. This restricts cardiac growth to CM hypertrophy in response to an increase in workload as occurs with stresses, such as high blood pressure and valvular heart disease. Thus, left ventricular hypertrophy (LVH) is a major risk factor for the development of adverse cardiovascular events sequelae, including HF, sudden cardiac death, and mortality (Levy *et al.*, 1990).

c-Kit, or stem cell factor receptor, is an important developmental signalling molecule for hematopoiesis, pigmentation, and reproduction. The compound heterozygous $\text{Kit}^{\text{W/W}^{\text{v}}}$ mouse (Figure 1.4; Chapter 1) carries a spontaneous W (null) and W^{v} (dominant negative missense mutation at T660M) mutation, leading to global impairment of c-Kit signalling (Nocka *et al.*, 1989), and mice are piebald, mildly anaemic, and have an altered immune response. Our laboratory has previously shown that cardiac regeneration is elicited in $\text{Kit}^{\text{W/W}^{\text{v}}}$ mice one week after hypertensive stress (Li *et al.*, 2008). At baseline, cardiac function and morphology in $\text{Kit}^{\text{W/W}^{\text{v}}}$ mice are indistinguishable from those of adult WT littermate controls, and when both are subjected to one week of suprarenal aortic constriction (SAC) they have equivalent increases in LV mass (Li *et al.*, 2008). Surprisingly, CMs in the $\text{Kit}^{\text{W/W}^{\text{v}}}$ hearts were found to have undergone less hypertrophy than WT controls, and the increase of LV mass in $\text{Kit}^{\text{W/W}^{\text{v}}}$ hearts was primarily the result of CM proliferation. At one week post-SAC, there was an addition of 40% CMs to the total $\text{Kit}^{\text{W/W}^{\text{v}}}$ CM population compared with $\text{Kit}^{\text{W/W}^{\text{v}}}$ shams. Cell cycle re-entry was evident in $\text{Kit}^{\text{W/W}^{\text{v}}}$ CMs that were in G1/S transit (BrdU⁺-stained nuclei), G2/M transit (H3P⁺-stained nuclei) and karyokinesis (aurora B⁺-staining between nuclei). This demonstrated that the newly formed CMs originated from the cell division of pre-existing CMs, similar to that observed after cardiac regeneration in neonatal mouse and in zebrafish after cardiac injury (Porrello *et al.*, 2013; Kikuchi *et al.*, 2010; Jopling *et al.*, 2010). Cardiac function and survival outcomes were also significantly better in $\text{Kit}^{\text{W/W}^{\text{v}}}$ (100% vs 59% survival) compared with WT mice post-SAC. Therefore, a hyperplastic response dramatically improved survival outcomes by generating more functional CMs.

Evidence that supports the association of inhibited cell cycle re-entry with c-Kit activity came from a transgenic mouse model, Tg(α MHC-Kit^{Wv}), in which c-Kit^{Wv} is overexpressed under the control of the α -MHC promoter, which leads to CM-restricted inactivation of c-Kit shortly after birth (Li *et al.*, 2008). One week after SAC surgery, there were significantly higher levels of the aforementioned cell cycle markers in the nuclei of Tg(α MHC-Kit^{Wv}) CM nuclei compared with sham controls, demonstrating an increase in CM cell cycle re-entry. This suggests that the inactivation of c-Kit in CMs shortly after birth prevents the terminal differentiation of CMs, and allows adult CMs to divide in response to an increased workload.

c-Kit is expressed in the WT heart during cardiac development. It is maximally expressed at P1-3 and barely detectable by P10-14 in cardiac stem and progenitor cells (Fransioli *et al.*, 2008; Tallini *et al.*, 2009) and in CMs (Li *et al.*, 2008), coinciding with CM maturation. Consequently, c-Kit is not detected in the adult myocardium (Fransioli *et al.*, 2008; Li *et al.*, 2008) and rarely observed within vascular compartments or CMs (Tallini *et al.*, 2009) by immunohistochemistry. These data support the hypothesis that c-Kit expression coincides with CM differentiation and cell cycle withdrawal.

Given the reported expression of c-Kit in the differentiation of CMs from stem cells and the proliferation of CMs in response to PO where c-Kit is inactivated, it is possible that c-Kit signalling prevents CM cell division by promoting terminal differentiation, thereby restricting CMs to hypertrophic growth. Preliminary immunohistochemistry data from our laboratory (not shown) suggested that c-Kit is re-expressed in adult WT CMs post-SAC. The re-expression of c-Kit has also been found occasionally in terminally differentiated adult CMs after cryo-injury (Tallini *et al.*, 2009). Thus, c-Kit may be a novel target for the development of pharmacological tools to inhibit c-Kit signalling after cardiac injury and thereby facilitate cardiac repair through CM proliferation, while also preventing pathological CM hypertrophy. To this end, the hypothesis underlying this study was that c-Kit is re-expressed after hypertensive stress in the adult heart, and that c-Kit signalling blocks CM cell cycle re-entry and restricts CMs to a hypertrophic response. The aim of this study was to evaluate the expression and activity of c-Kit in CMs from adult WT mice post-sham or SAC surgery.

4.2 Materials and Methods

General Methods are described in Chapter 2. Sham and SAC operations were performed as detailed in Chapter 3.

4.2.1 Animal models

C57BL/6J Tg(α MHC-Kit^{W^v}) mice overexpress the dominant-negative W^v c-Kit missense point mutation, T660M (Figure 1.4; Chapter 1), under the control of the α -MHC promoter (Figure 4.1); this leads to the inactivation of c-Kit signalling in CMs from birth. We also have two transgenic mouse models with CM-specific overexpression of wild-type c-Kit under the control of the α -MHC promoter: Tg(α MHC-Kit.1) and Tg(α MHC-Kit.2) (Figure 4.1).

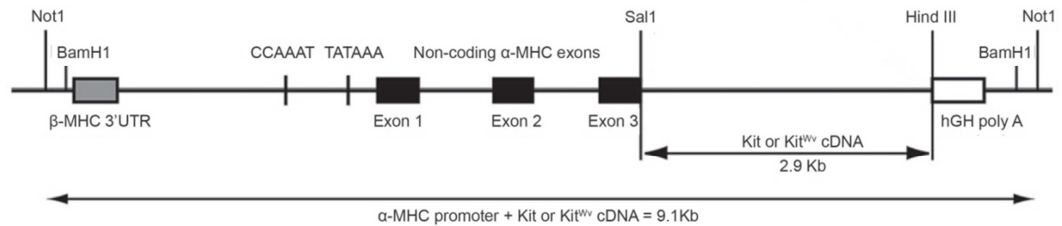


Figure 4.1: The construct used to generate transgenic c-Kit mouse models: Tg(α MHC-Kit^{W^v}), Tg(α MHC-Kit.1) and Tg(α MHC-Kit.2)

Kit or Kit^{W^v} cDNA was sub-cloned behind the α -MHC promoter into Sal I and Hind III sites.

4.2.2 Tissue and CM collection

In cohort 1, sham and SAC-operated LVs (see Chapter 3, Section 3.2.1) were dissected transversely into three sections, whereby the base and apex were snap-frozen in liquid nitrogen and stored at -80°C for downstream extraction of protein for Western blotting and RNA for RT-qPCR, respectively. The LV mid-section was fixed in 2% PFA for 3 hours and then stored in 70% ethanol for immunohistochemistry.

In cohort 2, CMs (3 ml) were isolated and enriched (see Chapter 2, Section 2.4) from sham- and SAC- operated hearts (see Chapter 3, Section 3.2.1) and separated into three aliquots for Western blotting (2 ml), RT-qPCR (0.8 ml), and immunocytochemistry (0.2 ml). CMs were snap-frozen in liquid nitrogen and stored at -80°C for downstream extraction of protein and RNA or fixed in 2% PFA for 5 minutes and subsequently stored in PBS for staining.

4.2.3 Cell culture of HEK293T and MEL cells

Cell culture was performed using aseptic techniques.

Human embryonic kidney (HEK293T) cells were stored in 1 ml of Dulbecco's modified Eagle's medium (DMEM) with 10% fetal bovine serum (FBS) and 20% dimethyl sulfoxide (DMSO) at -80°C . Cells were quickly thawed by agitation in a 37°C water bath and slowly resuspended and transferred drop by drop into a 15 ml polypropylene tube containing pre-warmed growth medium (5ml). Growth medium contained DMEM with sodium pyruvate and glutamate (Invitrogen) supplemented with 10% FBS and 1% penicillin and streptomycin. Cells were then centrifuged at 900 rpm ($\sim 140\text{ g}$) for 3 minutes at RT and resuspended in pre-warmed growth media (1 ml), which was then transferred to a T75cm^3 flask containing pre-warmed growth media (9 ml). HEK293T cells were cultured in a monolayer of a horizontally placed flask and incubated with 5% CO_2 at 37°C . Once HEK293T cells were confluent, cells were either passaged and/or removed for experimental use. For passaging cells, trypsin (1 ml) was added for 3 minutes at RT and cells were dislodged by tapping the sides of the flask. Cells were passaged by resuspending in pre-warmed media (5 ml) that was then split at 1:10 into new flasks containing pre-warmed medium (10 ml), twice a week. For protein or RNA extraction, cells were resuspended in 1

ml of chilled lysis buffer or TRizol that was spread across the monolayer with force using a pipette, and a cell scraper was used to aid the removal of cells. Cell lysates were then transferred to a 1.5 ml microfuge tube and placed on ice for immediate downstream processing of protein or RNA, or stored at -80°C.

Murine erythroleukemia (MEL) cells were stored in 1 ml of 90% FBS and 10% DMSO at a density of 1×10^7 cells/ml at -80°C. Cells were quickly thawed by agitation in a 37°C water bath and slowly resuspended and transferred drop by drop into a 15 ml polypropylene tube containing pre-warmed growth medium (5 ml). Growth medium contained high glucose DMEM with sodium pyruvate and glutamate that was supplemented with 10% FBS and 1% penicillin and streptomycin. Cells were centrifuged at 500 g for 3 minutes at RT and resuspended in pre-warmed growth media (1 ml), which was then transferred to a small T25cm³ flask containing pre-warmed medium (14 ml). MEL cells were cultured in suspension in an upright flask and incubated with 5% CO₂ at 37°C. Cells were counted using a Z2 Coulter Counter (Beckman) and seeded at a density of 1×10^6 cells/ml. MEL cells were passaged approximately every two days. To do this, cells were centrifuged at 500 g for 3 minutes at RT, media was aspirated and the cell pellet was resuspended in pre-warmed media (5 ml) that was then split at 1:10 into new flasks containing pre-warmed medium (10 ml). Alternatively, cells were collected for protein or RNA extraction, in which case MEL cells were transferred to a 15 ml polypropylene tube and washed with PBS at 500 g for 3 minutes at RT. For protein or RNA extraction, cells were resuspended in 1 ml of chilled lysis buffer or TRizol and transferred to a 1.5 ml microfuge tube. Cells were then placed on ice for immediate downstream processing of protein or RNA, or stored at -80°C.

4.2.4 Stem cell factor (SCF) stimulation of MEL cells

For stem cell factor stimulation, MEL cells were serum starved for 12 hours and resuspended at a density of 1×10^6 cells in 1 ml of DMEM containing recombinant mouse SCF protein (cat. #: 455-MC, R & D Systems) at 25 and 100 ng/ml. Cell treatments were seeded into a 12-well culture dish and incubated for 15 minutes with 5% CO₂ at 37°C. Treated cell lysates were collected in a 2 ml microfuge tube on wet ice and washed with PBS after centrifugation at 200 g for 3 minutes at 4°C, and cell pellets were stored at -80°C.

4.2.5 Protein extraction, immunoprecipitation and Western blotting

4.2.5.1 Protein extraction

Proteins were extracted in ice-cold lysis buffer (50 mM Tris-Cl, pH 7.5; 150 mM NaCl; 1 mM Na₄P₂O₇; 1 mM Benzamidine; 5 mM Na₃VO₄; 10 mM NaF; 0.5% NP-40). A cocktail of protease inhibitors in the form of a tablet (cat. #: 11836170001, Roche) was freshly added to the lysis buffer. The detergent was omitted from the lysis buffer (i.e., 0.5% NP-40) for immunoprecipitation experiments to retain the native form of a protein. Cells or tissues were homogenised in 500 µl or 1 ml of lysis buffer on ice with a Polytron homogeniser until cells or tissue were fully lysed. Proteins were further solubilised by gentle agitation for 30-60 minutes at 4°C on an orbital shaker. Lysates were pre-cleared of debris by collecting the supernatant after centrifugation at 12,000 rpm for 15 minutes at 4°C. The supernatant containing proteins was transferred into a fresh 1.5 ml microfuge tube on ice. Protein concentrations within a range of 0.2-5 mg/ml were determined using the Direct Detect method (Merck Millipore), which measures the amide bonds in protein chains by infrared spectrometry.

4.2.5.2 Immunoprecipitation

c-Kit protein was enriched by magnetic immunoprecipitation (IP) with a c-Kit Ab conjugated to Magna ChIP Protein A+G Magnetic Beads (cat. #:16-663, Millipore) or PureProteome Protein G Magnetic Beads (cat. #: LSKMAGG02, Millipore). Magna ChIP Protein A+G Magnetic Beads were mostly used for IP.

Beads were washed in ice-cold PBS (500 µl) twice by vortexing and were then placed on a MagnaRack for 1 minute and the supernatant was discarded. To prevent non-specific binding of proteins, lysates (3.5 mg of protein) were pre-cleared with magnetic beads (~100 µl) and lysis buffer (without detergent) making up to 1 ml in a 2 ml tube, which was incubated for 1 hour at 4°C on a rotating wheel. In a second tube, c-Kit Ab (D13A2 or M-14 at 1:50), was bound to pre-coated IgA and IgG beads (~100 µl) by incubating for 1 hour at 4°C on a rotating wheel. To remove excess Ab from the beads, the second tube was placed

on the MagnaRack for 1 minute and washed in ice-cold PBS (500 μ l) twice by vortexing and the supernatant was discarded. The first tube containing the lysate and beads was placed on the MagnaRack for 1 minute and the lysate was transferred to the second tube containing conjugated Ab-beads. c-Kit was then enriched from the lysate using the Ab-beads by gently resuspending and incubating overnight at 4°C. For all IP experiments, the quantity of Ab and beads were used as detailed above, unless otherwise stated in the figure legend.

To elute the bound c-Kit, the lysate and Ab-bead mixture was placed on MagnaRack for 1 minute and the supernatant was removed. The beads were washed (x4) with 500 μ l of NT2 buffer (50 mM Tris-Cl, pH 7.4; 150 mM NaCl; 1 mM MgCl₂; 0.05% IGEPAL) by placing onto the MagnaRack for 1 minute and the supernatant was discarded after each wash. The beads and eluted c-Kit were then finally resuspended in 20 μ l of lysis buffer (with 0.5% NP-40 detergent) and processed as described in the following SDS-PAGE and Western blotting sections.

4.2.5.3 SDS-PAGE and transfer

Laemmli sample buffer (0.35M Tris-Cl pH 6.8, 30% glycerol, 20% SDS, 0.012% bromophenol blue, and 30mM β -mercaptoethanol) was added to protein samples at a 1:6 dilution and proteins were denatured at 95°C for 5 minutes. Denatured protein samples and a 10-250 kDa protein ladder (cat. #: 1610374, Bio-Rad) were separated by size using sodium dodecyl sulphate polyacrylamide gel electrophoresis (SDS-PAGE) using the XCell SureLock Mini-Cell Electrophoresis System (Thermo Fisher). One or two gels were placed in a buffer chamber that was then filled with MOPS buffer or Tris-Acetate buffer depending on the type of gel used. Equivalent volumes of protein samples were loaded onto 4-12% Bis-Tris gels (Thermo Fisher) with MOPS buffer or a 3-8% Tris-Acetate gels (Thermo Fisher) with Tris-Acetate buffer. Electrophoresis was carried out at 180V for ~60-90 minutes at RT.

Proteins were transferred onto polyvinylidene fluoride (PVDF) membranes with transfer buffer at 35V for 90 minutes at RT. Briefly, gels were trimmed and placed onto PVDF membranes cut to size. These were cocooned with two pieces of blotting paper soaked with transfer buffer (10.5% glycine, 2.25% Tris, and 20% methanol) and at least two sponges

soaked with transfer buffer on either side of the gel. Blotting papers were cut slightly larger than the gel and were individually rolled onto sponges to prevent air bubbles. The layering of materials was performed onto an open cassette in the following order: sponges (x2), paper (x2), gel, membrane, paper (x2), and sponges (x4) from cathode to anode. The cassette was closed and placed in a buffer chamber that was then filled with transfer buffer. Transfer was carried out at 35V for ~90 minutes at RT.

4.2.5.4 Western blot

Membranes were blocked for 1 hour at RT or overnight at 4°C with blocking buffer (Tris-buffered saline with 0.1% Tween, TBS-TW, with 5% bovine serum albumin, BSA, or 5% skimmed milk, as per the manufacturer's recommendation for the primary antibody). The use of blocking buffer was important to prevent non-specific binding.

Membranes were incubated with primary antibodies (Table 4.1) that were diluted at 1:1000-1:2000 in blocking buffer for 1 hour at RT or overnight at 4°C on an orbital shaker. Excess primary Ab was removed by washing membranes with TBS-TW in a series of incubations: 10 seconds (x2), 10 minutes, 10 seconds (x2), and 10 minutes, at RT on an orbital shaker.

After the first series of washes, membranes were incubated with species-specific secondary antibodies conjugated to horseradish peroxidase at a 1:5,000-1:20,000 dilution for 1 hour at RT on an orbital shaker. The concentration of the secondary Ab was determined as per the enhanced chemiluminescence (ECL) guidelines. Excess secondary Ab was removed by washing membranes with TBS-TW in a series of incubations: 10 seconds (x2), 10 minutes, 10 seconds (x2) and 10 minutes (using TBS without TW), at RT on an orbital shaker.

Proteins were visualised on the membrane using one of the following ECL kits; Western Lightning Chemiluminescence Reagent Plus (Perkin Elmer), Pierce ECL Plus Western Blotting Substrate (Thermo Fisher), or SuperSignal West Pico Chemiluminescent Substrate (Thermo Fisher), as per manufacturer's recommendations. The chemiluminescent membrane was sealed in a plastic wallet, which was secured onto the bottom of an open Hyperfilm cassette. X-ray film (Hyperfilm ECL, Amersham) was placed on top of the

membrane and the cassette was closed for variable exposure times. Films were developed with a SRX-101A processor (Konica Minolta) in a dark room.

Table 4.1: c-Kit, phospho-c-Kit and GAPDH antibodies

Anti-c-Kit Abs	Company	Type of Ab	Targets
MAB1356	R&D Systems	rat monoclonal	C-terminus
D13A2	Cell Signaling	rabbit monoclonal	Residues surrounding Tyr703
In-house c-Kit ¹	Affinity BioReagents	rabbit polyclonal	Juxtamembrane domain
C-19	Santa Cruz	rabbit polyclonal	C-terminus
M-14	Santa Cruz	goat polyclonal	C-terminus
Phospho-c-Kit (Tyr719)	Cell Signaling	rabbit polyclonal	Phosphorylated tyrosine 719
GAPDH	Cell Signaling	rabbit monoclonal	C-terminus

4.2.5.5 Densitometry of Western blots

ImageJ was used to calculate the number of pixels per c-Kit protein bands or GAPDH protein band from sham and SAC samples. The eluted c-Kit proteins were normalised to GAPDH, which was measured using the IP input to control for IP loading.

¹ This personalised antibody was specifically produced for our laboratory's use by Affinity BioReagents and is denoted here as "In-house c-Kit".

4.2.6 RT-qPCR

To measure the expression of c-Kit mRNA, cDNA was synthesised using the Superscript III First Strand Synthesis System and RT-qPCR was performed using a Taqman assay. The Taqman probes (Applied Biosystems) used were: *Hprt* (Mm01545399_m1, 5'-GGACTGATTATGGACAGGACTGAAA-3'), and *Kit* (Mm00445212_m1, 5'-TTTACGTGAACACAAAACCAGAAAT-3'). *Kit* expression was normalised to the housekeeping gene, *Hprt*.

4.2.7 Immunocytochemistry

Immunostaining of fixed cells secured onto slides was performed as follows. Slides were incubated with blocking buffer (5% goat serum and 0.1% Triton X-100 in PBS; (80 µl per slide) for 1 hour at RT, after which blocking buffer was removed by individually flicking slides. Cells were incubated with primary antibodies diluted in blocking buffer (80 µl per slide) overnight at 4°C. The primary antibodies that were diluted in blocking buffer, included the CM-specific marker, mouse anti-myosin heavy chain (cat. #: ab 50967, Abcam) diluted at 1:800, and, the c-Kit Ab, rabbit anti-c-Kit D13A2 (cat. #: 3074S, Cell Signaling) diluted at 1:600. After overnight incubation, slides were washed in PBS for 5 minutes at RT on an orbital shaker (x5). The following steps were performed in the dark. Cells were incubated for 1 hour at RT with the species appropriate secondary antibodies, goat anti-mouse IgG Alexa Fluor 488 and goat anti-rabbit Alexa Fluor 594, diluted at 1:1000 (80 µl per slide). Cells were washed in PBS for 5 minutes on an orbital shaker (x5). Coverslips were secured onto each slide with hard mounting medium containing DAPI. Slides were then stored at 4°C. Stained cells were imaged with a confocal microscope (Axio Imager microscope equipped with a LSM 700 confocal scan head, Zeiss) using the same settings for all samples.

4.3 Results

4.3.1 Identification of specific anti-c-Kit antibodies for Western blot analyses

Before examining the expression of c-Kit in murine CMs, it was necessary to first identify a suitable Ab for Western blot analyses. c-Kit is comprised of 976 amino acids resulting in an ~110 kDa protein, but due to N-linked glycosylation the mature species migrates by SDS-PAGE fractionation at a relative molecular mass (Mr) between ~145-160 kDa, while the precursor is ~125 kDa (Lennartsson and Ronnstrand, 2012). Thus, c-Kit is expected to appear on a Western blot as two species, corresponding to the mature and immature form.

Five previously reported anti-c-Kit antibodies were sourced to detect c-Kit: MAB1356, D13A2, in-house c-Kit, C-19 and M-14, as outlined in Table 4.1. In addition, immortalised cell lines were obtained as a convenient and abundant supply of negative or positive c-Kit expressing controls. In keeping with the well-known role of c-Kit in cancer, suspension cultures of murine erythroleukaemia (MEL) cells were propagated as c-Kit positive controls (Hino *et al.*, 1995), and HEK293T cells were used as c-Kit negative controls (Tetsu *et al.*, 2010). All five anti-c-Kit antibodies were tested for their specificity and efficacy at detecting c-Kit protein in MEL cell lysates (10 µg) at a dilution of 1:1000 using the same film exposure time (Figure 4.2). D13A2 and M-14 anti-c-Kit antibodies detected two protein bands consistent with the predicted Mr's of c-Kit at ~125 and ~145 kDa. In contrast, MAB1356 and C-19 revealed a number of non-specific bands and failed to detect c-Kit. Finally, our in-house c-Kit Ab that had been previously used to detect the re-expression of c-Kit post-SAC by immunohistochemistry, did not detect c-Kit by Western blotting, most likely because it only detects the native conformation of the receptor. For the two specific antibodies D13A2 and M-14, titration experiments were performed to determine the optimal Ab dilution (Figure 4.2). A final dilution of 1:2000 was found to provide the best signal-to-noise ratio and film exposure time for both D13A2 and M-14.

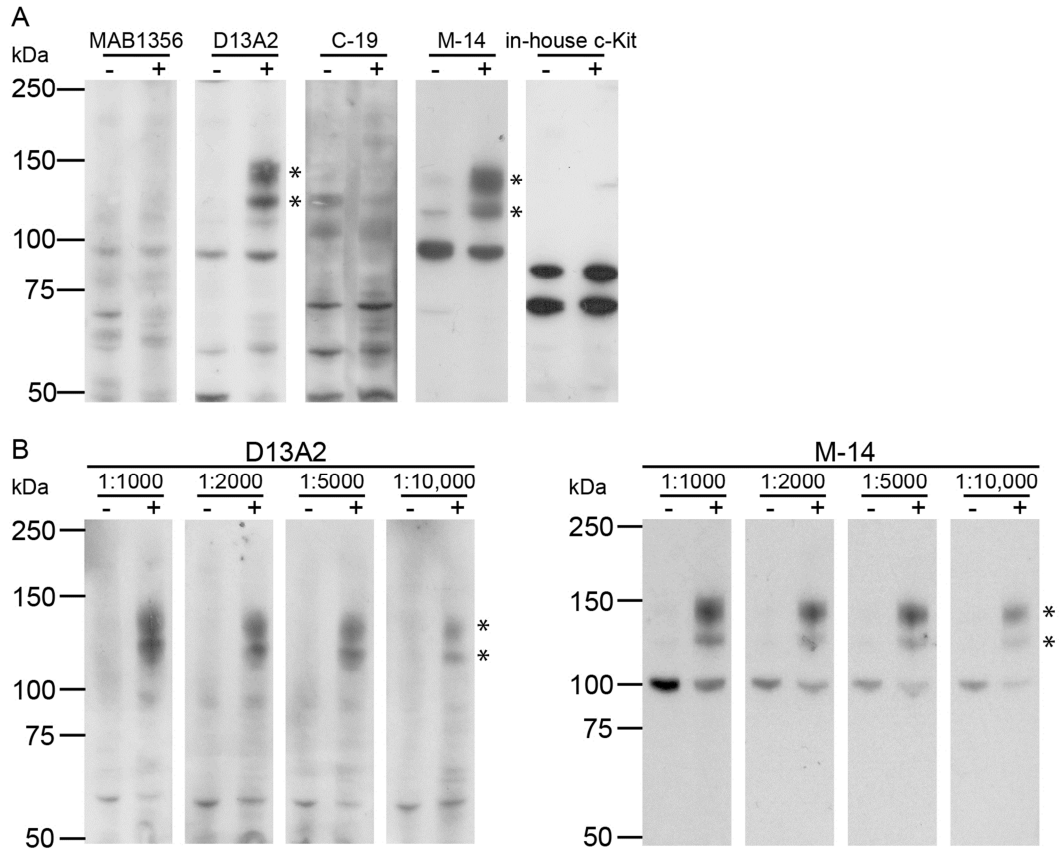


Figure 4.2: Western blot analyses to determine the specificity of c-Kit antibodies
 A, HEK293T or MEL cell lysates (10 μ g) served as negative and positive control cell lines for c-Kit expression, respectively, and were incubated with five reported c-Kit antibodies at a dilution of 1:1000. Membranes incubated with MAB1356, D13A2 or C-19 were blocked with 5% BSA, while membranes incubated with M-14 or in-house antibodies were blocked with 5% skimmed milk. All films were exposed for 30 minutes. B, HEK293T (-) or MEL (+) lysates (10 μ g) were probed with two c-kit antibodies at increasing dilutions: 1:1000, 1:2000, 1:5000 or 1:10,000. * indicates c-Kit species at 125 and 145 kDa.

4.3.2 Characterisation of c-Kit expression in MEL cells and in three cardiac-specific c-Kit transgenic mouse lines

The specific c-Kit antibodies, D13A2 and M-14, were then tested for their ability to detect c-Kit in whole heart tissue lysates from wild-type (WT) and Tg(α MHC-*Kit*^{Wv}) mice, including the cell line controls. D13A2 and M-14 detected two bands corresponding to the mature and immature forms of c-Kit in Tg(α MHC-*Kit*^{Wv}) heart tissue and in MEL cells (Figure 4.3A). As expected, Tg(α MHC-*Kit*^{Wv}) heart lysates had a greater abundance of c-Kit protein than MEL cells and more of the immature form of c-Kit was detected in Tg(α MHC-*Kit*^{Wv}) samples. Note that a longer film exposure time was necessary for D13A2 to display similar band intensities as M-14, suggesting that M-14 is the more sensitive Ab for Western blot analysis. Moreover, the expression of c-Kit mRNA (Figure 4.3B) was markedly higher by 2,000-fold in Tg(α MHC-*Kit*^{Wv}) hearts compared with an eight-fold increase in MEL cells, relative to WT hearts, corroborating the protein expression data. c-Kit protein was not detected by Western blot analysis in HEK293T cells or in WT heart tissue.

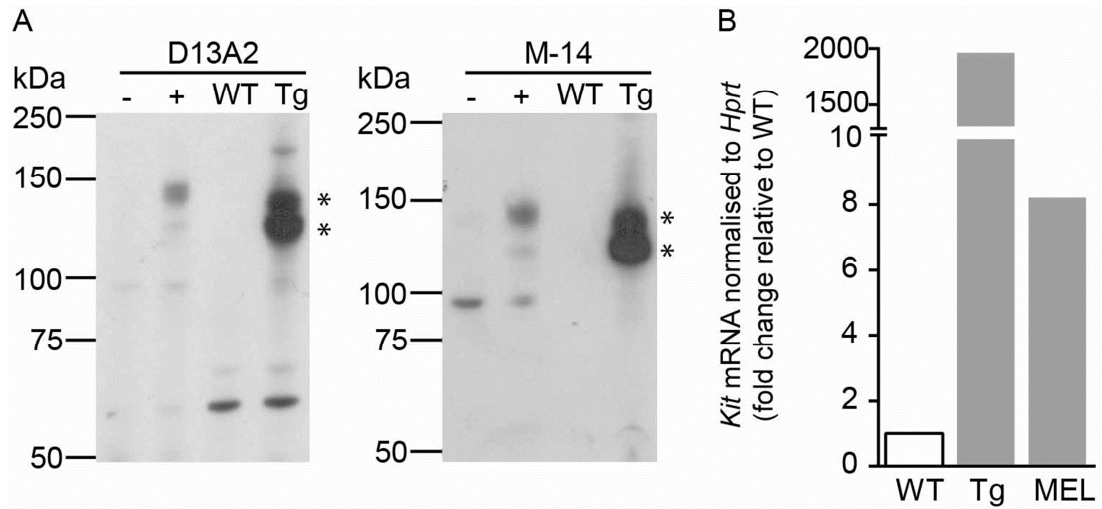


Figure 4.3: Characterisation of c-Kit expression in HEK293T and MEL cells, and in WT and Tg(α MHC-*Kit*^{Wv}) hearts

A, HEK293T or MEL cell lysates, and wild-type (WT) or Tg(α MHC-*Kit*^{Wv}) heart tissue lysates (10 μ g) were separated by SDS-PAGE, transferred to membranes, and membranes were probed with anti-c-Kit antibodies at a dilution of 1:2000. D13A2 and M-14 films were exposed for 10 minutes and 3 minutes, respectively. * indicates detection of c-Kit isoforms at 125 and 145 kDa. B, relative quantification of *Kit* was normalised to *Hprt* in WT or Tg(α MHC-*Kit*^{Wv}) hearts, or in MEL cells, relative to WT (n= 1). *Kit* encodes c-Kit and *Hprt* encodes HPRT.

Immunocytochemistry staining of MEL cells using D13A2 showed c-Kit was localised at the cell membrane (not shown). Staining of HEK293T cells (not shown) and WT CMs (Figure 4.4) failed to detect c-Kit. Interestingly, c-Kit localisation was subcellular in the perinuclear region in Tg(α MHC-*Kit*^{Wv}) CMs (Figure 4.4). This patterning, together with the predominance of the smaller immature species of c-Kit in Tg(α MHC-*Kit*^{Wv}) CMs (determined by Western blot analysis in Section 4.3.1) suggests the c-Kit^{Wv} protein may be misfolded, and, as a consequence, remains trapped in the endoplasmic reticulum or Golgi apparatus (Zheng *et al.*, 2014; Yang *et al.*, 2015). Note, M-14 was not a suitable Ab for detecting native c-Kit protein by immunocytochemistry.

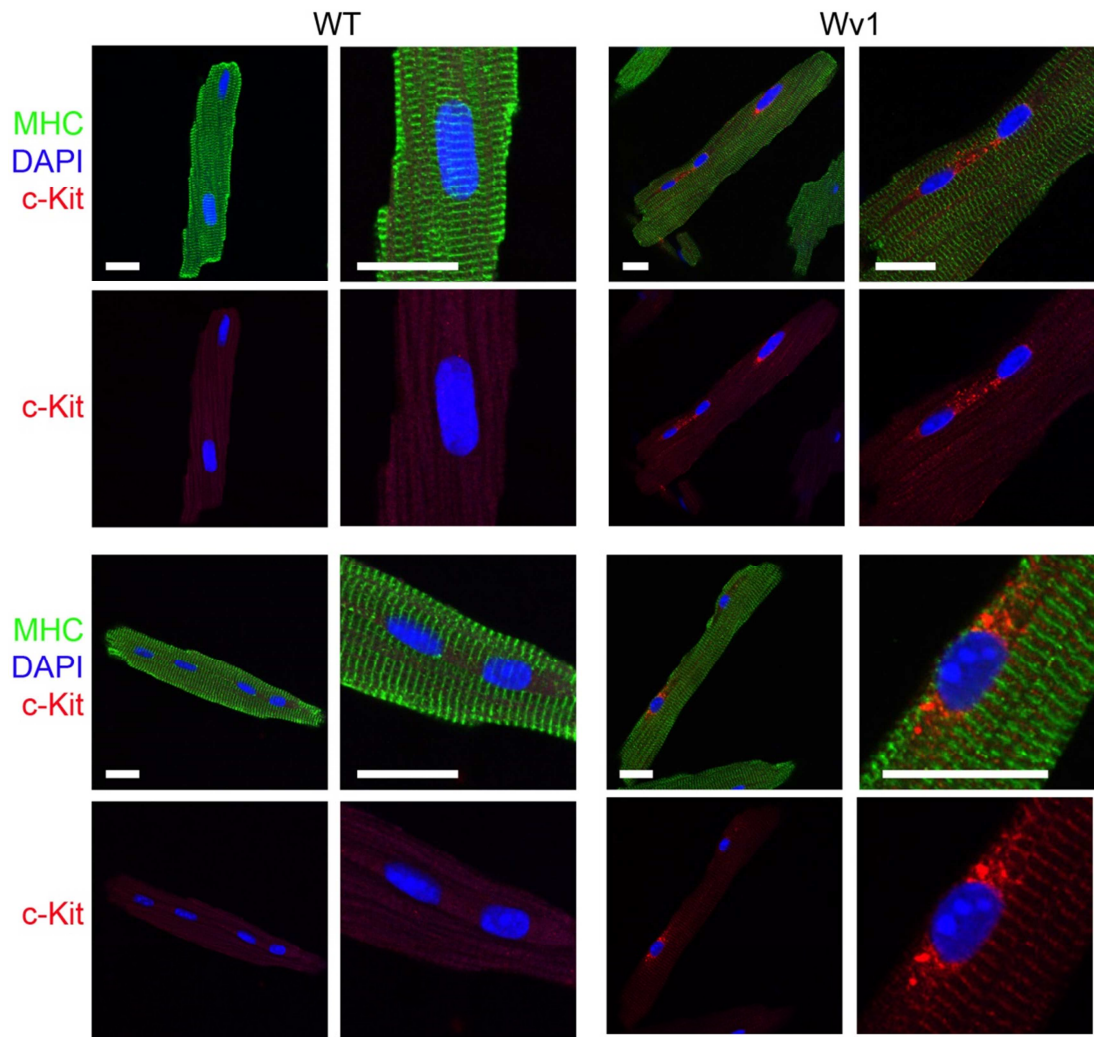


Figure 4.4: Characterisation of c-Kit expression in WT and Tg(α MHC-*Kit*^{Wv}) CMs

Representative confocal images of WT and Tg(α MHC-*Kit*^{Wv}) CMs co-stained with the CM-specific marker, myosin heavy chain (MHC, green), c-Kit with the D13A2 Ab (red), and DNA with DAPI (blue). Scale bar is 20 μ m.

M-14 and D13A2 were further tested for their specificity of c-Kit protein expression in heart lysates prepared from three c-Kit transgenic mouse lines [Tg(α MHC-*Kit*^{Wv}), Tg(α MHC-*Kit.1*) and Tg(α MHC-*Kit.2*)] and compared with WT mice (Figure 4.5). Interestingly, Western blot analyses revealed the following: (1) both M-14 and D13A2 detected the same c-Kit protein species, (2) M-14 has a greater affinity for the denatured linear c-Kit antigen than D13A2, thus producing a greater signal despite a much lower film exposure time (10 seconds vs 3 minutes, respectively), (3) comparatively, the relative abundance of c-Kit protein was: Tg(α MHC-*Kit*^{Wv}) > Tg(α MHC-*Kit.1*) > Tg(α MHC-*Kit.2*), in heart lysates, (4) the ratio of mature to immature c-Kit forms was greater in Tg(α MHC-*Kit.1*) and Tg(α MHC-*Kit.2*) compared with Tg(α MHC-*Kit*^{Wv}) hearts; the latter showing a higher expression of the immature c-Kit species, (5) c-Kit was not detected in WT heart lysates (50 μ g) with either Ab. The increased abundance of the immature c-Kit^{Wv} species in Tg(α MHC-*Kit*^{Wv}) relative to Tg(α MHC-*Kit.1*) and Tg(α MHC-*Kit.2*) hearts indicates an inability of the cell to properly process the c-Kit^{Wv} mutant protein during biosynthesis. These findings, therefore, reveal differential patterns of expression of c-Kit protein between WT mice, and transgenic mice overexpressing c-Kit or c-Kit^{Wv}. This likely reflects the altered biosynthesis and processing of c-Kit protein that is dependent on the transgene.

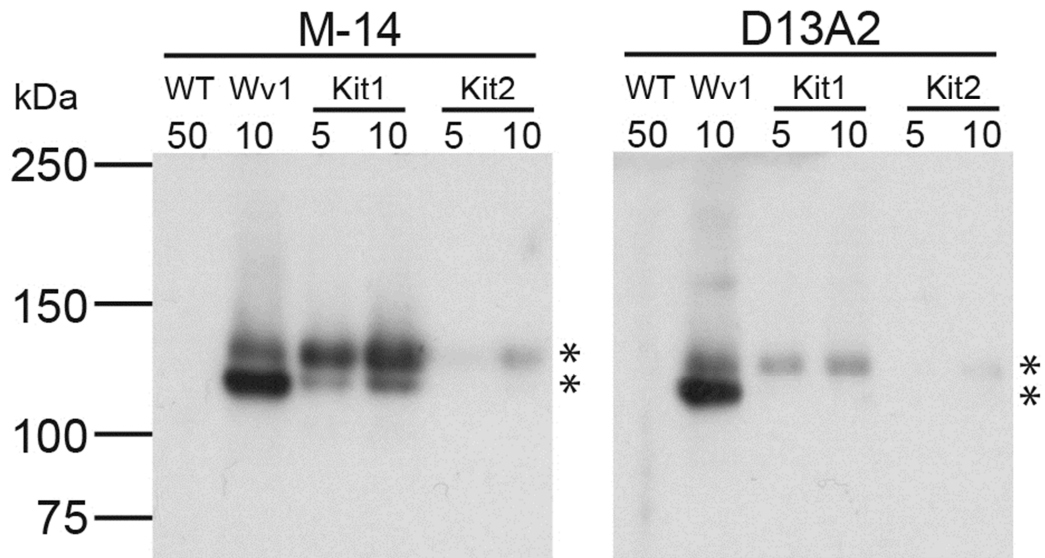


Figure 4.5: Characterisation of c-Kit expression in WT, Tg(α MHC-Kit^{Wv}), Tg(α MHC-Kit.1) and Tg(α MHC-Kit.2) transgenic mouse models

Wild-type (WT, 50 μ g), Tg(α MHC-Kit^{Wv}) (Wv1, 10 μ g); Tg(α MHC-Kit.1) (Kit1, 5 and 10 μ g), and Tg(α MHC-Kit.2) (Kit2, 5 and 10 μ g) heart lysates were separated by SDS-PAGE and c-Kit abundance detected using M-14 or D13A2 (1:1000) primary c-Kit antibodies. Membranes were probed with secondary antibodies at a dilution of 1:4000. Films for M-14 or D13A2 probed membranes were exposed for 10 seconds or 3 minutes, respectively. * indicates c-Kit species at 125 and 145 kDa.

4.3.3 Characterisation of c-Kit expression in the WT heart and in CMs

Given that our hypothesis was that c-Kit is re-expressed in the adult heart after hypertensive stress, it was important to establish the baseline abundance of c-Kit in the adult heart under normal physiological conditions in order to report a fold-increase. A low level of c-Kit should be detected in WT hearts, but not in adult CMs, because c-Kit is expressed by several other cell types in the heart, including adult CSCs, however, c-Kit was not detected in the small amount of heart lysate used for previous Western blots, as shown in Section 4.3.2. Therefore, to increase the sensitivity of c-Kit detection, c-Kit was immunoprecipitated from heart lysates before Western blotting and more sensitive ECL detection systems were sought.

The chemiluminescence kit, Western Lightning ECL, had been previously used to visualise proteins for Western blotting studies. Two alternative ECL kits were sourced for comparison: SuperSignal West Pico and Pierce ECL Plus; these allow for weaker dilutions of the HRP-conjugated secondary Ab compared with the original kit (at dilutions of 1:20,000 and 1:25,000, respectively, vs 1:5,000 using the Western Lightning kit). WT and Tg(α MHC-*Kit*^{Wv}) heart lysates were probed with the anti-c-Kit Ab, M-14, and both the SuperSignal West Pico and the Pierce ECL Plus markedly enhanced the detection of c-Kit (Figure 4.6A). Pierce ECL Plus was the most effective of all three kits. Nonetheless, c-Kit was still not detectable in WT heart lysates even when loading the maximum amount of protein sample per lane (100 μ g).

Since the amount of protein that can be loaded into a lane for Western blot analysis is limited, immunoprecipitation (IP) was employed to enrich for c-Kit from heart lysates using magnetic beads conjugated to an anti-c-Kit Ab. IP conditions were first optimised using Tg(α MHC-*Kit*^{Wv}) heart lysates as a positive control. c-Kit was immunoprecipitated from Tg(α MHC-*Kit*^{Wv}) heart lysates with either M-14 or D13A2 conjugated to Magna ChIP Protein A+G Magnetic Beads (Figure 4.6B). M-14 was more effective at enriching for c-Kit than D13A2, as demonstrated by the greater abundance of eluted c-Kit relative to IP input. Furthermore, given that M-14 is a goat polyclonal IgG Ab and Protein G beads are designed for binding IgG proteins, the M-14 Ab was tested with either Magna ChIP Protein A+G Magnetic Beads or PureProteome Protein G Magnetic Beads for IP and compared for their efficiency to pull down or elute c-Kit (Figure 4.6C). More c-Kit was eluted using the M-14 Ab conjugated to Magna ChIP Protein A+G Magnetic Beads. Thus, the combination of Magna ChIP Protein A+G Magnetic Beads conjugated to M-14, and Pierce ECL Plus, were determined as the optimal conditions for detecting c-Kit by Western blot in Tg(α MHC-*Kit*^{Wv}) heart lysates.

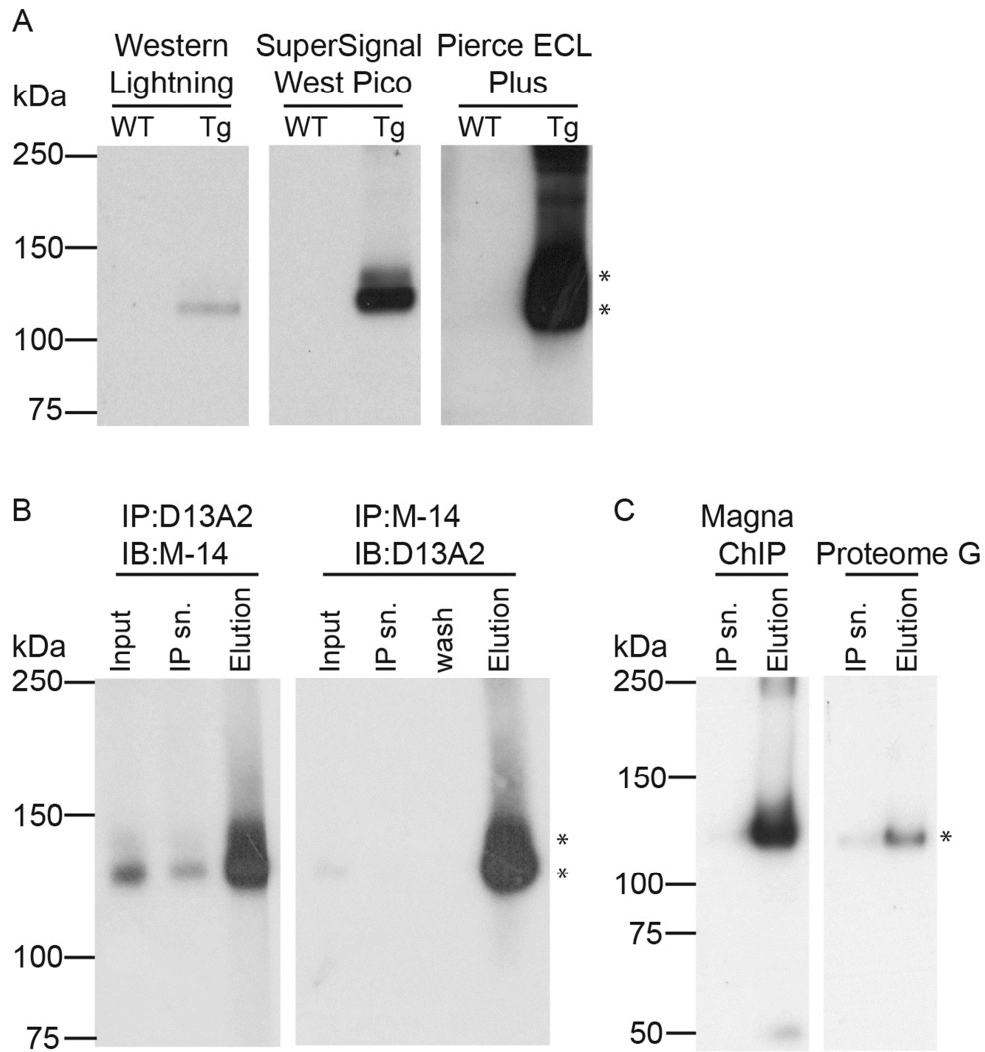


Figure 4.6: Western blotting and immunoprecipitation conditions were optimized to improve the detection of c-Kit protein

A, WT and Tg(α MHC-*Kit*^{Wv}) heart lysates (100 and 20 μ g, respectively) were separated by SDS-PAGE and c-Kit protein was detected with the M-14 Ab (diluted at 1:1000). The secondary Ab was diluted as per manufacturer's recommendations for each ECL kit, at 1:5,000 for Western Lightning, and at 1:25,000 for SuperSignal West Pico and Pierce ECL Plus. Films were exposed for 1 second. B, Tg(α MHC-*Kit*^{Wv}) heart lysates (400 μ g) were used for immunoprecipitation (IP) followed by size-fractionation and immunoblotting (IB). IP was performed using Magna ChIP beads (200 μ l) conjugated to either D13A2 or M-14 (1:50). The IP input and supernatant (sn.), and eluted c-Kit, were separated by SDS-PAGE and c-Kit abundance detected with M-14 (1:1000) or D13A2 (1:500). Films were exposed for 1 minute. C, Tg(α MHC-*Kit*^{Wv}) heart lysates (100 μ g) were used for IP followed by IB to detect c-Kit. IP was performed using Magna ChIP or PureProteome Protein G beads (20 μ l) conjugated to M-14 (5 μ l). The IP supernatant (sn.) and eluted c-Kit were separated by SDS-PAGE and c-Kit protein was detected using D13A2 (1:1000). Films were exposed for 1 second. * indicates c-Kit species at 125 and 145 kDa.

To test if c-Kit could be detected in WT hearts, lysates were processed using these optimised IP and IB techniques. Under these conditions, a robust c-Kit signal was observed at the expected molecular weights of 125 and 145 kDa in adult WT heart lysates (Figure 4.7). During the tissue solubilisation procedure, a substantial insoluble pellet was noticeable after homogenisation and centrifugation, and for this reason, an additional sonication step was incorporated to further solubilise proteins. WT heart lysates were then placed on gentle agitation for ~40 minutes at 4°C, and after centrifugation, an insoluble pellet was no longer visible and there was a marked increase in protein yield (post-sonication, 19 mg vs pre-sonication, 5.5 mg). This resulted in a greater elution of c-Kit protein (Figure 4.7).

To establish the baseline level of c-Kit protein in adult WT CMs, which was important to determine the fold-change in c-Kit expression after hypertensive stress, c-Kit was detected in WT CMs. CMs were isolated using the O'Connell *et al.* (2007) and enriched for by low-speed centrifugations, lysed by homogenisation and sonication, followed by gentle agitation for ~40 minutes at 4°C on an orbital shaker to further solubilise proteins. Cell lysates (1 mg or 2 mg, out of a total of 3 mg) were immunoprecipitated, however, despite using these carefully optimised conditions, c-Kit with a Mr of either 125 or 145 kDa was not detected in the WT CM-enriched fraction, shown in Figure 4.7. Thus, these results indicate that in agreement with the same findings of others, the expression of c-Kit in WT CMs is either extremely low or absent.

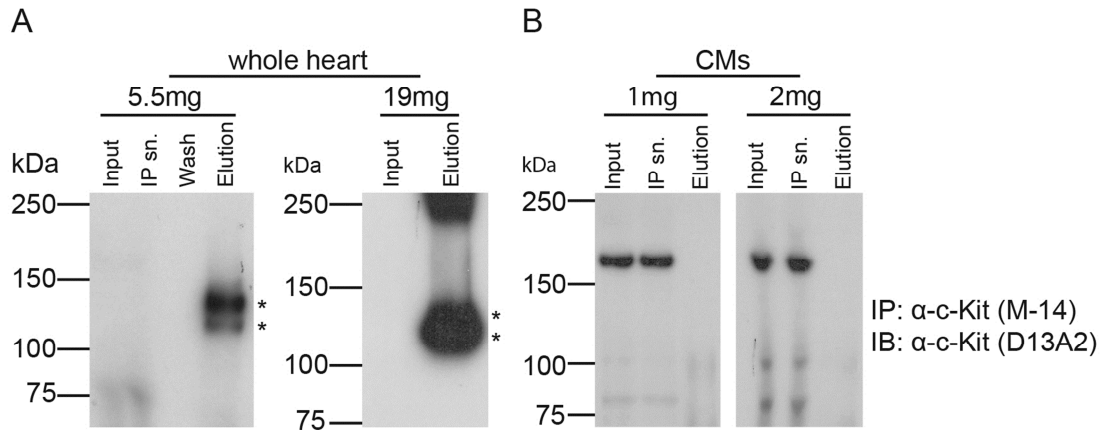


Figure 4.7: Characterisation of c-Kit in WT hearts and in CMs

A, WT whole heart (5.5 and 19 mg of protein) and B, CM-enriched fractions (1 mg and 2 mg) of lysates were subjected to IP and c-Kit was detected by IB. IP was performed using Magna ChIP beads conjugated to M-14. IP input and supernatant (sn.), wash, and elution, were separated by SDS-PAGE and c-Kit protein was detected using the D13A2 Ab (1:1000). Films for whole heart and CM-enriched fractions were exposed for 1 second and 10 minutes. * indicates c-Kit isoforms at 125 and 145 kDa.

4.3.4 c-Kit expression following SAC

To test the hypothesis that c-Kit is re-expressed in WT CMs after SAC-induced LVH, c-Kit protein levels were evaluated in enriched-CM fractions from sham- and SAC- operated hearts collected in cohort 2 (see Section 3.2.4 and 4.2.2). There was a robust elevation in SBP of 44 mmHg post-SAC (150 ± 14 SD mmHg, $n= 6$) relative to shams (106 ± 14 SD mmHg, $n=7$), and these CM samples were used in Figure 4.8 to detect c-Kit protein and mRNA. Micromanometry data were collected for all sham- operated mice, however, three animals had blood pressure traces that were obscured and could not be analysed, likely due to technical issues at the time of recording. Regardless, all sham- operated mice were included in this study. The amount of CM protein lysate used for the IP input was 3.5 mg (Figure 4.8A), which was the maximum protein yield that could be obtained from every SAC sample ($n= 6$), but in some cases two sham samples were combined to yield 3.5 mg ($n= 10$). Because c-Kit protein was not detected in WT CM-enriched fractions shown previously (see Figure 4.7B), the concentration of the secondary Ab was increased from

1:20,000 to 1:10,000 to boost the chemiluminescence signal. Nonetheless, c-Kit protein levels (normalised to GAPDH) were low and variable across sham and SAC CM samples (Figure 4.8A). Thus, the expression of c-Kit protein was not statistically significant between groups, as quantified by densitometry (Figure 4.8B).

c-Kit mRNA levels were also measured in the LV and in CMs post-SAC (Figure 4.8C). The LVs that were used in Figure 4.8C and collected in cohort 1 (see Section 3.2.1 and 4.2.2), had displayed a significant elevation in SBP of 46 mmHg post-SAC (156 ± 5 SD mmHg, n= 5) relative to shams (110 ± 2 SD mmHg, n= 7). Likewise, enriched-CM fractions that were used in Figure 4.8C and collected in cohort 2 (see Section 3.2.1 and 4.2.2), also had a robust elevation in SBP of 45 mmHg post-SAC (152 ± 13 SD mmHg, n= 8) relative to shams (107 ± 13 SD mmHg, n= 7). Although there was a trend towards an increase in c-Kit mRNA in both the LV and CMs post-SAC, neither reached a level of significance.

Furthermore, LV sections and isolated CMs were evaluated for c-Kit expression by confocal microscopy post -sham or -SAC surgery by immunohistochemistry and immunocytochemistry, respectively. Samples were co-stained with the CM-specific marker, myosin heavy chain Ab, and with the c-Kit Ab, D13A2, however, c-Kit was not detected in CMs post-SAC (data not shown).

Together, these results indicate that c-Kit expression is very low in CMs after PO and do not support the preliminary data that c-Kit is re-expressed in WT CMs after SAC-induced LVH.

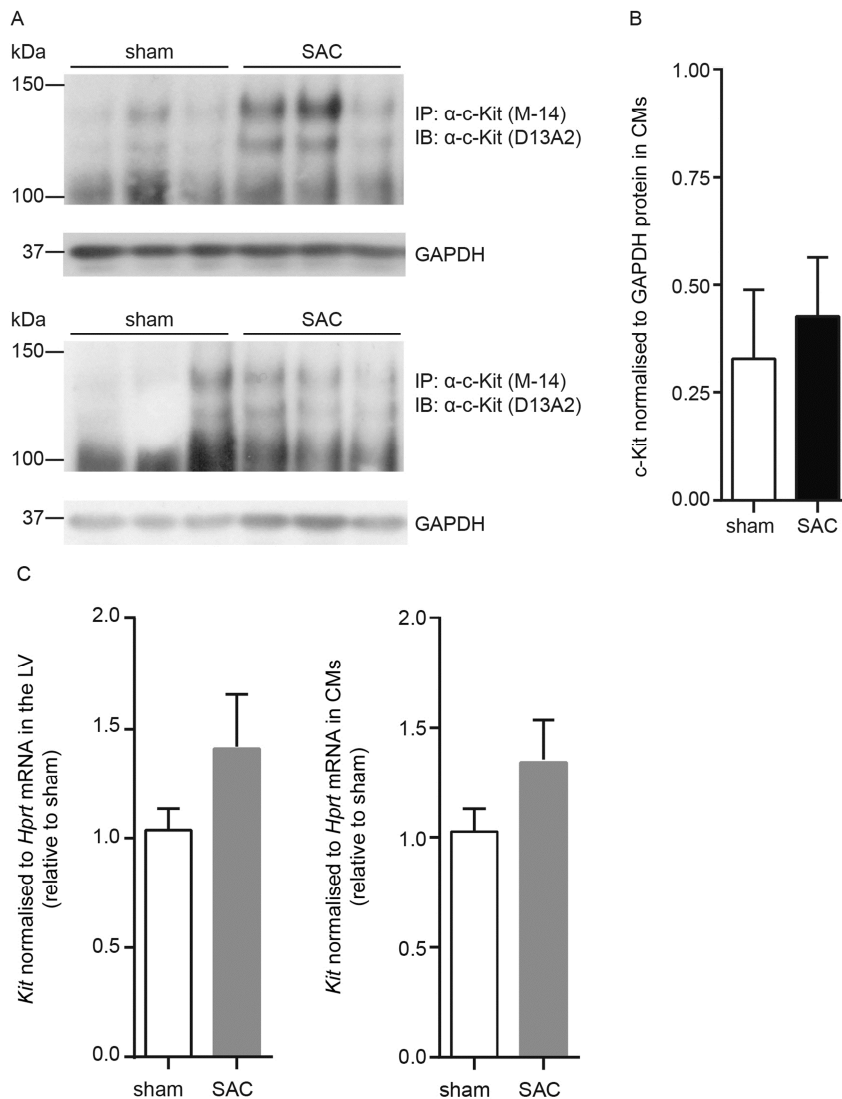


Figure 4.8: Characterisation of c-Kit in WT CMs and in LVs one week post -sham or -SAC surgery

A, WT CM lysates (3.5 mg) from C57BL/6J adult male mice (9-week old) one week post –sham or –SAC surgery (n=6) were used to detect c-Kit protein after immunoprecipitation (IP) and immunoblotting (IB). IP was performed using Magna ChIP beads conjugated to the c-Kit Ab, M-14. The elution was separated by SDS-PAGE and c-Kit was detected using the c-Kit Ab, D13A2 (1:1000). The secondary Ab was diluted at 1:1000 and c-Kit was detected with Pierce ECL Plus. Films were exposed for 10 minutes. B, c-Kit and GAPDH protein from the IBs produced in A were quantified by densitometry. C, WT LVs (sham=7; SAC= 5) and CM-enriched fractions (sham= 7; SAC= 8) from C57BL/6J adult male mice one week post –sham or –SAC surgery were used to detect the relative expression of *Kit* mRNA (normalised to *Hprt*). *Kit* encodes c-Kit and *Hprt* encodes HPRT. Data are presented as means \pm SEM, independent comparisons were made by two-tailed Student’s unpaired *t*-tests.

4.3.5 SCF stimulation of mature c-Kit in MEL cells

One of the original aims of this study was to test if c-Kit signalling, and thus activity, prevents CM cell cycle re-entry and confines CMs to a hypertrophic response. Therefore, concurrent with the experiments to detect c-Kit protein post-SAC, a protocol to detect c-Kit signalling was established using MEL cells were stimulated with SCF at 0, 25 or 100 ng/ml for 15 minutes. Lysates were immunoprecipitated with M14, proteins separated by SDS-PAGE and membranes were probed with an anti-phospho-c-Kit-antibody (Tyr719) to detect c-Kit phosphorylation at tyrosine 719, located in the kinase insert region, which is critical for c-Kit signalling. The mature form of c-Kit became phosphorylated when MEL cells were treated with the ligand SCF at either 25 or 100 ng/ml (Figure 4.9), confirming reports that the larger c-Kit species, expressed at the cell surface, is necessary for ligand-induced dimerization and c-Kit activity.

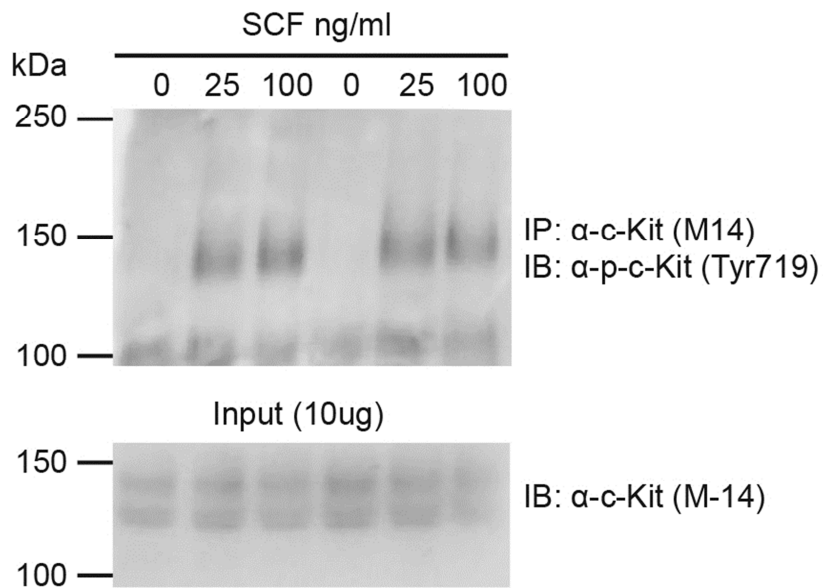


Figure 4.9: Detection of c-Kit activity after SCF stimulation of MEL cells

MEL cells (1×10^6 cells) were stimulated with SCF (0, 25, and 100 ng/ml) for 15 minutes, and cell lysates were immunoprecipitated (IP), and c-Kit phosphorylation (above) and protein (below) were detected by immunoblotting (IB). IP was performed using Magna ChIP beads conjugated to M-14. The eluted c-Kit and IP input (10 μ g) were separated by SDS-PAGE and c-Kit phosphorylation was detected by IB using the phospho-c-Kit (Tyr719) Ab (1:1000) and c-Kit was detected using D13A2 Ab (1:1000), respectively. Films were exposed for 1 second.

4.4 Discussion

This study showed that c-Kit is expressed at very low levels in adult WT CMs and does not increase in response to PO. The evidence, therefore, does not support the hypothesis that c-Kit re-expression and signalling is involved in the pathogenesis of LVH, inhibiting CM cell cycle re-entry, and thus, limiting the heart to hypertrophic growth.

Examining c-Kit expression in the adult WT heart required the optimisation of Western blotting and IP techniques, in which c-Kit⁺ cell and mouse line controls were used. c-Kit was not initially detected in WT heart lysates (100 µg of protein) by IB alone, but by increasing the total amount of protein that could be probed by IP with a c-Kit Ab, two c-Kit species were clearly observed (Figure 4.7). However, c-Kit was not detected in WT CM lysates (1 or 2 mg of protein), although a low level of c-Kit was detected in sham and SAC CM lysates (3.5 mg of protein), with enhanced chemiluminescent signal by increasing the concentration of the secondary Ab (from 1:20,000 to 1:10,000) and length of film exposure upto 10 minutes (Figure 4.8). Thus, despite using optimised techniques, the relative abundance of c-Kit protein one week post –sham or –SAC surgery did not change, and nor did the expression of *Kit* mRNA, in response to PO-induced LVH. To my knowledge, this is one of the first studies to show a lack of c-Kit expression in adult WT CMs at baseline and after LVH.

In support of this data, two elegant studies were published during the course of my candidature using a Cre-lox recombination strategy for genetic lineage tracing of the *Kit* locus in mice, which showed that c-Kit, detected by immunofluorescence, was minimally expressed in adult CMs before and after cardiac injury (van Berlo *et al.*, 2014; Sultana *et al.*, 2015; Liu *et al.*, 2016b). Furthermore, in contrast to Li *et al.* (2008) who reported c-Kit in P2 CMs, van Berlo *et al.* (2014) observed c-Kit⁺ cells were rarely CMs at P0-P1, and rather, they were non-myocytes (van Berlo *et al.*, 2014), which were specifically shown to be ECs by immunohistochemical analyses using the EC-specific marker, PECAM (Sultana *et al.*, 2015). This was different to the previous reports of others showing c-Kit⁺ cardiac stem and progenitor cells at this time point (Fransoli *et al.*, 2008; Tallini *et al.*, 2009). As reported by van Berlo *et al.* (2014) the cell size of non-myocytes and CMs at this age is similar and it is difficult to distinguish between cell types by immunohistochemistry. Although c-Kit expression was not assessed during development in this Chapter, high-throughput

sequencing data in Chapter 7 (see Section 7.3.6) showed expression levels of *Kit* mRNA very low in developing and adult CMs.

In adult hearts, flow cytometric analyses indicated that 77% of c-Kit⁺ cells were ECs (van Berlo *et al.*, 2014) and 43% of ECs were c-Kit⁺ (Sultana *et al.*, 2015). Moreover, the ECs that were generated from c-Kit⁺ cells doubled in number after MI (van Berlo *et al.*, 2014). Sultana *et al.* (2015) and colleagues used a similar lineage tracing strategy with the addition of an EC reporter mouse, Tie2^{Cre}, which was used to demonstrate that c-Kit⁺ cells were derived from an EC lineage, and furthermore, after 30 days of MI surgery the c-Kit⁺ cells had retained their EC identity in the infarct region. The overall consensus was that <0.04% of CMs were derived from c-Kit⁺ cells during development and in adulthood, and did not increase after MI (van Berlo *et al.*, 2014; Sultana *et al.*, 2015). The finding that a subpopulation of ECs are c-Kit⁺ and were not CSCs, is contrary to papers that previously identified c-Kit⁺ CSCs in the heart (Beltrami *et al.*, 2003; Ellison *et al.*, 2013; Fransioli *et al.*, 2008), adding further controversy as to the origin of c-Kit⁺ cells and their ability to form CMs. In this study, c-Kit protein was observed in WT hearts (Figure 4.7), and at very low and variable levels in enriched-CM fractions one week post –sham and –SAC surgery (Figure 4.8), while the former is likely due to the presence of other c-Kit⁺ cells in the heart, the latter is may be due to EC-contamination in the enriched-CM fractions (Figure 6.3, Chapter 6).

The hypothesis that c-Kit is re-expressed in CMs after PO and blocks CM cell cycle re-entry, offered a potential mechanism for c-Kit function that would explain the CM proliferation observed in Kit^{W/W^v} and in Tg(α MHC-*Kit*^{W^v}) hearts, post-SAC. The work described here has shown that c-Kit is not expressed in developing CMs, and therefore, is not “re-expressed” or expressed in adult WT CMs after PO. In the Kit^{W/W^v} mouse model, both the Kit^W and Kit^{W^v} mutations are under the control of the endogenous *Kit* locus, so it is unlikely that c-Kit, Kit^W or Kit^{W^v}, will be expressed in the adult CMs of these mice after PO. While it is also unlikely that c-Kit will be expressed from the *Kit* locus in the Tg(α MHC-*Kit*^{W^v}) mouse, there is constitutive overexpression of the transgene, Kit^{W^v}, under the control of the α -MHC promoter. Another indication that c-Kit is not a common mechanism for cell cycle re-entry in both mouse models is the vastly different CM transcriptomes of Kit^{W/W^v} or Tg(α MHC-*Kit*^{W^v}) at baseline, relative to WT littermate controls. Kit^{W/W^v} CMs had a

difference of 8 unrelated differentially expressed-mRNAs out of 40,000 compared with WT CMs (Li *et al.*, 2008), whereas there were >340 differentially expressed-mRNAs in Tg(α MHC-Kit^{Wv}) CMs relative to WT CMs (unpublished data). The combination of differences in these genetic mouse models and basal gene expression data indicate a highly dissimilar CM phenotype, and therefore, presumably, the mechanisms for CM proliferation after PO are distinct.

Hara *et al.* (2002) subjected Kit^{W/Wv} mice to mild PO by SAC for 15 weeks and reported cardioprotective effects abrogating cardiac remodelling and perivascular fibrosis that were attributed to a deficiency in mast cells. However, the contribution of CM proliferation to this cardioprotective effect was not evaluated. Nevertheless, Hara *et al.* (2002) offer another indirect mechanism for the cardioprotective effect observed in Kit^{W/Wv} mice that may also promote CM cell division. Indirect mechanisms of action may well be a source for cardiac regeneration since a number of physiological processes are impaired in the Kit^{W/Wv} mice, including hematopoiesis and the immune response, in which tissue mast cells are absent. Altogether, the original finding by Li *et al.* (2008) of CM proliferation in Kit^{W/Wv} mice after hypertensive stress is impressive but the mechanism is yet to be elucidated.

Further characterisation in our laboratory of Tg(α MHC-Kit^{Wv}) mice revealed that they had increased cardiac growth during postnatal development from P10 to P35, which was due to an increase in CM population number during adolescence relative to WT hearts (Iismaa *et al.*, submitted). However, adult Tg(α MHC-Kit^{Wv}) CMs had only slightly increased cell cycling relative to WT CMs (Iismaa *et al.*, submitted). Biochemical analyses in this study, showed that Tg(α MHC-Kit^{Wv}) hearts had high levels of c-Kit mRNA and protein compared with WT hearts (Figure 4.3). In addition, the 125 kDa immature species was more abundant than the 145 kDa mature protein in Tg(α MHC-Kit^{Wv}) hearts. This was in contrast to that observed in WT (Figure 4.7), Tg(α MHC-Kit.1) and Tg(α MHC-Kit.2) hearts (Figure 4.5), in which the larger c-Kit species was more abundant. Immunofluorescence showed that Kit^{Wv} localisation was perinuclear in isolated Tg(α MHC-Kit^{Wv}) CMs (Figure 4.4) and was not expressed at the cell surface, suggesting the entrapment of the Kit^{Wv} mutant in the endoplasmic reticulum (ER) or Golgi apparatus (Zheng *et al.*, 2014; Yang *et al.*, 2015). This is not without precedence, as the missense c-Kit^{W37} mutation has been reported to result in a greater abundance of the smaller c-Kit species, also detected by IB, and was also suggested

to accumulate in the ER of mast cells (Nocka *et al.*, 1990). The high level of mutant Kit^{Wv} protein that is overexpressed in Tg(α MHC-Kit^{Wv}) CMs may result in aggregates of the misfolded protein in the ER, and lead to aberrant processing, degradation, and ER stress. This may elicit the unfolded protein response (UPR) pathway, which is protective, but under prolonged stress may become pro-apoptotic (Chaudhari *et al.*, 2014). The mutant Kit^{Wv} protein may also be contained within the Golgi apparatus, as it is expressed in a similar pattern to that of the Golgi matrix protein, GM130 (Yang *et al.*, 2015). Altogether, the ER and Golgi may be involved in the processing and degradation of mutant Kit^{Wv} protein, however, staining Tg(α MHC-Kit^{Wv}) CMs with c-Kit with ER or Golgi markers for immunocytochemistry will be required to confirm its co-localisation with these organelles.

Microarray analyses performed by our laboratory using RNA extracted from baseline untreated WT or Tg(α MHC-Kit^{Wv}) CMs has revealed >340 statistically significant (>2-fold, $p < 0.05$) differentially-expressed mRNAs (unpublished observations). Interestingly, some of these up-regulated transcripts are involved in the immune (interferons and histocompatibility complexes) and ER stress response (*Eif2ak2*, *ATF5* and *CHOP/Gadd153*), protein ubiquitylation and degradation (*Usp18*, *Ube1*, and *COP9*) (Teske *et al.*, 2013; Ghigo *et al.*, 2014). Chronic ER stress evokes an inflammatory response through UPR pathways (Chaudhari *et al.*, 2014) and immune cells are mobilised to remove apoptotic and infected CMs (Ghigo *et al.*, 2014). To restrict the number of infiltrating immune cells, CMs secrete the macrophage-inhibiting cytokine 1 (GDF-15), the transcript for which was ~18-fold higher in Tg(α MHC-Kit^{Wv}) vs WT CMs (unpublished observations). There are many pathways involved in ER stress and the resulting cascade of activated stress-induced pathways involves many genes (Teske *et al.*, 2013). A recent report showed that when pancreatic β -cells increase the synthesis of proinsulin in response to high glucose, the UPR response is activated, which triggers β -cell proliferation (Sharma *et al.*, 2015). It is possible that the UPR may be balancing pro-survival and pro-apoptotic pathways involving ER stress-induced inflammation that subsequently leads to an increased population of CMs in Tg(α MHC-Kit^{Wv}) hearts. This warrants further investigation.

Overall, evidence indicates that c-Kit is not re-expressed in adult WT CMs after hypertensive stress. However, there may be other mechanisms involved that enable CMs to divide after cardiac injury in these two genetic mouse models of c-Kit inhibition that are

distinct. One possible mechanism in Tg(α MHC-*Kit*^{Wv}) mice is ER stress-induced inflammation resulting in CM cell division that may have a role in CM regeneration. Moreover, it is possible that using the CM-specific α -MHC promoter to overexpress proteins may result in ER-stress induced responses affecting the normal cellular physiology of CMs, which would have wider implications in the cardiac field for transgenic studies.

Chapter 5 Postnatal murine cardiac growth

5.1 Introduction

The prevalence of congenital heart disease (CHD) and premature births (<37 weeks) are 8 in 1000 and 1 in 10 births, respectively (Marelli *et al.*, 2014; Beck *et al.*, 2010). The majority of infants born with CHD require postnatal surgery and treatment to survive, which is often performed in the immediate postnatal period and has to be repeated. Normal cardiac development is disrupted in preterm infants (mainly as a result of preeclampsia), due to the early transition from the fetal to postnatal environment, predisposing infants and adults to CVD (Leipala *et al.*, 2003b; Lewandowski *et al.*, 2013; Norman, 2013; Beck *et al.*, 2010). Indeed, the hearts of children born prematurely or with CHD may have a reduced number of CMs. This is certainly the case for conditions such as hypoplastic left heart syndrome. The average adult human heart weighs ~260 g in females and ~340 g in males, (Friedman, 1951; Womack, 1983; Hanzlick and Rydzewski, 1990; Molina and DiMaio, 2012), whereas the newborn heart is ~20g (Coppoletta and Wolbach, 1933), and therefore, the extrapolated postnatal increase in heart weight is 13- to 17- fold from birth, with cardiac growth being most rapid in the first year of human life (Smith, 1928; Holt *et al.*, 1968). The heart is the first organ to form in the embryo and continues to grow throughout infancy, preadolescence and into adulthood as the body grows; heart growth is directly related to body surface area (Gutgesell *et al.* 1990) and weight (Scholz *et al.*, 1988). Therefore, CM endowment in the fetal and early postnatal period is critical for normal cardiac development.

Haemodynamic load is essential for normal cardiac growth (Leipala *et al.*, 2003a; Rudolph, 1970) and changes in blood flow directly affect cardiac afterload and preload; this is particularly accentuated and problematic in CHD. Furthermore, preterm newborns with low birth weights initially have immature smaller hearts, which consequently become larger in preterm-born infants and preterm-born adults compared with those born at full term (Kozak-Barany *et al.*, 2001; Leipala *et al.*, 2003a; Lewandowski *et al.*, 2013). This suggests that preterm birth leads to a disruption in cardiac growth during a period that is normally characterised by marked CM proliferation and, thus, the total CM population is reduced. This may be later compensated for by CM hypertrophy resulting in larger preterm born infant and adult hearts (Norman, 2013). Other external factors affecting cardiac growth

include nutrients and oxygen, whereby suboptimal levels also alter the total CM population number (Hollenberg *et al.*, 1977; Rakusan *et al.*, 1978; Bai *et al.*, 1990; Corstius *et al.*, 2005; Hollenberg *et al.*, 1976; Bae *et al.*, 2003).

Cardiac growth is achieved by CM proliferation and cellular enlargement, in which the transition from cell division to enlargement occurs soon after birth.(Li *et al.*, 1996; Leu *et al.*, 2001; Clubb and Bishop, 1984; Walsh *et al.*, 2010). It is widely suggested that in the mouse, CM proliferation ceases before birth (Soonpaa *et al.*, 1996) or up to P5 (Li *et al.*, 1996), coinciding with an increase in the binucleation of CMs up to P8-10, indicative of terminal differentiation (Soonpaa *et al.*, 1996; Walsh *et al.*, 2010). Moreover, studies performing apical resection of the heart or MI at P7 reported that there was no endogenous repair of the myocardium compared with P1, indicating that the regenerative capacity of the heart is lost by P7 (Porrello *et al.*, 2011b; Porrello *et al.*, 2013). However, our laboratory has recently shown that the proliferative capacity of CMs extends into preadolescence (up to P18), with a burst of cell division at P15 that further increases the total CM population by 1.4-fold during cardiac growth (Naqvi *et al.*, 2014). This was supported by the re-expression of mitosis-related genes at P15, the presence of mitotic figures in CM nuclei, and transient changes in cell dimensions and the proportion of mono- and bi-nucleated CMs, consistent with cell division giving rise to smaller daughter cells. In addition, CM proliferation and heart growth was abrogated in preadolescence if the biosynthesis of serum T₃ levels, which peaks at P12, was inhibited with propylthiouracil (PTU) administered at P7 (Naqvi *et al.*, 2014). The extension of cell division beyond the neonatal period has also been shown in human studies where cell division continues up to 20 years of age, resulting in a 3.4-fold increase in the total CM population number simultaneously with cellular enlargement (Mollova *et al.*, 2013). These studies question our understanding of postnatal cardiac development and raise the possibility of treating abnormal heart growth by stimulating CM proliferation during this preadolescent period.

The fetal and postnatal environments are critical in regulating normal cardiac growth, in which CMs permanently exit the cell cycle during postnatal development and become terminally differentiated. This limits the adult heart to maladaptive hypertrophy in response to hypertensive stress and CVDs. The timing and signals leading to CM proliferation, terminal differentiation, and cellular enlargement, during postnatal cardiac growth are not

completely understood. To this end, the following study characterises key periods in the CM growth trajectory of C57BL/6J mice and identifies time points that are important in CM development.

5.2 Materials and Methods

General Methods are described in Chapter 2.

5.2.1 Inbred C57BL/6J colony

Breeding pairs of C57BL/6J mice were set up to yield a high number of litters, and only litters of 6-8 pups were used in this study. Pregnant dams were checked twice daily, in the morning and evening, to confirm the day of birth and litter size. Litters were assessed according to the JAX guidelines (Figure 5.1) to further confirm the stage of postnatal development.

The stages of postnatal murine development were categorised as: P0 to P7, the neonatal period; P8 to P14, the transition from neonatal to preadolescence; P15 to P21 (weaning age), preadolescence; P22-P55, adolescence; and P56 onwards, fully grown adults.

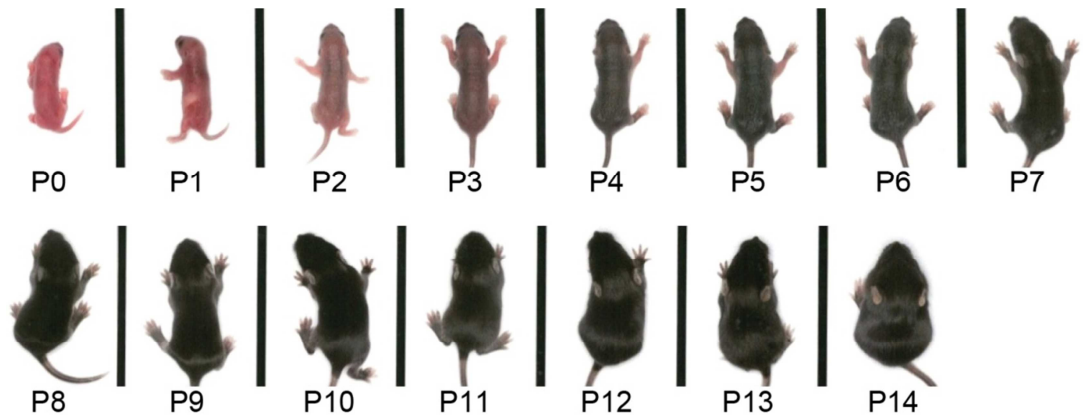


Figure 5.1: Phenotype of inbred C57BL/6J mouse pups from birth to two weeks

This image was adapted from a “JAX mouse pups appearance by age” poster (www.jax.org). Developmental characteristics are as follows (details provided by JAX); P0, blood red in colour with a slight milk spot; P1, lighter shade of red with milk spot present; P2, skin pigment begins to appear and ear nubs form; P3, ear flaps come away from the head; P4, skin colour develops and ears are fully formed; P5, increased colour density and thickness of skin with ears moving towards the back of the head; P6, milk spot has disappeared; P7, fur begins to cover pup; P8, belly begins to grow fur; P9, fur is much thicker and females begin to show nipples; P10, fur growth is complete and pups are more active; P11, teeth are protruding and eyes start to open; P12, eyes are open and pups begin to digest solids; P13, increased solid food intake; P14, pups gain weight by increasing food intake.

5.2.2 Heart collection, CM isolation and fixation

Hearts were excised as described in General Methods, and were collected at 9-11 am. CMs were isolated as described in Chapter 6. Cardiac cells were either fixed prior to or after the dissociation of cardiac tissues into a single suspension or after dissociation (described in General Methods). For fixing cardiac cells prior to the dissociation, hearts were fixed *in situ* immediately following Langendorff retrograde perfusion by mounting the cannulated heart onto a syringe containing 2% PFA (2 ml), and perfusing by pressing the syringe plunger slowly. The heart was then placed into a beaker with 2% PFA for 5 minutes at RT. After *in situ* fixation, cardiac tissues were dissociated as described in Chapter 6 and cardiac cells were fixed further as detailed in the General Methods.

5.2.3 Total T₃ assay

Mice were anaesthetised with 2-4% isoflurane. Blood was drawn by cardiac puncture at 9-11am and left to coagulate for 1 hour at RT. Supernatant containing blood plasma was collected after centrifugation at 1,500 g for 5 minutes at 4°C. Serum was stored at -80°C until use, when it was thawed on ice.

Endogenous total T₃ serum levels were determined using an ELISA assay (cat. #. 1700, Alpha Diagnostic) that is based on the competitive binding of human thyroxine from serum samples and enzyme-labelled T₃, to T₃-specific antibodies immobilised on ELISA plates. As per manufacturer's instructions, blood sera, standards and controls (50 µl) were dispensed in duplicate into wells on the ELISA plate followed by the addition of enzyme conjugate (100 µl of enzyme-labelled T₃) into each well. To enable competitive binding to immobilised T₃ antibodies, T₃ was released from its binding proteins in sera by a releasing agent. The plate was incubated and continually mixed for 1 hour on an orbital shaker at RT. After three washing steps, TMB "chromogenic" substrate (150 µl) was added to each well to allow the colour for each reaction to develop. The intensity of the colour (blue) is inversely proportional to the total amount of T₃ present in the sample. Stopping solution (50 µl; turns blue to yellow) was added after 15 minutes. The absorbance of each reaction was measured at 450 nm and a semi-log standard curve was calculated to extrapolate the approximate concentrations of T₃.

5.2.4 RT-qPCR

To measure the expression of mitosis-related genes, cDNA was synthesised using the QuantiTect Reverse Transcription Kit and RT-qPCR was performed using a SYBR Green assay. The primers (Integrated DNA Technologies) used for cell cycle genes and *18S* mRNA expression are shown in Table 5.1.

Table 5.1: Primers sequences for SYBR Green RT-qPCR

Gene	Forward primer	Reverse primer	Reference
<i>18S</i>	CTT AGA GGG ACA AGT GGC	ACG CTG AGC CAG TCA GTG TA	BMC
<i>Anln</i>	TAG AGT CCT CAT ATT AAC ATT AGC	CAG AGT TGT AGA AAG TGT CAT AG	Li <i>et al.</i> , 2008
<i>AurKA</i>	ACG CTC TGT CTT ACT GTC	GCC TTC AAT CAT CTC TGG	Li <i>et al.</i> , 2008
<i>Birc5</i>	CAT CTA AGC CAC GCA TCC	CGT CAC AAT AGA GCA AAG C	Li <i>et al.</i> , 2008
<i>Ccnb1</i>	CTA AAG TCG GAG AGG TTG	GTC TTC ACT GTA GGA TAG G	Li <i>et al.</i> , 2008
<i>Mki67</i>	ATC ATT GAC CGC TCC TTT AGG T	GCT CGC CTT GAT GGT TCC T	Primer Bank
<i>Plk1</i>	CAT TGA GTG CCA CCT TAG	GCC ATA CTT GTC CGA ATA G	Li <i>et al.</i> , 2008

Anln encodes Anillin; *Aurka* encodes Aurora kinase A; *Birc5* encodes Survivin; *Ccnb1* encodes Cyclin B1; *Mki67* encodes Ki67; *Plk1* encodes Polo-like kinase 1.

5.2.5 Immunocytochemistry

Immunostaining of fixed cells secured onto slides was performed as follows. Slides were incubated with blocking buffer (1% BSA and 0.2% Triton X-100 in PBS; 80 µl per slide) for 1 hour at RT, after which blocking buffer was removed by individually flicking slides. Cells were incubated for 1 hour at RT with the primary Ab, CM-specific mouse anti-cardiac troponin T (cTnT, cat. #: ab10214, Abcam), diluted at 1:400 in blocking buffer (80 µl per slide). Slides were then washed in PBS for 5 minutes at RT on an orbital shaker (x5). The following steps were performed in the dark. Cells were incubated for 1 hour at RT with the species appropriate secondary Ab, goat anti-mouse IgG Alexa Fluor 488, diluted at 1:1000 in blocking buffer (80 µl per slide). Cells were washed in PBS for 5 minutes on an orbital shaker (x5). Cell nuclei were stained with TO-PRO-3 (1 mg/ml), diluted at 1:1000 in

blocking buffer (80 μ l per slide), and incubated for 10 minutes at RT. Cells were washed in PBS for 5 minutes on an orbital shaker (x5). Coverslips were secured onto each slide with PVA-DABCO mounting medium. Slides were then stored at 4°C. Stained cells were imaged with a confocal microscope using the same settings for all samples (Axio Observer inverted microscope equipped with a LSM 710 confocal scan head, Zeiss).

5.3 Results

5.3.1 Postnatal heart and body weights

Biological variation due to nutrition-mediated effects of variable litter sizes was minimised by using animals only from a litter size of 6-8 pups to normalise body and cardiac weight development. The average litter size in our C57BL/6J colony was 6.8 pups, and the most frequent litter size was 8 pups (Figure 5.2A). Our lab has previously published using litter sizes of 6-7 pups (Naqvi *et al.*, 2014). A comparison of heart to body weight (HW/BW) measurements between litters of 6-7 pups and litters of 8 pups showed there were no statistically significant differences (Figure 5.2B). Thus, to increase the yield of useable litters, experiments were performed using litters of 6-8 pups.

Growth of the heart relative to body weight is rapid, increasing by 40% from P2 and 23% from P10 to the peak of growth at P18 (Figure 5.2C), as mice transition from the neonatal period to preadolescence. During the period of accelerated heart growth from P10 to P18, heart weight increased by ~45% while body weight increased by ~19% (Table 5.2). Interestingly, the neonatal heart weighed approximately one-eighteenth of the adult heart after birth (P2, 7.16mgs; vs P70, 129.7mgs) and at the peak of accelerated preadolescent heart growth, i.e. P18, the heart weighed approximately one-third of the adult heart size (P18, 46.36mgs).

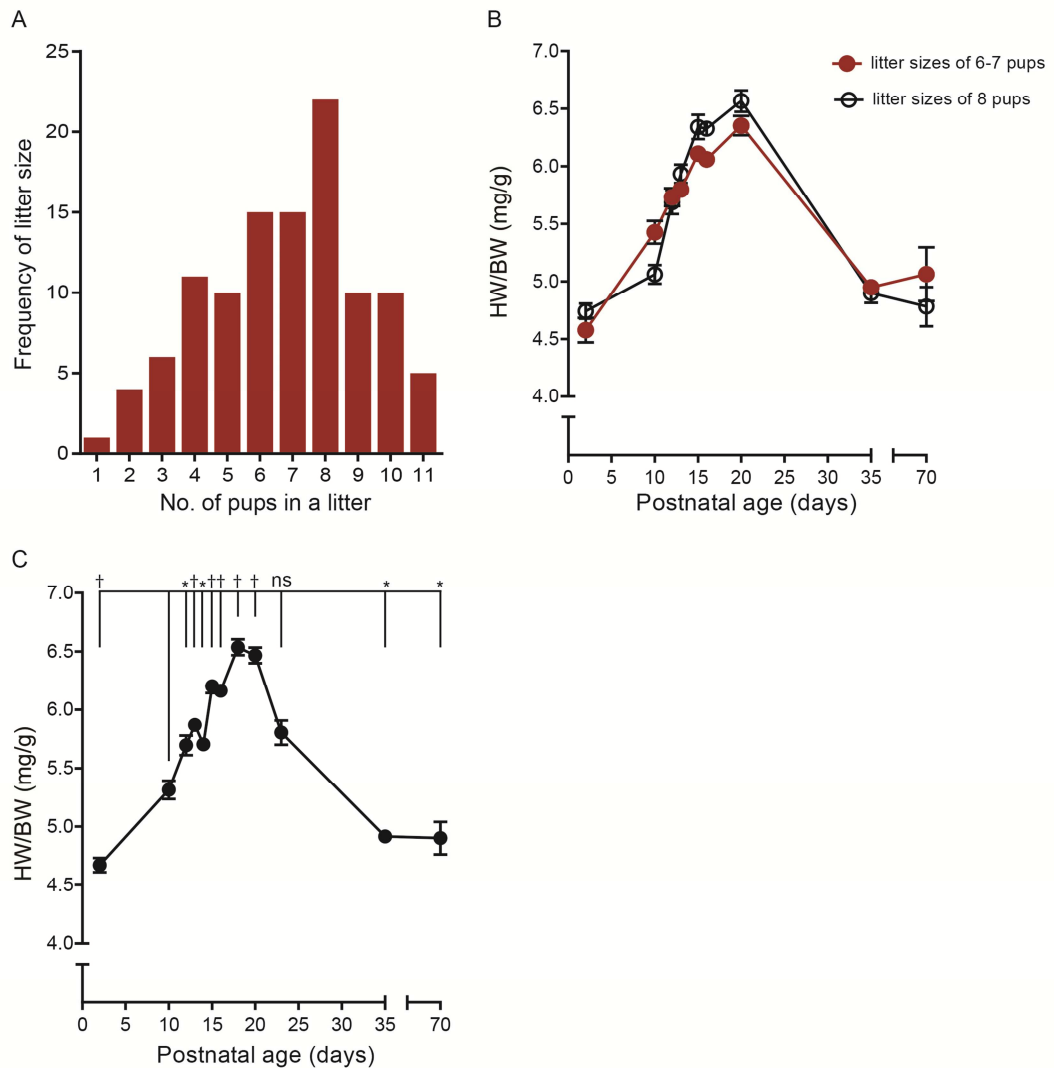


Figure 5.2: Heart-to-body weight ratios of C57BL/6J mice from litters of an average size

A, the histogram shows the frequency of litter sizes in our C57BL/6J colony. B, heart to body weight (HW/BW) ratio was compared between litters of 6-7 pups and litters of 8 pups, including adult male mice, which were not statistically significant. Statistical significances were determined by two-way ANOVA followed by Bonferroni's *post hoc* test, all points were non-significant. C, the HW/BW ratio during postnatal development from mice in litters of 6-8 pups ($n=6-60$ pups per time point, mostly $n \geq 14$ pups, except for P23, $n=6$), relative to P10. Data are presented as means \pm SEM bars. Statistical significances were determined by one-way ANOVA followed by Tukey's *post hoc* test; * $p < 0.05$, † $p < 0.0001$ and, non-significant, ns.

Table 5.2: Heart-to-body weight measurements in postnatal murine development

Postnatal age (<i>days</i>)	HW (mg)	BW (g)	HW/BW	n
2	7.16	1.533	4.671	14
10	31.87	5.989	5.314	26
12	35.07	6.170	5.696	30
13	36.03	6.148	5.870	45
14	39.82	6.982	5.705	16
15	47.15	7.618	6.202	60
16	47.17	7.663	6.162	21
18	46.36	7.111	6.536	21
20	54.40	8.429	6.467	15
23	60.40	10.500	5.805	6
35	87.83	17.910	4.916	33
70	129.70	26.410	4.902	14

The BW and HW of developing C57BL/6J mice born into litters of 6-8, were recorded and the number of animals analysed per time point (n) are shown. HW, heart weight; BW, body weight; and, HW/BW heart to body weight ratio. Statistics are presented in Figure 5.2C.

5.3.2 Levels of triiodothyronine (T₃) hormone in postnatal development

An important driver of heart and body growth during the transition from the neonatal to preadolescence period (P10-P18) is thyroid hormone, which increases markedly from P9-10 after birth (Chizzonite and Zak, 1984; Naqvi *et al.*, 2014). This was also determined in this study by collecting blood plasma from pups aged between P8 and P25, and total endogenous serum T₃ levels were assayed (Figure 5.3). There was a ~2.2-fold surge in serum T₃ levels between P10 (~0.6 ng/ml) and P12 (1.3 ng/ml). Serum T₃ levels further increased by ~2-fold as mice transitioned from preadolescence to adolescence (P18, 1.1 ng/ml; to P25, 2.1 ng/ml).

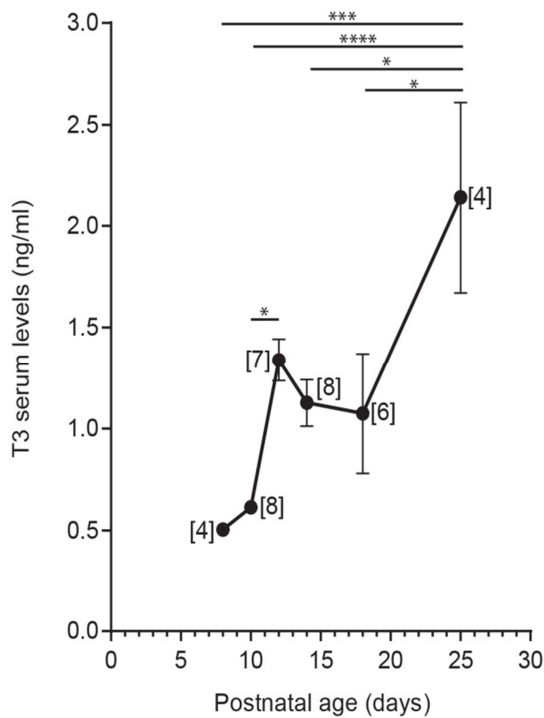


Figure 5.3: Endogenous serum total T₃ levels during postnatal development

Total T₃ levels were measured in blood plasma using mice from litters of 6-8 at the following ages; P8 (n=4), P10 (n=8), P12 (n=7), P14 (n=8), P18 (n=6) and P25 (n=4) pups. Data are presented as means \pm SEM. Statistical significances were determined by one-way ANOVA followed by Tukey's *post hoc* test; * $p < 0.05$, *** $p < 0.001$, and **** $p < 0.0001$.

5.3.3 Cell cycle gene expression during postnatal cardiac growth

Transcript levels for the following mitosis-related genes: anillin (*Anln*), aurora kinase A (*Aurka*), survivin (*Birc5*), cyclin B1 (*Ccnb1*), Ki67 (*Mki67*) and polo-like kinase 1 (*Plk1*) were determined in the ventricles of hearts at P2 and various postnatal days up to P56. The following three experiments were performed independently with new samples. In the first experiment, the expressions of cell cycle genes were evaluated during preadolescence (P13-P16). Transcripts for cell mitosis-related genes were more abundant at P13 as compared with P15 and P16, and at P14 relative to P15 (Figure 5.4A). Transcripts for survivin and Ki67 were more abundant at P13 than P14.

In the second experiment, temporal changes in the expression of mitosis-related gene transcripts were observed in hearts over a broader spectrum of ages that included neonatal (P2, highly proliferative), preadolescent (P13 and P15) and adult (P35, differentiated CM) hearts (Figure 5.4B). The greatest abundance of mitosis-related gene transcripts was observed at P2, approximately 4-fold higher than at P13 ($p < 0.0001$). In agreement with the first experiment, mitosis-related gene transcripts were more abundant at P13 than at P15 ($p < 0.01$) or P35 ($p < 0.01$).

In the third experiment, the expression of Ki67 transcripts was measured daily in the postnatal period between P10 and P18, and at P35 and P56 (Figure 5.4C). The abundance of Ki67 transcripts was equivalent at P10-P13, and was statistically significantly higher than at P14 -P18, P35 or P56. At P10-P13, Ki67 transcript levels were ~15-fold greater than in the adult heart at P56.

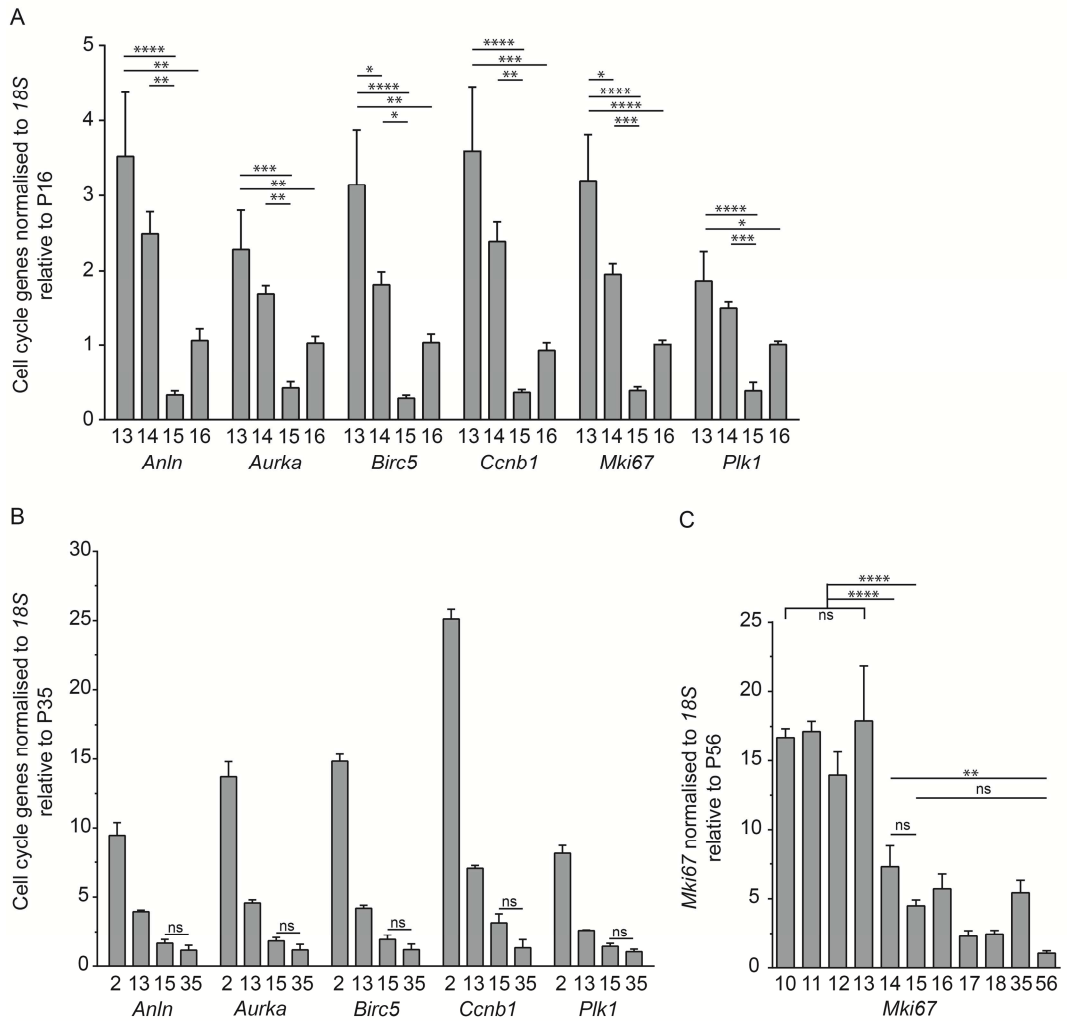


Figure 5.4: Expression of cell cycle genes throughout postnatal cardiac development

RNA was extracted from ventricles of P2-P56 mice born into litters of 6-8. The expression of cell cycle genes were normalised to *18S* ribosomal RNA. The fold-change was calculated relative to the oldest postnatal age in each experiment. Figures A, B and C were performed independently using independent samples. A, shows the expression of six cell cycle genes in hearts from P13-P16 pups, relative to P16 (n=6-8); B, shows the expression of five cell cycle genes in hearts from P2 (n=2), P13, P15 and P35 (n=4) mice, relative to P35; C, shows the expression of *Mki67* in hearts from P10-P18 (n=5-6), P35 (n=3) and P56 (n=4) mice, relative to P56. Data are presented as means \pm SEM. Statistics were calculated by one-way ANOVA followed by Tukey's *post hoc* test; * $p < 0.05$, ** $p < 0.01$, *** $p < 0.001$, **** $p < 0.0001$ or non-significant, ns. *Anln* encodes Anillin; *Aurka* encodes Aurora kinase A; *Birc5* encodes Survivin; *Ccnb1* encodes Cyclin B1; *Mki67* encodes Ki67; *Plk1* encodes Polo-like kinase 1.

5.3.4 Morphology of developing postnatal CMs

The morphology of maturing CMs was characterised at four stages of postnatal cardiac development where levels of mitosis-related gene transcripts ranged from high (P2), intermediate (P10 and P13) or low (P70). The preadolescent time points of P10 and P13 coincide with the rapid surge in serum T₃ levels (Figure 5.3), that is, P10 is immediately prior to the initial increase in serum T₃ levels and P13 is 24-hours after.

Hearts were digested by Langendorff retrograde perfusion of proteolytic enzymes (as detailed in Chapter 6) and cells were fixed *in situ* prior to tissue dissociation and CM isolation. This resulted in CMs that were almost 100% rod-shaped (Chapter 6, Figure 6.5 and Figure 5.5C). CMs were stained with the CM-specific protein, cardiac troponin T, cTnT, and nuclei were identified using the DNA dye, TO-PRO-3, for immunofluorescence microscopy to evaluate the nucleation status and area of CMs. Overlapping cells were excluded from measurements of CM nucleation and area. Cells with two overlapping nuclei, possibly indicative of karyokinesis, were counted as mononucleated. Mononucleated CMs accounted for >90% of P2 CMs, whereas 73%, 80% and 84% of CMs at P10, P13, and P70, respectively, were binucleated (Figure 5.5A).

CM areas were quantified using ImageJ, which automatically detects the outline of the cell in contrast to the background. This eliminates user variability, which usually involves selecting the diameter and width of a cell by eye. In addition, CMs are not uniform and the shape changes during development from small spindle-like cells to large cells with jagged edges located at the intercalated discs (Figure 5.5C). Average CM areas at P2, P10, P13 and P70 were 440, 1033, 1197 and 4286 μm^2 , respectively (Figure 5.5B). During the transition from the neonatal to preadolescent period (from P2 to P10 and P13), CM area increased by ~2.5-fold, while, the transition from preadolescence to adult saw CMs enlarge by ~3.8-fold. Overall postnatal CM maturation from P2 to P70 resulted in a ~9.7-fold enlargement of CM area.

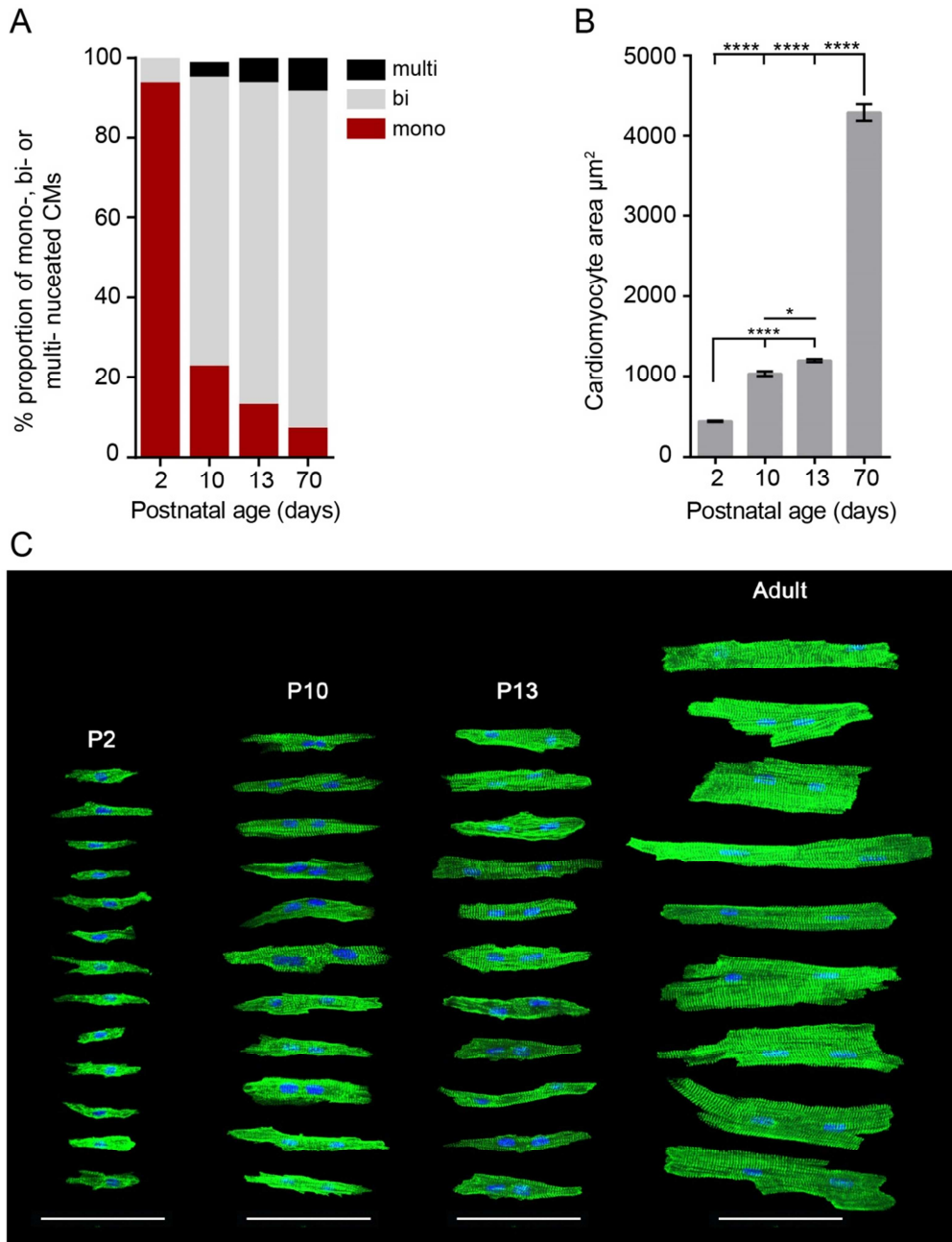


Figure 5.5: Gross morphology of developing postnatal CMs

Hearts were perfused with 2% PFA to fix cardiac cells *in situ* prior to the dissociation of cardiac tissue. The number of nuclei per cell (A) and the CM area (B) from postnatal ages: P2, P10, P13 and P70 (120-380 cells from 2-3 hearts per time point), were evaluated. ImageJ was used to calculate the CM area (μm^2). C, representative images of CMs from each time point were stained with the CM-specific marker, cTnT (green), and the nuclei dye, TO-PRO-3 (blue). Scale bar is 100 μm . Data are presented as the mean \pm SEM. Statistics were calculated by one-way ANOVA followed by Tukey's *post hoc* test; * $p < 0.05$, **** $p < 0.0001$.

5.4 Discussion

To elucidate mechanisms that regulate heart growth we first sought to characterise postnatal cardiac growth in C57BL/6J mice. Litter sizes of 6-8 pups were used to minimise biological variation in HW and BW during development. The murine heart undergoes profound growth between P10 and P18 due to both CM enlargement and proliferation, resulting in the rapid increase of HW/BW by 23%. This coincided with a surge in endogenous serum T₃ levels between P10 and P12. There was also evidence for an intermediate expression of mitosis-related transcripts at P10-13 relative to P2 (highly abundant) and adults (lowly abundant), indicating an incremental reduction in cell proliferation during postnatal development. This study highlights the importance of our recent findings (Naqvi *et al.*, 2014) and extends upon those that have been published previously (Li *et al.*, 1996; Soonpaa *et al.*, 1996; Leu *et al.*, 2001; Mollova *et al.*, 2013).

Careful characterisation and use of pups born into litters of 6-8 was particularly important in this study to reduce biological variation in all subsequent analyses of CMs, including morphological and molecular properties. In the postnatal period between P10 and P18, heart growth was rapid relative to body weight; and at P18 was one-third of the size of an adult heart. The neonatal heart was just one-eighteenth of the size of an adult male murine heart (Table 5.2). This is comparable to human heart growth from birth to adulthood, which I previously estimated to increase by ~17-fold in males (General Introduction). This suggests that cardiac growth is similar between rodents and humans.

HW/BW ratios obtained in this study were compared with those reported previously, see Figure 5.6. The study by Naqvi *et al.* (2014) was performed in a different animal house, and thus the animals from our facility were characterised. The HW/BW observed in this study and in the Naqvi *et al.* (2014) study were comparable that shows good reproducibility using a similar experimental design, in contrast to Leu *et al.* (2001) and Soonpaa *et al.* (1996) that were also quite different from each other. Curiously, the HW/BW ratio data presented by Soonpaa *et al.* (1996) and Leu *et al.* (2001) were not consistent with their conclusions. For example, the data from Soonpaa *et al.* (1996) showed variable HW/BW ratios from P0-P20 (Figure 5.6), yet their conclusion was that the HW/BW ratio was constant during murine development. On the other hand, Leu *et al.* (2001) showed a steady fall in the HW/BW ratio from P2 to P11 and an abrupt increase from P11 to P14 of 40% (Figure 5.6). Leu *et al.*

(2001) did not calculate HW/BW ratios, but rather presented their HW and BW data on the same graph, with HW plotted in milligrams and BW plotted in grams. Obviously, their graph showed a steeper rise in the heart weight trace using units of mg, compared with the smaller increase of the body weight trace using units of g, thereby leading them to conclude that heart growth was greater in relation to body weight. However, as previously described the calculated HW/BW ratio from Leu *et al.* (2001) shows otherwise (Figure 5.6), and thus their conclusion using different units on the same graph is misleading.

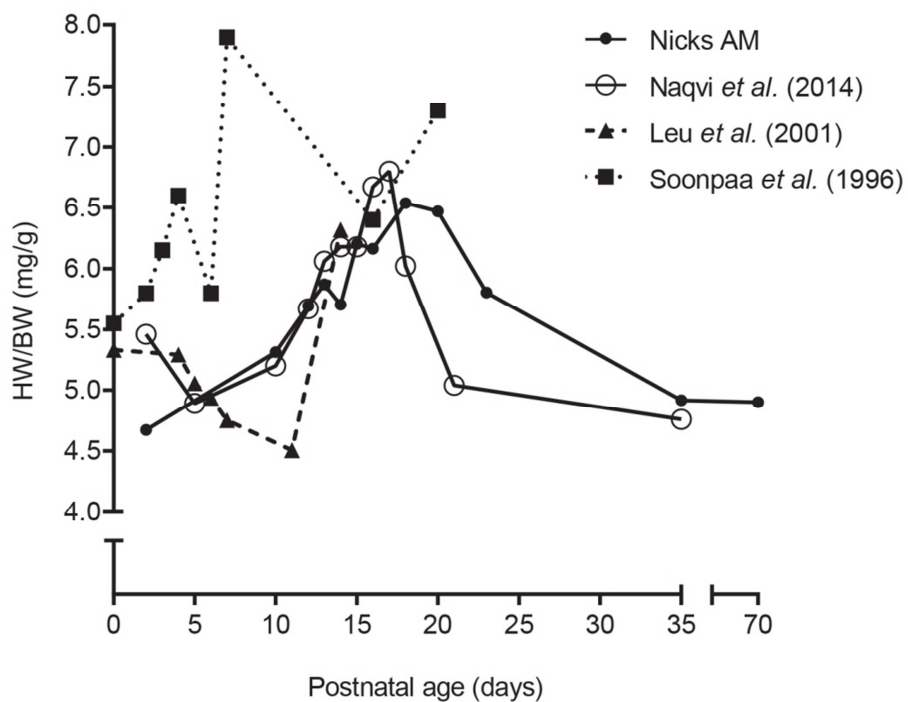


Figure 5.6: A comparison of reported murine heart-to-body weight ratios

HW/BW ratios during postnatal growth from previously published data are compared with those presented in this study. C57BL/6J mice were used by Naqvi *et al.* (2014), Leu *et al.* (2001) and in this study; C3Heb/FeJ mice were used by Soonpaa *et al.* (1996). Naturally-produced litters of 6-8 pups/litter or 6-7 pups/litter, were used in this study and by Naqvi *et al.* (2014), respectively, whereas litter sizes were adjusted to 6 pups/litter by Soonpaa *et al.* (1996) and there was no litter information from Leu *et al.* (2001). HW/BW data were obtained from n=6-60 (mostly n \geq 14 pups, except for P23, n=6) from P2-P70 in this study, n=5-15 from P2-P35 by Naqvi *et al.* (2014), n=4 from P0-P20 by Soonpaa *et al.* (1996), and n \geq 5 from P0-P14 by Leu *et al.* (2001).

There are apparent differences in HW/BW ratios, which might be explained by different experimental conditions, such as mouse strain, the size of the litter used, number of mice per time point, and/or period of sampling intervals. For example, Soonpaa *et al.* (1996) used C3Heb/FeJ mice, and other studies use C57BL/6J mice. Both the C3Heb/FeJ and C57BL/6J strains have similar body weights (Jackson Laboratories), so one may expect similar heart weights. In this study and that of Naqvi *et al.* (2014), only animals from naturally-occurring litter sizes of 6-8 were used, whereas Soonpaa *et al.* (1996) adjusted litters to 6 pups/litter by adding or removing pups after birth. Adjusting litter sizes after birth to normalise litter growth does not take into account different nutritional environments during gestation, which may affect postnatal development. Leu *et al.* (2001) provided no information about the litter sizes that were used. Another difference was the number of mice used to calculate the HW, specifically a smaller sample size of $n=4$ (Soonpaa *et al.*, 1996) and $n \geq 5$ (Leu *et al.*, 2001), whereas Naqvi *et al.* (2014) and I analysed larger numbers of mice of $n=5-15$ and $n=6-60$ ($n \geq 14$ at all intervals except at P23, $n=6$), respectively. Lastly, there were differences in the period and intervals of sampling. Soonpaa *et al.* (1996) and Leu *et al.* (2001) collected the majority of data points before P10, while most of our data points were collected after P10. This comparative analysis highlights the importance of accurately detailing experimental procedures in order to identify sources of variation.

Another important factor for cardiac growth is TH, which more than doubles between P10 and P12 (Figure 5.3). This is similar to that observed in rats (Chizzonite and Zak, 1984) and in other mouse studies (Hadj-Sahraoui *et al.*, 2000; Naqvi *et al.*, 2014) and corresponds to the maturation of the hypothalamic-pituitary-axis at P12-P15 in rodents, which is completed by birth in humans (Fisher and Klein, 1981; Li *et al.*, 2014b). The level of T_3 was constant from P12 to P14 and P18, and further increased at P25. These concentrations overlap with those observed in other euthyroid rodents (Chizzonite and Zak, 1984; Shimoni *et al.*, 1997; Naqvi *et al.*, 2014; Hernandez *et al.*, 2006; Hadj-Sahraoui *et al.*, 2000). Moreover, there have also been reports showing T_3 decreases at P20 ($n=6$) and P21 ($n=3$) (Hadj-Sahraoui *et al.*, 2000; Hernandez *et al.*, 2006), although T_3 remains constant in other studies (Chizzonite and Zak, 1984; Naqvi *et al.*, 2014). Thus, additional time points would be necessary to determine the pattern of serum T_3 levels during this stage of development. One observation that may explain the specific increase between P10 and P12 is that according to the Jackson Laboratories developmental stages chart (Figure 5.1), mouse pups start teething at P11 and

digesting solid food at P12. This may increase dietary substrates such as iodine that contributes to the surge in T₃ levels.

In agreement with the literature, mitosis-related gene transcripts were highly expressed in the early neonatal period at P2 (Figure 5.4). Furthermore, it was clear in all three independent experiments that these transcripts were more abundant at P10-P13 than at P15, which was comparable to adult levels of expression. Thus, in this study we did not see an increase in the abundance of cell cycle gene transcripts at P15 relative to P13, P14 and P16 (Naqvi *et al.*, 2014). Rather there was a progressive decrease in cell cycle gene transcripts. One difference between these two studies is the subtle shift in the HW/BW curve, which could potentially be due to different litter sizes (6-8 pups vs 6-7 pups), although the HW/BWs were comparable (Figure 5.2B). Regardless, both datasets show the expression of mitosis-related genes beyond the neonatal period of P7, when CMs are believed to cease division, and growth had been mainly attributed to cellular enlargement (Soonpaa *et al.*, 1996). As early as the 1960s, however, Sasaki *et al.* (1968) used the mitotic inhibitor, Colcemid (demecolcine, which is related to colchicine), to arrest cell mitosis in metaphase, which showed the presence of mitotic figures in dividing CM nuclei up to 3 weeks after birth in rat cardiac tissue sections. More recently, Ikenishi *et al.* (2012) evaluated the abundance of cyclins (D1/E/A/B1) and their corresponding holoenzyme partners, CDKs (1/2/4), by Western blot analyses in murine cardiac ventricles from the embryo and at the following postnatal time points: P0, P3, P5, P7, P10, P14, P21, including adults. In the postnatal period, cell cycle proteins were most abundant at P5, lower at P10, but were very low after P14 and comparable to adults. Therefore, the abundance of cell cycle proteins correlate well with the expression of mitosis-related genes presented here. One of the limitations of these studies is the use of cardiac tissues that comprise a heterogeneous population of cells that includes ECs, VSMCs and fibroblasts, which also proliferate and cell proportions change during postnatal development (Soonpaa *et al.*, 1996; Olivetti *et al.*, 1980). An accurate delineation of CM proliferation and cell cycle gene changes during postnatal development would thus require analyses of purified CMs.

CM morphology was also assessed at each of the developmental time points corresponding to high cell cycle activity at P2, intermediate cell cycle activity at P10 and P13, as well as extremely low cell cycle activity at P70. Firstly, the nucleation status of CMs was evaluated

by immunocytochemistry, and as expected, the proportion of CMs that were binucleated increased from 6% at P2 to 72% at P10 to 81% at P13, and to 85% at P70 (Figure 5.5A). This was similar to Li *et al.* (1996) and Naqvi *et al.* (2014), as well as Ikenishi *et al.* (2012) excluding the P10 time point, which indicated 60% of CMs were binucleated. In contrast, Soonpaa *et al.* (1996) and Walsh *et al.* (2010) calculated that >95% of CMs were binucleated by ~P8. This may indicate faster cardiac growth and a more rapid maturation of CMs (Soonpaa *et al.*, 1996; Walsh *et al.*, 2010) that is different from the three aforementioned studies, including this study. Moreover, the CM area increased significantly throughout the time course, even between P10 and P13, and the time points have different proportions of binucleated CMs of 72% and 81%, respectively. The cell shape of adult CMs was highly variable as shown by the CM images in Figure 5.5C. Nonetheless, the absolute cell area correlated well to heart weight (Figure 5.7). However, there is a discrepancy in the adult CM areas that were measured in this Chapter (~4300 μm^2) and in Chapter 3 (Figure 3.4, sham: ~3300 μm^2). In both experiments, CMs were isolated from C57BL/6J mice at 9-10 weeks but two different buffers were used in this Chapter (Liao and Jain, 2007) and in Chapter 3 (O'Connell *et al.*, 2007). The latter solution has a higher osmolality (~15% higher)² and this difference in osmolality may contribute to changes in cell area that causes cells to swell or shrink depending on the intracellular osmolality of CMs. This is important to note for other studies, in which different protocols could lead to slight differences in reported cell areas and volumes.

² Calculated according to the osmolality:

$\text{mOsM/L} = \sum \text{ of mOsM per buffer component (mOsM= molecular conc.(mM) x number of species (e.g. ions) into which the molecule dissociates)}$

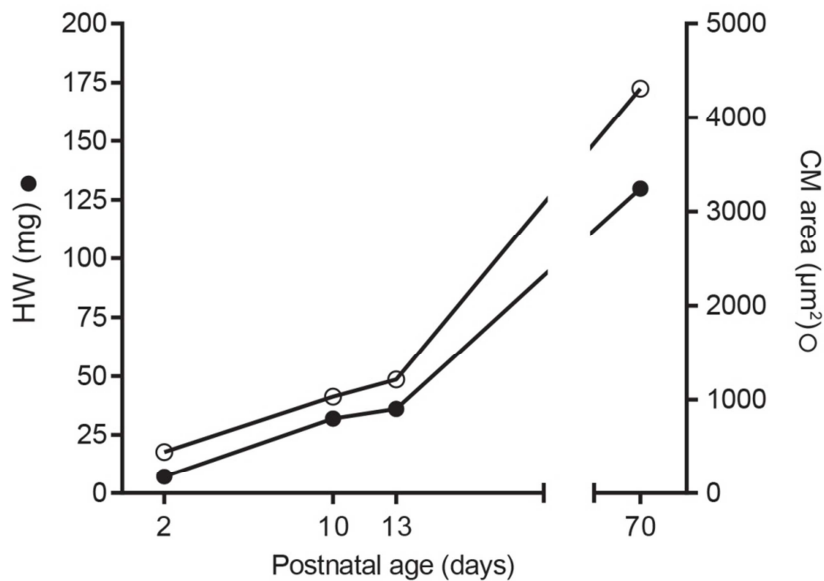


Figure 5.7: Correlation between heart weight and CM size in postnatal cardiac development

HW (●) and CM area (○) are compared during postnatal cardiac growth from the ages: P2, P10, P13 and P70 mice that were also presented in Figure 5.2 and Figure 5.5, respectively.

In conclusion, this study describes the relationship of CM division and enlargement during postnatal cardiac growth, particularly in the transition from neonatal to preadolescent development. It is a potentially exciting finding that the overall postnatal growth of the heart in mice may be similarly conserved to that of humans (adult male mice, 18-fold; vs adult male human 17-fold). During this period of cardiac growth, cell cycle activity was intermediate at P10 and P13, compared with P2 and adult time points that had high and low levels of cell cycle genes, respectively. Furthermore, these time points coincide with a surge in serum T_3 levels between P10 and P12, in which P10 was immediately before and P13 was 24-hours after the surge. In addition, P10 and P13 CMs were different in size and binucleation status and therefore, both of these time points are of interest for phenotyping CM maturation. Many unanswered questions remain, for example, what role does T_3 have during this period of growth in an *in vivo* setting? Do CMs stop dividing at P13, and if so, is there a master switch that triggers cell cycle exit? To this end, I decided to isolate and purify CMs (Chapter 6) at these pivotal time points during CM growth and evaluate the whole cellular transcriptome using RNA-Seq technology (Chapter 7).

Chapter 6 Purification of cardiomyocytes from neonatal, preadolescent, and adult mouse hearts

6.1 Introduction

CMs were first isolated in the late 1950's and 1960's from the embryonic chick heart (Cavanaugh, 1955), neonatal rat heart (Harary and Farley, 1960), and adult rat heart (Kono, 1969), and since then protocols have been continually modified for particular experimental end-points. Isolated CMs provide a system to study: cell morphology and ultrastructure, contractility, electrophysiology, Ca^{2+} homeostasis, intracellular signalling, as well as gene and protein expression, contributing to a wealth of knowledge in fundamental CM physiology. In the era of revolutionary technologies that enable interrogation of the whole genome, transcriptome, and epigenome from the lab bench, new experimental end-points are now possible.

In the previous Chapter, postnatal cardiac growth was characterised at pivotal developmental time points of CM proliferation, enlargement, and terminal differentiation. These three phases of CM growth have important implications for cardiac regenerative therapies, which are highly sought after but, thus far, have only achieved limited success. Hence, a better understanding of the developmental transitions of CMs from cell division to terminal differentiation is necessary. To delineate the cellular changes that take place during CM maturation at the transcript level, high-throughput sequencing provides nucleotide-base resolution and absolute numbers of RNA molecules, and is a tool for the discovery of novel transcripts, and the identification of candidate genes and gene networks. The cardiac milieu is intricate comprising contracting myocardium, capillaries, extracellular matrix, and gap junctions, along with other supporting cells. Thus, a homogenous population of CMs from heterogeneous cardiac tissues is needed for cell type-specific information. The adult rat heart has been reported to contain 30-40% CMs (Zak, 1974; Nag, 1980), and there are two conflicting estimations of the CM population in the adult mouse heart. In one study, ~56% of cardiac cells were determined to be CMs by flow cytometry (Banerjee *et al.*, 2007), and in two others, ~30% of cardiac nuclei were reported to be CMs by immunohistochemistry (Raulf *et al.*, 2015; Pinto *et al.*, 2016), although if the binucleation of rodent CMs is taken into account, the latter estimate would be reduced to ~15% CMs. Furthermore, the

proportion of cardiac cell types, including CMs, ECs, fibroblasts, and VSMCs, also change during development (Banerjee *et al.*, 2007).

Isolating highly enriched populations of CMs is not trivial and different protocols are used for adult vs neonatal hearts. Currently, there is no universal method to isolate and purify rodent CMs from neonate through to adult hearts. The problem with having two different methods for neonatal and adult CM isolations is that they are not consistent and therefore experimental results may be less comparable. For example, the method for tissue digestion and the time taken (3-48 hours) to isolate and purify CMs from adult vs neonatal mice varies. In addition, an individual adult heart can be used for an independent biological replicate, whereas a number of neonatal hearts are pooled to provide a single biological replicate, which obviates the ability to evaluate biological variability between animals. Furthermore, protocols that require cell culture can lead to changes in gene expression and CM de-differentiation (Ehler *et al.*, 2013). To preserve the *in vivo* status of CMs as closely as possible, a protocol that easily and rapidly results in purified populations of CMs from neonates through to adults, without cell culture, is required.

To this end, my aim was to develop a standardised method that enables the rapid isolation and purification of viable CMs from hearts across all postnatal ages, within a comparable timeframe. Homogenous populations of CMs could then be used for RNA-Seq analyses to obtain cell type-specific information (Chapter 7).

6.2 Materials and Methods

General Methods are described in Chapter 2 and animal use in Chapter 5. In this Chapter, preadolescence ascribes P10 and P13 to differentiate from neonatal mice.

6.2.1 CM isolation, enrichment and purification from neonatal, preadolescent, and adult hearts

Because we have perfected the technique of cannulating even neonatal hearts, we elected to isolate CMs from neonatal (P0-P3), preadolescent (P10 and P13) or adult (> P56) hearts by Langendorff retrograde perfusion with proteolytic enzymes to digest cardiac tissue. After enzymatic digestion of the extracellular matrix, the atria were removed and the ventricles were dissected into fragments, which were dissociated into a cell suspension by trituration using a pipette tip that had been trimmed to provide a large bore that easily accommodates CMs, which are much larger than other cell types in the heart. The heterogeneous cardiac cell suspension was then enriched for CMs by multiple low-speed centrifugations to separate the larger CMs into a pellet from the smaller non-myocytes, which remained in the supernatant and were discarded. This step was omitted for neonatal CMs, which are similar in size to non-myocytes. CMs were then purified by immuno-magnetic cell separation whereby non-myocytes were bound to magnetic beads pre-coated with antibodies against their cell surface proteins. The bead-bound non-myocyte fraction was then separated from CMs using a magnet, and the supernatant fraction containing CMs was collected by aspiration. This resulted in a large yield of viable and highly purified CMs (>90%) from a range of postnatal ages (neonatal to adult). This standardised method of CM purification can be utilised by other researchers, and hence, extensive details are provided below.

6.2.1.1 Materials for cannulation and perfusion of the heart

For the cannulation and perfusion of the murine heart, the following equipment and reagents were used:

Heparin (5000IU/5ml, cat. #: 02112115, Pfizer), isoflurane chamber and VetQuip Isotec 3, BD Falcon 15 and 50 ml tubes, Corning 500 ml filter system (0.22 μm), 1.5 ml microfuge tubes, surgical instruments (shown in Figure 6.1A), non-sterile 6.0 silk suture spool, cannulas (a 24 G gavage needle, blunted-end 30 G and 25 G needles), 2 ml syringe secured to a circular weighted board (approx. 8 cm), operating board, 70% ethanol, 18.2 Ω Milli-Q water, Langendorff perfusion system (shown in Figure 6.1C), and a digital thermometer probe.

For the isolation and enrichment of CMs, the following equipment was used:

Petri dish (60 x 15 mm), fine sharp scissors, fine straight forceps, transfer pipettes (1 ml and 3 ml), sterile BD Filcon 200 μM cup filter, sterile BD Falcon 70 μM cell strainer, and a Neubauer haemocytometer (cat. #: AC1000, Hawksley).

For the purification of preadolescent and adult CMs, the following equipment and reagents were used:

Dynabeads Sheep Anti-Rat IgG, which are 4.5 μm superparamagnetic beads with affinity purified polyclonal sheep anti-rat IgG covalently bound to the bead surface (cat. #: 11035, ThermoFisher Scientific), rat anti-mouse CD31 Ab (cat. #: 550274, BD Biosciences), MagnaRack Magnetic Separation Rack (ThermoFisher), and 2 ml round-bottom microfuge tubes.

For the purification of neonatal CMs, which are smaller and cannot be readily enriched, the following equipment and reagents were used:

Neonatal Cardiomyocyte Isolation Kit (cat. #: 130-100-825, Miltenyi Biotec), MS columns (cat. #: 130-042-201, Miltenyi Biotec), and a MultiStand with an OctoMACS Separator Magnet (Miltenyi Biotec).

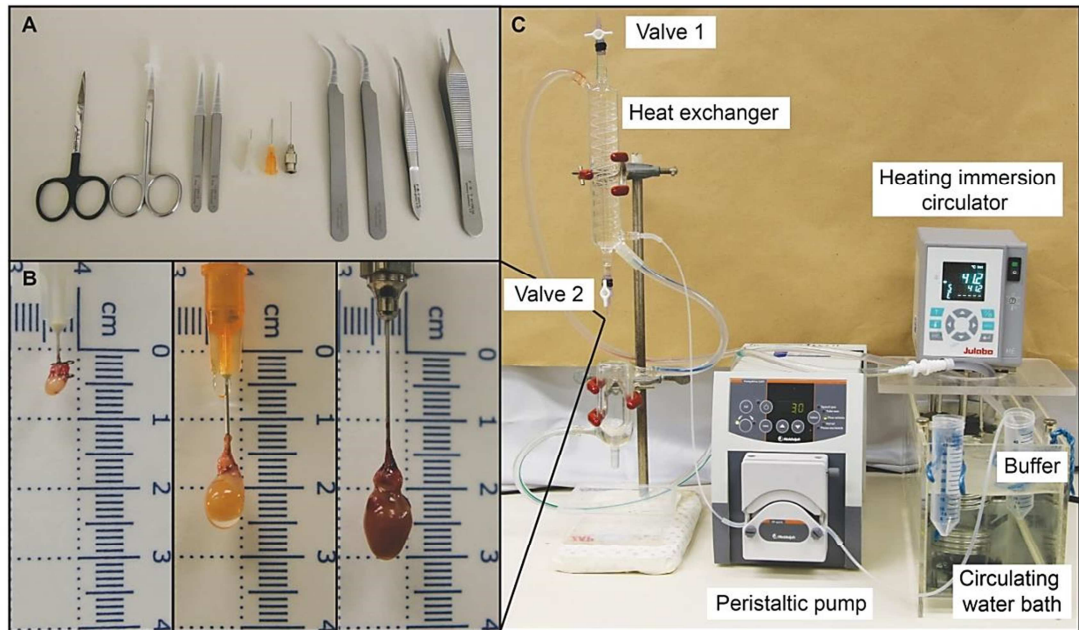


Figure 6.1: Surgical instruments and Langendorff apparatus used to cannulated and perfuse murine hearts

A, surgical equipment used for the cannulation of the heart include (from left to right): tough cut straight sharp scissors, fine sharp scissors, mini forceps x2, blunted needles at 30 G and 25 G, 24 G gavage needle, curved forceps x2, curved serrated forceps, and straight serrated forceps. B, murine hearts from the postnatal ages of P1, P10 and P70 (left to right) are mounted onto the Langendorff apparatus with a scale to show the differences in heart size. C, the Langendorff apparatus consists of a heating immersion circulator that regulates the temperature of the water bath, which is adjusted to maintain the perfusate at 37°C. The heated water is circulated through the insulating jacket of the heat exchanger. Buffers are incubated in the water bath and pumped through the coil of the heat exchanger by the peristaltic pump that controls the rate of perfusion. A pressure gradient in the heat exchanger is created by closing valve 1 (in the horizontal position) and opening valve 2 (in the vertical position), which allows the perfusate to circulate. A water-jacketed insulating organ bath is then moved upwards to encapsulate the mounted heart.

6.2.1.2 Buffers

Perfusion (PB), digestion (DB) and transfer (TB) buffers were modified from Liao and Jain (2007) listed in Table 6.1. Chemical components for each buffer were dissolved in 18.2 Ω Milli-Q water and the pH was adjusted to 7.2 for PB and to 7.4 for TB. Buffers were filter-sterilised using a Corning 500 ml filter system. Isolation buffer (IB) for use with Dynabeads comprised 0.1% BSA and 2 mM EDTA in PBS, which was adjusted to a pH of 7.4. IB used with the Neonatal Cardiomyocyte Isolation Kit (cat. #: 130-100-825, MACS Miltenyi Biotec) comprised 0.5% BSA and 2 mM EDTA in PBS, which was adjusted to pH 7.2 (Table 6.1). IB and DB were freshly prepared at the start of the experimental day, whereas PB and TB can be stored for up to two weeks at 4°C.

Table 6.1: Buffers for CM isolation and purification

Compound	MW (g/mol)	Stock conc. (M)	Final conc. (mM)	To add (ml or g)	Supplier
Perfusion buffer (PB), pH 7.2				/L	
NaCl	58.44	5	135	27 ml	Sigma
KCl	1.98	1	4	4 ml	Sigma
MgCl ₂	203.30	1	1	1 ml	Merck
NaHPO ₄		0.6	0.33	0.55 ml	
HEPES	238.31		10	2.38 g	Panreac Appli Chem
BDM	101.10		15	1.5 g	Sigma
Taurine	125.1		5	0.63 g	Sigma
Glucose	180.16		10	1.8 g	Sigma
Digestion buffer (DB), pH 7.2					
PB, pH 7.2					
Collagenase			0.3 mg/g		Roche
Collagenase			0.4 mg/g		Roche
Protease XIV			0.05 mg/g		Roche
Transfer buffer (TB), pH 7.4				/500ml	
NaCl		5	135	13.5 ml	
KCl		1	4	2 ml	
MgCl ₂		1	1	0.5 ml	
NaHPO ₄		0.6	0.33	0.275 ml	
HEPES			10	1.19 g	
BDM			15	0.75 g	
BSA			5 g/ml	2.5 g	
Glucose			10	0.9 g	
Isolation buffer (IB), pH 7.2				/50 ml	

PBS					
EDTA	372.2	0.5	2	200 µl	Sigma
BSA			0.5%	0.25 g	
MW, molecular weight					

To prepare the DB, the proteolytic enzymes collagenase B, collagenase D and protease XIV were added to PB at 0.3, 0.4 and 0.05 mg/g depending on the adult body weight (BW). Enzyme concentrations were empirically standardised for optimal heart digestion for each particular age. Thus, the minimum amount of enzyme required for a good quality CM preparation was determined for P0-P3 neonate hearts to be equivalent to the amount that would be used for a mouse with a BW of 5g, as listed in Table 6.3, and for P10-13 pups to be equivalent to the amount that would be used for a mouse with a BW of 8g. The total amounts of digestion enzymes required on any one day were calculated based on the total number of mice from which hearts were to be collected in that day. An example calculation is shown in Table 6.2, where the amounts of digestion enzymes were calculated for a litter of 6 pups aged P0-P3 for a mouse with a BW of 5 g. Enzymes were prepared as separate stock solutions by weighing each one separately into a 1.5 ml microfuge tube, and dissolving in 1 ml of PB. Individual DB aliquots were prepared for each mouse by adding enzyme stocks into PB, i.e., 16 ml of PB minus the required enzyme volumes for a pup, or, 25 ml of PB minus the required enzyme volumes for an adult. The volume of DB used took into account the flow rate to standardise the overall time taken to perfuse pup and adult hearts (see Table 6.3). All buffers were kept at RT throughout the procedure.

Table 6.2: Preparing digestion buffer (DB) for neonatal hearts

	No. of mice	Set BW (g)	Total BW (g)	Col B (0.3mg/g BW)	Col D (0.4mg/g BW)	P XIV (0.05mg/g BW)
Litter of 6 pups (P0-3)	6	5	30			
Stock conc. of enzymes (mg/ml)				= 30 x 0.3 = 9	= 30 x 0.4 = 12	= 30 x 0.05 = 1.5
For one pup	1	5	5			
Conc. of enzymes per pup (mg)				= 5 x 0.3 = 1.5	= 5 x 0.4 = 2	= 5 x 0.05 = 0.25
Vol. of stock to add to DB per pup (µl)				= (1.59 / 9) x 1000 = 167	= (2 / 12) x 1000 = 167	= (0.25 / 1.5) x 1000 = 167
Total vol. of DB buffer per pup (ml)					16	

BW, body weight; Col B, Collagenase B; Col D, Collagenase D; P XIV, Protease XIV

6.2.1.3 Extraction and cannulation of the heart

The following steps were performed in preparation for the cannulation of the heart. A cannula of an appropriate size that is dependent on the heart size (see Table 6.3 and Figure 6.1A) was attached to a 2 ml syringe filled with PB. The filled syringe-cannula was secured onto a circular weighted board to prevent movement of the cannula during the procedure. To ensure that no air bubbles entered the heart during perfusion, the cannula was primed with PB. A loop of 6.0 silk (~3 cm) was tied around the base of the cannula and set aside.

Mice were heparinised by intraperitoneal injection (volumes listed in Table 6.3) to prevent blood coagulation, which would obstruct the perfusion of the myocardium through the coronaries. Surgical tools were surface sterilised with 70% ethanol. Twenty to thirty minutes after heparin administration, the mouse was euthanised by decapitation, cervical dislocation (CD), or isoflurane and CD, and immediately placed onto the operating board directly under a dissection microscope and was secured in a supine position with surgical

tape. The chest region was sterilised with 70% ethanol before a longitudinal incision was made above the diaphragm using small tough cut scissors and serrated forceps (surgical instruments are shown in Figure 6.1A). The thoracic cavity was exposed by cutting the lateral sides of the ribcage along with the skin, and the front of the ribcage was retracted and removed, exposing the heart. Surrounding tissues were removed including the lungs and the oesophagus, which was severed with a transverse cut. The heart was still attached to the aorta and via connective tissue to the thymus but was freed from other connective tissues.

Cannulations were performed *in situ* whereby the heart was gently elevated by gripping the thymus with serrated forceps. Fine scissors were opened and placed horizontally underneath the heart at the back of the cavity, pressed against the posterior wall of the ribcage. The aorta was carefully isolated by cutting the connective fatty tissue that keeps the aorta in place along the spine, starting from the aortic arch down to the diaphragm. The aorta was then cut transversely so that approx. 0.5-1 cm of the ascending aorta remained intact. This aorta length was necessary to enable the successful cannulation of the smaller pup hearts as the aorta is very delicate and susceptible to breakage. The thymus and heart were released from the grip of the forceps and placed back into the open cavity. The operating board was rotated 90° clockwise so that the head of the mouse was to the left. The syringe-cannula was placed perpendicular to the mouse so that the tip was near the opening of the aorta. Under a dissection microscope, the aorta was drawn onto the cannula until the end of the cannula was approx. 1 mm above the aortic valves, using two fine forceps to grip either side of the aortic wall (fine curved forceps were used for adult and preadolescent aortae or fine mini forceps were used for neonatal aortae). This placement of the cannula enables retrograde perfusion of the heart, in which the leaflets of the aortic valve close, resulting in the perfusion of the myocardium via the coronary arteries. The aorta was then secured to the cannula by tying a silk suture twice around the tip, and the thymus and extraneous tissue were dissected away. The time taken to cannulate the heart after extraction was less than one minute.

Table 6.3: Detailed procedure for the purification of CMs from murine neonatal and adult hearts

	P0-P3	P10-P13	Adult
Heparin (1000IU/ml)	10 μ l	20 μ l	100 μ l
Incubation period after heparin injection (min)	20-30	20-30	20-30
Cannulation of the heart			
Euthanasia	Decapitation	CD	2-4% Isoflurane and CD
Cannula	30 G blunt needle	25 G blunt needle	24 G gavage needle
Time taken to dissect, extract and cannulate the heart (min)	3	3	3
Perfusion of the heart			
Flow rate (ml/min)	1.5	2	3
Volume of PB (ml)	4	6	9
Time taken to perfuse with PB (min:sec)	2:40	3	3
BW per mouse for enzyme conc. calculation (g)	5	8	BW
Volume of DB (ml)	16	16	25
Time taken for DB perfusion (min:sec)	10:40	8:00	8:20
Isolation of CMs			
Buffer for isolation	Isolation buffer	Transfer buffer	Transfer buffer
Filter (μ m)	70	200	200
Enrichment of CMs			
Centrifugation	NA	55 g for 3 min (x3)	20 g for 3min (x3)
Volume of buffer (ml)	NA	8	10
Purification of CMs			

Method of purification	Miltenyi Neonatal CM	CD31 Ab conjugated to Dynabeads	CD31 Ab conjugated to Dynabeads
Volume of Ab-beads (μ l)	10	12.5	25
Incubation time with Ab-beads (min)	15	15	15
Total time taken for purification (min)	18	18	18
Total time taken from heart cannulation to purifying CMs (min)	55	60	60

P, postnatal day; CD, cervical dislocation; PB, perfusion buffer; BW, body weight; DB, digestion buffer; CM, cardiomyocyte; Ab, antibody.

6.2.1.4 Perfusion of postnatal hearts

The Langendorff apparatus was prepared at the beginning of each experimental day by cleaning the perfusate line with 70% ethanol (10 ml) followed by Milli-Q water (20 ml). The perfusion system was also cleaned with HCl (1M) and rinsed with Milli-Q water each month. Once cleaned, the heating immersion circulator was turned on and set to a temperature that maintains the perfusate at 37°C. This was monitored with a digital thermometer probe at the outflow nozzle below valve 2 (see Figure 6.1C). Prior to perfusion, the Langendorff apparatus was cleared with PB (30 ml) to remove air bubbles in the perfusate line, mainly in the coil of the heat exchanger. The Langendorff apparatus was then primed with PB and DB. Prior to the start of the experiment, the peristaltic pump was set to the appropriate flow rate (Table 6.3), which was determined according to the size of the heart (Figure 6.1B).

Immediately after cannulation of the heart, the peristaltic pump was turned on to begin the flow of perfusate and the cannulated heart was mounted onto the Langendorff system at the outflow nozzle (Figure 6.1B & C). The pre-heated water-jacketed organ bath was moved upwards around the heart to maintain a warm environment. The heart was digested by retrograde perfusion with PB and DB for ~13 minutes (Table 6.3). PB was used to pre-clear the heart of blood from the coronary arteries, turning the cardiac tissue from red to white,

indicative of blood clearing, as well as the uniform perfusion, and thus, digestion of the heart. Towards the end of perfusion, TB was added to a petri dish at either 2 ml for preadolescent hearts or 3 ml for adult hearts (Table 6.3). For neonatal hearts, 2 ml of IB was added to a petri dish. The peristaltic pump was turned off immediately before the DB emptied to avoid the introducing air bubbles into the heart that would reduce cell viability. The water-jacketed insulating organ bath was then lowered and the atria were dissected away by cutting the atria-ventricular junction. The ventricles were collected into a petri dish containing TB or IB.

6.2.1.5 Isolation of CMs

Following the digestion of the heart, tissues were dissociated into a cell suspension containing isolated CMs. This was either carried out on the lab bench, or if CMs were to be cultured this was performed under sterile conditions in a biohazard hood.

To dissociate the myocardium into a cell suspension, the ventricles of the heart were teased apart with fine scissors and sharp forceps into ~10 pieces in the petri dish containing TB or IB. Tissues were triturated by gently pipetting up and down 20-40 times using a 1 ml transfer pipette with trimmed tip to provide a large bore, and, thus, minimise mechanical shear stress. The cardiac cell suspension was then transferred from the petri dish into a 15 ml Falcon tube. Cells were resuspended in buffer of a specified volume with either IB (3 ml) for neonatal preparations, or, TB for preadolescent (6 ml) or adult (10 ml) preparations. The cell suspension was then passed through a filter cup (filter sizes are detailed in Table 6.3) to remove any undigested clumps of tissue. Immediately prior to counting, cells were uniformly resuspended by gently pipetting and loaded onto a haemocytometer (10 μ l). The number of CMs and percentage of rod-shaped CMs in each corner square of the grid were determined. Rod-shaped CMs are viable cells with an intact ultrastructure, whereas rounded cells with collapsed cell structures are dead, as identified by positive trypan blue staining (O'Connell *et al.*, 2007; Louch *et al.*, 2011). It was thus important to determine the yield and viability of the isolated CMs and only preparations with >60% rod-shaped CMs were used. In contrast, neonatal CMs are more robust and are usually round-shaped after isolation (Ehler *et al.*, 2013).

6.2.1.6 Enrichment of preadolescent and adult CMs

Preadolescent and adult CMs were enriched from cell suspensions by low-speed centrifugation to remove the smaller non-myocytes that remained suspended in the supernatant and were aspirated. This step was omitted for neonatal CMs because they are comparable in cell size to non-myocytes.

Centrifugations to enrich for adult CMs were performed at 20 g for 3 minutes at RT, as previously detailed by O'Connell *et al.* (2007). Preadolescent (P10 and P13) CMs were smaller and optimisation of the centrifugal force was required. The number of CMs present in the supernatant vs pellet was assessed following centrifugation at different speeds. A centrifugal force of 55 g for 3 minutes at RT was determined to be optimal for preadolescent CMs as this resulted in a high yield of CMs in the pellet with minimal losses to the supernatant. After the first centrifugation, the supernatant was aspirated and cell pellets were resuspended in TB for preadolescent (6 ml) or adult preparations (10 ml), respectively. Cells were then centrifuged and washed two more times. Immediately prior to counting, cells were uniformly resuspended by gently pipetting and loaded onto a haemocytometer (10 μ l). The number of CMs and percentage of rod-shaped CMs in each corner square of the grid were determined.

6.2.1.7 Purification of preadolescent and adult CMs

Preparations of enriched preadolescent and adult CMs were observed under a light microscope and showed there were ECs present, existing as single cells or as undigested threads or clumps that were separate from or attached to CMs. Immuno-magnetic cell separation was thus employed to remove these contaminating ECs (Figure 6.2). This technique is commonly used in other fields, particularly immunology. For immuno-magnetic cell separation, Dynabeads (4.5 μ m superparamagnetic beads) covalently bound to purified sheep anti-rat IgG were pre-coated overnight with the EC-specific cell surface Ab, rat anti-CD31 Ab.

In preparation for immuno-magnetic cell separation, Dynabeads (250 μ l of 10x stock, sufficient for a total of 10 adult or 20 preadolescent preparations) were added to a 2 ml tube

and washed with IB (1 ml) and then the tube was placed onto the MagnaRack for 1 minute to allow beads to separate on the magnet, following which the supernatant was removed and discarded. CD31 Ab (100 µg, i.e., 10 µg of Ab was used for every 25 µl of original 10X Dynabead stock) was added to the Dynabeads, which were resuspended in a total volume of 1 ml using IB. To conjugate the Ab to the beads, the mixture was incubated overnight at 4°C on a roller mixer. The Ab was then conjugated to the magnetic beads (Ab-beads), and stored at 4°C.

Immediately prior to CM purification, the Ab-beads (100 µl for adult or 50 µl for preadolescent preparations) were aliquoted into a 2 ml tube. The Ab-beads were then washed with IB (1 ml) by placing the tube onto the MagnaRack for 1 minute after which excess non-conjugated Ab was discarded in the supernatant. This wash step was repeated two more times. Immuno-magnetic cell separation was performed by adding CM-enriched cell preparations (2 ml) to the pre-washed Ab-beads, which were incubated on a roller mixer for 15 minutes at RT. The supernatant containing the CMs (unbound cells) was collected after placing the tube onto the MagnaRack for 2 minutes, and transferred into a fresh tube that was placed onto the MagnaRack for a further 2 minutes. This was repeated once more to ensure the complete removal of EC-bound beads from the cell suspension. To increase the CM yield, some of the isolated CMs were trapped in the collection of EC-bound beads to the magnet in the original tube, and were subsequently recovered by washing the beads IB (2ml) twice. After each wash, the supernatant was transferred into a fresh tube on the MagnaRack, and this was repeated with a second tube on the MagnaRack, to ensure all EC-bound beads were removed. After all the washes and transfers, the three supernatants containing purified CMs were combined into a 15 ml Falcon tube to a total volume of 6 ml for preadolescent and 8 ml for adult cell preparations. The bead-bound fraction was transferred into a separate 15 ml Falcon tube. Immediately prior to counting, CMs were uniformly resuspended by gently pipetting and loaded onto a haemocytometer (10 µl). The number of CMs and percentage of rod-shaped CMs in each corner square of the grid were determined.

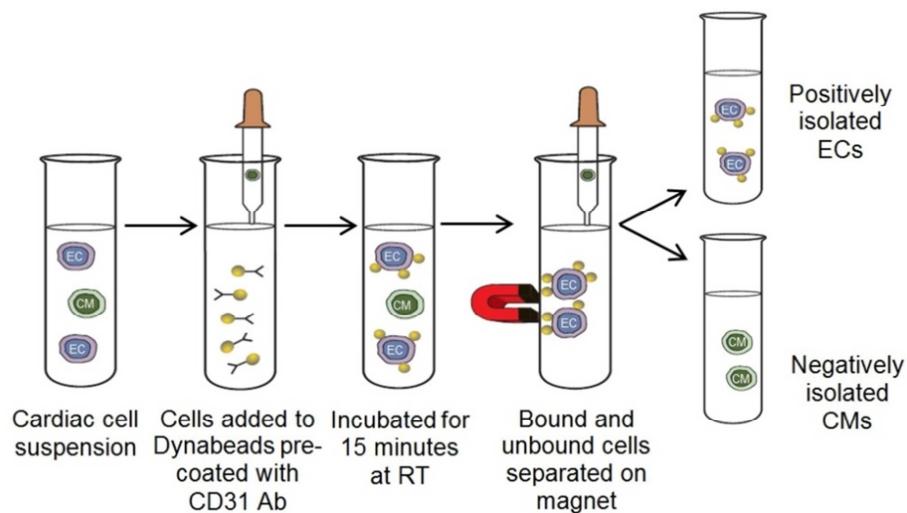


Figure 6.2: Immuno-magnetic separation of ECs from CMs

CM-enriched cell suspensions were transferred to a 2 ml tube containing Dynabeads pre-coated with CD31 Ab, and incubated on a roller mixer for 15 minutes at RT. Immuno-magnetic separation was used to remove bead-bound ECs from unbound CMs. The CM-containing supernatant was transferred to a new tube, leaving behind the bead-bound ECs. This figure was adapted from the “Dynabeads Cell Separation Guide”.

6.2.1.8 Purification of neonatal CMs

Neonatal CMs were purified using the Neonatal Cardiomyocyte Isolation Kit (Miltenyi Biotec) that utilises an OctoMACS™ Separator magnet on a MultiStand.

Neonatal CMs were purified as per the manufacturers’ instructions for the Neonatal Cardiomyocyte Isolation Kit. Briefly, isolated cells were centrifuged at 300 g for 5 minutes and the supernatant was aspirated and discarded. Cells were resuspended in cold IB (90 µl) and Neonatal Cardiomyocyte Isolation solution (10 µl) containing MicroBeads-conjugated to Abs against non-myocytes (the combination of Abs is proprietary information), and incubated for 15 minutes at 4°C with occasional mixing. During the incubation period, a MS column, containing ferromagnetic spheres in a matrix, was placed onto the OctoMACS magnet to apply a magnetic field (10,000-fold). The MS column was primed by applying cold IB (500 µl). After the incubation of cells and Abs, cold IB (500 µl) was added to the

cells, which were then applied to the MS column. Magnetically-labelled cells were retained in the column while the flow-through containing unlabelled CMs was collected into a 15 ml Falcon tube. To increase the yield of CMs, IB (500 µl) was applied three more times and the flow-through was collected each time. Non-myocytes, i.e. the magnetically-labelled cells, were collected separately by removing the column from the magnet and flushing the column with IB (1 ml) using a MS plunger. Immediately prior to counting, cells were uniformly resuspended by gently pipetting in IB (3 ml) and loading onto a haemocytometer (10 µl). The number of CMs and percentage of rod-shaped CMs in each corner square of the grid were determined. Trypan blue was initially used to assess cell viability but dye was routinely excluded from neonatal cells, indicating 100% cell viability.

6.2.2 Histology

For H&E staining of hearts and aortae see Chapter 3 (Section 3.2.8, staining with PicroSirius Red and Fast Green was omitted).

6.2.3 Flow cytometry

6.2.3.1 Fixing cells for flow cytometry

Cell suspensions were fixed with 2% PFA for 5 minutes at RT. After fixation, cells were resuspended in PBS (10 ml) and centrifuged at 300 g for 5 minutes at RT. The supernatant was aspirated and the cell pellet was resuspended in PBS (1 ml) and stored at 4°C.

6.2.3.2 Staining for flow cytometry

Cell suspensions were washed with BD Perm/Wash Buffer (200 µl) twice by centrifugation at 300 g, and the supernatant was discarded. Cell pellets were resuspended in BD Perm/Wash Buffer (100 µl) and incubated for 10 minutes at RT. Cells were then centrifuged at 300 g for 3 minutes and the supernatant was discarded. The following steps were

performed in the dark. CMs were stained with the CM-specific cTnT Ab Alexa Fluor 647 (cat. #: 565744, BD Pharmingen) that was diluted at 1:200 in BD Perm/Wash Buffer (100 μ l), and incubated for 30 minutes at RT in the dark. Samples were then washed with BD Perm/Wash Buffer (200 μ l) two times by centrifugation at 300 g for 3 minutes and the supernatant was discarded. Cell pellets were resuspended in PBS and 0.1% BSA in FACS tubes at approx. ~50,000 cells per 100 μ l. Nuclei were stained with propidium iodide (cat. #: 81845, Sigma) at 1:100 (stock concentration:1 mg/ml), which was added 10 minutes before using the flow cytometer. An unstained control, using buffer without Ab, was also prepared in a similar manner to determine the gating strategy against each stained sample (i.e., non-fluorescent samples vs the intensity of the fluorescent sample).

6.2.3.3 Flow cytometry

Tubes were loaded onto either a BD FACS Canto (BD Biosciences) or CytoFLEX (Beckman Coulter) flow cytometer. Nucleated cells were selected by gating those that were positive for propidium iodide, and CMs were selected by gating nucleated cells that were positive for cTnT. The gating strategy was determined by comparing the fluorescence intensity to unstained samples. Data were analysed and presented using FlowJo software.

6.2.4 Immunocytochemistry

Cell preparations were obtained after initial cell isolation, CM enrichment, and CM purification (including the bead-bound fraction) from each sample.

Immunostaining of fixed cells secured onto slides was performed as follows. Slides were incubated with blocking buffer (3% BSA in PBS; 80 μ l per slide) for 1 hour at RT, after which blocking buffer was removed by individually flicking slides. Cells were incubated overnight at 4°C with the primary Ab, mouse anti-cTnT (cat. #: ab10214, Abcam), diluted at 1:400 in blocking buffer (80 μ l per slide). Slides were washed in PBS twice and in lectin buffer (50mM Tris base, 0.87% NaCl, 0.02% MgCl₂, 0.01% CaCl₂, pH 7.6) twice for 5 minutes at RT on an orbital shaker. The following steps were performed in the dark. Cells were incubated for 1 hour at RT with the species appropriate secondary Ab, goat anti-mouse

IgG Alex Fluor 488, diluted at 1:1000 in blocking buffer, as well as an EC marker, Isolectin GS-IB₄-568 conjugate, diluted at 1:100 (cat. #: I21412, Life Technologies), and the DNA dye TO-PRO-3, diluted at 1:1000 (cat. #: T3605, Life Technologies) that were mixed together and added at 80 µl per slide. Cells were washed in lectin buffer for 5 minutes on an orbital shaker (x3). Coverslips were secured onto each slide with PVA-DABCO mounting medium. Slides were then stored at 4°C. Stained cells were imaged on a confocal microscope at 25x or 40x magnification using the same settings for all samples (Axio Observer inverted microscope equipped with a LSM 710 confocal scan head, Zeiss). Multiple fields of view (10 or 15 fields) were joined using the tiling function and at least 6 planes were summated using the z-stack function for each slide.

6.2.4.1 Counting cell populations

Cells were counted using ZEN software to select each nucleated cell that was: cTnT⁺ or IB₄⁺ or cTnT⁻ and IB₄⁻, using the arrow tool, which records a tally. All cells were counted excluding those that were not wholly visible, i.e., if the whole of an individual cell was indistinguishable due to overlapping cells. The percentages of CMs, ECs, or other cell types were calculated as a proportion of the total number of cells from each sample.

6.3 Results

6.3.1 Modification of the method for isolation and enrichment of adult CMs

Our laboratory is experienced in producing freshly isolated preparations of enriched CMs that can be used for cell culture using the O'Connell *et al.* (2007) method. This protocol was developed for measuring Ca^{2+} transients and contractility, and for biochemical assays that use freshly isolated adult CMs, as well as for biochemical assays and gene transduction that use cultured adult CMs. However, for transcriptomic analyses of CM gene expression profiles during cardiac growth (Chapter 7), it was essential to obtain freshly isolated, viable and highly purified populations of CMs without cell culture, from neonatal, preadolescent and adult hearts. Thus, the O'Connell *et al.* (2007) protocol was changed and adapted for this experimental end-point.

The main issue with the O'Connell *et al.* (2007) protocol was the use of the crude enzyme, collagenase II (Worthington), for tissue digestion, as it is well-known to have high batch-to-batch variation in enzymatic activity (Wolska and Solaro, 1996; Louch *et al.*, 2011). This leads to inconsistencies in tissue digestion, which affects cell viability and requires batch-to-batch optimisation. For this reason, I sought another protocol from Liao and Jain (2007), which uses a combination of three proteolytic enzymes that are more refined: collagenase B, collagenase D and protease XIV. These enzymes resulted in consistent tissue digestion and cell viability. A second issue of both the O'Connell *et al.* (2007) and Liao and Jain (2007) protocols was that they perform CM enrichment by sedimentation of these larger cells in parallel with Ca^{2+} re-introduction. Non-myocytes, which are smaller than CMs, are removed in the supernatant that is discarded and the cell pellet is resuspended in buffer with increasing concentrations of Ca^{2+} , and this is repeated two more times. Although Ca^{2+} -tolerant CMs are used for other experimental end-points (such as measuring Ca^{2+} transients and contractility), it reduces cell viability and, thus, was omitted from this protocol. Thirdly, the sedimentation of CMs can be performed by low-speed centrifugation for 3 minutes (O'Connell *et al.*, 2007), or by settling CMs into a pellet by gravity for 15 minutes (Liao and Jain, 2007). In this protocol, cells were centrifuged to ensure rapid isolation and

enrichment for CMs. Lastly, although both the O'Connell *et al.* (2007) and Liao and Jain (2007) protocols enrich for CMs, these fractions are contaminated with ECs that can be observed under a light microscope and by immunofluorescence (Figure 6.3). To remove ECs from enriched-CM fractions, I introduced a purification step using immuno-magnetic cell separation (see Section 6.3.4).

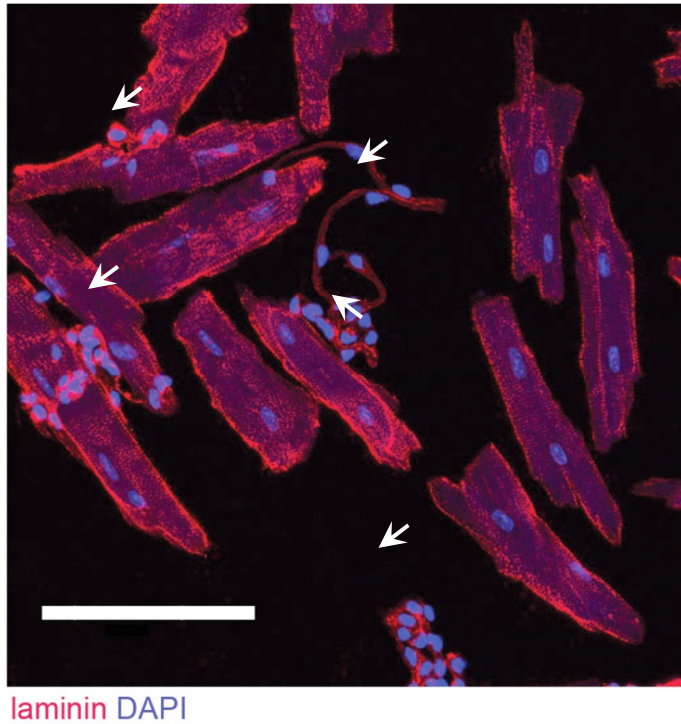


Figure 6.3: Enriched CM fraction contaminated with ECs

CMs were enriched for using the O'Connell *et al.* (2007) protocol, as detailed in Chapter 2, see Section 2.4. Cell membranes were stained with laminin (red) and DNA with DAPI (blue). ECs contaminate the CM-enriched preparation, and are present as undigested strings and clump together (white arrows). The scale bar is 100 μm .

6.3.2 Adapting the purification of CMs from adult hearts to neonatal and preadolescent hearts

The procedure for cardiac tissue digestion by Langendorff retrograde perfusion, isolation and purification of CMs was optimised for adult hearts and then adapted for neonatal and preadolescent hearts. The size of the heart and aorta varies markedly between adults and pups. Histological sections of aortic rings and whole hearts show the relative differences in size (Figure 6.4). Thus, every parameter of the procedure, from the cannulation and Langendorff retrograde perfusion of the heart to CM purification, including concentrations of proteolytic enzymes, volumes of buffers, *in situ* cannulation techniques, sizes of the cannula, sizes of surgical instruments, perfusate flow rate, the centrifugational force, volumes of Ab-beads used for CM purification and the incubation period with the Ab-beads, was modified (see Table 6.3). Hence, appropriately sized cannulae and surgical instruments were used for cannulation and Langendorff perfusion of hearts. Furthermore, for effective tissue digestion the concentration of digestion enzymes was adjusted to a specific “body weight” that was empirically determined as 5 g for neonatal and 8 g for preadolescent pups. The total perfusion time of hearts was comparable between neonates, preadolescents, and adults, resulting in reproducible and consistent CM yields and viability.

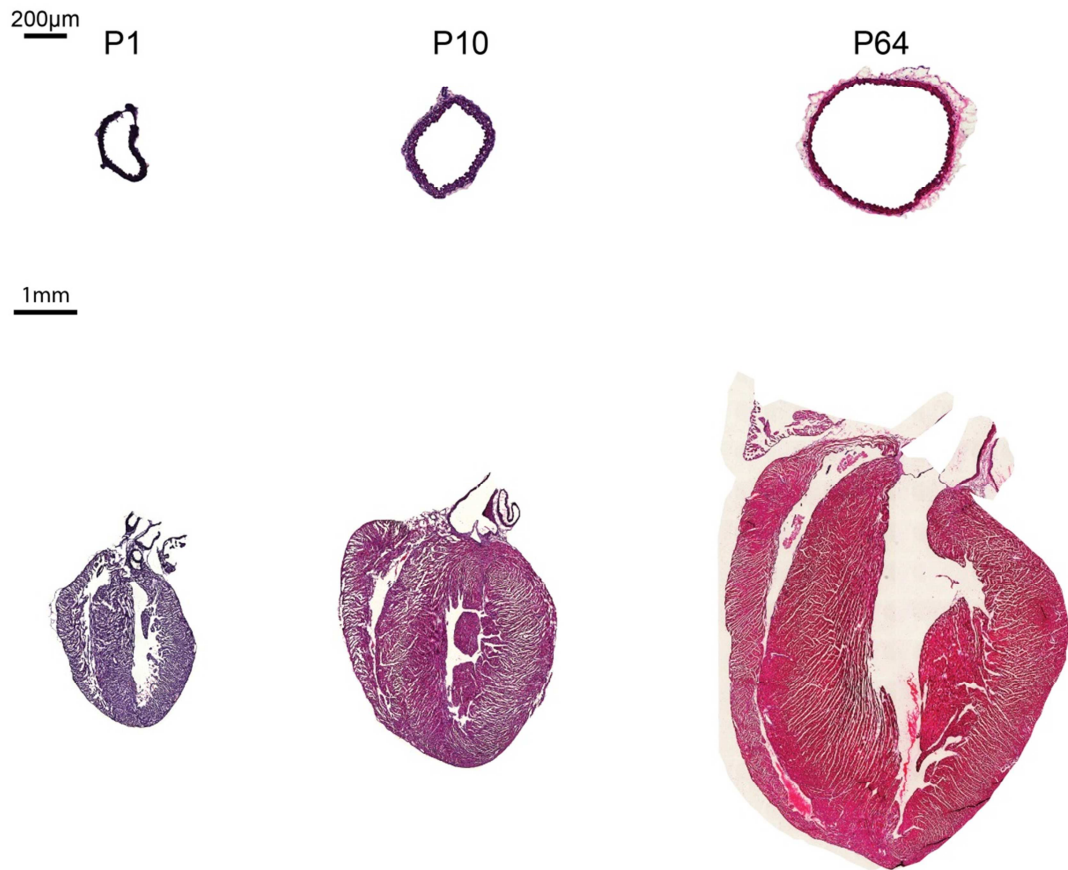


Figure 6.4: Histological sections of aortae and hearts from neonatal, preadolescent and adult mice

Histological sections of aortae (transversely sectioned at the level of the diaphragm) and hearts (sectioned coronally) from neonatal (P1), preadolescent (P10), and adult (P64) mice, were stained with H & E (DNA, blue; cell cytoplasm, red).

6.3.3 Characterisation of isolated and enriched CMs

After enzymatic digestion of the heart by Langendorff retrograde perfusion, tissue fragments were teased apart and dissociated into a cell suspension by gently pipetting, thereby isolating CMs. The estimated yield of CMs isolated from hearts at each age was: $\sim 1.2 \times 10^6$ at P2, $\sim 1.4 \times 10^6$ at P10, $\sim 1.6 \times 10^6$ at P13, and $\sim 2.3 \times 10^6$ at P70 (also presented in Chapter 7, Table 7.1). After CM enrichment by a series of low-speed centrifugations, the yield of CMs decreased by $\sim 20\%$, $\sim 17\%$, and $\sim 12\%$, in P10, P13, and P70 cell preparations, respectively.

During postnatal development, the proportion of cardiac cell types changed, whereby 58%, 36%, 37%, and 51% of the cells isolated from the heart were CMs at P2, P10, P13, and P70, respectively. In addition, the proportions of ECs were 34%, 61%, 50%, and 39%, at P2, P10, P13, and P70, respectively. CM enrichment resulted in an increase in the proportion of CMs that were 56%, 52%, and 86%, of the total cell population in P10, P13, and P70 cell preparations, respectively. The CM enrichment step was omitted for P2 cell preparation due to the comparable size of CMs and non-myocytes that are not so easily separated by centrifugation.

The average proportion of rod-shaped CMs, indicative of good cell viability, after cell isolation was 65-85% of CMs at P10 (Figure 6.8A), P13 (Figure 6.9A), and P70 (Figure 6.10A), also shown in Chapter 7 (Table 7.1). Although neonatal CMs are usually round rather than rod-shaped after cells are isolated from cardiac tissues that have been mechanically minced and sequentially incubated with proteolytic enzymes, a high proportion of neonatal CMs were rod-shaped ($\sim 50\%$) at P2 after cells were isolated by Langendorff perfusion and gentle trituration (Figure 6.5 and Figure 6.7A). Moreover, all neonatal cells excluded trypan blue, indicating 100% cell viability.

Additionally, *in situ* fixing of hearts with 2% PFA immediately after Langendorff perfusion (instead of fixing only after producing the cell suspensions) yielded $>95\%$ rod-shaped CMs for all ages. Hence, when cells were fixed after tissues were dissociated into a cell suspension, the proportion of rod-shaped CMs was lower (Figure 6.5), as mentioned above. This indicates high cell viability following enzymatic digestion by Langendorff perfusion

that only decreases with the mechanical shear stress associated with gentle trituration, which is required to dissociate cardiac tissues into cell suspensions.

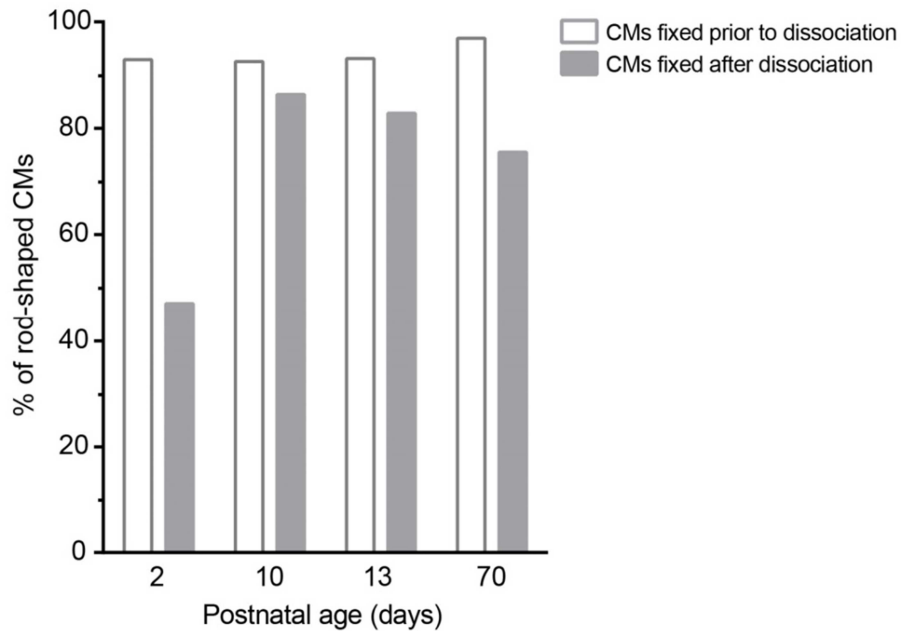


Figure 6.5: The percentage of rod-shaped CMs that were fixed prior to the dissociation of cardiac tissue or after

Cardiac cells were fixed prior to (*in situ*), or after the dissociation of cardiac tissues into isolated CMs by gentle trituration. The percentage of rod-shaped CMs was quantified for P2, P10, P13, or P70 preparations (n=2-4, 120-420 CMs per slide). Representative immunocytochemistry images of CMs fixed prior to dissociation are shown in Chapter 5 (Figure 5.5) and those fixed after dissociation are shown in Figure 6.7A (P2), Figure 6.8A (P10), Figure 6.9A (P13), and Figure 6.10A (P70).

6.3.4 Characterisation of purified CMs

Preadolescent (P10 and P13) and adult CMs were purified from enriched fractions by removing ECs using immuno-magnetic cell separation (Figure 6.2) with a CD31 Ab bound to Dynabeads. Neonatal CMs were purified from isolated cell suspensions by immuno-magnetic cell separation using the Neonatal Cardiomyocyte Isolation Kit (Miltenyi Biotec), which employs magnetic beads bound to multiple Abs against non-myocytes. The proportion of rod-shaped CMs after purification remained at 65-85% for P10, P13, and P70 (also presented in Chapter 7, Table 7.1), but decreased for P2 preparations to ~40%, although all P2 cells excluded trypan blue, indicating 100% cell viability. The estimated yield of purified CMs from heart at each age was: 9.3×10^5 at P2, 6.3×10^5 at P10, 7.9×10^5 at P13, and 1.6×10^6 at P70. After CM purification, there was an overall reduction in CM yield of ~23% , ~55%, ~51%, and ~30% in P2, P10, P13, and P70 cell preparations, respectively.

Preliminary data was collected by flow cytometry to quantify the proportion of CMs that stained positively for cTnT after purification. The CM-specific cTnT Ab was diluted at 1:200, resulting in the least overlap with an unstained control of cells from the same sample (Figure 6.6). Flow cytometry (Figure 6.6) indicated that there was a high proportion of CMs after purification of 96%, 91%, and 97% CMs from P2, P10, and P70 cell populations, respectively. However, this flow cytometric analysis did not provide quantitative or qualitative data for the EC population. If ECs were undigested and remained attached to CMs, they may be present in the gated cTnT⁺ cell population (Figure 6.6).

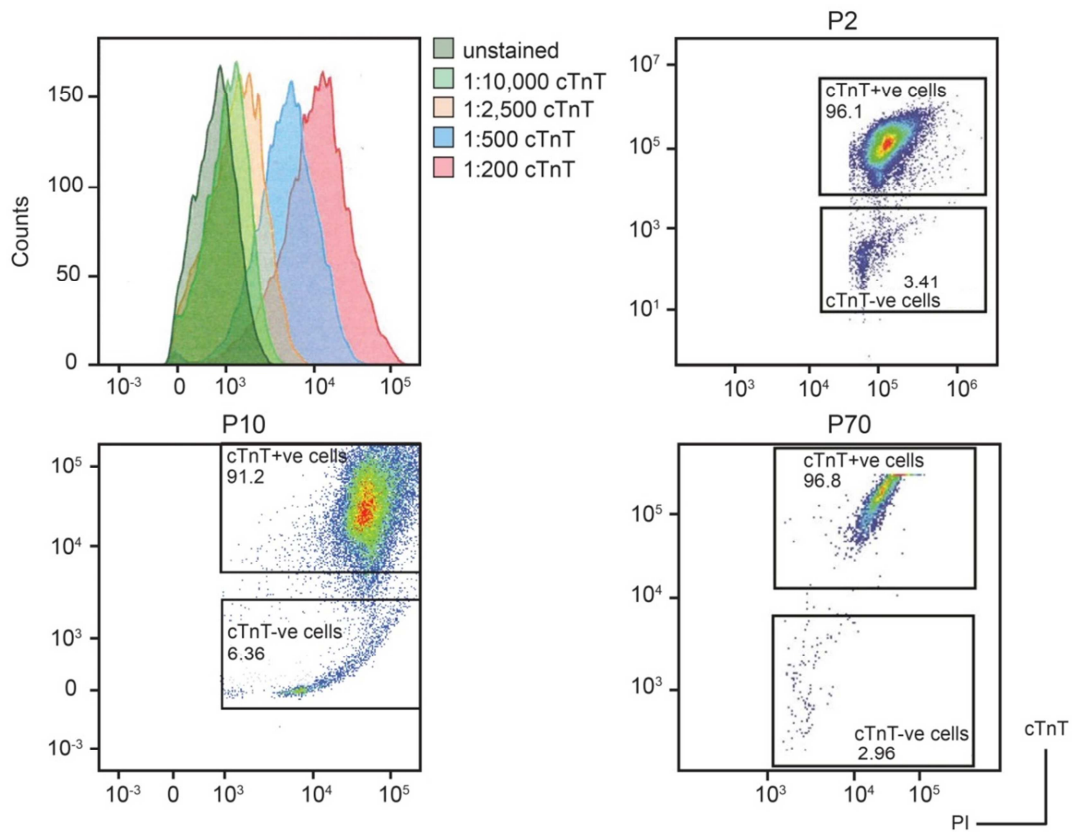


Figure 6.6: Flow cytometric analyses of purified neonatal, preadolescent, or adult CMs

Serial dilutions of the cTnT Ab (1:10000, 1:2500, 1:500, and 1:200) were used to determine the appropriate Ab concentration for flow cytometry such that there is minimal overlap of the cTnT⁺ population with the unstained control of the cell population using the same sample. The purity of CMs after purification by immune-magnetic cell separation was evaluated by flow cytometry in CM preparations from P2, P10, and P70 hearts. Nucleated cells were identified with propidium iodide (PI) and CMs with cTnT (1:200). The gating strategy was established using the unstained control.

To account for the EC population, cell preparations were assessed by immunocytochemistry after CM isolation, enrichment, and purification (including the bead-bound fraction), from P2 (Figure 6.7), P10 (Figure 6.8), P13 (Figure 6.9), or adult hearts (Figure 6.10). CMs were stained with cTnT, ECs were stained with isolectin B4 (IB4), and DNA was stained with TO-PRO-3. The number of nucleated (TO-PRO-3⁺) CMs (cTnT⁺), endothelial (IB4⁺), and other cell types (cTnT⁻ and IB4⁻), were counted and quantified as a percentage of the total number of cells (Figure 6.11). After purification by immuno-magnetic cell separation, the purity of CMs, quantified by immunocytochemistry, was 96%, 96%, 93% and 95% from P2, P10, P13 or P70 cell preparations, respectively. Following CM purification, the bead-bound fraction contained approximately 69%, 90%, 85%, and 85% of the ECs from P2, P10, P13, or P70 cell suspensions, respectively. The proportion of other cell types was very low (cTnT⁻, and IB4⁻) throughout the CM isolation, enrichment and purification procedure, although they did decrease after CM enrichment and purification (Figure 6.11).

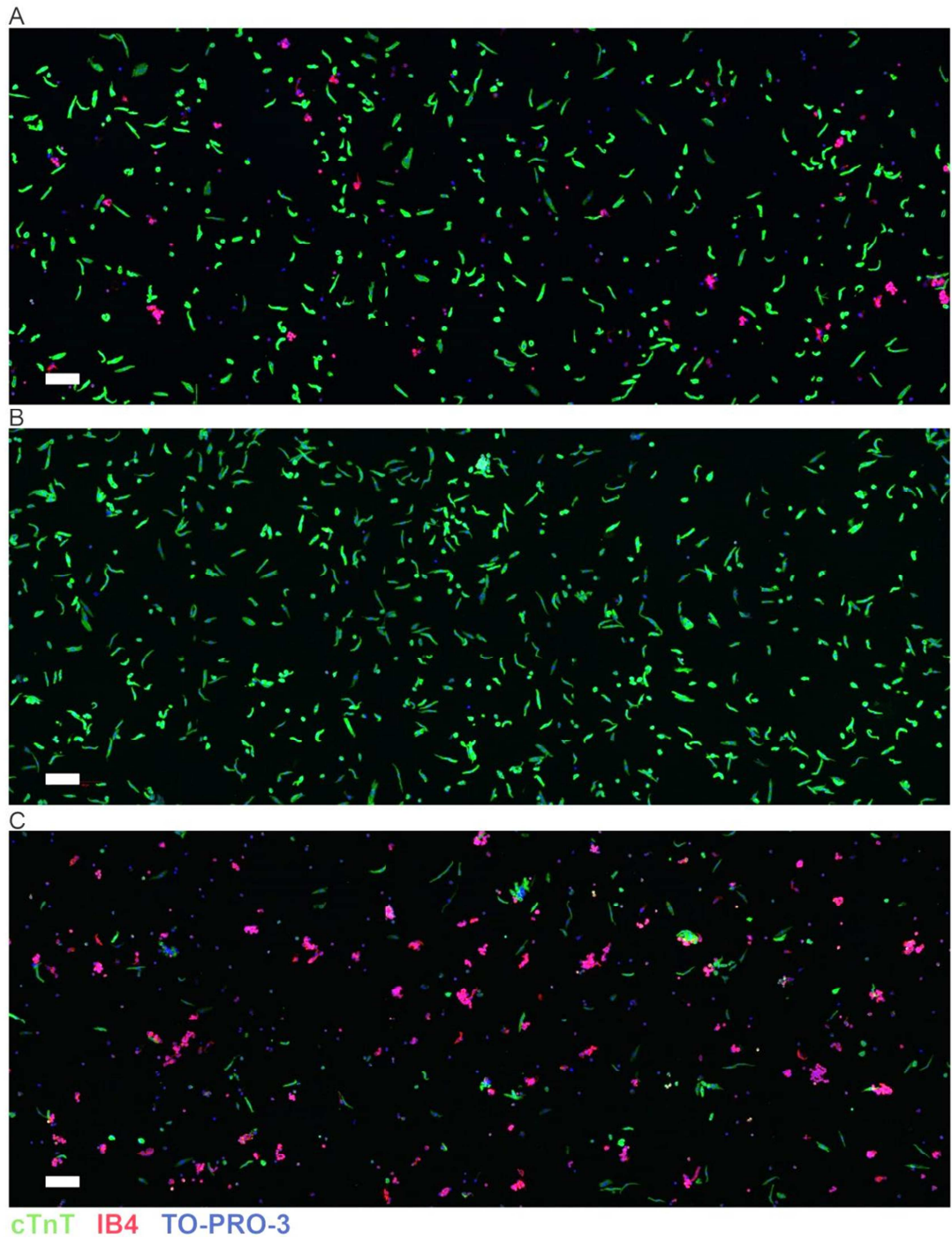


Figure 6.7: Isolation and purification of P2 CMs

Cells from P2 hearts were fixed and collected after isolation (A) or purification (B), and the bead-bound fraction (C) was collected (n=4, 10 fields of view per image at 25x). Cardiac cells were identified as CMs (TO-PRO-3⁺, cTnT⁺), ECs (TO-PRO-3⁺, IB4⁺), or other (TO-PRO-3⁺, cTnT⁻, IB4⁻). Scale bar is 100 μ m.

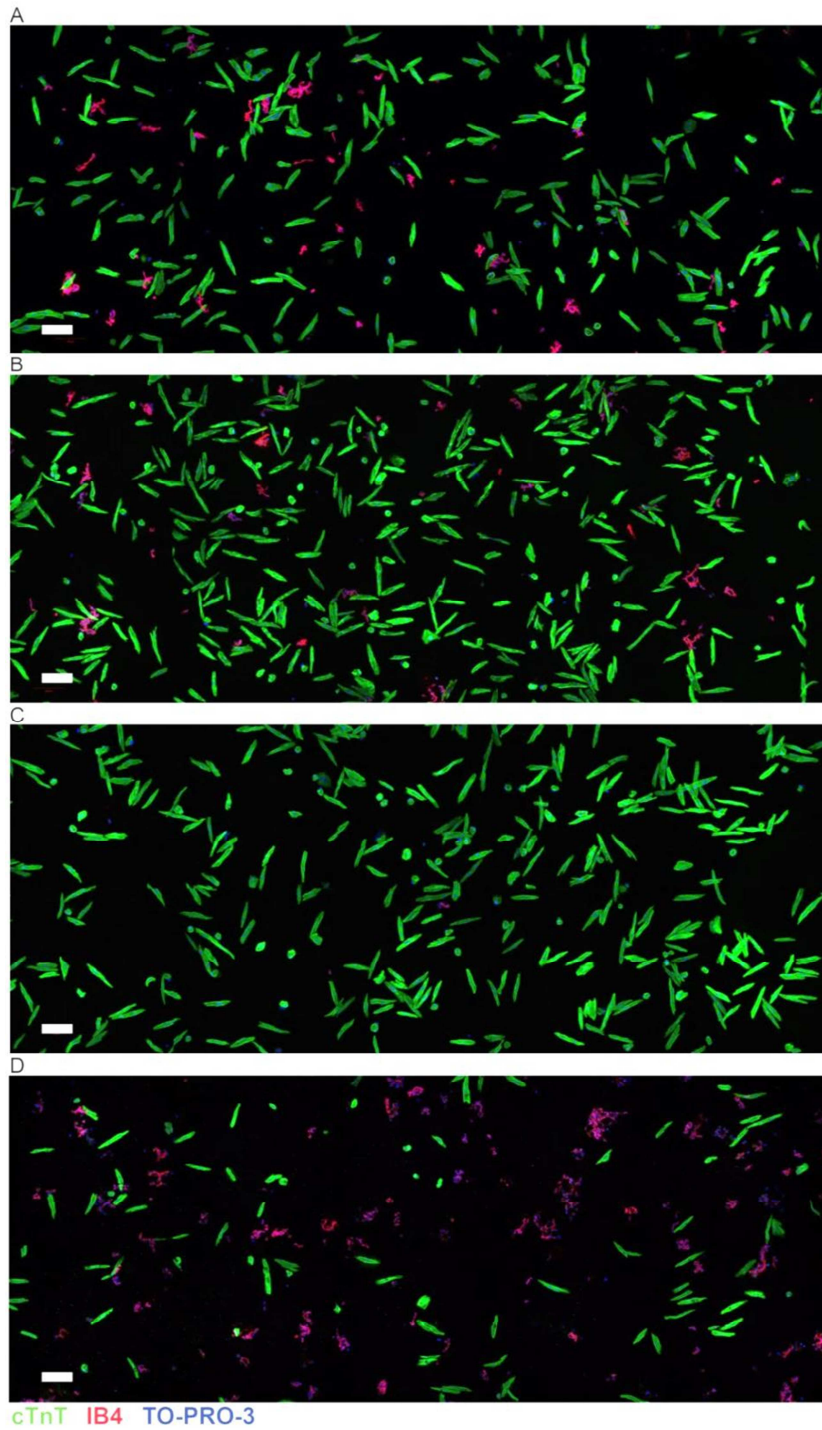


Figure 6.8: Isolation, enrichment and purification of P10 CMs

Cells from P10 hearts were fixed and collected after isolation (A), enrichment (B) or purification (C), and the bead-bound fraction (D) was collected (n=4, 10 fields of view per image at 25x). Cardiac cells were identified as CMs (TO-PRO-3⁺, cTnT⁺), ECs (TO-PRO-3⁺, IB4⁺), or other (TO-PRO-3⁺, cTnT⁻, IB4⁻). Scale bar is 100µm.

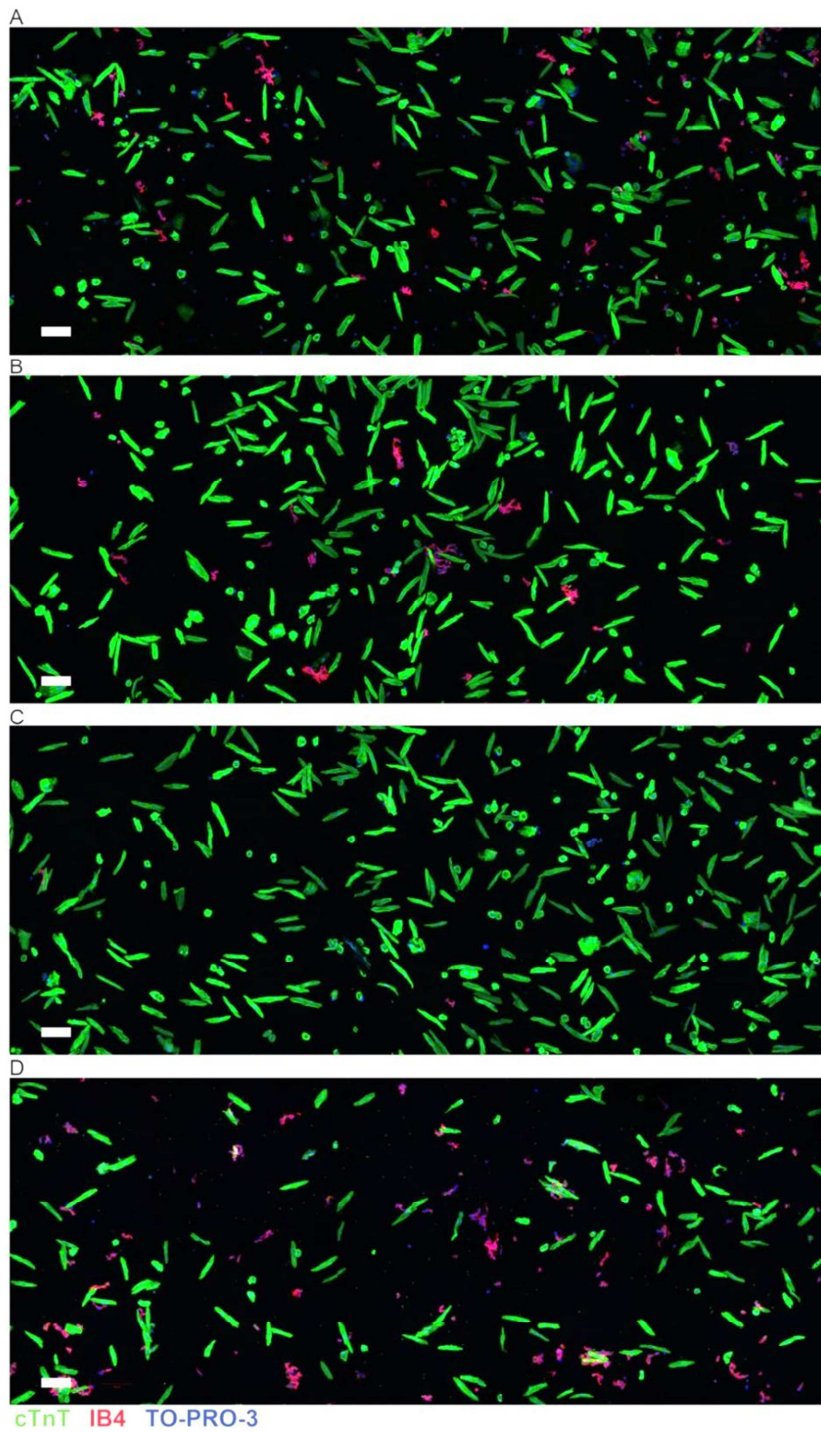


Figure 6.9: Isolation, enrichment and purification of P13 CMs

Cells from P13 hearts were fixed and collected after isolation (A), enrichment (B) or purification (C), and the bead-bound fraction (D) was collected (n=3, 10 fields of view per image at 25x). Cardiac cells were identified as CMs (TO-PRO-3⁺, cTnT⁺), ECs (TO-PRO-3⁺, IB4⁺), or other (TO-PRO-3⁺, cTnT⁻, IB4⁻). Scale bar is 100 μm .

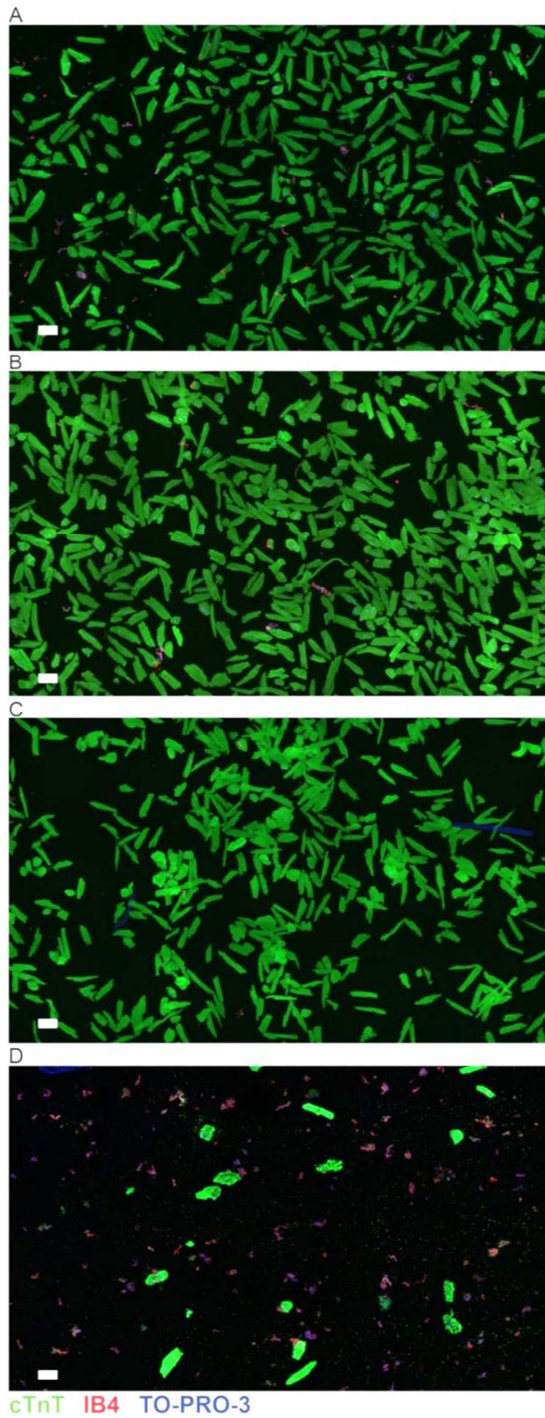


Figure 6.10: Isolation, enrichment and purification of adult CMs

Cells from P10 hearts were fixed and collected after isolation (A), enrichment (B) or purification (C), and the bead-bound fraction (D) was collected (n=3, 15 fields of view per image at 25x). Cardiac cells were identified as CMs (TO-PRO-3⁺, cTnT⁺), ECs (TO-PRO-3⁺, IB4⁺), or other (TO-PRO-3⁺, cTnT⁻, IB4⁻). Scale bar is 100 μ m.

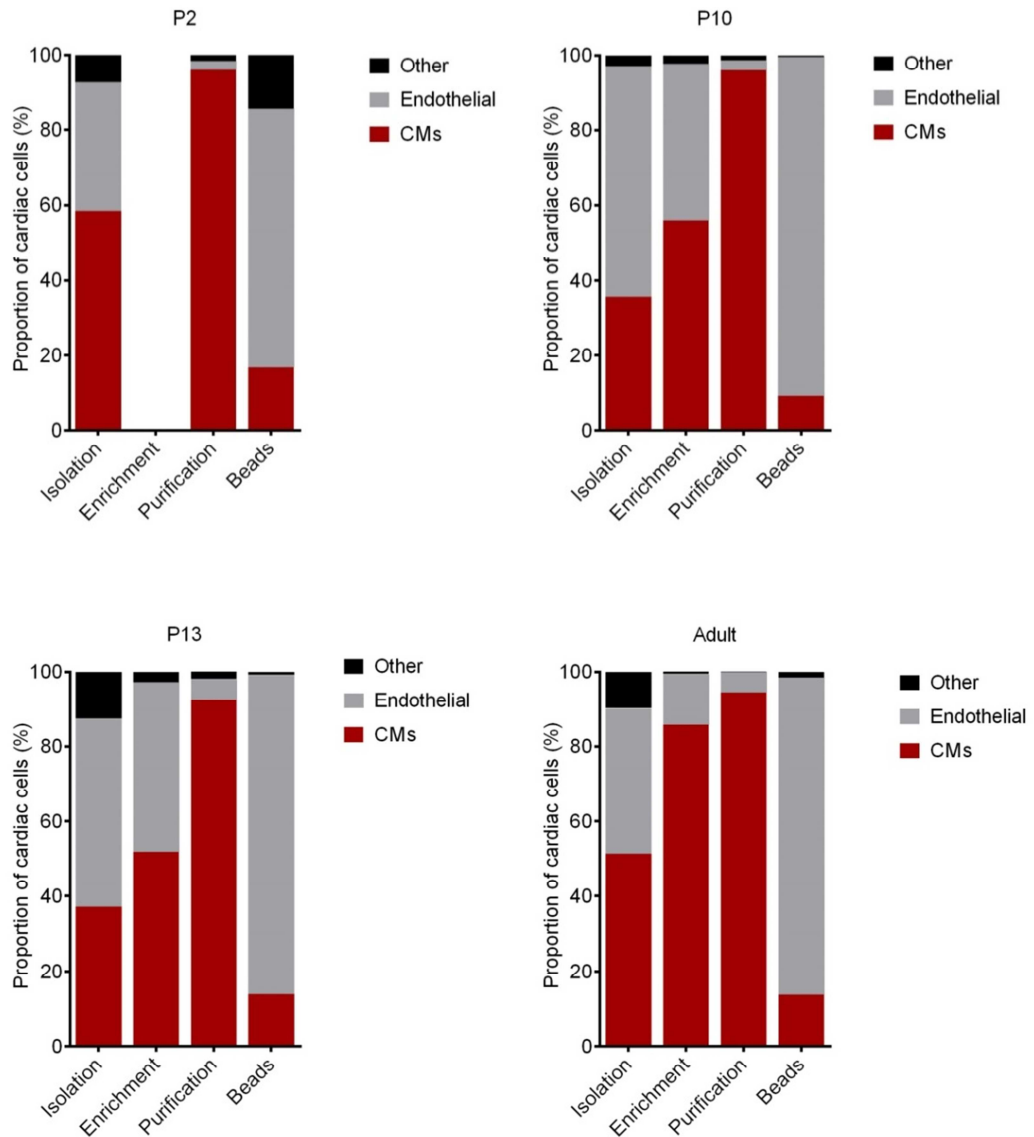


Figure 6.11: The proportion of CMs, ECs or other cell types quantified at various stages of the CM purification procedure

Cardiac cells from P2 (n= 3, ~2000 cells per n), P10 (n=4, ~1500 cells per n), P13 (n=3, ~1500 cells per n), or adult (n=3, ~1500 cells per n) hearts, were collected following the isolation, enrichment or purification steps, and the number of nucleated CMs (cTnT⁺), endothelial (IB4⁺), or other cells (cTnT⁻, IB4⁻) were quantified as a percentage of the total number of cardiac cells counted.

6.4 Discussion

Here I have reported on the development of standardised methods to isolate and purify CMs from neonatal, preadolescent or adult hearts using Langendorff retrograde perfusion and immuno-magnetic cell separation. This involves *in situ* cannulation of the heart, enzymatic digestion of the myocardium, and subsequent isolation, enrichment and purification of CMs. Using this approach, a high yield of viable and pure CMs (~95%) is reproducibly obtained across a range of postnatal ages.

The isolation and purification of CMs can be categorised into four steps that each require careful consideration: i) digestion of the heart by Langendorff retrograde perfusion, ii) dissociation of cardiac tissue into isolated CMs, iii) enrichment of CMs by removing non-myocytes, and iv) purification of CMs by further removing non-myocytes. This procedure was developed and optimised for adult hearts, and was then adapted for neonatal and preadolescent hearts, which vary greatly in size (Figure 6.4). The advantage of this method is that neonatal, preadolescent and adult CMs are collected in a comparable timeframe of ~1 hour from the time of euthanasia (Table 6.3). Optimisation took the following parameters into account: sizes of surgical instruments, *in situ* cannulation technique, cannula size, concentrations of proteolytic enzymes, perfusate volumes, perfusate flow rates, centrifugal forces required for CM enrichment, and immuno-magnetic cell separation (including the volume and incubation time with magnetic beads).

The main consideration for CM isolation from neonatal and adult hearts was the large difference in size of the heart, CMs and aortae, between pups and adults (Figure 6.4). In addition, the aortae from P2, P10, and P13 pups are more delicate and, thus, more likely to tear than those of adults, hence the wide recognition of the technical challenges in cannulation and Langendorff retrograde perfusion of younger hearts (Ehler *et al.*, 2013; Louch *et al.*, 2011). This has resulted in two different methods being commonly used to digest heart tissues from neonatal vs adult mice. For the cannulation of adult hearts, most methods involve cutting the aorta just proximal to the aortic valve. The heart is then removed and placed into a petri dish containing ice cold buffer where it is cannulated *ex vivo* (Roth *et al.*, 2014; Li *et al.*, 2014a; Liao and Jain, 2007; O'Connell *et al.*, 2007; Louch *et al.*, 2011). The method described here performs cannulations *in situ* using most of the ascending aorta (0.5-1 cm), which is sufficient in length to guide the aorta onto the cannula.

This has enabled the cannulation of both pup and adult hearts to be successful. Once the heart is mounted onto the Langendorff apparatus, it is digested using proteolytic enzymes to break down the extracellular matrix. It is important at this step that hearts are not under- or over- digested so that CM structural integrity, cell yield or viability, are not compromised. Collagenase II is usually used in digestion buffers (Wolska and Solaro, 1996; Louch *et al.*, 2011), however, the batch-to-batch variation of enzyme activity requires optimisation to ensure consistent tissue digestions, cell yields and viability. This optimisation process leads to the use of extra animals, time, and reagents. An alternative digestion buffer using collagenase B, collagenase D, and protease XIV, according to the Liao and Jain (2007) method, provided consistent tissue digestion, cell yield and viability, relative to collagenase II (O'Connell *et al.*, 2007). Moreover, both of these protocols were developed for adult hearts, and thus, all the parameters of Langendorff perfusion with proteolytic enzymes were tested to ensure consistent digestion of neonatal and preadolescent hearts.

CMs were isolated after Langendorff retrograde perfusion by dissociating tissues into a cell suspension. Thereafter, the proportions of cardiac cells were quantified by immunocytochemistry (Figure 6.11), showing that the majority of isolated cells in the adult heart were CMs (51%) or ECs (39%). This is similar to the report of Banerjee *et al.* (2007) who estimated that 56% of adult cardiac cells were CMs by flow cytometry, but contrasts with others who estimated that ~30% of adult cardiac nuclei were CMs by immunohistochemistry (Raulf *et al.*, 2015; Pinto *et al.*, 2016). The main caveat for immunohistochemical analysis is that 20% of the nuclei were unaccounted for, and although ~31% of nuclei were reported as CMs, rodent adult CMs are binucleated, which would mean only ~15% of cells were CMs. This work has found that the second major cell type in the adult heart was ECs and not fibroblasts, and hence on this issue, is in agreement with Pinto *et al.* (2016) but not Banerjee *et al.* (2007). The proportion of CMs and non-myocytes also changed during postnatal cardiac development, in that most P2 cells were CMs (58%) rather than ECs (34%), similar to that reported by Banerjee *et al.* (2007). At P10 and P13, the majority of cells were ECs (61% and 50%, respectively) and there were less CMs (~36%), however, Banerjee *et al.* (2007) reported that ~62% of cardiac cells were CMs and ~18% were fibroblasts at P15. It is clear that the proportion of the various cardiac cell types changes during postnatal cardiac growth but determining the exact percentages does require further evaluation with more replicates and at least two methods of quantification.

Cell viability was assessed by the proportion of rod-shaped vs round CMs (Louch *et al.*, 2011; O'Connell *et al.*, 2007; Liao and Jain, 2007). The range of viable preadolescent and adult CMs was 65-85% after both the isolation and purification steps, similarly reported by O'Connell *et al.* (2007) and Liao and Jain (2007). Most neonatal CM isolation protocols and commercial kits yield round CMs (Ehler *et al.*, 2013) and, thus, it was a surprise that a high proportion of neonatal CMs were rod-shaped after Langendorff retrograde perfusion. The majority of neonatal CMs remained rod-shaped after purification through the magnetic column using the Neonatal Cardiomyocyte Isolation Kit. All neonatal CMs that were purified using this method excluded trypan blue dye, likely due to the more gentle digestion of heart tissue by coronary perfusion with digestion enzymes, which takes ~13 minutes, rather than mincing heart tissues with scissors and then incubating in digestion enzymes overnight and/or serial incubations for >15 minutes 5-8 times (Ehler *et al.*, 2013; Louch *et al.*, 2011). It was also clear that the physical dissociation of tissues by pipetting causes mechanical shear stress, resulting in a fewer proportion of rod-shaped CMs (Figure 6.5). This was evident after fixing cardiac cell *in situ* immediately after Langendorff perfusion followed by dissociating tissues into a cell suspension, which yielded a high proportion of rod-shaped CMs (>95%) from P2, P10, P13, and P70 hearts. Hence, the mechanical shear stress from gentle trituration reduces the proportion of rod-shaped CMs from >95% to 65-85% (when cells were fixed after isolation), decreasing cell viability.

Protocols and commercial kits for neonatal CM isolations are lengthy and use multiple hearts (5-15) that are pooled to increase CM yield. The use of multiple hearts per preparation does not allow use of independent biological replicates. One of the commercial kits (Pierce Cardiomyocyte Isolation Kit, Thermo Scientific) for CM isolation has reduced this time to 1 hour (without CM purification) and reports a yield of ~2 million neonatal CMs per 100 mg of tissue, which is reported to be a higher yield than other commercially available kits. In comparison, the protocol described here yields 1.2 million CMs per neonatal heart, which weighs approx. ~7 mg (Chapter 5, Table 5.2). This would be equivalent to 17 million CMs per 100 mg of tissue, which yields ~9-fold more CMs from a single heart. Therefore, the method detailed here is substantially higher than current protocols. The yield of adult CMs was 2.2 million CMs per adult heart, which was also higher by almost twice the number of CMs than the average 1.1-1.5 million CMs per adult heart that has been previously reported (O'Connell *et al.*, 2007). Most protocols omit details of CM yield. Previous reports from our laboratory (Naqvi *et al.*, 2014), are more

comparable to the CM yields reported in this work for the different ages, although they are reduced by $\sim 2 \times 10^5$ CMs at P1, P10, and adult time points. This may be because in this study CMs were counted 1-2 times after each step of CM isolation, enrichment, and purification, to minimise delays in the length of process, and therefore, the yield is reported as an estimation. Another factor may be the choice of enzymes used for CM isolation, which was collagenase II in the O'Connell *et al.* (2007) protocol used by Naqvi *et al.* (2014), whereas this study used a combination of enzymes from the Liao and Jain (2007) protocol. In general, the estimated yield of neonatal, preadolescent and adult CMs in this study was higher than those reported previously.

Careful consideration was given to the enrichment step, since CM size varies at different postnatal ages (see Chapter 5, Figure 5.5B and C). Low-speed centrifugations at 20 g enriches for adult CMs O'Connell *et al.* (2007). This was optimised for P10 and P13 CMs to 55 g to minimise the loss of CMs in the supernatant that resulted in a 20% and 17% reduction in yield after enrichment, respectively. Because neonatal CMs are similar in size to non-myocytes, the enrichment step by centrifugation was omitted. Thus, it was difficult to distinguish with confidence round neonatal CMs from neonatal non-myocytes when counting cells under a light microscope, although round CMs appear to be more irregular in shape. Therefore, the yield of neonatal CMs is also an estimate. CM purity increased after enrichment by 15-20% in P10 and P13 isolated cardiac cell preparations, and by 35% in P70 isolated cardiac cell preparations, however, contaminating ECs were still present (Figure 6.3, Figure 6.8B, Figure 6.9B and Figure 6.10B). This is likely due to the incomplete digestion of ECs. ECs are usually isolated by incubating cardiac tissues with collagenase A for 45-60 minutes with continuous agitation (Jelonek *et al.*, 2011). Perhaps an improvement to this protocol may be to incorporate the use of this enzyme provided the viability of the CM population is not compromised.

Although cell culture is often used to improve the purity of adult and neonatal CMs by incubation for $\sim 1-48$ hours, it may lead to changes in gene expression and the de-differentiation of CMs (Louch *et al.*, 2011; Ehler *et al.*, 2013). Employing immunomagnetic cell separation (< 20 minutes) rapidly purifies CMs without the need of cell culture to remove ECs from individual preadolescent and adult cardiac cell preparations, while the Neonatal CM Isolation Kit was used for individual neonatal cardiac cell

preparations. This resulted in a CM purity of ~95% that is consistent across the postnatal ages (Figure 6.10), as evaluated by immunocytochemistry (P2, 96%; P10, 96%; P13, 93%; and P70, 95%; Figure 6.11), and is comparable to the CM percentages determined by flow cytometry (Figure 6.6). In rats, Percoll gradients used to purify adult or neonatal CMs yielded similar purities of 90-95% (Maisch, 1981; Chlopcikova *et al.*, 2001), however, CM purification using Percoll has been reported to be complicated and time-consuming (Louch *et al.*, 2011; Chlopcikova *et al.*, 2001). Purification of CM-enriched fractions from P10 and P13 hearts reduced the yield of CMs by ~30%. This may be due to a number of CMs that were trapped in the magnetic bead pellet, or, non-specific binding of CMs to magnetic beads. The first issue was addressed by washing the bead pellet a few times to release CMs, and the latter was partly addressed by reducing the volume of magnetic beads to half the amount used for adult preparations. Purification of CM-enriched fractions from the adult heart also resulted in a loss of ~18% CMs. Nevertheless, the yield and purity of CMs remained high, whereby the majority of contaminating ECs (~70-90%) were removed. Overall, immuno-magnetic cell separation is an easy and effective method to rapidly purify CMs.

In summary, this protocol provides a standardised method that rapidly produces freshly purified CMs using Langendorff retrograde perfusion and immuno-magnetic cell separation from individual mouse hearts at any postnatal age. As evident from the studies shown in Chapter 7, the resulting homogenous and viable population of CMs provided high-quality input material for downstream profiling of CM transcriptomic signatures.

Chapter 7 Transcriptional profiles of CM maturation

7.1 Introduction

The postnatal murine heart grows rapidly, increasing in mass by ~3-fold between P10 and P35, commensurate with a similar increase in body weight over this period. However, heart (HW/BW) growth is rapid between P10 and P18, increasing by ~23%. During this period, serum T₃ levels increase from P10 to P12, while the expression of mitosis-related genes decreases from P10 to P18, CMs enlarge between P10 and P13, and the proportion of binucleated CMs increases (a possible indicator of terminal differentiation) (Chapter 5). Thus, in addition to the time points of P2 and P70, which are characterised by highly proliferative neonatal or differentiated adult CMs (Li *et al.*, 1996; Clubb and Bishop, 1984; Naqvi *et al.*, 2014; Porrello *et al.*, 2011b), respectively, P10 and P13 are also pivotal time points for cardiac growth. Together, these four developmental time points span the key phases of postnatal CM growth that include CM division, enlargement, and terminal differentiation. Although the exact timing and determinants of these events are unclear, they are likely to be driven by changes in gene expression.

In the past decade high-throughput sequencing technologies have become commercially available, and have enabled the discovery of novel genes, exons or splicing events as well as the quantitation of transcripts between different conditions or developmental stages (Morozova and Marra, 2008). RNA sequencing (RNA-Seq) is now more affordable and accessible, and is used to interrogate the transcriptome and the transcriptional changes that occur with CM maturation. Poly(A) RNA is most commonly used for RNA-Seq that captures protein-coding mRNA and a considerable number of long noncoding RNAs (lncRNAs) that are also polyadenylated, >200 nucleotides, and overlap with exons, introns, and intergenic regions (Ma *et al.*, 2013) (Gao and Wang, 2014). The role of lncRNAs during development has not been established but distinct patterns of expression have been reported, relating to cell type and different stages of development (Batista and Chang, 2013; Matkovich *et al.*, 2014). However, a couple of lncRNAs have recently been discovered and assigned a function in the heart to mediate cardiac hypertrophy (Wang *et al.*, 2014; Viereck *et al.*, 2016; Wang *et al.*, 2016) and establish cardiac lineages in cardiac development (Klattenhoff *et al.*, 2013). Another population of smaller noncoding RNAs are micro RNAs

(miRNAs), which are ~22 nucleotides and negatively regulate gene expression through post-transcriptional regulation. Mature miRNAs bind to partially complementary mRNA sequences, usually in the 3'-untranslated region (UTR). This reduces the efficiency of translation, or leads to mRNA destabilisation through shortening of the poly(A) tail or mRNA cleavage (Lai, 2002). miRNAs have been implicated in stimulating or inhibiting CM proliferation (Porrello *et al.*, 2011a; Katz *et al.*, 2016; Eulalio *et al.*, 2012; Liu *et al.*, 2008; Liang *et al.*, 2015; Zhao *et al.*, 2007) and also in mediating cardiac hypertrophy (Wang *et al.*, 2014).

Cardiac gene expression datasets predominantly use input samples from hearts or CMs at a limited range of ages (embryonic, neonatal or adult), cultured CMs, or immortal CM cell lines. The major limitations of using such samples are that the results may be misleading due to the constraints of these models, whereby cell culture conditions (often used to purify CMs) may cause changes in the expression of genes, while cardiac tissues are heterogeneous containing a large proportion of cell populations that are non-myocytes. Hence, datasets from primary homogenous CM populations at specific postnatal stages of development are currently lacking. Therefore, a method to rapidly purify CMs at these time points was optimised (Chapter 6).

This study describes the generation of RNA-seq datasets from purified CMs from neonatal (P2), preadolescent (P10 and P13) and adult (P70) mouse hearts, and provides an overview of the dynamic and complex changes in genes that are expressed over the course of CM maturation.

7.2 Materials and Methods

7.2.1 Purification of CMs

CMs were purified from individual mouse pups or adults from litters of 6-8, and three litters were collected per time point at P2, P10, P13 and P70. CMs were collected from mouse pups using the whole litter, regardless of gender, whereas P70 CMs were collected only from adult males due to differences in female and male cardiac growth after puberty (de Simone *et al.*, 1995). CMs were isolated and purified by Langendorff retrograde perfusion and immuno-magnetic cell separation, as detailed in Chapter 6. Collecting a litter (i.e., 6-8 animals) of hearts individually within a day was a time-consuming process, and so CMs were isolated and purified from two hearts in parallel to minimise the experimental duration. This involved cannulating and mounting two hearts within 5 minutes of each other onto separate Langendorff apparatus. Cells were re-suspended in PBS (100 μ l) and stored at -80°C, and one-quarter of each CM preparation was dedicated to RNA extraction.

7.2.2 RNA extraction

RNA was extracted using the miRNeasy Mini Kit (this kit contains RNeasy Mini Spin Columns, 1.5 and 2 ml Collection Tubes, QIAzol Lysis Reagent, RNAase-free water, RWT and RPE Buffers, cat. #: 217004, Qiagen Sciences) from 63 samples of purified CMs isolated from mice at the following ages: P2 (n=19), P10 (n=16), P13 (n=18), and P70 (n=10). CM samples were kept on dry ice and were then rapidly thawed in QIAzol Lysis Reagent (600 μ l) before homogenising for 3 seconds (x5) on wet ice; thereafter samples were incubated for 5 minutes at RT. Chloroform (140 μ l) was added to each sample, which was mixed thoroughly and incubated for 2-3 minutes. Samples were centrifuged at 12,000 *g* for 15 minutes at 4°C to separate the phenol/chloroform solution into layers, whereby the upper aqueous layer, containing RNA, was carefully transferred to a new 1.5 ml microfuge tube at RT. To capture and bind RNA, each sample was mixed with 1.5 vol. of 100% ethanol (~450 μ l) and applied to a silica-membrane contained within an RNeasy Mini column. The column was placed into a 2 ml collection tube, which was centrifuged at 8,000 *g* for 15 seconds and the flow-through was discarded. This was repeated once more using

the remainder of the sample. Concentrated RWT and RPE Buffers were diluted with 100% ethanol to obtain a final volume of 67% and 80% ethanol, respectively. To remove residual contaminants (including phenol), the RNA-bound silica-membrane was washed with RWT Buffer (700 μ l) and then washed with RPE Buffer (500 μ l) by centrifuging at 8,000 g for 15 seconds and the flow-through was discarded. In the final wash, RPE Buffer (500 μ l) was added to the column, which was centrifuged at 8,000 g for 2 minutes and the flow-through was discarded. The column was transferred to a new 2 ml collection tube, which was centrifuged at maximal speed for an additional minute to dry the membrane. RNA was eluted by placing the RNeasy Mini column into a fresh 1.5 ml microfuge tube, and adding RNase-free water (30 μ l) directly to the membrane, which was centrifuged at 8,000 g for 1 minute and the RNA was collected in the microfuge tube. The eluted RNA was either placed on wet ice or stored at -80°C . All steps were performed at RT, unless otherwise stated.

7.2.3 RNA concentration and quality

The concentration and purity of RNA was assayed by adding RNA (2 μ l) to a NanoDrop Spectrophotometer (ND-1000) and measuring UV absorbance at 260 nm and 280 nm. The concentration of RNA per sample was measured at 260 nm, as 1 OD_{260} unit is equivalent to 40 $\mu\text{g}/\text{ml}$ for single-stranded DNA and RNA. The purity of RNA per sample was measured using the absorbance ratio of A 260 nm: 280 nm ($A_{260/280}$), whereby $A_{260/280}$ of 2 indicates pure RNA. Strong absorbance at 280 nm indicates potential contamination with protein or phenol.

The concentration and quality of RNA was also assessed using the Agilent RNA 6000 Nano Assay and Agilent 2100 Bioanalyzer System, as per manufacturer's recommendations. Briefly, gel, intercalating dye, RNA samples (100 ng as determined from the NanoDrop) and an RNA ladder, were added to channels of an RNA Nano Chip, which was vortexed for 1 minute at 2400 rpm. The chip was loaded onto an Agilent 2100 Bioanalyzer, which uses microcapillary electrophoresis to record the size distribution of RNA molecules and assigns a RNA integrity number (RIN) based on an algorithm that uses multiple dimensions of the electropherogram using 2100 Expert Software; this algorithm takes into account the ratio of ribosomal RNA of 28S:18S (Schroeder *et al.*, 2006). RNA samples were given a RIN score between 1 (degraded RNA) and 10 (highest quality RNA). For RNA-Seq, a high RIN

(>8) is considered optimal (Sigurgeirsson *et al.*, 2014); the average RIN score in this study was 8.9.

The RNA concentration that was determined using NanoDrop, was a more conservative estimate than the Agilent assay, and thus, was used to calculate the amount of input RNA required for generating cDNA libraries.

7.2.4 cDNA library construction from poly(A) and small RNA

To minimise biological variability, equivalent amounts of RNA were taken from each CM sample in the same litter and pooled to generate one cDNA library per litter (n=3 litters per time point at P2, P10, P13, and P70). Hence, a total of 12 poly(A) cDNA libraries (1 µg of pooled RNA per library) were generated and 12 miRNA cDNA libraries were generated (1 µg of pooled RNA per library). cDNA libraries from poly(A) RNA and miRNA libraries were constructed using the Total RNA-Seq v2 Kit (Life Technologies, cat. #: 4479789), please refer to the Ion Total RNA-Seq Kit v2 user guide for exact the quantities of the following reagents.

7.2.4.1 Enrichment of poly(A) and small RNA

Poly(A) RNA (including some lncRNAs) was purified from 1 µg of pooled RNA using Dynabeads mRNA DIRECT Micro Kit (that kit contains: Dynabeads Oligo (dT)₂₅, Lysis/Binding Buffer, Washing Buffer A, Washing Buffer B and 10 mM Tris-HCl; Life Technologies; cat. #: 61021). Total RNA was heated at 70°C for 2 minutes and resuspended in Lysis/Binding Buffer that was transferred to a tube containing Dynabeads Oligo (dT)₂₅. Samples were mixed thoroughly and incubated for 5 minutes at RT. This enables poly(A) RNA to bind to the oligo (dT)₂₅ sequences covalently bound to magnetic beads. After separating the poly(A) bound magnetic beads with a magnet, other unbound contaminating RNA species (including ribosomal RNA and small RNA) present in the supernatant were removed. Beads were washed with Washing Buffers (A followed by B) and poly(A) RNA was eluted in Nuclease-Free Water (pre-heated to 80°C). The elution step was repeated once

more. The amount of poly(A) RNA recovered is assumed to be ~1% of total RNA, thus it is estimated that ~10 ng of poly(A) RNA was used in the following steps.

Poly(A) RNA was enzymatically fragmented (to ~100 nucleotides) using the Total RNA-Seq v2 Kit (Life Technologies, cat. #: 4479789). Briefly, poly(A) RNA samples were fragmented by incubating with RNase III and Reaction Buffer for 3 minutes at 37°C and then water was added. The fragmented poly(A) RNA was then purified by adding Nucleic Acid Binding Beads and Binding Solution Concentrate into the 1.5ml microfuge tube, which was incubated for 5 minutes at RT. Bead-bound poly(A) RNA fragments were separated with a magnet and the supernatant was discarded. Bead-bound poly(A) RNA fragments were incubated for 30 seconds at RT in Wash Solution Concentrate (80% ethanol), which was then carefully removed and discarded after separation with a magnet. The bead-bound poly(A) RNA fragments were air-dried for 1 minute. Fragmented poly(A) RNA was then eluted from the beads in Nuclease-Free Water (pre-heated to 37°C) and incubated for 1 minute at RT, after which RNA samples were placed on ice. To check for a consistent size of fragments (100-200 nucleotides), samples were loaded onto an Agilent Pico Chip (Agilent RNA 6000 Pico Kit) and analysed using the Agilent 2100 Bioanalyzer System (see Section 7.2.3). Small RNA was similarly enriched using Nucleic Acid Binding Beads as per manufacturer's instructions (Ion Total RNA-Seq Kit v2), but the fragmentation step was omitted for small miRNA. Both poly(A) RNAs and small RNAs were concentrated from a volume of 10 µl to 3 µl using a Concentrator for 5-10 minutes at 60°C that were then used to generate cDNA libraries.

7.2.4.2 cDNA library construction

Poly (A) RNA fragments or small RNA were hybridized at the 3' and 5' ends to double-stranded adaptors (specific DNA sequences). To do this, a hybridization master mix (Ion Adaptor Mix v2 and Hybridization Solution) was prepared on ice and added to RNA samples. The solution was mixed by trituration, briefly centrifuged and incubated on a thermocycler for 10 minutes at 65°C, and then for 5 minutes at 30°C for poly(A) RNA or 16°C for small RNA. Samples were placed on ice and 2x Ligation Buffer and Ligation Enzyme Mix were added to each sample, and mixed by trituration. Samples were incubated for 1 hour at 30°C for poly(A) RNA or at 16°C for small RNA overnight on a thermocycler.

To perform reverse-transcription (RT), RT master mix was prepared on ice using Nuclease-Free Water, 10x RT Buffer, 2.5 mM dNTP Mix, and Ion RT Primer v2. RT master mix was added to the ligated RNA sample, which was mixed by vortexing and centrifuged prior to incubating at 70°C for 10 minutes on a thermocycler. After incubation, 10x SuperScript III Enzyme Mix was added to the ligated RNA sample, which was mixed by vortexing and centrifuged briefly prior to incubating at 42°C for 30 minutes.

To purify cDNA, cDNA samples were mixed with Nuclease-Free Water and transferred to PCR tubes containing Nucleic Acid Binding Beads and Binding Solution Concentrate that were mixed thoroughly by trituration. cDNA bound to the beads after adding ethanol (100%) and mixing samples thoroughly by trituration that were then incubated for 5 minutes at RT. Bead-bound cDNA was separated on a magnet for 5 minutes and then the supernatant was discarded. Wash Solution Concentrate was added to the samples while on the magnet and incubated for 30 seconds at RT, and then the supernatant was discarded. The samples of bead-bound cDNA were air-dried on the magnet for 1 minute. To elute the cDNA from the beads, PCR tubes were removed from the magnet and Nuclease-Free Water (pre-heated to 37°C) was added to each sample, which was mixed thoroughly by trituration and incubated for 1 minute at RT. Samples were placed on the magnet for 1 minute and the beads were separated from the eluted cDNA, which was collected in the supernatant into a new PCR tube.

To amplify barcoded cDNA libraries, a PCR mixture was prepared with Platinum PCR SuperMix High Fidelity and Ion Xpress RNA 3' Barcode Primer. cDNA samples were transferred to new PCR tubes and the PCR mixture was added to the each sample. A unique Ion Xpress RNA-Seq Barcode BC primer (ranging from BC01-B016) was added to each cDNA sample that was then mixed by trituration and briefly centrifuged. PCR was carried out by placing the samples in a thermocycler and incubating with the following PCR conditions: hold at 94°C for 2 minutes; 2x cycles of 94°C for 30 seconds, 50°C for 30 seconds, 68°C for 30 seconds; 16x cycles for poly(A) RNA or 14x cycles for small RNA of 94°C for 30 seconds, 62°C for 30 seconds, 68°C for 30 seconds; hold at 68°C for 5 minutes. The amplified cDNA was purified with Nucleic Acid Binding Beads using the same method as detailed in the previous paragraph.

The yield of cDNA was measured using an Agilent High Sensitivity DNA Chip (Agilent High Sensitivity DNA Kit) on an Agilent 2100 Bioanalyzer System (see Section 7.2.3). Barcoded samples were diluted to 1000 pM and pooled, and the pooled sample was diluted to 100 pM, of which 10 µl of cDNA was used for sequencing. cDNA libraries were sent to the Genomic Core Facility at the Victor Chang Cardiac Research Institute for sequencing using the Ion Torrent Proton System.

Gel size selection was performed after cDNA amplification of small RNAs to remove primer dimers. Samples were separated by electrophoresis on a 10% urea polyacrylamide gel and cDNA of 100-120 nucleotides was excised and eluted overnight in gel elution buffer at 4°C. On the following day, cDNA was then ethanol-precipitated.

7.2.5 Alignment of reads and gene counts

Sequenced reads were aligned or mapped to the mouse reference genome (version mm10) using the Torrent Suite software's RNA-Seq plugin, which uses STAR and Bowtie 2 aligners. Gene counts represent the expression value of each gene (i.e., the number of reads that uniquely aligned to a reference gene), which were generated for poly(A) libraries using HTSeq software from the RNA-Seq plugin. This plugin also uses a Picard tool that provides the RNA alignment metrics (including the distribution of uniquely aligned reads that overlap with coding or intergenic bases etc.) for quality control assessment of the sequencing data output.

Small RNA-Seq data are not compatible with the RNA-Seq plugin, and therefore, small reads were aligned to the mouse reference genome (version mm10) using the Bowtie aligner and counts were generated using miRspring tools (Humphreys and Suter, 2013).

7.2.6 Analyses of RNA-Seq data

The following data analyses were performed using R (v 3.2.3) and R Studio software.

Gene counts of unique reads that were assembled using HTSeq were imported into R, and from here onwards this output is referred to as raw counts. Principle component analyses (PCA) were performed using raw counts for an unbiased analysis of the variance and correlation of genes between time points. The raw count dataset was normalised to the size of each library, which range between ~14 and 19 million coding reads per library, and the normalised count data was used to compare the expression or counts per million (cpm) of specific genes of interest across time points.

The number of differentially-expressed (DE)-mRNAs were calculated using VOOM analysis tools (Law *et al.*, 2014) with a minimum of 2 cpm per gene in at least 3 samples (25% of the 12 datasets). The threshold for a DE-mRNA was determined as genes with a 2 fold-change in expression (≥ 2 fold, up-regulated; or ≤ -2 fold, down-regulated) that were statistically significant with an adjusted p-value of < 0.05 . DE-mRNAs were determined using VOOM by pairwise comparisons of: 2 vs 10, 10 vs 13, 13 vs 70, 2 vs 13, 2 vs 70, and 10 vs 70, which were all combined to establish the total number of DE-mRNAs.

7.2.7 Functional biological category analyses of differentially expressed (DE)-mRNAs

The following data analyses were performed using R (v 3.2.3) and R studio software.

The cpm of DE-mRNAs was normalised across time points by assigning a z-score.

$$z = \frac{x - \mu}{\sigma}$$

where x is the cpm, and μ and σ are the mean and standard deviation of the population, respectively.

DE-mRNAs were clustered by the k-means clustering algorithm, which identifies genes with similar patterns of expression across the time course using the z-score value. These clustered patterns of gene expression are presented as a heatmap. Each cluster of genes was enriched for functional biological categories that were statistically significant using Fisher's exact test ($p < 0.001$). A knowledgebase of functional biological categories for murine genes was kindly provided by Dr Joshua Ho (O'Connell *et al.*, 2012), and draws upon multiple databases including: gene ontology terms, Kyoto Encyclopedia of Genes and Genomes (KEGG) pathways, MouseCyc pathways, Mouse Genome Informatics (MGI) mouse phenotype-associated genes, Functional Annotation of the Mammalian Genome 4 (FANTOM4), and mouse tissue-specific transcription factor gene sets.

7.3 Results

7.3.1 Characterisation of CM inputs for RNA-Seq

CMs were isolated and purified from individual pups (P2, n=19; P10, n=16; and P13, n=18) or adult male mice (P70, n=10) by Langendorff retrograde perfusion and immuno-magnetic cell separation using litters of 6-8 mice (n=3 litters per time point). These samples were used for RNA-Seq experiments as detailed in Table 7.1, which includes: the average BW of mice, CM yield, CM viability, RNA yield, RNA $A_{260/280}$ ratio, and the RIN score per time point. The RNA yield was obtained from one-quarter of the purified CM samples; and thus, the estimated amount of RNA per CM cell is: ~5 pg/cell, 9 pg/cell, 16 pg/cell and 25 pg/cell at P2, P10, P13, and P70, respectively. The RNA yield at the later time points was higher than the average amount for a mammalian cell of 10 pg/cell (Tang *et al.*, 2011). Furthermore, the average RIN score was ~8.9 across all samples, indicating high quality RNA that was not degraded.

Table 7.1: CM input samples for RNA-Seq

P	BW (g)	Isolated CMs		Purified CMs		RNA (μ g)	260/280 ratio	RIN score	n
		CM yield	Rod-shaped CMs (%)	CM yield	Rod-shaped CMs (%)				
2	1.83	1.35×10^6	51	0.98×10^6	39	1.7	1.94	8.9	19
10	5.43	1.42×10^6	70	0.63×10^6	70	3.3	1.98	9	16
13	6.62	1.55×10^6	68	0.79×10^6	66	6.2	2.04	8.7	18
Adult	26.56	2.22×10^6	71	1.56×10^6	69	14.2	2.07	8.8	10

P, postnatal age (days)

7.3.2 Alignment of unique reads

As expected, the majority of uniquely aligned reads (reads that did not align to more than one area of the genome, i.e., a “multi-mapper”) were either in exons (~60%) or UTRs (~25%), thus, mostly aligning to coding regions (Figure 7.1). A much smaller proportion of reads aligned to intergenic and intronic bases. In total there were ~14-19 million single-end reads per sample that mapped to coding regions with an average length of ~100 nucleotides.

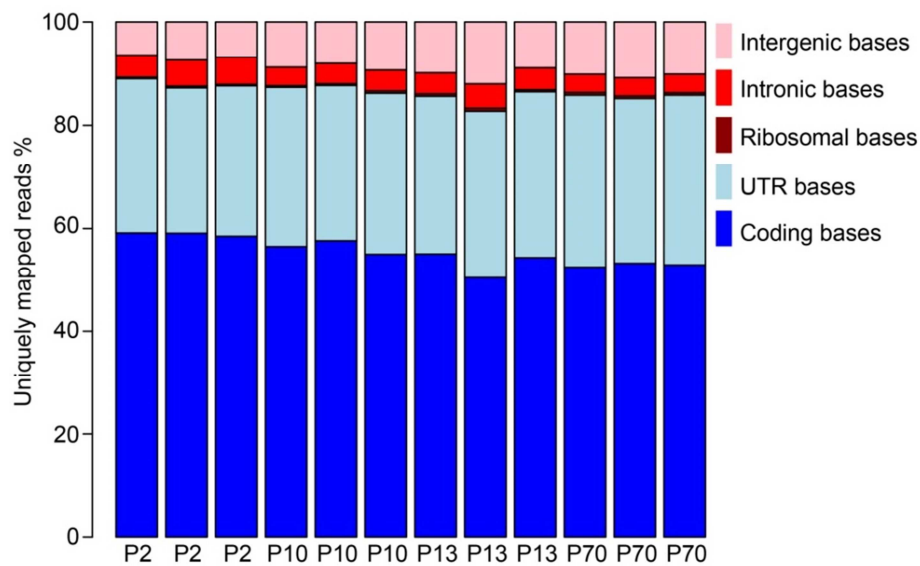


Figure 7.1: The distribution of unique poly(A) reads to the reference genome from CMs across postnatal cardiac development

Poly(A) libraries were generated from CMs purified from P2, P10, P13 and P70 C57BL/6J litters (n=3 litters per time point). The majority of unique reads aligned to coding and untranslated region (UTR) bases, while a smaller proportion aligned to intergenic and intronic bases, and a minimal number of reads aligning to ribosomal bases.

7.3.3 Distinct transcriptional profiles of postnatal CMs

Unbiased principal component analyses (PCA) were performed on mRNAs, lncRNAs, and miRNAs for each sample to assess the variance and correlation between biological replicates and time points. PCA plots (Figure 7.2) of mRNA, lncRNA, and miRNA datasets, showed biological replicates were grouped together in each time point and separated along the PC1 axis in order of developmental age: P2, P10, P13, and P70. The most closely related time points were P10 and P13, while P2 and P70 separated from P10 and P13 time points on the PC2 axis. Altogether, these CM datasets indicate biological replicates were highly reproducible and have distinct transcriptomic profiles along the postnatal trajectory of cardiac growth.

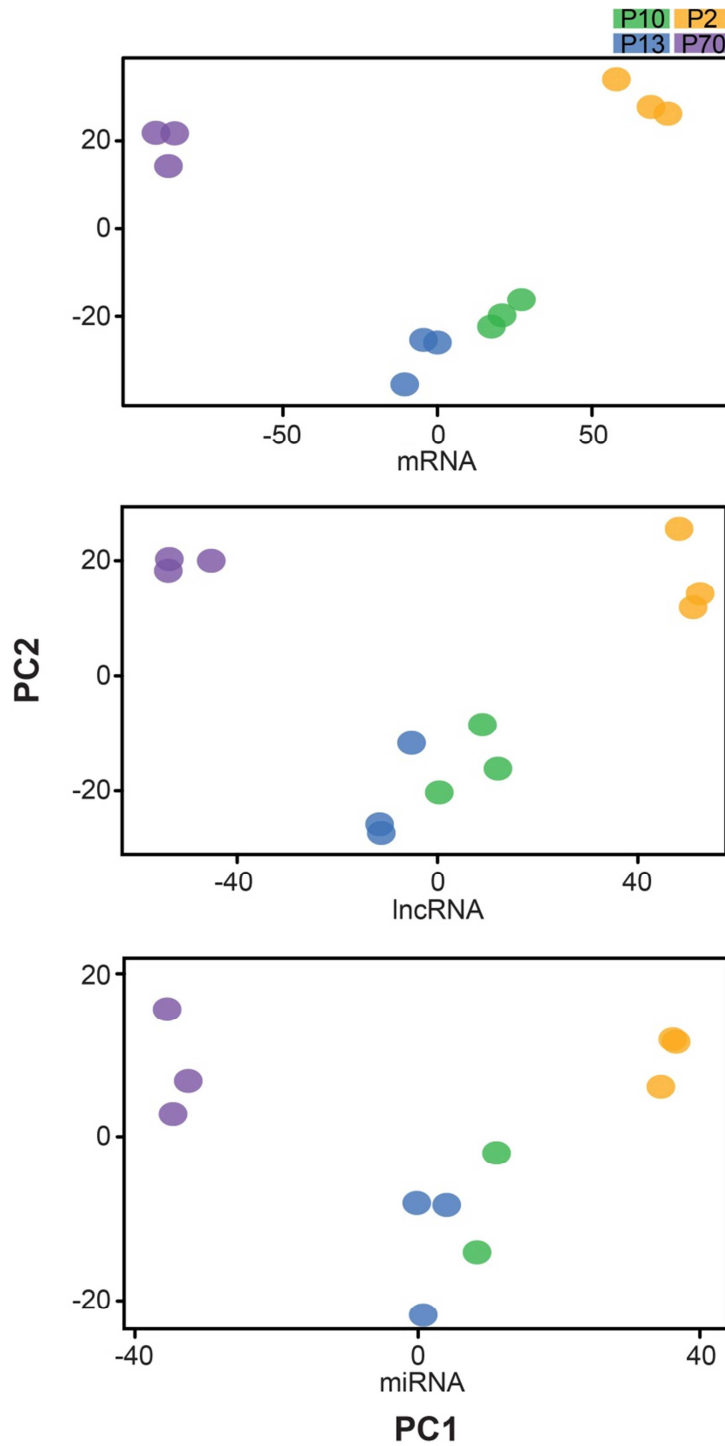


Figure 7.2: Principle component analyses (PCA) of mRNA, lncRNA and miRNA, from CMs across postnatal cardiac development

Unbiased PCA plots of mRNA, lncRNA and miRNA, from purified CMs show biological replicates grouped together and separated time points according to postnatal age during CM maturation (P2, P10, P13, and P70, n=3, except for P10 miRNA replicates, where n=2).

7.3.4 Identifying DE-mRNAs in CM maturation

Prior to identifying DE-mRNAs, it was important to filter out the lowly abundant reads (i.e. the noise) from the datasets. The majority of genes fall within a normal distribution between 2 and 10 counts per million (cpm). A smaller proportion of genes have counts greater than 10 cpm. The remaining genes at the far left of the histograms in Figure 7.3A had 0 cpm or low abundance (< 2 cpm), and thus, a threshold of 2 cpm was set to filter out potential noise. DE-mRNAs were identified using VOOM analyses, and the criteria for robust changes in gene expression was ≤ -2 or ≥ 2 fold-change with statistical significance using an adjusted p-value < 0.05, as shown in the volcano plots in. The proportion of DE-mRNAs after applying the fold-change and statistical significance criteria are shown in volcano plots, whereby DE-mRNAs are presented as orange coloured data points (Figure 7.3B). There were fewer DE-mRNAs identified at P10 vs P13 compared with P2 vs P70 (Figure 7.3B). The total number of up- or down-regulated DE-mRNAs for each pairwise comparison (i.e., P2 vs P10, P2 vs P13, P2 vs P70, P10 vs P13, P10 vs P70, and P13 vs P70) is shown in Figure 7.3C. Overall, a higher proportion of DE-mRNAs were down-regulated than up-regulated during postnatal cardiac development (~60%).

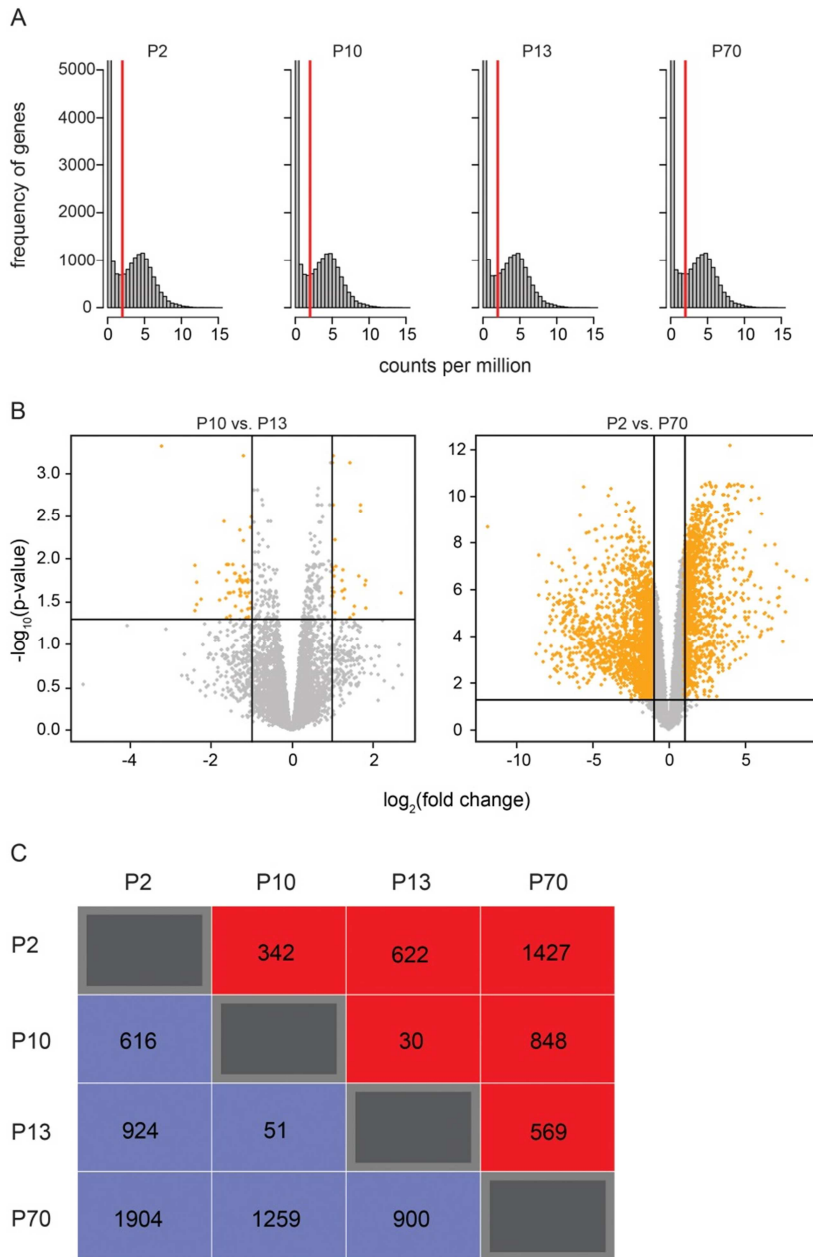


Figure 7.3: The number of DE-mRNAs from CMs across postnatal cardiac growth were determined using cpm, fold-change, and statistical significance criteria

A, the distribution of gene counts from poly(A) libraries constructed from P2, P10, P13, and P70 CMs, with a threshold of >2 cpm to exclude genes with very low abundance from subsequent DE-mRNA analyses. B, volcano plots of genes to determine DE-mRNAs for P10 vs P13 and P2 vs P70, using the criteria of \log_2 fold-change (≤ -2 or ≥ 2) and $-\log_{10}$ of the adjusted p-value (<0.05). DE-mRNAs are represented as orange data points, while mRNAs that do not meet the criteria are represented by grey data points. C, the number of DE-mRNAs that are up (red)- or down (blue)- regulated between different pairwise comparisons. P, postnatal age (days)

7.3.5 Expression levels of cardiac cell-type specific markers in purified preparations of CMs

To ensure the preparations of CMs represent mostly CM mRNAs, cell type-specific markers that are well-defined for CMs (*Myh6* and *Tnnt2*), ECs (*Pecam1* and *Vcam1*), and fibroblasts (*Ddr2* and *Vim*), were assessed to confirm the purity of CMs for each time point. The expression of CM markers was higher at all of the time points compared with non-myocyte markers (Figure 7.4), and were statistically significant (see Appendix A).

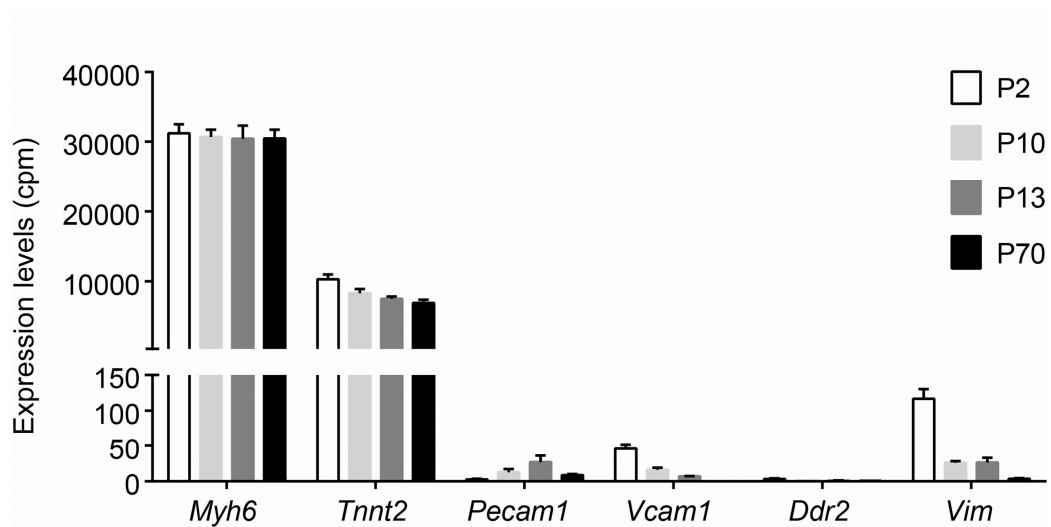


Figure 7.4: Expression of cardiac cell markers in purified CMs

Expression levels of mRNAs (cpm) for cardiac cell type-specific markers are shown in preparations of purified CMs from P2, P10, P13, or P70 mice (n=3 litters per time point). CMs (*Myh6* encodes α -MHC; *Tnnt2* encodes cTnT), ECs (*Pecam1* and *Vcam1*), and fibroblasts (*Ddr2* encodes discoidin domain receptor tyrosine kinase 2; *Vim* encodes vimentin).

7.3.6 Expression of developmental and growth signals across postnatal CM maturation

The expression of genes relating to the cell cycle, physiological hypertrophy, and some TFs were evaluated. The expression of the mitosis-related genes that were evaluated in cardiac ventricles (Chapter 5, Figure 5.4) were also determined in purified CMs (Figure 7.5A). The abundance of these cell cycle mRNAs progressively decreased from P2 to P70 in purified CMs, with the exception to *Rb1* (Figure 7.5A). This panel of cell cycle genes included *E2f1*, which is a TF that positively regulates the cell cycle (Ahuja *et al.*, 2007) and its reduced expression correlates well with the downward trend in the expression of cell cycle genes (Figure 7.5A). Most of the mitosis-related genes were statistically significant between P2 vs P13 CMs and P2 vs P70 CMs (see Appendix B). The expression levels of *Rb1*, which negatively regulates the activity of *E2f1*, were steady throughout development and did not change with *E2f1* expression.

Cardiac growth signals were also assessed, including *Igf1* and TH-related genes, which are both associated with CM proliferation and physiological hypertrophy, i.e., the IGF1/PI3K/Akt pathway. *Igf1*, *Igf1r*, *Pi3kca*, and *Akt1* mRNAs, were more abundant in neonatal CMs (P2) and significantly decreased over the time course of CM maturation (Figure 7.5B). Moreover, while the expression of *Thrb* (TR β) increased significantly, *Thra* (TR α) progressively decreased in CMs across postnatal development (Figure 7.5B). Most growth signals were statistically significantly different across the time course of CM maturation, see Appendix B.

Finally, TFs that have an established role in embryonic cardiac development (*Nkx2-5*, *Gata4*, and *Mef2c*), hypertrophy (*Nfatc4*), and CM differentiation (*Meis1*), were determined in CMs across postnatal cardiac growth. In general, the expression of TFs decreased significantly during CM maturation (Figure 7.5C), mainly between P2 vs P10, P2 vs P13, and P2 vs P70 (see Appendix B for statistical analyses). In addition, the expression of *Kit* mRNA (encoding c-Kit) was very low in CMs at all postnatal ages (P2, ~1.4 cpm; P10, ~1 cpm, P13, ~1 cpm; and P70, ~0.1 cpm).

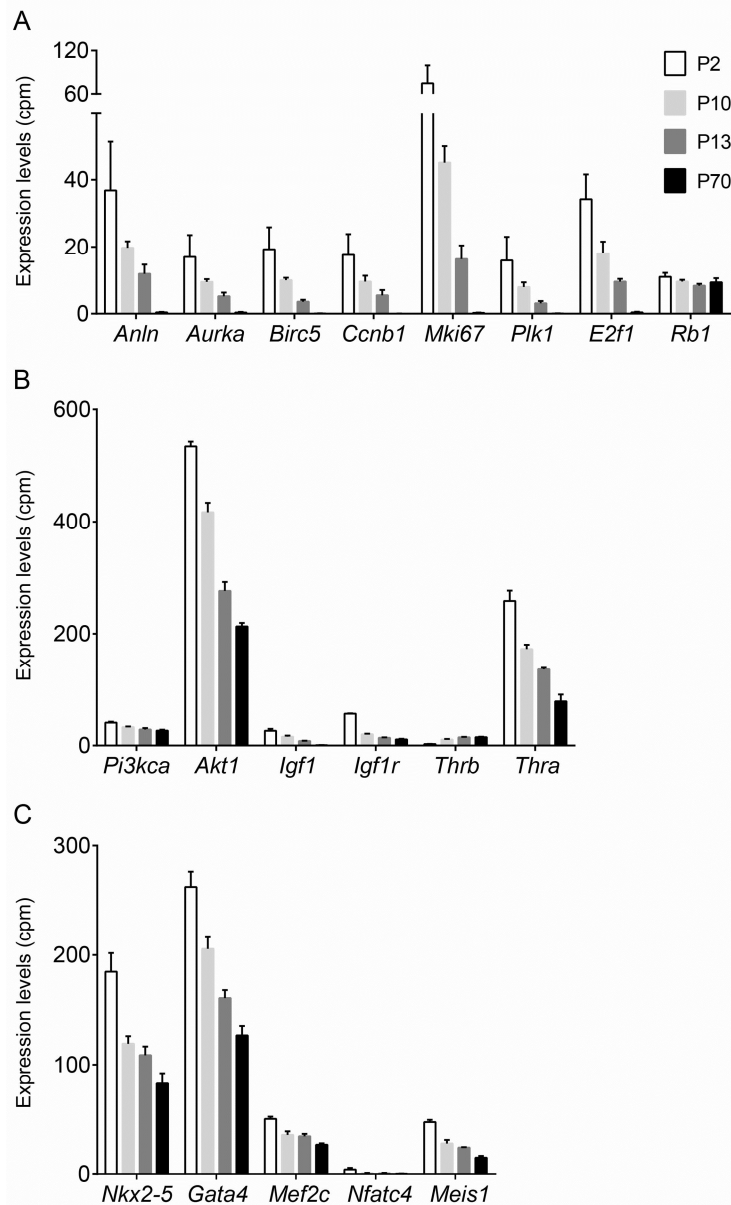


Figure 7.5: Expression of developmental and growth signalling genes in CMs purified over the course of postnatal cardiac development

Expression levels (cpm) of cardiac developmental and growth signalling mRNAs in purified CMs from mice aged P2, P10, P13, and P70 (n=3 litters per time point). A, cell cycle genes: anillin (*Anln*), aurora kinase A (*Aurka*), survivin (*Birc5*), cyclin B1 (*Ccnb1*), Ki67 (*Mki67*), polo-like kinase 1 (*Plk1*), E2 promoter binding factor 1 (*E2f1*), and retinoblastoma (*Rb1*); B, growth signals: phosphatidylinositol-4,5-bisphosphate 3-kinase catalytic subunit α (*Pi3kca*), serine/threonine kinase 1 (*Akt1*), insulin-like growth factor 1 (*Igf1*), insulin-like growth factor 1 receptor (*Igf1r*), thyroid hormone receptor β (*Thrb*), thyroid hormone receptor α (*Thra*); C, TFs: NK2 homeobox 5 (*Nkx2-5*), *Gata4*, myocyte enhancer factor 2 (*Mef2c*), nuclear factor of activated T cells (*Nfatc4*), and meis homeobox 1 (*Meis1*).

7.3.7 Functional biological category analyses of DE-mRNAs

The total number of DE-mRNAs from all pairwise comparisons of time points (P2, P10, P13, and P70) across postnatal CM maturation was ~3,800 (with ≤ -2 or ≥ 2 fold-change in expression; adjusted p-value < 0.05). DE-mRNAs were clustered into seven unique patterns of expression by k-means clustering presented in a heatmap using the z-score (Figure 7.6). The expression profiles of all the DE-mRNAs were similar across biological replicates for each time point, further validating the high reproducibility of these datasets. Each cluster of DE-mRNAs has a defined pattern expression, shown below the heatmap as line graphs in Figure 7.6. The number of DE-mRNAs that were clustered together is shown beside the heatmap, and were associated with multiple functional biological categories (O'Connell *et al.*, 2012). For example, cluster 4 represents genes that steadily decreased from P2 to P13 and then declined more rapidly from P13 to P70 that are involved in cell cycle pathways and mitosis (Figure 7.6). Thus, these DE-mRNAs may identify biological processes and pathways that correlate with CM proliferation, enlargement and terminal differentiation during postnatal cardiac growth.

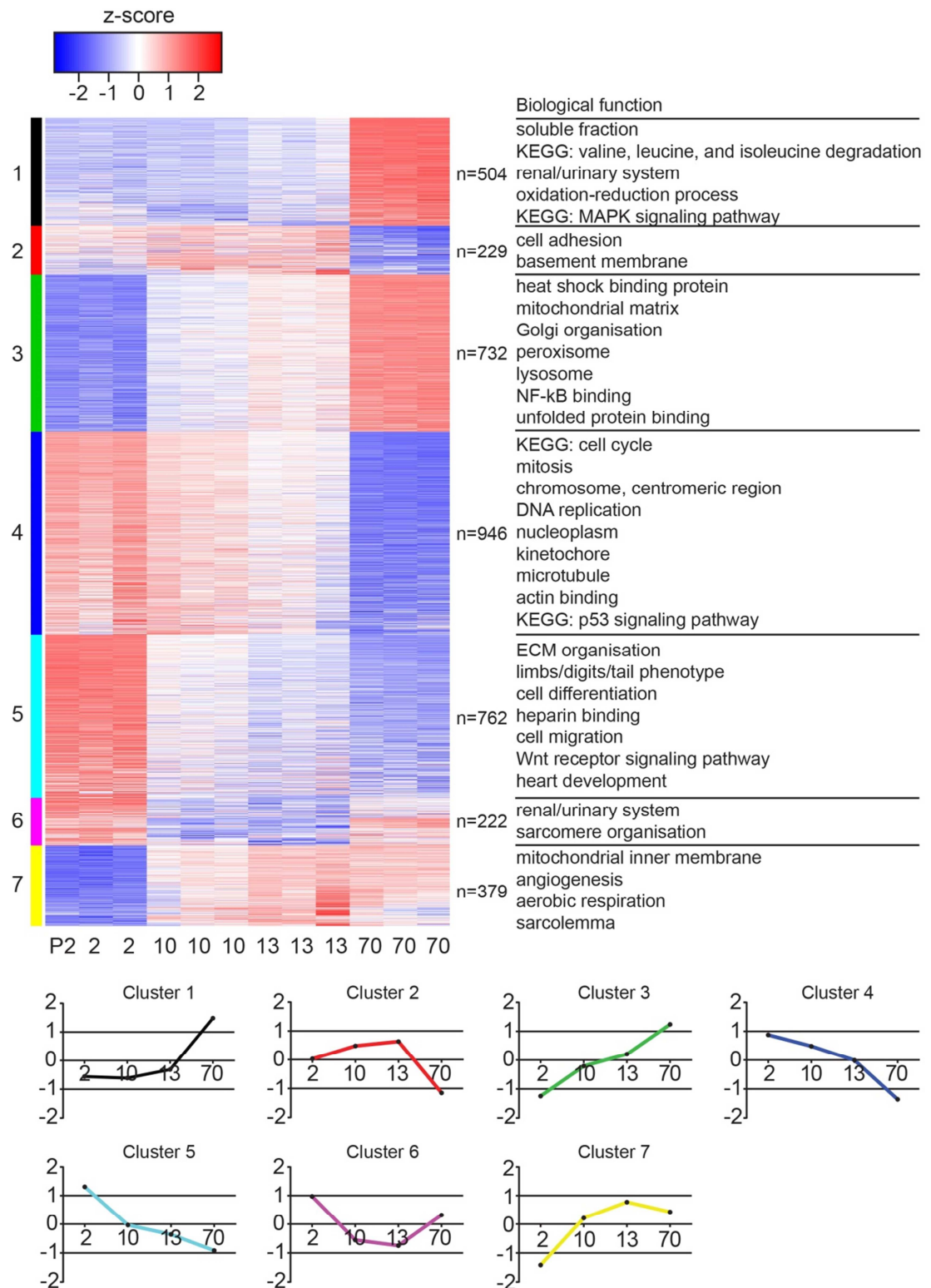


Figure 7.6: Heatmap of clustered DE-mRNAs reveal functional biological categories that associate with key developmental time points in postnatal CM maturation

Figure 7.6: Rows correspond to DE-mRNAs (3,800 DE-mRNAs; ≤ -2 or ≥ 2 fold-change; $p < 0.05$) clustered by the k-means algorithm and presented as a heatmap. Columns represent CM samples from different postnatal time points (P2, P10, P13, and P70, n=3 litters per time point). The z-score scale bar indicates low expression (blue) to high expression (red) of DE-mRNAs, which clustered into seven unique patterns of gene expression. The number of DE-mRNAs in each cluster and their associated functional biological categories are annotated to the right of the heatmap. The defined patterns of gene expression that correspond to each cluster are shown in separate line graphs (using the z-score) below the heatmap.

7.4 Discussion

This chapter describes the transcriptional profiles of purified CMs over the course of postnatal cardiac development. CMs were rapidly purified from three litters per time point (P2, P10, P13, and P70) and high quality total RNA was extracted with an average RIN scores of ~8.9 (Table 7.1). Poly(A) and small RNA libraries were constructed and sequenced. The purity of CMs using the purification method developed in Chapter 6 was further evident by the very low expression of non-myocyte mRNAs (ECs and fibroblasts) relative to CM mRNAs (Figure 7.4). Unbiased PCA of mRNAs, lncRNAs, and miRNAs, identified the variance and correlation of genes expressed in each library, grouping biological replicates together and separating time points in order of postnatal age (Figure 7.2), demonstrating high reproducibility. A further indication of this was shown in the heatmap of DE-mRNAs, whereby gene expression profiles of biological replicates were nearly identical at each time point (Figure 7.6). Thus, these dataset show that the high quality input RNA from purified CMs used for sequencing yielded highly reproducible transcriptomic signatures that were distinct at time points across postnatal cardiac growth.

The RNA-Seq experiment was designed to capture the transcriptome across key developmental time points at P2, P10, P13, and P70. RNA was prepared from CMs from littermates (born into litters of 6-8) that was then pooled per biological replicate at each time point. The combination of methods had the following advantages: i) litters of 6-8 mice were used to reduce biological variation in cardiac growth; ii) CMs were collected from all pups in a litter to minimise bias (e.g., instead of selecting an individual small/large pup from a litter); and iii) fresh CMs were purified rapidly. Of note, adult male CMs (i.e. P70) were pooled separately from adult females (these will be sequenced at a later time) since there are sex-related differences in cardiac growth and morphology after puberty (de Simone *et al.*, 1995). Altogether, these considerations are likely to have contributed to the highly reproducible biological replicates that are evident from PCA (Figure 7.2) and the heatmap of DE-mRNAs (Figure 7.6). This shows each replicate was grouped into the same time point along the PC1 axis by PCA and the hierarchical clustering of DE-mRNAs in the heatmap had comparable patterns of gene expression across replicates.

This Chapter focusses on mRNAs, which can be used to identify biological processes and pathways that are important in postnatal CM maturation. The number of DE-mRNAs (≤ -2

or ≥ 2 fold-change; adjusted p value <0.05) was greater between neonatal (P2) and adult (P70) time points than between P10 and P13, which is not unexpected given that the number of days between ages is higher. Nonetheless, there were still ~80 DE-mRNAs between P10 and P13, while overall there were ~3,800 DE-mRNAs over the course of CM maturation that dynamically changed and were distinct for each time point. In general, more DE-mRNAs were down-regulated during postnatal cardiac development, coincidentally TFs also decreased in expression (*E2f1*, *Nkx2-5*, *Gata4*, *Mef2c*, *Nfatc4*, and *Meis1*), many of which have been implicated in CM proliferation, enlargement, and differentiation (Oka *et al.*, 2007). These TFs (with the exception of *Meis1*) are established core networks that regulate gene expression in embryonic heart development, in which protein-protein interactions of TFs (such as: *Gata4* and *Nkx2-5*; *Gata4* and *Nfatc4*; *Mef2c*, *Gata4*, and *Nfatc4*; *Mef2c* and *Nkx2-5*) synergistically enhance the expression of multiple target genes (Akazawa and Komuro, 2003; Vincentz *et al.*, 2008; Olson, 2006). Thus, if expression levels of the majority of TFs decrease during postnatal cardiac development, this may possibly explain why more DE-mRNAs were down-regulated.

E2F1 is another TF that has a positive role in regulating the cell cycle. When E2F1 is bound to Rb1, transcription is repressed, however, upon Rb1 phosphorylation, E2F1 becomes transcriptionally active, increasing the expression of cell cycle genes (Ahuja *et al.*, 2007). *E2f1* mRNA expression decreased, whereas *Rb1* mRNA expression did not change during postnatal CM development (Figure 7.5A). Previously in Chapter 5 (Figure 5.4), mitosis-related genes were evaluated in cardiac ventricles and were more abundant in P13 hearts relative to adult hearts. The RNA-Seq data generated in this Chapter also showed a downward trend of the expression of cell cycle genes in CMs over postnatal cardiac growth (Figure 7.5A) Moreover, hierarchical clustering highlighted that a number of the down-regulated DE-mRNAs over the time course were linked to the biological processes of mitosis, cell cycling, and DNA replication (cluster 4, Figure 7.6). Nonetheless, cell cycle gene expression was evident at P2, P10, and P13. Therefore, these datasets demonstrate that the expression of cell cycle genes extend beyond the first week of birth to P10 and P13, which has been similarly reported for protein levels (Walsh *et al.*, 2010; Ikenishi *et al.*, 2012). This is interesting since CMs are widely regarded to cease cell division within the first week of birth.

DE-mRNAs that were down-regulated over the developmental time course were associated with cell differentiation, heart development, and Wnt receptor signalling (cluster 5, Figure 7.6). Those genes associated with cell differentiation (cluster 5) may provide clues for candidate genes that regulate the differentiation and maturation of CMs. Indeed, one such pathway that was clustered with cell differentiation was Wnt receptor signalling, which is negatively regulated by the Hippo pathway, and has been previously identified for its role in cell proliferation and controlling heart size (Heallen *et al.*, 2011). In contrast to genes that were down-regulated, DE-mRNAs that continually increased over the time course were related to the development of organelles, such as Golgi, mitochondria and sarcolemma, as well as a shift in metabolism to aerobic respiration (cluster 3 and 7, Figure 7.6), all of which have been previously documented in postnatal CM maturation (Lopaschuk and Jaswal, 2010). One may expect the expression of genes involved in physiological hypertrophy, including the IGF1/PI3K/Akt pathway, (Dorn, 2007; Maillet *et al.*, 2013; DeBosch *et al.*, 2006) to increase. However, these particular genes actually decreased over the time course of cardiac growth (Figure 7.5C). It is important to remember that transcript expression levels may not necessarily correlate with protein abundance or signalling activity as there are numerous mechanisms for post-transcriptional and post-translational regulation. A number of up-regulated DE-mRNAs were associated with MAPK signalling (cluster 1, Figure 7.6), which has been implicated in pathological hypertrophy, CM differentiation, and cell cycle exit (Heineke and Molkenin, 2006; McMullen and Jennings, 2007; Bernardo *et al.*, 2010; Liang and Molkenin, 2003). Although the role of MAPK signalling in CMs during postnatal cardiac growth has not been well defined, this makes it an interesting pathway to investigate further.

It is nearly impossible to elucidate the contribution and mechanisms of all of these mRNAs to the biological processes and pathways that are prominent in CM maturation based on gene expression levels alone. Indeed, future work will be required to mine the literature for genes that have known functions in CM maturation and those that are potentially novel. In conjunction with the lncRNA and miRNA datasets, bioinformatic analyses of all three RNA species datasets will also help to identify genes of interest (Wang *et al.*, 2014; Matkovich *et al.*, 2014). While less sensitive than RNA-Seq, RT-qPCR can be used to independently verify relative changes in gene expression across samples, but more importantly, protein abundance should be confirmed by Western blot. There are many *in vitro* tools available to study a gene of interest. An example of this is to use small interfering RNA (siRNA) to

knock down the transcript in cultured CMs. This has been performed to test CM proliferation or assess components of a biochemical signalling pathway (Mahmoud *et al.*, 2013; O'Meara *et al.*, 2015). However, to fully understand the *in vivo* function of the gene, there are many genetic strategies (Mahmoud *et al.*, 2013) that can be employed to overexpress or delete the gene of interest in a tissue-specific or ubiquitous manner that is either constitutive or inducible. Delineation of the function of a candidate mRNA product in normal cardiac development is highly dependent on the nature of the protein it encodes, i.e., if it is a growth hormone or TF. For example, another up-regulated pathway that was highlighted from this dataset was NFκB binding (cluster 3, Figure 7.6). NFκB is a TF that has an undefined role in the heart but previous reports have related NFκB to hypertrophy, cardioprotection and cardiotoxicity (Gordon *et al.*, 2011). Recent *in vitro* methods have been developed to confirm the novel interaction of NFκB binding to the promoter of VEGF by chromatin immunoprecipitation (ChIP)-qPCR (Walton and Matter, 2015). This is carried out by: cross-linking proteins to the DNA, lysing cells, sonicating DNA, performing IP with a NFκB Ab to pull down bound DNA, and then RT-qPCR using VEGF primers. Thus, many techniques are available to validate and determine gene function that is primarily dependent on the inherent features of the protein it encodes. The next challenge is to systematically mine my datasets for candidate genes.

Recently, O'Meara *et al.* (2015) sequenced poly(A) RNA from multiple input samples to investigate CM differentiation and regeneration that included: the stages of *in vitro* differentiation of embryonic stem cells to CMs; time points of CM maturation using neonatal (P0, P4, and P7) and adult CMs; cultured adult CMs, as well as cardiac ventricles and CMs at 7 days post the apical resection of a P1 heart. O'Meara *et al.* (2015) isolated and purified CMs at neonatal time points by mechanical homogenisation of cardiac tissues that were then incubated with proteolytic enzymes from the Neonatal Heart Dissociation kit (Miltenyi) and purified using the Neonatal Cardiomyocyte Isolation kit (Miltenyi) to yield 95% CMs. Adult CMs were isolated and enriched for using the Liao and Jain (2007) method by Langendorff perfusion. The purity of neonatal CMs reported by this group was similar to that reported in Chapter 6. O'Meara *et al.* (2015) also performed gene ontology term analyses and DE-mRNAs in developing postnatal CMs were related to mitochondria, sarcomere, and the cell cycle, which were also documented here. However, there are many more processes and pathways that have been highlighted from my dataset that were not shown in their study. O'Meara *et al.* (2015) focussed on interleukin 13 signalling that

regulates CM differentiation and regeneration, and is mediated by STAT3/periostin and STAT6. This pathway was identified by mining the dataset using bioinformatics tools, literature referencing, and *in vitro* validation of signalling by treating CMs with interleukin 13 and carrying out siRNA knockdown of interleukin 13 receptors.

O'Meara *et al.* (2015) also noted that some of the DE-mRNAs determined in cardiac ventricles at 7 days post apical resection of a P1 heart were not reproducible in CMs, and they suggested this was due to the sensitivity of mouse hearts to the methods of digesting and purifying CMs at P7/8. Indeed, the commercial kits that were used in their study were developed for P0-P3 neonatal hearts, and thus, larger CMs (i.e., P7/8) may not filter through the iron matrix contained within the MS columns. Thus, this is further evidence of the challenges that are involved in isolating CMs at different ages that may have caused differences in DE-mRNAs.

In summary, this Chapter describes the generation of a valuable data resource that comprises mRNAs, lncRNAs, and miRNAs, generated from purified populations of CMs at key postnatal time points during CM maturation. These RNA-Seq datasets show high reproducibility between biological replicates, reflecting the robustness of the CM purification method and the experimental design that revealed a dynamically changing transcriptome over the course of CM maturation. DE-mRNAs were strongly enriched for multiple biological processes and pathways that are well established in postnatal cardiac development, such as aerobic respiration, and others that are not, such as NF κ B binding and MAPK signalling. There are also DE -lncRNAs and -miRNAs in these datasets that have not yet been fully analysed, and thus, future work is required to perform systematic bioinformatic analyses and *in vitro* validation of genes and their pathways that are involved in CM maturation. This may reveal candidates that are crucial in promoting or inhibiting CM proliferation, enlargement, and terminal differentiation, providing important insights into some of the molecular roadblocks that prevent CM regeneration in the adult heart.

Chapter 8 General Discussion

The overarching focus of the work described in this thesis was to provide a detailed understanding of the molecular signals that contribute to CM proliferation, enlargement and terminal differentiation; critical processes in the postnatal maturation of CMs. To this end, the aims of this study were to determine the role of c-Kit in maintaining the differentiated state of adult CMs following cardiac injury, and, profile the CM transcriptome at pivotal time points during postnatal cardiac development. Insights into CM maturation at the molecular level may lead to the development of strategies to enhance cardiac regeneration through endogenous CM proliferation. It is generally believed that a molecular switch exists for the terminal differentiation of CMs that would control normal cardiac growth but the mechanisms involved in this process remain largely unknown in cardiovascular physiology (Chien *et al.*, 1993; Li *et al.*, 1996; O'Meara *et al.*, 2015). Developmental signals of postnatal CM growth are defined here as molecules that are expressed or show altered expression that have a function in CM maturation. This work addresses questions that are current and highly relevant to the field of cardiac development and regeneration by focussing on the physiology and pathophysiology of CMs. As a result, my work has (1) characterised an *in vivo* model of pathological cardiac growth (SAC), a useful tool to evaluate whether candidate molecules have cardiac regenerative potential; (2) determined that c-Kit does not contribute to maintenance of CM terminal differentiation; (3) identified pivotal time points in CM maturation that contribute to normal postnatal cardiac growth; (4) developed a standardised protocol for the isolation and purification of CMs from mice of any postnatal age; and (5) profiled genes in purified populations of CMs that dynamically change in expression across the identified pivotal time points in postnatal CM maturation, thus generating the first comprehensive library of CM mRNAs, lncRNAs, and miRNAs, using a directly comparable method of CM isolation for P2, P10, P13, and P70 hearts.

c-Kit is not a candidate for CM regeneration

c-Kit has attracted attention as a marker of CSCs and CPCs that can differentiate into all cardiac lineages, including CMs, during development and after cardiac injury (Beltrami *et*

et al., 2003; Hsieh *et al.*, 2007; Ellison *et al.*, 2013). c-Kit⁺ CSCs have been used in clinical trials for the treatment of post-MI HF patients, with moderate improvements in cardiac function observed (Bolli *et al.*, 2011). However, the cardiomyogenic potential of CSCs in adult cardiac regeneration and repair has been challenged (Zaruba *et al.*, 2010; Jesty *et al.*, 2012; Sultana *et al.*, 2015; Wallner *et al.*, 2016), and concerns have surfaced with respect to the robustness of the data presented using CSCs in the clinical trial (The Lancet Editors, 2014). When c-Kit signalling was inhibited from birth in two mouse models, our laboratory previously found that CMs proliferate in response to SAC-induced PO, whereas CMs from WT littermates were restricted to cellular hypertrophy. The work presented in this thesis shows that c-Kit mRNA is expressed at very low levels in developing CMs (Chapter 7) and both c-Kit mRNA and protein are expressed at very low levels in adult CMs, and are not re-expressed following SAC (Chapter 4). Thus, it is unlikely that c-Kit is “re-expressed” or expressed post-SAC, and does not contribute to maintaining a differentiated state of CMs. Since the commencement of this study, these findings have been corroborated with the work of others using genetic lineage tracing to show that developing and adult CMs rarely express c-Kit, and does not change in adult CMs after MI (van Berlo *et al.*, 2014; Sultana *et al.*, 2015). Rather, c-Kit⁺ cells contributed to a subpopulation of ECs (van Berlo *et al.*, 2014; Sultana *et al.*, 2015), and furthermore, c-Kit⁺ cells were determined to have an EC origin that were not CSCs in the developing or adult heart (Sultana *et al.*, 2015). Thus, although c-Kit may not be expressed in CMs preventing cell cycle re-entry, its expression and role in CSCs and ECs, regardless of the disparity in cell type, may still be an important signal in postnatal cardiac growth and regeneration. Altogether, this suggests that c-Kit is not a suitable therapeutic target for the regeneration of CMs.

CM-specific overexpression of mutant Kit^{Wv} under the α -MHC promoter

The original observations from our group indicated that CMs from adult Kit^{W/Wv} and Tg(α MHC-Kit^{Wv}) mice were not terminally differentiated, since they can proliferate in response to cardiac injury. While it is not clear intrinsically how this occurs, Tg(α MHC-Kit^{Wv}) CMs show robust Kit^{Wv} protein and mRNA expression relative to WT CMs, and the immature c-Kit protein (~125 kDa) was more abundant than the mature form (~145-160

kDa); that may have accumulated in subcellular compartments (Chapter 4). In addition, microarray profiling of Tg(α MHC-*Kit^{W^v}*) CMs revealed up-regulated mRNAs were involved in the inflammatory and ER stress response, as well as in protein degradation (unpublished observations). As discussed in Chapter 4, this indicates aberrant processing of the mutant protein and altered cellular physiology, which together may enable adult CMs to re-enter the cell cycle and proliferate in response to PO. This may be due to the overexpression of a mutant protein under the α -MHC promoter, which is widely used for cardiac-specific overexpression of proteins in transgenic mouse studies. There are reports that α -MHC-driven overexpression of a protein can lead to deleterious effects on cardiac morphology and function. For example, Huang *et al.* (2000) showed that the overexpression of the biologically inert GFP, in four independent transgenic mouse lines resulted in two of the lines with the highest GFP expression developing LVH, systolic dysfunction and HF. This phenotype has also been reported in inducible transgenic models using Cre-recombinase overexpression driven by the α -MHC promoter (Buerger *et al.*, 2006). Hence, neither the insertion site nor the copy number of a transgene using the random integration approach can be controlled and CM-specific overexpression of a protein may result in unphysiological consequences (Yutzey and Robbins, 2007). Therefore, transgenic mouse models that overexpress proteins under the α -MHC promoter should be interpreted with caution.

Phases of CM maturation in particular terminal differentiation

Rapid growth of the preadolescent mouse heart (P10-P18) was observed by Naqvi *et al.* (2014) using litters of 6-7 C57BL/6J mice bred in the animal facility at Emory University (Atlanta). This specific period of substantial cardiac growth was recapitulated in this study using litters of 6-8 C57BL/6J mice (Chapter 5), but bred in the animal facility at the Victor Chang Cardiac Research Institute (Sydney). However, a specific burst in CM proliferation at P15 (Naqvi *et al.*, 2014) was not observed at the level of myocardial gene expression despite comparable increases in HW/BW and a comparable surge in serum T₃ levels from P10 to P12 (Chapter 5). Of course, the expression of mitosis-related genes *per se* does not confirm cell division. Rather, this has to be evaluated directly at the cellular level, preferably by counting CM numbers or, at least by *in vivo* staining for cytokinesis-related

events (immunocytochemistry) specifically in CMs. Although this is a difficult event to capture given that cytokinesis lasts for only 1 hour, and is dependent on the synchronicity and number of cells undergoing mitosis. Nonetheless, both studies demonstrate that substantial cardiac growth is achieved in the postnatal period and the presence of mitosis-related genes in the preadolescent period indicates that cell division extends beyond the perinatal period.

Three phases of CM growth have been defined (Clubb and Bishop, 1984): CM proliferation at P0-4, a transitional phase from proliferation to cellular enlargement between P4 and P15, and a quiescent stage from P16, in which CMs no longer proliferate but continue to enlarge, although some disagreement remains as to the exact timing of these events. Indeed, Soonpaa *et al.* (1996) suggested CM proliferation ceases before birth and terminal differentiation occurs as CMs become binucleated in the postnatal period between P4 and P10. Li *et al.* (1996) reported a rapid transition from CM proliferation to hypertrophy just after birth at P3-4. However, others have reported a gradual decrease in cell cycle genes and proteins within the first 3 weeks after birth (Clubb and Bishop, 1984; Walsh *et al.*, 2010; Ikenishi *et al.*, 2012). In agreement with Clubb and Bishop (1984), a similar delineation of CM growth phases was apparent from the work described in Chapter 5. The expression of mitosis-related genes in the myocardium decreased progressively from P2 to preadolescence; transcript abundance at P13 was greater than the low levels observed at P15 and P70 (Chapter 5, Figure 5.4). This pattern of expression is consistent with the RNA-Seq data from CMs, which show the expression of DE-mRNAs that progressively decrease but are still clearly evident at P13, compared with P70, were associated with the cell cycle, mitosis, and DNA replication (Chapter 7, Figure 7.6: cluster 4). This is interesting since these results correlate with a gradual fall in the abundance of cell cycle proteins after birth, which were very low at P14 (Ikenishi *et al.*, 2012; Walsh *et al.*, 2010). In the period of growth from P10 to P18, there was an increase in the proportion of binucleated CMs and cellular enlargement, particularly at P10 and P13, which coincide with an intermediate expression of mitosis-related genes in the myocardium (Chapter 5). Furthermore, P10 marks the start of the period before rapid heart growth and the immediate time point before the surge in serum T₃ levels, while P13 is 24-hours after the initial peak in serum T₃ levels. Thus, it was determined from these parameters that these postnatal days may mark pivotal time points during the P10-18 period of cardiac growth. Future studies should characterise CMs at multiple sampling intervals between P2 and P35 to gain a complete picture of the time course of CM

maturation. Taken together, the data presented in this thesis indicate that the ~P13-P15 time points potentially mark the end of cell division, which is important since it may coincide with the initiation of terminal differentiation. Thus, pivotal stages of cardiac growth were identified using two time points from opposite spectrums of CM maturation including highly proliferative (P2) vs differentiated (P70) CM states; and P10 and P13, which represent the transitional state between CM cell division and enlargement.

RNA-Seq discovery of developmental mRNA signals in cardiac growth

The regulatory events that orchestrate CM proliferation and enlargement during normal cardiac growth remain poorly defined, as recognised by many in the field (Matkovich *et al.*, 2014; Li *et al.*, 1996; Chien *et al.*, 1993; Soonpaa *et al.*, 1996). To begin to elucidate these events more clearly, methods were developed to rapidly purify CMs (Chapter 6) from time points that were identified to be pivotal in the process of postnatal CM maturation (P2, P10, P13, or P70). RNA was then extracted from CMs at these developmental time points to construct poly(A) and small RNA libraries used to generate RNA-Seq datasets (Chapter 7). This revealed ~3,800 DE-mRNAs over the time course of postnatal CM maturation, and were associated with a number of interesting biological signalling pathways and processes (Chapter 7). Although the main purpose was to relate candidate genes specifically to each phase of CM growth, this was more difficult to ascertain with large datasets because DE-mRNAs are also involved in a number of other cellular processes, such as sarcomere or mitochondria development, which may not directly contribute to CM proliferation, enlargement or terminal differentiation. This highlights the challenges in teasing out functional relationships. Future work will involve mining the mRNA datasets by referring to the literature to identify genes of interest with novel or known roles in the heart. Moreover, it will be important to determine the protein level of genes of interest at the relevant time points to elucidate a function and signalling pathway. Delineating the mechanisms for CM proliferation, enlargement, and terminal differentiation, to understand normal cardiac growth would also, in time, reveal underlying interruptions of transcriptional activity in postnatal hearts that grow abnormally. Furthermore, this may lead to finding ways to stimulate cardiac regeneration and develop novel regenerative therapies. These datasets,

therefore, provide a foundation for the discovery of complex gene regulatory networks that drive CM maturation, the scope of which has enormous potential.

Tools for investigating developmental CM biology and cardiac regeneration

The ultimate goal for our group and many others is to harness the very limited innate ability of the heart to repair after injury by stimulating CM cell division, or reversing the terminally differentiated state of adult CMs that would then allow cell cycle re-entry and proliferation in response to injury. This is not only pertinent for MI patients but is also relevant to patients with other types of CVD, including LVH and CHD. In LVH, CMs undergo hypertrophy, and in CHD, CMs may also be reduced in number, leading to impaired cardiac function. Thus, pathways that stimulate or promote endogenous CM proliferation would increase the number of functional CMs, which is key to restoring or improving cardiac function. Currently, cardiac regeneration is mainly studied in the context of MI models, resulting in the death of cardiac tissue and in this setting, the aim is to replace the region of death with healthy myocardium to restore cardiac morphology and function. Cardiac regeneration has been assessed in early postnatal hearts by their response post-MI at different ages (Porrello *et al.*, 2013; Naqvi *et al.*, 2014). Is this regeneration or were the hearts in a phase of growth by CM proliferation at the time of injury and had continued to grow regardless?

Another cardiac injury model that should be explored more widely in the context of cardiac regeneration is SAC-induced LVH, detailed in Chapter 3. The PO overload injury model lead to concentric hypertrophy that was associated with reduced CO, left ventricular ejection fraction, and fractional shortening; fibrosis; and the re-expression of fetal genes. Unlike MI that leads to regional death of the heart, which often has a variable infarct size, PO overload uniformly affects the whole heart, whereby CM cell size and numbers can be assessed as parameters for cardiac regeneration when using genetic mouse models or after treatment with potential regenerative therapeutics. SAC is also reliable and reproducible model of cardiac hypertrophy. SAC can be used as a tool to determine the function of novel candidate mRNAs, lncRNAs, and miRNAs, in the adult heart following cardiac injury (Wang *et al.*,

2014) that may lead to the development of therapeutic agents that ameliorate LVH. Thus, future studies should use various cardiac injury models to investigate the expression and function of molecular candidates, and moreover, to realise the potential for regenerative therapies in treating multiple CVDs, including LVH and MI.

This thesis describes the detailed development of methods to isolate and purify a high yield of CMs by Langendorff retrograde perfusion and immuno-magnetic separation at any postnatal age (Chapter 6). The resulting high quality RNA and reproducibility between biological replicates (gene expression profiles of replicates shown in Figure 7.2 and Figure 7.6, Chapter 7) was further testament to the protocols developed to purify CMs. In addition to the quality of these datasets and to the best of my knowledge, there are no other RNA-Seq datasets available from CMs isolated and purified using a universal method for all postnatal murine ages (P2, P10, P13 and P70). Hence, we are well placed to use this unique dataset to investigate the transcriptional changes that occur with CM maturation. This protocol may also be useful for primary cell culture with CMs from any postnatal age, rather than only those from neonatal or adult hearts. This would allow us to study downstream signalling pathways at any developmental age by treating CMs with candidate molecules, such as T₃, or siRNA knockdown of transcripts. Overall, this CM purification protocol is a valuable research tool to study postnatal cardiac development.

Future perspectives: the mRNA-lncRNA-miRNA relationship

In this study, an unbiased integrative approach was employed to concurrently profile mRNA, lncRNA and miRNA, and comprehensively evaluate the transcriptome. Because lncRNAs are less abundant than mRNAs, it is possible to prioritise DE-mRNAs of interest by locating adjacent DE-lncRNAs to genomic regions that are active. Matkovich *et al.* (2014) recently reported ~120 cardiac-specific lncRNAs, whereby gene expression profiles of embryonic and adult hearts were compared, and ~22 neighbouring lncRNA-mRNA pairs were identified to have concordant expression, whereas 11 pairs had reciprocal expression. A brief exploration of gene expression datasets (Chapter 7) revealed the concordant expression of functionally relevant mRNA-lncRNAs-miRNAs at the Igf2/H19 locus (Figure

8.1A). Interestingly, both the lncRNA, *H19*, and the miRNA that it encodes, miR-675, were highly abundant in P2 CMs and at later time points the expression of *H19* and miR-675 fell coincidentally with the adjacent DE-mRNA, *Igf2* (Figure 8.1B). Furthermore, *Igf2*, which encodes miR-483, and partially overlaps with the antisense lncRNA transcript, *Igf2os*, were all down-regulated over the time course of CM maturation (Figure 8.1B). *H19* mediates skeletal muscle differentiation and regeneration (Dey *et al.*, 2014), and more recently, a function for *H19* and miR-675 has been elucidated in the heart to both negatively regulate CM hypertrophy (Liu *et al.*, 2016a). *Igf2* also affects embryonic heart development in *Igf2*-deficient mice resulting in CM hypoplasia (Li *et al.*, 2011), whereas miR-483 has more recently been implicated to cause CM apoptosis in response to high blood- glucose (Qiao *et al.*, 2016). However, a role for *Igf2os* has not yet been reported.

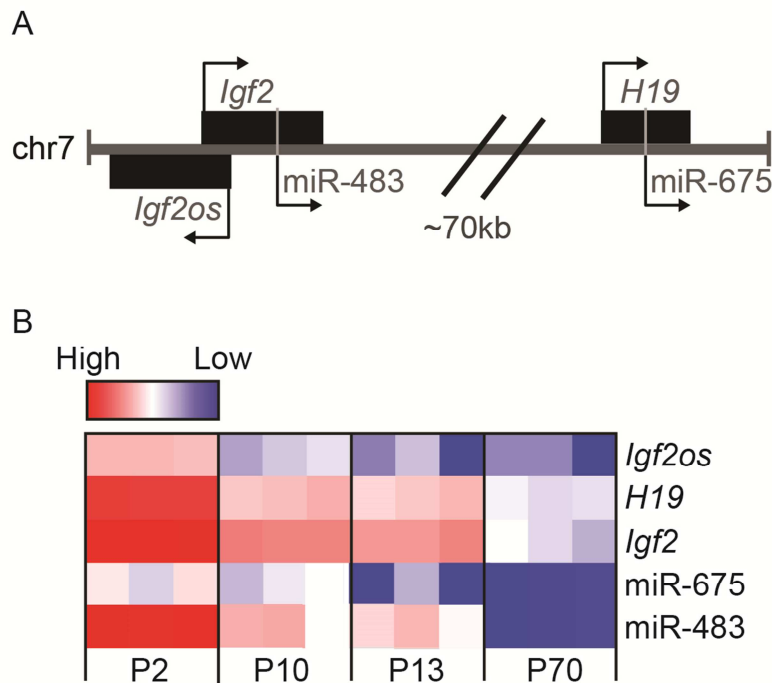


Figure 8.1: Expression patterns of mRNA-lncRNAs-miRNAs from the *Igf2/H19* locus over the time course of postnatal CM maturation

A, schematic of the structural organisation of the *Igf2/H19* locus encoding transcripts, including the antisense lncRNA (*Igf2os* and *H19*), mRNA (*Igf2*), miRNA (miR-483 and miR-675). B, the normalised gene count data of each transcript in the *Igf2/H19* locus is shown with high (red) or low (blue) expression, and expression of these decrease across the time course of CM maturation (P2, P10, P13 and P70, n=3 litter per time point).

By analysing the expression of miRNAs after Ang II-induced hypertrophy, Wang *et al.* (2014) identified a functional mRNA-lncRNA-miRNA relationship. The expression of miR-489 decreased after Ang II-induced hypertrophy. Interestingly, overexpression of this miRNA attenuated the hypertrophic response, and was found to target myeloid differentiation primary response gene 88 (*Myd88*) mRNA, the expression of which increased following Ang II-induced hypertrophy. In *Myd88*-knockout mice, Ang II-induced cardiac hypertrophy was attenuated with reduced HW/BW and CM cross-sectional area; fibrosis; and the re-expression of fetal genes. Wang *et al.* (2014) also evaluated the expression of a subset of lncRNAs following Ang II treatment and found that the expression of the lncRNA, AK04851, which was named cardiac hypertrophy related factor (CHRF) thereafter, had increased. CHRF also binds miR-489 and acts as a sponge to sequester miR-489. Therefore, CHRF reduced the availability of miR-489 to bind to *Myd88* resulting in the enhanced expression of *Myd88* after Ang II-induced hypertrophy, ultimately regulating cardiac hypertrophy (Wang *et al.*, 2014). This regulatory relationship demonstrates the combined power of such RNA-Seq datasets in uncovering multiple and novel mRNA, lncRNA, and miRNA, functions.

Future perspectives: exploring the function of candidate lncRNAs and miRNAs

The miRNA dataset can be probed using bioinformatics tools such as Target Scan to predict potential mRNA targets based on the complementarity of the miRNA seed region (a specific sequence of 6-8 nucleotides at the 5' end) to mRNA that either results in target mRNA degradation or prevents its translation. In contrast to miRNAs, there are not many bioinformatic tools available to analyse lncRNAs, presumably because their annotation and function are not yet well defined (Matkovich *et al.*, 2014). The poly(A) lncRNAs captured in my dataset (Chapter 7) may be intergenic, intronic, or partially overlapping with protein-coding genes on either the sense or antisense strand, and have been classified in many different ways due to challenges in the annotation and interpretation of lncRNA (Batista and Chang, 2013; Ma *et al.*, 2013; St Laurent *et al.*, 2015). LncRNAs may regulate gene expression by acting sequestering miRNAs, also known as competing endogenous RNAs (Cesana *et al.*, 2011; Wang *et al.*, 2014) or they may lead to epigenetic changes that silence

or activate genes by mediating DNA methylation or chromatin modifications (Rinn and Chang, 2012; Wamstad *et al.*, 2012; Batista and Chang, 2013).

There are many *in vitro* and *in vivo* techniques available to explore the functions of candidate lncRNAs and miRNAs from these RNA-Seq datasets (similar to those discussed for mRNAs in Chapter 7). For *in vitro* evaluation of function, transcripts are often overexpressed or knocked down by transfecting CMs using: cloned vectors expressing the transcript or mutant transcript, synthetic RNA mimics, small interfering RNA (siRNA), or antisense sequences of oligonucleotides flanked with locked nucleic acids (LNAs) that perfectly complement the RNA sequence (Liang *et al.*, 2015; Viereck *et al.*, 2016; Wang *et al.*, 2016; Eulalio *et al.*, 2012; Wang *et al.*, 2014). Proliferative markers or changes in cell size have been evaluated to determine their effect on CM proliferation or CM hypertrophy, respectively (Liang *et al.*, 2015; Viereck *et al.*, 2016; Porrello *et al.*, 2011a; Wang *et al.*, 2016; Eulalio *et al.*, 2012). For *in vivo* evaluation, genetic mouse models that overexpress or have the gene of interest deleted are characterised for changes in cardiac morphology and function. These are generated by cardiac-specific overexpression of the gene, or by targeted deletion of a gene using FLPe or Cre recombinase-mediated homologous recombination to excise the gene of interest, or by CRISPR-Cas9 mediated genome-editing (Zhao *et al.*, 2007; Liu *et al.*, 2008; Liang *et al.*, 2015; Wang *et al.*, 2016; Wang *et al.*, 2014). Alternatively, the transcript may be knocked down *in vivo* by injecting synthetic siRNA or LNA-modified antisense oligonucleotides (antimiRs or GapmeRs) (Porrello *et al.*, 2011a; Porrello *et al.*, 2013; Viereck *et al.*, 2016; Wang *et al.*, 2016; Eulalio *et al.*, 2012; Wang *et al.*, 2014). In the event that there is no apparent phenotype, these genetic mouse models may then be subjected to cardiac stressors, such as SAC, TAC, or MI, to further elucidate the function of the transcript (Viereck *et al.*, 2016; Wang *et al.*, 2016; Wang *et al.*, 2014) (Porrello *et al.*, 2013; Eulalio *et al.*, 2012).

Interactions between protein, mRNAs, lncRNAs, miRNAs and/or DNA can also be explored. Luciferase reporter assays have been used to detect transcript interactions by creating reporter constructs that contain luciferase fused to the DNA sequence of the transcript of interest. The luciferase activity is then compared to the same construct that has also been co-transfected with a second transcript of interest. For example, if the primary transcript is a mRNA and the second transcript is a miRNA, a reduction in luciferase

activity would confirm that the miRNA targets and inhibits expression of the mRNA (Liu *et al.*, 2008; Liang *et al.*, 2015; Porrello *et al.*, 2011a; Wang *et al.*, 2014). In addition, if a mutation of the mRNA 3'UTR abolishes the reduction in luciferase activity, this would further confirm a specific mRNA-miRNA interaction (Liu *et al.*, 2008; Liang *et al.*, 2015; Porrello *et al.*, 2011a; Wang *et al.*, 2014). Depending on the nature of the protein encoded by the mRNA (i.e. if the protein binds to DNA), novel lncRNA-protein interactions may be defined using chromatin IP (ChIP) of the protein that is bound to the promoter of the lncRNA (Viereck *et al.*, 2016; Wang *et al.*, 2016).

Future perspectives: the epigenome

Epigenetic modifications, such as temporal changes in chromatin and DNA methylation have been shown to regulate the differentiation of embryonic stem cells into CMs, and widespread changes also occur in the postnatal murine heart within two week of birth (Wamstad *et al.*, 2012; Sim *et al.*, 2015). In particular, the differentiation of embryonic stem cells into CMs was reported to involve an “epigenetic switch” (Wamstad *et al.*, 2012). One-quarter of each CM sample collected in Chapter 7 was allocated for the RNA-Seq experiment, and the remaining three-quarters were reserved for parallel sequencing of the epigenome either by evaluating DNA methylation, histone modifications, or accessible regions of DNA. These complementary datasets will enable active genomic regions to be identified, and thereby provide some insights into the epigenetic regulation of gene expression.

Conclusion

In summary, the substantial growth of the postnatal heart is likely to be coordinated by transcriptional networks that are already established regulators of embryonic cardiac development. To profile the postnatal CM transcriptome, a universal protocol for the rapid purification of CMs from any postnatal age was developed as a valuable research tool,

producing high quality poly(A) and small RNA as inputs for high-throughput sequencing. This has led to the identification of ~3,800 DE-mRNAs that contribute to the distinct and dynamically changing transcriptional profiles of CMs at pivotal time points in CM maturation. These transcripts were associated with many different pathways that can be investigated to unravel regulatory gene networks and gene functions that regulate postnatal cardiac growth. To elucidate the function of novel candidates we can use this CM purification protocol for *in vitro* studies and use SAC as a of cardiac injury model for *in vivo* experiments. Without question there is a lot to be gained from these large datasets in terms of providing a framework for understanding the molecular changes that underpin postnatal cardiac growth. However, further systematic analyses and experiments will be required to discover molecular targets to stimulate cardiac regeneration.

List of References

- Ahuja, P., Sdek, P. & Maclellan, W. R. 2007. Cardiac myocyte cell cycle control in development, disease, and regeneration. *Physiol Rev*, 87, 521-544.
- Akazawa, H. & Komuro, I. 2003. Roles of cardiac transcription factors in cardiac hypertrophy. *Circ Res*, 92, 1079-1088.
- Anversa, P., Olivetti, G. & Loud, A. V. 1980. Morphometric study of early postnatal development in the left and right ventricular myocardium of the rat. I. Hypertrophy, hyperplasia, and binucleation of myocytes. *Circ Res*, 46, 495-502.
- Archambault, V. & Glover, D. M. 2009. Polo-like kinases: conservation and divergence in their functions and regulation. *Nat Rev Mol Cell Bio*, 10, 265-275.
- Atlas, S. A. 2007. The renin-angiotensin aldosterone system: pathophysiological role and pharmacologic inhibition. *J Manag Care Pharm*, 13, 9-20.
- Atlas, S. A., Volpe, M., Sosa, R. E., Laragh, J. H., Camargo, M. J. F. & Maack, T. 1986. Effects of atrial natriuretic factor on blood pressure and the renin-angiotensin-aldosterone system. *Faseb J*, 45, 2115-2121.
- Bae, S., Xiao, Y. H., Li, G. H., Casiano, C. A. & Zhang, L. B. 2003. Effect of maternal chronic hypoxic exposure during gestation on apoptosis in fetal rat heart. *Am J Physiol-Heart C*, 285, H983-H990.
- Bai, S. L., Campbell, S. E., Moore, J. A., Morales, M. C. & Gerdes, A. M. 1990. Influence of age, growth, and sex on cardiac myocyte size and number in rats. *Anat Rec*, 226, 207-12.
- Baker, K. M., Chernin, M. I., Wixson, S. K. & Aceto, J. F. 1990. Renin-angiotensin system involvement in pressure-overload cardiac hypertrophy in rats. *Am J Physiol*, 259, H324-32.
- Banerjee, I., Fuseler, J. W., Price, R. L., Borg, T. K. & Baudino, T. A. 2007. Determination of cell types and numbers during cardiac development in the neonatal and adult rat and mouse. *Am J Physiol-Heart C*, 293, H1883-H1891.
- Barile, L., Messina, E., Giacomello, A. & Marban, E. 2007. Endogenous cardiac stem cells. *Prog Cardiovasc Dis*, 50, 31-48.
- Barker, D. J. P., Winter, P. D., Osmond, C., Margetts, B. & Simmonds, S. J. 1989. Weight in infancy and death from ischemic heart disease. *Lancet*, 2, 577-580.
- Batista, P. J. & Chang, H. Y. 2013. Long noncoding RNAs: cellular address codes in development and disease. *Cell*, 152, 1298-307.
- Beck, S., Wojdyla, D., Say, L., Betran, A. P., Merialdi, M., Requejo, J. H., . . . Van Look, P. F. 2010. The worldwide incidence of preterm birth: a systematic review of maternal mortality and morbidity. *Bull World Health Organ*, 88, 31-8.

- Beltrami, A. P., Barlucchi, L., Torella, D., Baker, M., Limana, F., Chimenti, S., . . . Anversa, P. 2003. Adult cardiac stem cells are multipotent and support myocardial regeneration. *Cell*, 114, 763-776.
- Bergmann, O., Bhardwaj, R. D., Bernard, S., Zdunek, S., Barnabe-Heider, F., Walsh, S., . . . Frisen, J. 2009. Evidence for cardiomyocyte renewal in humans. *Science*, 324, 98-102.
- Bernardo, B. C., Weeks, K. L., Pretorius, L. & McMullen, J. R. 2010. Molecular distinction between physiological and pathological cardiac hypertrophy: Experimental findings and therapeutic strategies. *Pharmacol Ther*, 128, 191-227.
- Besmer, P., Murphy, J. E., George, P. C., Qiu, F. H., Bergold, P. J., Lederman, L., . . . Hardy, W. D. 1986. A new acute transforming feline retrovirus and relationship of its oncogene v-kit with the protein kinase gene family. *Nature*, 320, 415-21.
- Bettendorf, M., Schmidt, K. G., Grulich-Henn, J., Ulmer, H. E. & Heinrich, U. E. 2000. Triiodothyronine treatment in children after cardiac surgery: a double-blind, randomised, placebo-controlled study. *Lancet*, 356, 529-534.
- Blume-Jensen, P., Claesson-Welsh, L., Siegbahn, A., Zsebo, K. M., Westermark, B. & Heldin, C. H. 1991. Activation of the human c-kit product by ligand-induced dimerization mediates circular actin reorganization and chemotaxis. *Embo J*, 10, 4121-8.
- Bolli, R., Chugh, A. R., D'amario, D., Loughran, J. H., Stoddard, M. F., Ikram, S., . . . Anversa, P. 2011. Cardiac stem cells in patients with ischaemic cardiomyopathy (SCIPIO): initial results of a randomised phase 1 trial. *Lancet*, 378, 1847-57.
- Breckenridge, R. 2010. Heart failure and mouse models. *Dis Model Mech*, 3, 138-43.
- Brodsky, V., Chernyaev, A. L. & Vasilyeva, I. A. 1991. Variability of the cardiomyocyte ploidy in normal human hearts. *Virchows Arch B Cell Pathol Incl Mol Pathol*, 61, 289-94.
- Brown, R. S. 2000. Disorders of the Thyroid Gland in Infancy, Childhood and Adolescence. In: De Groot, L. J., Beck-Peccoz, P., Chrousos, G., Dungan, K., Grossman, A., Hershman, J. M., . . . Weickert, M. O. (eds.) *Endotext*. South Dartmouth (MA).
- Bruneau, B. G. 2008. The developmental genetics of congenital heart disease. *Nature*, 451, 943-948.
- Buerger, A., Rozhitskaya, O., Sherwood, M. C., Dorfman, A. L., Bisping, E., Abel, E. D., . . . Jay, P. Y. 2006. Dilated cardiomyopathy resulting from high-level myocardial expression of Cre-recombinase. *J Card Fail*, 12, 392-398.
- Campbell, S. E., Gerdes, A. M. & Smith, T. D. 1987. Comparison of regional differences in cardiac myocyte dimensions in rats, hamsters, and guinea pigs. *Anatomical Record*, 219, 53-59.
- Cavanaugh, M. W. 1955. Pulsation, migration and division in dissociated chick embryo heart cells in vitro. *J Exp Zool*, 128, 573-589.

- Cesana, M., Cacchiarelli, D., Legnini, I., Santini, T., Sthandier, O., Chinappi, M., . . . Bozzoni, I. 2011. A Long Noncoding RNA Controls Muscle Differentiation by Functioning as a Competing Endogenous RNA. *Cell*, 147, 358-369.
- Chaudhari, N., Talwar, P., Parimisetty, A., Lefebvre D'hellencourt, C. & Ravanan, P. 2014. A molecular web: endoplasmic reticulum stress, inflammation, and oxidative stress. *Front Cell Neurosci*, 8, 213.
- Chien, K. R., Zhu, H., Knowlton, K. U., Millerhance, W., Vanbilsen, M., O'Brien, T. X. & Evans, S. M. 1993. Transcriptional Regulation during Cardiac Growth and Development. *Annu Rev Physiol*, 55, 77-95.
- Chizzonite, R. A. & Zak, R. 1984. Regulation of myosin isoenzyme composition in fetal and neonatal rat ventricle by endogenous thyroid hormones. *J Biol Chem*, 259, 12628-32.
- Chlopčikova, S., Psotova, J. & Miletova, P. 2001. Neonatal rat cardiomyocytes--a model for the study of morphological, biochemical and electrophysiological characteristics of the heart. *Biomed Pap Med Fac Univ Palacky Olomouc Czech Repub*, 145, 49-55.
- Chu, Y. J. & Corey, D. R. 2012. RNA sequencing: platform selection, experimental design, and data interpretation. *Nucleic Acid Ther*, 22, 271-274.
- Claycomb, W. C. 1975. Biochemical aspects of cardiac muscle differentiation. Deoxyribonucleic acid synthesis and nuclear and cytoplasmic deoxyribonucleic acid polymerase activity. *J Biol Chem*, 250, 3229-3235.
- Clubb, F. J., Jr. & Bishop, S. P. 1984. Formation of binucleated myocardial cells in the neonatal rat. An index for growth hypertrophy. *Lab Invest*, 50, 571-7.
- Cooper, G. M. 2000. The Cell: A Molecular Approach. *The Eukaryotic Cell Cycle*. 2nd edition ed. Sunderland (MA): Sinauer Associates; 2000. .
- Coppoletta, J. M. & Wolbach, S. B. 1933. Body Length and Organ Weights of Infants and Children: A Study of the Body Length and Normal Weights of the More Important Vital Organs of the Body between Birth and Twelve Years of Age. *Am J Pathol*, 9, 55-70.
- Corstius, H. B., Zimanyi, M. A., Maka, N., Herath, T., Thomas, W., Van Der Laarse, A., . . . Black, M. J. 2005. Effect of intrauterine growth restriction on the number of cardiomyocytes in rat hearts. *Pediatr Res*, 57, 796-800.
- Crane, R., Gadea, B., Littlepage, L., Wu, H. & Ruderman, J. V. 2004. Aurora A, meiosis and mitosis. *Biol Cell*, 96, 215-229.
- Cuspidi, C., Ciulla, M. & Zanchetti, A. 2006. Hypertensive myocardial fibrosis. *Nephrol Dial Transpl*, 21, 20-23.
- De Simone, G., Devereux, R. B., Daniels, S. R. & Meyer, R. A. 1995. Gender differences in left ventricular growth. *Hypertension*, 26, 979-83.

- De Windt, L. J., Lim, H. W., Bueno, O. F., Liang, Q., Delling, U., Braz, J. C., . . . Molkentin, J. D. 2001. Targeted inhibition of calcineurin attenuates cardiac hypertrophy in vivo. *Proc Natl Acad Sci U S A*, 98, 3322-7.
- Dealmeida, A. C., Van Oort, R. J. & Wehrens, X. H. 2010. Transverse aortic constriction in mice. *J Vis Exp*.
- Debosch, B., Treskov, I., Lupu, T. S., Weinheimer, C., Kovacs, A., Courtois, M. & Muslin, A. J. 2006. Akt1 is required for physiological cardiac growth. *Circulation*, 113, 2097-2104.
- Dey, B. K., Pfeifer, K. & Dutta, A. 2014. The H19 long noncoding RNA gives rise to microRNAs miR-675-3p and miR-675-5p to promote skeletal muscle differentiation and regeneration. *Genes Dev*, 28, 491-501.
- Diez, J. 2007. Mechanisms of cardiac fibrosis in hypertension. *J Clin Hypertens (Greenwich)*, 9, 546-50.
- Dobson, G. P. 2003. On being the right size: heart design, mitochondrial efficiency and lifespan potential. *Clin Exp Pharmacol P*, 30, 590-597.
- Doree, M. & Hunt, T. 2002. From Cdc2 to Cdk1: when did the cell cycle kinase join its cyclin partner? *J Cell Sci*, 115, 2461-2464.
- Dorn, G. W. 2007. The fuzzy logic of physiological cardiac hypertrophy. *Hypertension*, 49, 962-970.
- Drazner, M. H. 2011. The progression of hypertensive heart disease. *Circulation*, 123, 327-34.
- Drazner, M. H., Dries, D. L., Peshock, R. M., Cooper, R. S., Klassen, C., Kazi, F., . . . Victor, R. G. 2005. Left ventricular hypertrophy is more prevalent in blacks than whites in the general population: the Dallas Heart Study. *Hypertension*, 46, 124-9.
- Duan, S. Z., Ivashchenko, C. Y., Whitesall, S. E., D'alecy, L. G. & Mortensen, R. M. 2007. Direct monitoring pressure overload predicts cardiac hypertrophy in mice. *Physiol Meas*, 28, 1329-39.
- Durham, F. M. 1908. A preliminary account of the inheritance of coat colour in mice. *Rep. Evol. Com. Roy. Soc.*, 41-53.
- Eggert, U. S., Mitchison, T. J. & Field, C. M. 2006. Animal cytokinesis: from parts list to mechanisms. *Annu Rev Biochem*, 75, 543-66.
- Ehler, E., Moore-Morris, T. & Lange, S. 2013. Isolation and culture of neonatal mouse cardiomyocytes. *J Vis Exp*.
- Eisenstein, R. W., G. L. 1970. Myocardial DNA and protein in maturing and hypertrophied human hearts. *P Soc Exp Biol Med*, 133, 176-+.
- Ellison, G. M., Vicinanza, C., Smith, A. J., Aquila, I., Leone, A., Waring, C. D., . . . Nadal-Ginard, B. 2013. Adult c-kit(pos) cardiac stem cells are necessary and sufficient for functional cardiac regeneration and repair. *Cell*, 154, 827-842.

- Eulalio, A., Mano, M., Dal Ferro, M., Zentilin, L., Sinagra, G., Zacchigna, S. & Giacca, M. 2012. Functional screening identifies miRNAs inducing cardiac regeneration. *Nature*, 492, 376-81.
- Evans, H. J. & Goodwin, R. L. 2007. Western array analysis of cell cycle protein changes during the hyperplastic to hypertrophic transition in heart development. *Mol Cell Biochem*, 303, 189-199.
- Fazel, S., Cimini, M., Chen, L., Li, S., Angoulvant, D., Fedak, P., . . . Li, R. K. 2006. Cardioprotective c-kit⁺ cells are from the bone marrow and regulate the myocardial balance of angiogenic cytokines. *J Clin Invest*, 116, 1865-77.
- Fisher, D. A. & Klein, A. H. 1981. Thyroid development and disorders of thyroid function in the newborn. *N Engl J Med*, 304, 702-12.
- Fleming, S., Thompson, M., Stevens, R., Heneghan, C., Pluddemann, A., Maconochie, I., . . . Mant, D. 2011. Normal ranges of heart rate and respiratory rate in children from birth to 18 years of age: a systematic review of observational studies. *Lancet*, 377, 1011-1018.
- Francis, G. S. 2001. Pathophysiology of chronic heart failure. *Am J Med*, 110 Suppl 7A, 37S-46S.
- Fransioli, J., Bailey, B., Gude, N. A., Cottage, C. T., Muraski, J. A., Emmanuel, G., . . . Sussman, M. A. 2008. Evolution of the c-kit-positive cell response to pathological challenge in the myocardium. *Stem cells*, 26, 1315-24.
- Freeman, R. H., Davis, J. O. & Spielman, W. S. 1977. Renin-angiotensin system and aldosterone secretion during aortic constriction in the rat. *Am J Physiol*, 232, F434-7.
- Friedman, C.-E. 1951. The Normal Size of the Heart Muscle Weight. *Acta Medica Scandinavica*, 139, 15-19.
- Galli, S. J., Arizono, N., Murakami, T., Dvorak, A. M. & Fox, J. G. 1987. Development of large numbers of mast cells at sites of idiopathic chronic dermatitis in genetically mast cell-deficient WBB6F1-W/W^v mice. *Blood*, 69, 1661-6.
- Gao, C. & Wang, Y. B. 2014. Transcriptome complexity in cardiac development and diseases - an expanding universe between genome and phenome. *Circ J*, 78, 1038-1047.
- Gardner, D. G. 2003. Natriuretic peptides: markers or modulators of cardiac hypertrophy? *Trends Endocrinol Metab*, 14, 411-6.
- Ghigo, A., Franco, I., Morello, F. & Hirsch, E. 2014. Myocyte signalling in leucocyte recruitment to the heart. *Cardiovasc Res*, 102, 270-80.
- Goldenberg, R. L., Culhane, J. F., Iams, J. D. & Romero, R. 2008. Epidemiology and causes of preterm birth. *Lancet*, 371, 75-84.
- Gordon, J. W., Shaw, J. A. & Kirshenbaum, L. A. 2011. Multiple facets of NF-kappa B in the heart: to be or not to NF-kappa B. *Circ Res*, 108, 1122-1132.

- Grossman, W., Jones, D. & McLaurin, L. P. 1975. Wall stress and patterns of hypertrophy in the human left ventricle. *J Clin Invest*, 56, 56-64.
- Gulick, J., Subramaniam, A., Neumann, J. & Robbins, J. 1991. Isolation and characterization of the mouse cardiac myosin heavy chain genes. *J Biol Chem*, 266, 9180-5.
- Gutgesell, H. P. & Rembold, C. M. 1990. Growth of the human heart relative to body surface area. *Am J Cardiol*, 65, 662-8.
- Hadj-Sahraoui, N., Seugnet, I., Ghorbel, M. T. & Demeneix, B. 2000. Hypothyroidism prolongs mitotic activity in the post-natal mouse brain. *Neurosci Lett*, 280, 79-82.
- Hanzlick, R. & Rydzewski, D. 1990. Heart weights of white men 20 to 39 years of age. An analysis of 218 autopsy cases. *Am J Foren Med Path*, 11, 202-204.
- Hara, M., Ono, K., Hwang, M. W., Iwasaki, A., Okada, M., Nakatani, K., . . . Matsumori, A. 2002. Evidence for a role of mast cells in the evolution to congestive heart failure. *J Exp Med*, 195, 375-81.
- Harada, M., Qin, Y., Takano, H., Minamino, T., Zou, Y., Toko, H., . . . Komuro, I. 2005. G-CSF prevents cardiac remodeling after myocardial infarction by activating the Jak-Stat pathway in cardiomyocytes. *Nat Med*, 11, 305-11.
- Harary, I. & Farley, B. 1960. In vitro studies of single isolated beating heart cells. *Science*, 131, 1674-1675.
- Heallen, T., Zhang, M., Wang, J., Bonilla-Claudio, M., Klysik, E., Johnson, R. L. & Martin, J. F. 2011. Hippo pathway inhibits Wnt signaling to restrain cardiomyocyte proliferation and heart size. *Science*, 332, 458-461.
- Heckbert, S. R., Post, W., Pearson, G. D., Arnett, D. K., Gomes, A. S., Jerosch-Herold, M., . . . Bluemke, D. A. 2006. Traditional cardiovascular risk factors in relation to left ventricular mass, volume, and systolic function by cardiac magnetic resonance imaging: the Multiethnic Study of Atherosclerosis. *J Am Coll Cardiol*, 48, 2285-92.
- Heineke, J. & Molkentin, J. D. 2006. Regulation of cardiac hypertrophy by intracellular signalling pathways. *Nat Rev Mol Cell Bio*, 7, 589-600.
- Heller, L. J., Opsahl, J. A., Wernsing, S. E., Saxena, R. & Katz, S. A. 1998. Myocardial and plasma renin-angiotensinogen dynamics during pressure-induced cardiac hypertrophy. *Am J Physiol*, 274, R849-56.
- Hernandez, A., Martinez, M. E., Fiering, S., Galton, V. A. & St Germain, D. 2006. Type 3 deiodinase is critical for the maturation and function of the thyroid axis. *J Clin Invest*, 116, 476-484.
- Hewett, T. E., Grupp, I. L., Grupp, G. & Robbins, J. 1994. Alpha-skeletal actin is associated with increased contractility in the mouse heart. *Circ Res*, 74, 740-746.
- Ho, K. K., Pinsky, J. L., Kannel, W. B. & Levy, D. 1993. The epidemiology of heart failure: the Framingham Study. *J Am Coll Cardiol*, 22, 6A-13A.

- Hochegger, H., Takeda, S. & Hunt, T. 2008. Cyclin-dependent kinases and cell-cycle transitions: does one fit all? *Nat Rev Mol Cell Bio*, 9, 910-U26.
- Hollenberg, M., Honbo, N. & Samorodin, A. J. 1976. Effects of hypoxia on cardiac growth in neonatal rat. *Am J Physiol*, 231, 1445-1450.
- Hollenberg, M., Honbo, N. & Samorodin, A. J. 1977. Cardiac cellular responses to altered nutrition in the neonatal rat. *Am J Physiol*, 233, H356-60.
- Holt, J. P., Rhode, E. A. & Kines, H. 1968. Ventricular volumes and body weight in mammals. *Am J Physiol*, 215, 704-&.
- Horwich, T. B., Patel, J., Maclellan, W. R. & Fonarow, G. C. 2003. Cardiac troponin I is associated with impaired hemodynamics, progressive left ventricular dysfunction, and increased mortality rates in advanced heart failure. *Circulation*, 108, 833-838.
- Hosoda, T., D'amario, D., Cabral-Da-Silva, M. C., Zheng, H. Q., Padin-Iruegas, M. E., Ogorek, B., . . . Leri, A. 2009. Clonality of mouse and human cardiomyogenesis in vivo. *Proc Natl Acad Sci U S A*, 106, 17169-17174.
- Hou, J. & Kang, Y. J. 2012. Regression of pathological cardiac hypertrophy: signaling pathways and therapeutic targets. *Pharmacol Ther*, 135, 337-54.
- Houser, S. R., Margulies, K. B., Murphy, A. M., Spinale, F. G., Francis, G. S., Prabhu, S. D., . . . Genomics, C. F. 2012. Animal models of heart failure: a scientific statement from the American Heart Association. *Circ Res*, 111, 131-150.
- Hsieh, P. C., Segers, V. F., Davis, M. E., Macgillivray, C., Gannon, J., Molkentin, J. D., . . . Lee, R. T. 2007. Evidence from a genetic fate-mapping study that stem cells refresh adult mammalian cardiomyocytes after injury. *Nat Med*, 13, 970-4.
- Huang, W. Y., Aramburu, J., Douglas, P. S. & Izumo, S. 2000. Transgenic expression of green fluorescence protein can cause dilated cardiomyopathy. *Nat Med*, 6, 482-483.
- Hudlicka, O. & Brown, M. D. 1996. Postnatal growth of the heart and its blood vessels. *J Vasc Res*, 33, 266-287.
- Humphreys, D. T. & Suter, C. M. 2013. miRspring: a compact standalone research tool for analyzing miRNA-seq data. *Nucleic Acids Res*, 41.
- Ikenishi, A., Okayama, H., Iwamoto, N., Yoshitome, S., Tane, S., Nakamura, K., . . . Takeuchi, T. 2012. Cell cycle regulation in mouse heart during embryonic and postnatal stages. *Dev Growth Differ*, 54, 731-738.
- Iwaki, K., Sukhatme, V. P., Shubeita, H. E. & Chien, K. R. 1990. Alpha- and beta-adrenergic stimulation induces distinct patterns of immediate early gene expression in neonatal rat myocardial cells. fos/jun expression is associated with sarcomere assembly; Egr-1 induction is primarily an alpha 1-mediated response. *J Biol Chem*, 265, 13809-17.
- Jelonek, K., Walaszczyk, A., Gabrys, D., Pietrowska, M., Kanthou, C. & Widlak, P. 2011. Cardiac endothelial cells isolated from mouse heart - a novel model for radiobiology. *Acta Biochim Pol*, 58, 397-404.

- Jessup, M., Abraham, W. T., Casey, D. E., Feldman, A. M., Francis, G. S., Ganiats, T. G., . . . Yancy, C. W. 2009. 2009 focused update: ACCF/AHA Guidelines for the Diagnosis and Management of Heart Failure in Adults: a report of the American College of Cardiology Foundation/American Heart Association Task Force on Practice Guidelines: developed in collaboration with the International Society for Heart and Lung Transplantation. *Circulation*, 119, 1977-2016.
- Jesty, S. A., Steffey, M. A., Lee, F. K., Breitbach, M., Hesse, M., Reining, S., . . . Kotlikoff, M. I. 2012. c-kit(+) precursors support postinfarction myogenesis in the neonatal, but not adult, heart. *Proc Natl Acad Sci U S A*, 109, 13380-13385.
- Jonker, S. S. & Louey, S. 2016. Endocrine and other physiologic modulators of perinatal cardiomyocyte endowment. *The Journal of endocrinology*, 228, R1-18.
- Jopling, C., Sleep, E., Raya, M., Marti, M., Raya, A. & Belmonte, J. C. I. 2010. Zebrafish heart regeneration occurs by cardiomyocyte dedifferentiation and proliferation. *Nature*, 464, 606-U168.
- Jung, H. J. & Suh, Y. 2014. Regulation of IGF -1 signaling by microRNAs. *Frontiers in genetics*, 5, 472.
- Kahan, T. & Bergfeldt, L. 2005. Left ventricular hypertrophy in hypertension: Its arrhythmogenic potential. *Heart*, 91, 250-256.
- Kajstura, J., Gurusamy, N., Ogorek, B., Goichberg, P., Clavo-Rondon, C., Hosoda, T., . . . Anversa, P. 2010. Myocyte turnover in the aging human heart. *Circ Res*, 107, 1374-86.
- Katz, M. G., Fargnoli, A. S., Kendle, A. P., Hajjar, R. J. & Bridges, C. R. 2016. The role of microRNAs in cardiac development and regenerative capacity. *Am J Physiol-Heart C*, 310, H528-H541.
- Kikuchi, K., Holdway, J. E., Werdich, A. A., Anderson, R. M., Fang, Y., Egnaczyk, G. F., . . . Poss, K. D. 2010. Primary contribution to zebrafish heart regeneration by gata4(+) cardiomyocytes. *Nature*, 464, 601-5.
- Kim, H. L., Kim, Y. J., Kim, K. H., Lee, S. P., Kim, H. K., Sohn, D. W., . . . Park, Y. B. 2015. Therapeutic effects of udenafil on pressure-overload cardiac hypertrophy. *Hypertens Res*, 38, 597-604.
- Klattenhoff, C. A., Scheuermann, J. C., Surface, L. E., Bradley, R. K., Fields, P. A., Steinhauser, M. L., . . . Boyer, L. A. 2013. Braveheart, a long noncoding RNA required for cardiovascular lineage commitment. *Cell*, 152, 570-583.
- Kolar, F., Seppet, E. K., Vetter, R., Prochazka, J., Grunermel, J., Zilmer, K. & Ostadal, B. 1992. Thyroid control of contractile function and calcium handling in neonatal rat heart. *Pflug Arch Eur J Phy*, 421, 26-31.
- Kono, T. 1969. Roles of collagenases and other proteolytic enzymes in dispersal of animal tissues. *Biochim Biophys Acta*, 178, 397-&.
- Kovacic, J. C., Muller, D. W., Harvey, R. & Graham, R. M. 2005. Update on the use of stem cells for cardiac disease. *Intern Med J*, 35, 348-56.

- Kozak-Barany, A., Jokinen, E., Saraste, M., Tuominen, J. & Valimaki, I. 2001. Development of left ventricular systolic and diastolic function in preterm infants during the first month of life: a prospective follow-up study. *J Pediatr*, 139, 539-45.
- Krenz, M. & Robbins, J. 2004. Impact of beta-myosin heavy chain expression on cardiac function during stress. *J Am Coll Cardiol*, 44, 2390-7.
- Kurtz, A., Dellabruna, R., Pfeilschifter, J. & Bauer, C. 1986. Atrial natriuretic peptide (ANP) inhibits renin release from juxtaglomerular cells. *Experientia*, 42, 638-638.
- Kuwahara, F., Kai, H., Tokuda, K., Kai, M., Takeshita, A., Egashira, K. & Imaizumi, T. 2002. Transforming growth factor-beta function blocking prevents myocardial fibrosis and diastolic dysfunction in pressure-overloaded rats. *Circulation*, 106, 130-5.
- Lacroix, B. & Maddox, A. S. 2012. Cytokinesis, ploidy and aneuploidy. *J Pathol*, 226, 338-351.
- Laflamme, M. A. & Murry, C. E. 2011. Heart regeneration. *Nature*, 473, 326-335.
- Lai, E. C. 2002. Micro RNAs are complementary to 3' UTR sequence motifs that mediate negative post-transcriptional regulation. *Nat Genet*, 30, 363-364.
- Lam, M. L., Bartoli, M. & Claycomb, W. C. 2002. The 21-day postnatal rat ventricular cardiac muscle cell in culture as an experimental model to study adult cardiomyocyte gene expression. *Mol Cell Biochem*, 229, 51-62.
- Latif, S. & Garry, D. J. 2010. Genomic Analyses in the Developing and Diseased Heart. In: Rosenthal, N. & Harvey, R. P. (eds.) *Heart Development and Regeneration*. Elsevier.
- Law, C. W., Chen, Y. S., Shi, W. & Smyth, G. K. 2014. voom: precision weights unlock linear model analysis tools for RNA-seq read counts. *Genome Biol*, 15.
- Lawn, J. E., Wilczynska-Ketende, K. & Cousens, S. N. 2006. Estimating the causes of 4 million neonatal deaths in the year 2000. *Int J Epidemiol*, 35, 706-18.
- Leipala, J. A., Boldt, T., Turpeinen, U., Vuolteenaho, O. & Fellman, V. 2003a. Cardiac hypertrophy and altered hemodynamic adaptation in growth-restricted preterm infants. *Pediatr Res*, 53, 989-93.
- Leipala, J. A., Boldt, T., Turpeinen, U., Vuolteenaho, O. & Fellman, V. 2003b. Cardiac hypertrophy and altered hemodynamic adaptation in growth-restricted preterm infants. *Pediatr Res*, 53, 989-993.
- Lennartsson, J. & Ronnstrand, L. 2012. Stem cell factor receptor/c-Kit: from basic science to clinical implications. *Physiol Rev*, 92, 1619-49.
- Leu, M., Ehler, E. & Perriard, J. C. 2001. Characterisation of postnatal growth of the murine heart. *Anat Embryol (Berl)*, 204, 217-24.

- Levy, D., Anderson, K. M., Savage, D. D., Kannel, W. B., Christiansen, J. C. & Castelli, W. P. 1988. Echocardiographically detected left ventricular hypertrophy: prevalence and risk factors. The Framingham Heart Study. *Ann Intern Med*, 108, 7-13.
- Levy, D., Garrison, R. J., Savage, D. D., Kannel, W. B. & Castelli, W. P. 1990. Prognostic implications of echocardiographically determined left ventricular mass in the Framingham Heart Study. *New Engl J Med*, 322, 1561-1566.
- Lewandowski, A. J., Augustine, D., Lamata, P., Davis, E. F., Lazdam, M., Francis, J., . . . Leeson, P. 2013. Preterm heart in adult life: cardiovascular magnetic resonance reveals distinct differences in left ventricular mass, geometry, and function. *Circulation*, 127, 197-206.
- Li, D. X., Wu, J., Bai, Y., Zhao, X. C. & Liu, L. J. 2014a. Isolation and culture of adult mouse cardiomyocytes for cell signaling and in vitro cardiac hypertrophy. *Jove-J Vis Exp*.
- Li, F., Wang, X., Capasso, J. M. & Gerdes, A. M. 1996. Rapid transition of cardiac myocytes from hyperplasia to hypertrophy during postnatal development. *J Mol Cell Cardiol*, 28, 1737-46.
- Li, L., Zhou, N., Gong, H., Wu, J. A., Lin, L., Komuro, I., . . . Zou, Y. Z. 2010. Comparison of angiotensin II type 1-receptor blockers to regress pressure overload-induced cardiac hypertrophy in mice. *Hypertens Res*, 33, 1289-1297.
- Li, M., Iismaa, S. E., Naqvi, N., Nicks, A., Husain, A. & Graham, R. M. 2014b. Thyroid hormone action in postnatal heart development. *Stem Cell Res*, 13, 582-91.
- Li, M., Liu, K., Michalicek, J., Angus, J. A., Hunt, J. E., Dell'italia, L. J., . . . Husain, A. 2004. Involvement of chymase-mediated angiotensin II generation in blood pressure regulation. *J Clin Invest*, 114, 112-20.
- Li, M., Naqvi, N., Yahiro, E., Liu, K., Powell, P. C., Bradley, W. E., . . . Husain, A. 2008. c-kit is required for cardiomyocyte terminal differentiation. *Circ Res*, 102, 677-85.
- Li, P., Cavallero, S., Gu, Y., Chen, T. H. P., Hughes, J., Hassan, A. B., . . . Sucov, H. M. 2011. IGF signaling directs ventricular cardiomyocyte proliferation during embryonic heart development. *Development*, 138, 1795-1805.
- Li, S., Tighe, S. W., Nicolet, C. M., Grove, D., Levy, S., Farmerie, W., . . . Mason, C. E. 2014c. Multi-platform assessment of transcriptome profiling using RNA-seq in the ABRF next-generation sequencing study. *Nat Biotechnol*, 32, 915-925.
- Liang, D. D., Li, J., Wu, Y. H., Zhen, L. X., Li, C. M., Qi, M., . . . Chen, Y. H. 2015. miRNA-204 drives cardiomyocyte proliferation via targeting Jarid2. *Int J Cardiol*, 201, 38-48.
- Liang, Q. R. & Molkenin, J. D. 2003. Redefining the roles of p38 and JNK signaling in cardiac hypertrophy: dichotomy between cultured myocytes and animal models. *J Mol Cell Cardiol*, 35, 1385-1394.
- Liao, R. & Jain, M. 2007. Isolation, culture, and functional analysis of adult mouse cardiomyocytes. *Methods Mol Med*, 139, 251-62.

- Liao, Y., Takashima, S., Asano, Y., Asakura, M., Ogai, A., Shintani, Y., . . . Kitakaze, M. 2003. Activation of adenosine A1 receptor attenuates cardiac hypertrophy and prevents heart failure in murine left ventricular pressure-overload model. *Circ Res*, 93, 759-66.
- Licatalosi, D. D. & Darnell, R. B. 2010. RNA processing and its regulation: global insights into biological networks. *Nat Rev Genet*, 11, 75-87.
- Lim, S. H. & Kaldis, P. 2013. Cdks, cyclins and CKIs: roles beyond cell cycle regulation. *Development*, 140, 3079-3093.
- Linder, N., Sela, B., German, B., Davidovitch, N., Kuint, I., Hegesh, T., . . . Sack, J. 1996. Iodine and hypothyroidism in neonates with congenital heart disease. *Pediatr Res*, 39, 1338-1338.
- Little, C. C. 1917. The relation of yellow coat color and black-eyed white spotting of mice in inheritance. *Genetics*, 2, 433-444.
- Liu, L. T., An, X. B., Li, Z. H., Song, Y., Li, L. L., Zuo, S., . . . Wang, J. 2016a. The H19 long noncoding RNA is a novel negative regulator of cardiomyocyte hypertrophy. *Cardiovasc Res*, 111, 56-65.
- Liu, N., Bezprozvannaya, S., Williams, A. H., Qi, X. X., Richardson, J. A., Bassel-Duby, R. & Olson, E. N. 2008. microRNA-133a regulates cardiomyocyte proliferation and suppresses smooth muscle gene expression in the heart. *Genes Dev*, 22, 3242-3254.
- Liu, Q., Yang, R., Huang, X., Zhang, H., He, L., Zhang, L., . . . Zhou, B. 2016b. Genetic lineage tracing identifies in situ Kit-expressing cardiomyocytes. *Cell Res*, 26, 119-30.
- Lloyd-Jones, D. M., Larson, M. G., Leip, E. P., Beiser, A., D'agostino, R. B., Kannel, W. B., . . . Framingham Heart, S. 2002. Lifetime risk for developing congestive heart failure: the Framingham Heart Study. *Circulation*, 106, 3068-72.
- Lodish, H., Berk, A. & Zipursky, S. 2000. Oxidation of Glucose and Fatty Acids to CO₂. *Molecular Cell Biology*. 4th edition ed. New York: W. H. Freeman.
- Loman, N. J., Misra, R. V., Dallman, T. J., Constantinidou, C., Gharbia, S. E., Wain, J. & Pallen, M. J. 2012. Performance comparison of benchtop high-throughput sequencing platforms. *Nat Biotechnol*, 30, 434-+.
- Lopaschuk, G. D. & Jaswal, J. S. 2010. Energy metabolic phenotype of the cardiomyocyte during development, differentiation, and postnatal maturation. *J Cardiovasc Pharmacol*, 56, 130-40.
- Lorell, B. H. & Carabello, B. A. 2000. Left ventricular hypertrophy: pathogenesis, detection, and prognosis. *Circulation*, 102, 470-9.
- Louch, W. E., Sheehan, K. A. & Wolska, B. M. 2011. Methods in cardiomyocyte isolation, culture, and gene transfer. *J Mol Cell Cardiol*, 51, 288-298.
- Ma, L. N., Bajic, V. B. & Zhang, Z. 2013. On the classification of long non-coding RNAs. *Rna Biol*, 10, 925-934.

- Mahmoud, A. I., Kocabas, F., Muralidhar, S. A., Kimura, W., Koura, A. S., Thet, S., . . . Sadek, H. A. 2013. Meis1 regulates postnatal cardiomyocyte cell cycle arrest. *Nature*, 497, 249-253.
- Mai, W., Janier, M. F., Allioli, N., Quignodon, L., Chuzel, T., Flamant, F. & Samarut, J. 2004. Thyroid hormone receptor alpha is a molecular switch of cardiac function between fetal and postnatal life. *Proc Natl Acad Sci U S A*, 101, 10332-10337.
- Maillet, M., Van Berlo, J. H. & Molkenin, J. D. 2013. Molecular basis of physiological heart growth: fundamental concepts and new players. *Nat Rev Mol Cell Biol*, 14, 38-48.
- Maisch, B. 1981. Enrichment of vital adult cardiac muscle cells by continuous silica sol gradient centrifugation. *Basic Res Cardiol*, 76, 622-9.
- Marelli, A. J., Ionescu-Ittu, R., Mackie, A. S., Guo, L. M., Dendukuri, N. & Kaouache, M. 2014. Lifetime prevalence of congenital heart disease in the general population from 2000 to 2010. *Circulation*, 130, 749-+.
- Masino, A. M., Gallardo, T. D., Wilcox, C. A., Olson, E. N., Williams, R. S. & Garry, D. J. 2004. Transcriptional regulation of cardiac progenitor cell populations. *Circ Res*, 95, 389-397.
- Matkovich, S. J., Edwards, J. R., Grossenheider, T. C., De Guzman Strong, C. & Dorn, G. W., 2nd 2014. Epigenetic coordination of embryonic heart transcription by dynamically regulated long noncoding RNAs. *Proc Natl Acad Sci U S A*, 111, 12264-9.
- Mcmullen, J. R. & Jennings, G. L. 2007. Differences between pathological and physiological cardiac hypertrophy: novel therapeutic strategies to treat heart failure. *Clin Exp Pharmacol P*, 34, 255-262.
- Mcmullen, J. R., Shioi, T., Zhang, L., Tarnavski, O., Sherwood, M. C., Kang, P. M. & Izumo, S. 2003. Phosphoinositide 3-kinase(p110 alpha) plays a critical role for the induction of physiological, but not pathological, cardiac hypertrophy. *Proc Natl Acad Sci U S A*, 100, 12355-12360.
- Melo, L. G., Pang, S. C. & Ackermann, U. 2000. Atrial Natriuretic Peptide: Regulator of Chronic Arterial Blood Pressure. *News Physiol Sci*, 15, 143-149.
- Miyata, S., Minobe, W., Bristow, M. R. & Leinwand, L. A. 2000. Myosin heavy chain isoform expression in the failing and nonfailing human heart. *Circ Res*, 86, 386-390.
- Moffett, R. B., MCGowan, R. A. & Gross, K. W. 1986. Modulation of kidney renin messenger RNA levels during experimentally induced hypertension. *Hypertension*, 8, 874-82.
- Molina, D. K. & Dimaio, V. J. M. 2012. Normal Organ Weights in Men Part I-The Heart. *Am J Foren Med Path*, 33, 362-367.
- Mollova, M., Bersell, K., Walsh, S., Savla, J., Das, L. T., Park, S. Y., . . . Kuhn, B. 2013. Cardiomyocyte proliferation contributes to heart growth in young humans. *Proc Natl Acad Sci U S A*, 110, 1446-51.

- Morozova, O. & Marra, M. A. 2008. Applications of next-generation sequencing technologies in functional genomics. *Genomics*, 92, 255-264.
- Morris, B. J., Davis, J. O., Zatzman, M. L. & Williams, G. M. 1977. The renin-angiotensin-aldosterone system in rabbits with congestive heart failure produced by aortic constriction. *Circ Res*, 40, 275-82.
- Mrowka, R., Patzak, A., Schubert, E. & Persson, P. B. 1996. Linear and non-linear properties of heart rate in postnatal maturation. *Cardiovasc Res*, 31, 447-454.
- Nag, A. C. 1980. Study of non-muscle cells of the adult mammalian heart - a fine structural analysis and distribution. *Cytobios*, 28, 41-61.
- Naghavi, M., Wang, H., Lozano, R., Davis, A., Liang, X., Zhou, M., . . . Murray, J. L. M. 2015. Global, regional, and national age-sex specific all-cause and cause-specific mortality for 240 causes of death, 1990-2013: a systematic analysis for the Global Burden of Disease Study 2013. *Lancet*, 385, 117-71.
- Nakagawa, O., Ogawa, Y., Itoh, H., Suga, S., Komatsu, Y., Kishimoto, I., . . . Nakao, K. 1995. Rapid transcriptional activation and early mRNA turnover of brain natriuretic peptide in cardiocyte hypertrophy. Evidence for brain natriuretic peptide as an "emergency" cardiac hormone against ventricular overload. *J Clin Invest*, 96, 1280-7.
- Naqvi, N., Li, M., Calvert, J. W., Tejada, T., Lambert, J. P., Wu, J. X., . . . Husain, A. 2014. A proliferative burst during preadolescence establishes the final cardiomyocyte number. *Cell*, 157, 795-807.
- Nickson, P., Toth, A. & Erhardt, P. 2007. PUMA is critical for neonatal cardiomyocyte apoptosis induced by endoplasmic reticulum stress. *Cardiovasc Res*, 73, 48-56.
- Nishimura, H., Hoffmann, S., Baltatu, O., Sugimura, K., Ganten, D. & Urata, H. 1996. Angiotensin I converting enzyme and chymase in cardiovascular tissues. *Kidney Int*, S18-S23.
- Nocka, K., Majumder, S., Chabot, B., Ray, P., Cervone, M., Bernstein, A. & Besmer, P. 1989. Expression of c-kit gene products in known cellular targets of W mutations in normal and W mutant mice--evidence for an impaired c-kit kinase in mutant mice. *Genes Dev*, 3, 816-26.
- Nocka, K., Tan, J. C., Chiu, E., Chu, T. Y., Ray, P., Traktman, P. & Besmer, P. 1990. Molecular bases of dominant negative and loss of function mutations at the murine c-Kit/white spotting locus: W37, Wv, W41 and W. *Embo J*, 9, 1805-1813.
- Norman, M. 2013. Preterm Birth and the Shape of the Heart. *Circulation*, 127, 160-161.
- O'connell, D. J., Ho, J. W. K., Mammoto, T., Turbe-Doan, A., O'connell, J. T., Haseley, P. S., . . . Maas, R. L. 2012. A Wnt-bmp feedback circuit controls intertissue signaling dynamics in tooth organogenesis. *Sci Signal*, 5.
- O'meara, C. C., Wamstad, J. A., Gladstone, R. A., Fomovsky, G. M., Butty, V. L., Shrikumar, A., . . . Lee, R. T. 2015. Transcriptional reversion of cardiac myocyte fate during mammalian cardiac regeneration. *Circ Res*, 116, 804-815.

- O'connell, T. D., Rodrigo, M. C. & Simpson, P. C. 2007. Isolation and culture of adult mouse cardiac myocytes. *In: Vivanco, F. (ed.) Cardiovascular Proteomics: Methods and Protocols.* Totowa, NJ: Humana Press.
- Odum, E. P. 1945. The Heart Rate of Small Birds. *Science*, 101, 153-4.
- Ogawa, T., Linz, W., Scholkens, B. A. & De Bold, A. J. 1999. Variable renal atrial natriuretic factor gene expression in hypertension. *Hypertension*, 33, 1342-7.
- Oka, T., Xu, J. & Molkenin, J. D. 2007. Re-employment of developmental transcription factors in adult heart disease. *Semin Cell Dev Biol*, 18, 117-131.
- Olivetti, G., Anversa, P. & Loud, A. V. 1980. Morphometric study of early postnatal development in the left and right ventricular myocardium of the rat. II. Tissue composition, capillary growth, and sarcoplasmic alterations. *Circ Res*, 46, 503-12.
- Olivetti, G., Cigola, E., Maestri, R., Corradi, D., Lagrasta, C., Gambert, S. R. & Anversa, P. 1996. Aging, cardiac hypertrophy and ischemic cardiomyopathy do not affect the proportion of mononucleated and multinucleated myocytes in the human heart. *J Mol Cell Cardiol*, 28, 1463-77.
- Olson, E. N. 2006. Gene regulatory networks in the evolution and development of the heart. *Science*, 313, 1922-7.
- Patten, R. D. & Hall-Porter, M. R. 2009. Small animal models of heart failure: development of novel therapies, past and present. *Circ-Heart Fail*, 2, 138-144.
- Pinto, A. R., Ilinykh, A., Ivey, M. J., Kuwabara, J. T., D'antoni, M. L., Debuque, R., . . . Tallquist, M. D. 2016. Revisiting Cardiac Cellular Composition. *Circ Res*, 118, 400-409.
- Porrello, E. R., Johnson, B. A., Aurora, A. B., Simpson, E., Nam, Y. J., Matkovich, S. J., . . . Olson, E. N. 2011a. miR-15 family regulates postnatal mitotic arrest of cardiomyocytes. *Circ Res*, 109, 670-U208.
- Porrello, E. R., Mahmoud, A. I., Simpson, E., Hill, J. A., Richardson, J. A., Olson, E. N. & Sadek, H. A. 2011b. Transient regenerative potential of the neonatal mouse heart. *Science*, 331, 1078-80.
- Porrello, E. R., Mahmoud, A. I., Simpson, E., Johnson, B. A., Grinsfelder, D., Canseco, D., . . . Sadek, H. A. 2013. Regulation of neonatal and adult mammalian heart regeneration by the miR-15 family. *Proc Natl Acad Sci U S A*, 110, 187-192.
- Puente, B. N., Kimura, W., Muralidhar, S. A., Moon, J., Amatruda, J. F., Phelps, K. L., . . . Sadek, H. A. 2014. The oxygen-rich postnatal environment induces cardiomyocyte cell-cycle arrest through DNA damage response. *Cell*, 157, 565-579.
- Qiao, Y., Zhao, Y. L., Liu, Y., Ma, N., Wang, C. X., Zou, J. Q., . . . Huang, H. 2016. miR-483-3p regulates hyperglycaemia-induced cardiomyocyte apoptosis in transgenic mice. *Biochem Biophys Res Commun*, 477, 541-547.

- Quail, M. A., Smith, M., Coupland, P., Otto, T. D., Harris, S. R., Connor, T. R., . . . Gu, Y. 2012. A tale of three next generation sequencing platforms: comparison of Ion Torrent, Pacific Biosciences and Illumina MiSeq sequencers. *Bmc Genomics*, 13.
- Rakusan, K., Raman, S., Layberry, R. & Korecky, B. 1978. The influence of aging and growth on the postnatal development of cardiac muscle in rats. *Circ Res*, 42, 212-8.
- Raulf, A., Horder, H., Tarnawski, L., Geisen, C., Ottersbach, A., Roll, W., . . . Hesse, M. 2015. Transgenic systems for unequivocal identification of cardiac myocyte nuclei and analysis of cardiomyocyte cell cycle status. *Basic Res Cardiol*, 110.
- Reiss, K., Cheng, W., Ferber, A., Kajstura, J., Li, P., Li, B., . . . Anversa, P. 1996. Overexpression of insulin-like growth factor-1 in the heart is coupled with myocyte proliferation in transgenic mice. *Proc Natl Acad Sci U S A*, 93, 8630-5.
- Ren, B., Cam, H., Takahashi, Y., Volkert, T., Terragni, J., Young, R. A. & Dynlacht, B. D. 2002. E2F integrates cell cycle progression with DNA repair, replication, and G(2)/M checkpoints. *Genes Dev*, 16, 245-256.
- Rinn, J. L. & Chang, H. Y. 2012. Genome Regulation by Long Noncoding RNAs. *Annual Review of Biochemistry*, Vol 81, 81, 145-166.
- Rockman, H. A., Ross, R. S., Harris, A. N., Knowlton, K. U., Steinhilper, M. E., Field, L. J., . . . Chien, K. R. 1991. Segregation of atrial-specific and inducible expression of an atrial natriuretic factor transgene in an in vivo murine model of cardiac hypertrophy. *Proc Natl Acad Sci U S A*, 88, 8277-81.
- Rosa, J., Canovas, P., Islam, A., Altieri, D. C. & Doxsey, S. J. 2006. Survivin modulates microtubule dynamics and nucleation throughout the cell cycle. *Mol Biol Cell*, 17, 1483-93.
- Roskoski, R. 2005. Structure and regulation of Kit protein-tyrosine kinase - The stem cell factor receptor. *Biochem Bioph Res Co*, 338, 1307-1315.
- Roth, G. A., Forouzanfar, M. H., Moran, A. E., Barber, R., Nguyen, G., Feigin, V. L., . . . Murray, C. J. 2015. Demographic and epidemiologic drivers of global cardiovascular mortality. *N Engl J Med*, 372, 1333-41.
- Roth, G. M., Bader, D. M. & Pfaltzgraff, E. R. 2014. Isolation and physiological analysis of mouse cardiomyocytes. *Jove-J Vis Exp*.
- Rudolph, A. M. 1970. The changes in the circulation after birth. Their importance in congenital heart disease. *Circulation*, 41, 343-59.
- Rumyantsev, P. P. 1977. Interrelations of the proliferation and differentiation processes during cardiac myogenesis and regeneration. *Int Rev Cytol*, 51, 186-273.
- Salazar, N. C., Chen, J. & Rockman, H. A. 2007. Cardiac GPCRs: GPCR signaling in healthy and failing hearts. *Bba-Biomembranes*, 1768, 1006-1018.
- Sandritter, W. & Scomazzoni, G. 1964. Deoxyribonucleic Acid Content (Feulgen Photometry) and Dry Weight (Interference Microscopy) of Normal and Hypertrophic Heart Muscle Fibers. *Nature*, 202, 100-1.

- Sasaki, R., Watanabe, Y., Morishit.T & Yamagata, S. 1968. Estimation of cell number of heart muscles in normal rats. *Tohoku J Exp Med*, 95, 177-184.
- Schoenfeld, J. R., Vasser, M., Jhurani, P., Ng, P., Hunter, J. J., Ross, J., . . . Lowe, D. G. 1998. Distinct molecular phenotypes in murine cardiac muscle development, growth, and hypertrophy. *J Mol Cell Cardiol*, 30, 2269-2280.
- Scholz, D. G., Kitzman, D. W., Hagen, P. T., Ilstrup, D. M. & Edwards, W. D. 1988. Age-related changes in normal human hearts during the first 10 decades of life. Part I (Growth): A quantitative anatomic study of 200 specimens from subjects from birth to 19 years old. *Mayo Clin Proc*, 63, 126-36.
- Schroeder, A., Mueller, O., Stocker, S., Salowsky, R., Leiber, M., Gassmann, M., . . . Ragg, T. 2006. The RIN: an RNA integrity number for assigning integrity values to RNA measurements. *Bmc Mol Biol*, 7.
- Sealey, J. E. 1991. Plasma renin activity and plasma prorenin assays. *Clin Chem*, 37, 1811-9.
- Segar, J. L., Volk, K. A., Lipman, M. H. B. & Scholz, T. D. 2013. Thyroid hormone is required for growth adaptation to pressure load in the ovine fetal heart. *Exp Physiol*, 98, 722-733.
- Senyo, S. E., Steinhauser, M. L., Pizzimenti, C. L., Yang, V. K., Cai, L., Wang, M., . . . Lee, R. T. 2013. Mammalian heart renewal by pre-existing cardiomyocytes. *Nature*, 493, 433-U186.
- Sharma, R. B., O'donnell, A. C., Stamateris, R. E., Ha, B., Mccloskey, K. M., Reynolds, P. R., . . . Alonso, L. C. 2015. Insulin demand regulates beta cell number via the unfolded protein response. *J Clin Invest*, 125, 3831-46.
- Shendure, J. & Ji, H. L. 2008. Next-generation DNA sequencing. *Nat Biotechnol*, 26, 1135-1145.
- Shimoni, Y., Fiset, C., Clark, R. B., Dixon, J. E., Mckinnon, D. & Giles, W. R. 1997. Thyroid hormone regulates postnatal expression of transient K⁺ channel isoforms in rat ventricle. *J Physiol*, 500 (Pt 1), 65-73.
- Shioi, T., Kang, P. M., Douglas, P. S., Hampe, J., Yballe, C. M., Lawitts, J., . . . Izumo, S. 2000. The conserved phosphoinositide 3-kinase pathway determines heart size in mice. *Embo J*, 19, 2537-48.
- Sigurgeirsson, B., Emanuelsson, O. & Lundeberg, J. 2014. Sequencing Degraded RNA Addressed by 3' Tag Counting. *PloS one*, 9.
- Sim, C. B., Ziemann, M., Kaspi, A., Harikrishnan, K. N., Ooi, J., Khurana, I., . . . Porrello, E. R. 2015. Dynamic changes in the cardiac methylome during postnatal development. *Faseb Journal*, 29, 1329-1343.
- Slattery, M. M. & Morrison, J. J. 2002. Preterm delivery. *Lancet*, 360, 1489-97.
- Smith, H. L. 1928. The relation of the weight of the heart to the weight of the body and of the weight of the heart to age. *Am Heart J*, 4, 79-93.

- Soonpaa, M. H., Kim, K. K., Pajak, L., Franklin, M. & Field, L. J. 1996. Cardiomyocyte DNA synthesis and binucleation during murine development. *Am J Physiol*, 271, H2183-9.
- St Laurent, G., Wahlestedt, C. & Kapranov, P. 2015. The Landscape of long noncoding RNA classification. *Trends Genet*, 31, 239-251.
- Steigemann, P. & Gerlich, D. W. 2009. Cytokinetic abscission: cellular dynamics at the midbody. *Trends Cell Biol*, 19, 606-616.
- Subramaniam, A., Jones, W. K., Gulick, J., Wert, S., Neumann, J. & Robbins, J. 1991. Tissue-specific regulation of the alpha-myosin heavy chain gene promoter in transgenic mice. *J Biol Chem*, 266, 24613-24620.
- Sultana, N., Zhang, L., Yan, J., Chen, J., Cai, W., Razzaque, S., . . . Cai, C. L. 2015. Resident c-kit(+) cells in the heart are not cardiac stem cells. *Nat Commun*, 6, 8701.
- Takeda, N., Manabe, I., Uchino, Y., Eguchi, K., Matsumoto, S., Nishimura, S., . . . Nagai, R. 2010. Cardiac fibroblasts are essential for the adaptive response of the murine heart to pressure overload. *J Clin Invest*, 120, 254-265.
- Tallini, Y. N., Greene, K. S., Craven, M., Spealman, A., Breitbach, M., Smith, J., . . . Kotlikoff, M. I. 2009. c-kit expression identifies cardiovascular precursors in the neonatal heart. *Proc Natl Acad Sci U S A*, 106, 1808-13.
- Tamura, N., Ogawa, Y., Chusho, H., Nakamura, K., Nakao, K., Suda, M., . . . Katsuki, M. 2000. Cardiac fibrosis in mice lacking brain natriuretic peptide. *Proc Natl Acad Sci U S A*, 97, 4239-44.
- Tang, F. C., Lao, K. Q. & Surani, M. A. 2011. Development and applications of single-cell transcriptome analysis. *Nat Methods*, 8, S6-S11.
- Tarnavski, O., McMullen, J. R., Schinke, M., Nie, Q., Kong, S. & Izumo, S. 2004. Mouse cardiac surgery: comprehensive techniques for the generation of mouse models of human diseases and their application for genomic studies. *Physiol Genomics*, 16, 349-60.
- Teske, B. F., Fusakio, M. E., Zhou, D., Shan, J., McClintick, J. N., Kilberg, M. S. & Wek, R. C. 2013. CHOP induces activating transcription factor 5 (ATF5) to trigger apoptosis in response to perturbations in protein homeostasis. *Mol Biol Cell*, 24, 2477-90.
- Tetsu, O., Phuchareon, J., Chou, A., Cox, D. P., Eisele, D. W. & Jordan, R. C. 2010. Mutations in the c-Kit gene disrupt mitogen-activated protein kinase signaling during tumor development in adenoid cystic carcinoma of the salivary glands. *Neoplasia*, 12, 708-17.
- Thaker, V. V., Leung, A. M., Braverman, L. E., Brown, R. S. & Levine, B. 2014. Iodine-induced hypothyroidism in full-term infants with congenital heart disease: more common than currently appreciated? *J Clin Endocr Metab*, 99, 3521-3526.
- The Lancet Editors. 2014. Expression of concern: the SCIPIO trial. *The Lancet*, 383, 1279.

- Theoharides, T. C., Elmansoury, M., Letourneau, R., Boucher, W. & Rozniecki, J. J. 1993. Dermatitis characterized by mastocytosis at immunization sites in mast-cell-deficient W/W^v mice. *Int Arch Allergy Imm*, 102, 352-361.
- Tsuruda, T., Boerrigter, G., Huntley, B. K., Noser, J. A., Cataliotti, A., Costello-Boerrigter, L. C., . . . Burnett, J. C., Jr. 2002. Brain Natriuretic Peptide is Produced in Cardiac Fibroblasts and Induces Matrix Metalloproteinases. *Circ Res*, 91, 1127-34.
- Van Berlo, J. H., Kanisicak, O., Maillet, M., Vagnozzi, R. J., Karch, J., Lin, S. C., . . . Molkenkin, J. D. 2014. c-kit⁺ cells minimally contribute cardiomyocytes to the heart. *Nature*, 509, 337-41.
- Van Nierop, B. J., Van Assen, H. C., Van Deel, E. D., Niesen, L. B., Duncker, D. J., Strijkers, G. J. & Nicolay, K. 2013. Phenotyping of left and right ventricular function in mouse models of compensated hypertrophy and heart failure with cardiac MRI. *PloS one*, 8, e55424.
- Viereck, J., Kumarswamy, R., Foinquinos, A., Xiao, K., Avramopoulos, P., Kunz, M., . . . Thum, T. 2016. Long noncoding RNA Chast promotes cardiac remodeling. *Sci Transl Med*, 8.
- Villarreal, D., Davis, J. O., Freeman, R. H., Sweet, W. D. & Dietz, J. R. 1984. Effects of meclofenamate on the renin response to aortic constriction in the rat. *Am J Physiol*, 247, R546-51.
- Vincentz, J. W., Barnes, R. M., Firulli, B. A., Conway, S. J. & Firulli, A. B. 2008. Cooperative interaction of Nkx2.5 and Mef2c transcription factors during heart development. *Dev Dynam*, 237, 3809-3819.
- Vogel, C. & Marcotte, E. M. 2012. Insights into the regulation of protein abundance from proteomic and transcriptomic analyses. *Nat Rev Genet*, 13, 227-232.
- Wallner, M., Duran, J. M., Mohsin, S., Troupes, C. D., Vanhoutte, D., Borghetti, G., . . . Houser, S. R. 2016. Acute Catecholamine Exposure Causes Reversible Myocyte Injury Without Cardiac Regeneration. *Circ Res*, 119, 865-79.
- Walsh, S., Ponten, A., Fleischmann, B. K. & Jovinge, S. 2010. Cardiomyocyte cell cycle control and growth estimation in vivo--an analysis based on cardiomyocyte nuclei. *Cardiovasc Res*, 86, 365-73.
- Walton, C. B. & Matter, M. L. 2015. Chromatin Immunoprecipitation Assay: Examining the Interaction of NFκB with the VEGF Promoter. *Methods Mol Biol*, 1332, 75-87.
- Wamstad, J. A., Alexander, J. M., Truty, R. M., Shrikumar, A., Li, F. G., Eilertson, K. E., . . . Bruneau, B. G. 2012. Dynamic and Coordinated Epigenetic Regulation of Developmental Transitions in the Cardiac Lineage. *Cell*, 151, 206-220.
- Wang, K., Liu, F., Zhou, L. Y., Long, B., Yuan, S. M., Wang, Y., . . . Li, P. F. 2014. The long noncoding RNA CHRF regulates cardiac hypertrophy by targeting miR-489. *Circ Res*, 114, 1377-1388.
- Wang, Z., Gerstein, M. & Snyder, M. 2009. RNA-Seq: a revolutionary tool for transcriptomics. *Nat Rev Genet*, 10, 57-63.

- Wang, Z., Zhang, X. J., Ji, Y. X., Zhang, P., Deng, K. Q., Gong, J., . . . Wang, Y. 2016. The long noncoding RNA Chaer defines an epigenetic checkpoint in cardiac hypertrophy. *Nat Med*, 22, 1131-1139.
- Weber, K. T. & Brilla, C. G. 1991. Pathological hypertrophy and cardiac interstitium. Fibrosis and renin-angiotensin-aldosterone system. *Circulation*, 83, 1849-65.
- Wettschureck, N., Rutten, H., Zywiets, A., Gehring, D., Wilkie, T. M., Chen, J., . . . Offermanns, S. 2001. Absence of pressure overload induced myocardial hypertrophy after conditional inactivation of Galphaq/Galpha11 in cardiomyocytes. *Nat Med*, 7, 1236-40.
- Wiesel, P., Mazzolai, L., Nussberger, J. & Pedrazzini, T. 1997. Two-kidney, one clip and one-kidney, one clip hypertension in mice. *Hypertension*, 29, 1025-30.
- Winer, J., Jung, C. K. S., Shackel, I. & Williams, P. M. 1999. Development and validation of real-time quantitative reverse transcriptase-polymerase chain reaction for monitoring gene expression in cardiac myocytes in vitro. *Anal Biochem*, 270, 41-49.
- Wolska, B. M. & Solaro, R. J. 1996. Method for isolation of adult mouse cardiac myocytes for studies of contraction and microfluorimetry. *Am J Physiol-Heart C*, 271, H1250-H1255.
- Womack, H. C. 1983. The Relationship Between Human Body Weight, Subcutaneous Fat, Heart Weight, and Epicardial Fat. *Human Biology*, 55, 667-676.
- Wu, J. H., Hagaman, J., Kim, S., Reddick, R. L. & Maeda, N. 2002. Aortic constriction exacerbates atherosclerosis and induces cardiac dysfunction in mice lacking apolipoprotein E. *Arterioscler Thromb Vasc Biol*, 22, 469-75.
- Xiang, F. L., Lu, X., Hammoud, L., Zhu, P., Chidiac, P., Robbins, J. & Feng, Q. 2009. Cardiomyocyte-specific overexpression of human stem cell factor improves cardiac function and survival after myocardial infarction in mice. *Circulation*, 120, 1065-74, 9 p following 1074.
- Xin, M., Olson, E. N. & Bassel-Duby, R. 2013. Mending broken hearts: cardiac development as a basis for adult heart regeneration and repair. *Nat Rev Mol Cell Bio*, 14, 529-541.
- Xing, W. R., Govoni, K. E., Donahue, L. R., Kesavan, C., Wergedal, J., Long, C. L., . . . Mohan, S. 2012. Genetic evidence that thyroid hormone is indispensable for prepubertal insulin-like growth factor-I expression and bone acquisition in mice. *J Bone Miner Res*, 27, 1067-1079.
- Yang, Z. K., Kirton, H. M., Macdougall, D. A., Boyle, J. P., Deuchars, J., Frater, B., . . . Steele, D. S. 2015. The Golgi apparatus is a functionally distinct Ca²⁺ store regulated by the PKA and Epac branches of the beta(1)-adrenergic signaling pathway. *Sci Signal*, 8.
- Yarden, Y., Kuang, W. J., Yang-Feng, T., Coussens, L., Munemitsu, S., Dull, T. J., . . . Ullrich, A. 1987. Human proto-oncogene c-kit: a new cell surface receptor tyrosine kinase for an unidentified ligand. *Embo J*, 6, 3341-51.

- Yutzey, K. E. & Robbins, J. 2007. Principles of genetic murine models for cardiac disease. *Circulation*, 115, 792-799.
- Zak, R. 1973. Cell proliferation during cardiac growth. *Am J Cardiol*, 31, 211-9.
- Zak, R. 1974. Development and proliferative capacity of cardiac muscle cells. *Circ Res*, 35, suppl II:17-26.
- Zaruba, M. M., Soonpaa, M., Reuter, S. & Field, L. J. 2010. Cardiomyogenic potential of c-Kit(+)-expressing cells derived from neonatal and adult mouse hearts. *Circulation*, 121, 1992-U56.
- Zeng, S., Xu, Z., Lipkowitz, S. & Longley, J. B. 2005. Regulation of stem cell factor receptor signaling by Cbl family proteins (Cbl-b/c-Cbl). *Blood*, 105, 226-32.
- Zhang, D. Y. & Morgan, T. O. 1999. Effects of aortic ligation on the renin angiotensin system in hydronephrotic mice. *Blood Press*, 8, 122-7.
- Zhao, Y., Ransom, J. F., Li, A., Vedantham, V., Von Drehle, M., Muth, A. N., . . . Srivastava, D. 2007. Dysregulation of cardiogenesis, cardiac conduction, and cell cycle in mice lacking miRNA-1-2. *Cell*, 129, 303-317.
- Zheng, J. Y., Wei, C. C., Hase, N., Shi, K., Killingsworth, C. R., Litovsky, S. H., . . . Dell'italia, L. J. 2014. Chymase mediates injury and mitochondrial damage in cardiomyocytes during acute ischemia/reperfusion in the dog. *PloS one*, 9.
- Zimmerman, B. G. & Kraft, E. 1979. Blockade by saralasin of adrenergic potentiation induced by renin-angiotensin system. *J Pharmacol Exp Ther*, 210, 101-5.
- Zitouni, S., Nabais, C., Jana, S. C., Guerrero, A. & Bettencourt-Dias, M. 2014. Polo-like kinases: structural variations lead to multiple functions. *Nat Rev Mol Cell Biol*, 15, 433-452.

Appendix

Appendix A

	P2	P10	P13	P70
Cardiac cell markers				
<i>Myh6</i> vs <i>Tnnt2</i>	****	****	****	****
<i>Myh6</i> vs <i>Pecam1</i>	****	****	****	****
<i>Myh6</i> vs <i>Vcam1</i>	****	****	****	****
<i>Myh6</i> vs <i>Ddr2</i>	****	****	****	****
<i>Myh6</i> vs <i>Vim</i>	****	****	****	****
<i>Tnnt2</i> vs <i>Pecam1</i>	****	****	****	****
<i>Tnnt2</i> vs <i>Vcam1</i>	****	****	****	****
<i>Tnnt2</i> vs <i>Ddr2</i>	****	****	****	****
<i>Tnnt2</i> vs <i>Vim</i>	****	****	****	****
<i>Pecam1</i> vs <i>Vcam1</i>	ns	ns	ns	ns
<i>Pecam1</i> vs <i>Ddr2</i>	ns	ns	ns	ns
<i>Pecam1</i> vs <i>Vim</i>	ns	ns	ns	ns
<i>Vcam1</i> vs <i>Ddr2</i>	ns	ns	ns	ns
<i>Vcam1</i> vs <i>Vim</i>	ns	ns	ns	ns
<i>Ddr2</i> vs <i>Vim</i>	ns	ns	ns	ns

Expression levels of mRNA (cpm) for cardiac cell type-specific markers for CMs, ECs, and fibroblasts, were compared in preparations of purified CMs from P2, P10, P13, or P70 mice (n=3 litters per time point). CMs (*Myh6* encodes α -MHC; *Tnnt2* encodes cTnT), ECs (*Pecam1* and *Vcam1*), and fibroblasts (*Ddr2* encodes discoidin domain receptor tyrosine kinase 2; *Vim* encodes vimentin). Statistical significances were determined using two-way ANOVA followed by Tukey's *post hoc* test; **** p<0.0001, and non-significant, ns.

Appendix B

	2 vs 10	2 vs 13	2 vs 70	10 vs 13	10 vs 70	13 vs 70
Cell cycle						
<i>Anln</i>	ns	ns	*	ns	ns	ns
<i>Aurka</i>	ns	ns	*	ns	ns	ns
<i>Birc5</i>	ns	*	*	ns	ns	ns
<i>Ccnb1</i>	ns	ns	*	ns	ns	ns
<i>Ki67</i>	ns	*	*	ns	ns	ns
<i>Plk1</i>	ns	ns	ns	ns	ns	ns
<i>E2f1</i>	ns	*	**	ns	ns	ns
<i>Rb1</i>	ns	ns	ns	ns	ns	ns
Growth signals						
<i>Pi3kca</i>	ns	**	**	ns	ns	ns
<i>Akt1</i>	***	****	****	***	****	*
<i>Igf1</i>	*	**	****	ns	**	ns
<i>Igf1r</i>	****	****	****	**	***	ns
<i>Thrb</i>	***	****	****	*	*	ns
<i>Thra</i>	**	***	****	ns	**	*
TFs						
<i>Nkx2.5</i>	*	**	***	ns	ns	ns
<i>Gata4</i>	*	***	****	ns	**	ns
<i>Mef2c</i>	**	**	***	ns	ns	ns
<i>Nfatc4</i>	ns	ns	*	ns	ns	ns
<i>Meis1</i>	***	***	****	ns	**	ns

Expression levels (cpm) of cardiac developmental and growth signalling mRNAs in purified CMs from mice aged P2, P10, P13, and P70 (n=3 litters per time point). Cell cycle genes: anillin (*Anln*), aurora kinase A (*Aurka*), survivin (*Birc5*), cyclin B1 (*Ccnb1*), Ki67 (*Mki67*), polo-like kinase 1 (*Plk1*), E2 promoter binding factor 1 (*E2f1*), and retinoblastoma (*Rb1*). Growth signals: phosphatidylinositol-4,5-bisphosphate 3-kinase catalytic subunit α (*Pi3kca*), serine/threonine kinase 1 (*Akt1*), insulin-like growth factor 1 (*Igf1*), insulin-like growth factor 1 receptor (*Igf1r*), thyroid hormone receptor β (*Thrb*), thyroid hormone receptor α (*Thra*). TFs: NK2 homeobox 5 (*Nkx2-5*), *Gata4*, myocyte enhancer factor 2 (*Mef2c*), nuclear factor of activated T cells (*Nfatc4*), and meis homeobox 1 (*Meis1*). Statistical significances were determined using one-way ANOVA followed by Tukey's *post hoc* test; p<0.05, **p<0.01, ***p<0.001, ****p<0.0001, and non-significant, ns.